

NEW STRATEGIES
FOR THE CONTROL OF ELECTROHEAT PROCESSES

THESIS

DOCTOR OF PHILOSOPHY

at the

UNIVERSITY OF ASTON IN BIRMINGHAM

by

Güney Cönenç

January 1970

University of Aston in Birmingham
Electrical Engineering Department

THE UNIVERSITY
OF
BIRMINGHAM.
LIBRARY

13 FEB 1970

THESIS 127013

621.365

GÖN

SUMMARY

NEW STRATEGIES

FOR THE CONTROL OF ELECTROHEAT PROCESSES

The increasing use of electroheat in complicated industrial processes makes it necessary to investigate the current electroheat control methods with a view to developing new strategies.

First, various models of electroheat processes are investigated. Methods for obtaining approximate models are evaluated in terms of their accuracy in the time domain.

An analytical investigation of on-off control systems is presented. Digital simulation techniques for on-off control systems are discussed, and computer programmes are given.

Open loop control of first and second order systems is investigated. The advantages and disadvantages of open-loop control are discussed. An indirect electroheat control scheme which uses a model of the plant in the feedback loop is proposed and discussed. It is shown that, by a suitable choice of the model parameters, performance criteria can be substantially improved.

Pulse-width modulation (PWM) control of electroheat processes is presented as an alternative to indirect control. An analysis of PWM control systems, with particular reference to electroheat processes, is given. Digital simulation programmes based on this analysis are also included. Stability conditions are investigated analytically and the results are verified both by digital and analogue simulation. An exact analysis of limit cycling in PWM electroheat control systems is presented. The results of this analysis are verified by using analogue and digital simulation. The potential advantages of PWM for electroheat control are discussed.

ACKNOWLEDGEMENTS

I wish to thank the late Professor W.K.Roots for his guidance and encouragement. I also thank Professor J.E.Flood who kindly consented to be my adviser for the latter portion of the work. Thanks are also due to Mr. J.L.Murgatroyd who provided many useful suggestions.

I thank the Scientific and Technical Research Council of Turkey for the financial support provided during my studies.

TABLE OF CONTENTS

1	INTRODUCTION	1
2	APPROXIMATE MODELS FOR ELECTROHEAT PROCESSES	4
	2.1 Introduction	4
	2.2 The Ziegler-Nichols Model	4
	2.3 Other Approximate Models	5
	2.4 Typical Electroheat Processes	7
	2.5 Discussion	17
	2.6 Summary	18
3	ON-OFF CONTROL OF ELECTROHEAT PROCESSES	19
	3.1 Introduction	19
	3.2 The on-off Controller	19
	3.3 On-off Control	21
	3.4 Illustrative Example	34
	3.5 Digital Simulation of On-off Control Systems	36
	3.5.1 Method Used for Simulation	36
	3.5.2 Simulation Programme	39
	3.5.3 Simulation Results	40
	3.5.4 Discussion	48
	3.6 Summary	53
4	OPEN-LOOP AND INDIRECT CONTROL	55
	4.1 Introduction	55
	4.2 Open-loop Control	56
	4.2.1 First Order Systems	56
	4.2.2 Higher Order Systems	66
	4.2.3 Digital Simulation of Open-loop Control Systems	74
	4.2.3.1 Method Used for Simulation	74
	4.2.3.2 Simulation Programme	74
	4.2.3.3 Simulation Results	75
	4.3 Indirect Control	80
	4.3.1 Description and Design Criteria	82
	4.3.2 Applications	88
	4.4 Summary	93

5	PULSE-WIDTH MODULATION (PWM) CONTROL	94
5.1	Introduction	94
5.2	PWM as a Sampling Process	99
5.3	Analysis of PWM Control Systems	104
5.3.1	Description of the System	104
5.3.2	Solution of System Differential Equations for Sampled-data Systems	108
5.3.3	Analysis of the PWM System	111
5.4	Digital Simulation of PWM Control Systems	122
5.5	Summary	129
6	LIMIT CYCLES IN PWM CONTROL SYSTEMS	130
6.1	Introduction	130
6.2	Graphical Analysis of PWM Control Systems	132
6.2.1	Difference Equation Formulation of the System	132
6.2.2	Graphical Solution	137
6.2.3	Bias Considerations	139
6.3	An Exact Analysis of Limit Cycles in PWM Electroheat Control Systems	143
6.3.1	Basic Definitions	143
6.3.2	Saturated-saturated Oscillations	146
6.3.3	Linear and Saturated-linear Oscillations	179
6.3.4	Plants with Transit Delay	190
6.4	Effects of Mode Dependence	209
6.5	Effects of Disturbance	210
6.5.1	Effects of Disturbance on Regulation Characteristic	210
6.5.2	Effects of Disturbance on Limit Cycles	212
6.6	Summary	214
7	ANALOGUE SIMULATION OF PWM SYSTEMS	217
7.1	Introduction	217
7.2	The Pulse-width Modulator	218
7.3	Analogue Simulation of the PWM Control System	222
7.3.1	Actual Variables and Their Analogues	222
7.3.2	Description of the Circuit used in Simulation	223
7.4	Experimental Results	228
7.4.1	Practical Considerations	228
7.4.2	Qualitative Results	229
7.4.3	Quantitative Results	231
7.5	Summary	240

8	GENERAL CONCLUSIONS	242
APPENDIX A	DIGITAL SIMULATION PROGRAMMES	245
APPENDIX B	APPROXIMATIONS USED IN THE TEXT	267
LIST OF SYMBOLS		270
REFERENCES		273
PRESENT PUBLICATIONS RESULTED FROM THIS WORK		276

1

INTRODUCTION

The use of electroheat in industrial processes has been continuously increasing for the last three decades. Today electroheat plays an important role in nearly all branches of industry and this role is acquiring even more importance as the processes become more and more complicated. In thermal processes the main objective is to achieve certain thermal conditions and to maintain them within acceptable limits. Therefore the control of electroheat processes is the most important factor in determining the quality of the output product. On-off control methods have been widely used to control electroheat processes since these methods often represent the simplest and most economical means of control. In on-off control the control element is usually a relay. Relays are capable of handling large powers, operate with very small amounts of power, and reasonably cheap. It is now possible to utilise electronic on-off controllers (silicon controlled rectifiers, unijunction transistors etc.) which have the advantage of high speed switching and less hysteresis over the conventional relay controllers.

Although on-off control is still the most common technique used in electroheat processes, it presents serious disadvantages, which can be summarized as follows:

- a. the existence of long cycling periods, especially when the transit delays in the system are large.
- b. the existence of large amplitude oscillations in the output temperature
- c. the undesirable effects of controller hysteresis.

Therefore it is found necessary to examine existing on-off control methods with a view to developing new techniques. This study is done for the most general case viz. mode dependent processes with transit delay which are controlled by hysteretic controllers.

A new electroheat control technique must have better performance while still using conventional controllers (electromechanical or electronic relays) to be regarded as an improvement. Two such techniques are proposed in this work. The first is the indirect control scheme which is analysed with emphasis on the design aspects. The second strategy is the use of pulse width modulation (PWM) control. Up to the present time PWM has not been studied in the literature as a means of electroheat control. PWM systems encountered in communication and control systems have been associated with bang-bang type outputs rather than on-off. Thus, a detailed study of PWM control of electroheat was required to assess the suitability of such techniques to practical processes. An exact analysis of stability, including limit cycling phenomena in PWM electroheat control systems, is presented in this work for the first time.

Special emphasis is given to the digital simulation aspects of electroheat control throughout the work. Digital simulation programmes for on-off, open-loop, and PWM control systems are developed. These programmes are not only a powerful tool in the analysis and design of such systems, but also serve the purpose

of checking the results derived analytically.

An analogue simulation method for PWM control systems and the experimental implementation of this method are also described. The analytical results derived throughout this study were checked by using digital and analogue computers and they were found to be in complete agreement with the simulation results.

In this thesis the presentation of PWM control is from an analytical viewpoint, though it must be conceded that for a complete treatment there are further investigations which should be made in the application of PWM to the control of electroheat processes. The accuracy of control obtained as the result of the use of PWM in preference to comparative schemes for electroheat control has not been investigated for reasons of space and time.

2

APPROXIMATE MODELS FOR ELECTROHEAT PROCESSES

2.1 INTRODUCTION

Electroheat processes encountered in practice usually possess irrational transfer functions leading to cumbersome calculations. This necessitates the use of approximate models. In this chapter some of the approximations encountered in the literature are discussed. The Ziegler-Nichols model is shown to be the most suitable approximation for the analysis and design of control systems. Even in dealing with simple electroheat processes one is usually involved in complex calculations. To illustrate this point a typical electroheat process model is investigated briefly later in this chapter.

2.2 THE ZIEGLER-NICHOLS MODEL

All electroheat processes possess a low-pass transfer characteristic of an order higher than one, therefore they exhibit an S-shaped step response. This property suggests the use of Ziegler-Nichols⁴⁸ approximation. The Ziegler-Nichols approximate model consists of a transport delay and a first order system, therefore its transfer function is given by:

$$F = \exp(-sL_e)/(1 + sT_e) \quad (2.1)$$

The determination of the model parameters from the process step response is shown in fig. 2.1a. In this figure $a(t)$ is the step response of the actual process. The tangent to $a(t)$ at its inflection point is denoted by AB. The inverse slope of AB gives the time constant of the model, and its intersection point with the time axis gives the equivalent delay.

The Ziegler-Nichols model is extensively used in electro-heat control applications^{5,25,26,32,36,37,47}. Among the reasons for this wide acceptance are:

1. The Ziegler-Nichols model is relatively simple; hence it simplifies the analysis both in time and in the frequency domain.
2. It provides a good approximation to most electroheat processes.
3. Most important of all, the Ziegler-Nichols model has a delay/time-constant ratio which is larger than any other reasonable first order approximation (fig. 2.1b). As is well known, the L/T ratio is the most important factor on system stability. As L/T increases the tendency of the system to become unstable increases. Because of the conservative L/T value of the Ziegler-Nichols model, the stability analysis of control systems carried out by using a Ziegler-Nichols model of the process will have a safety margin, i.e. the actual system will always be stable whenever the analysis using this model gives stable results.

2.3 OTHER APPROXIMATE MODELS

Other approximate models have been proposed instead of the Ziegler-Nichols model. Two of these models will be briefly mentioned in this section.

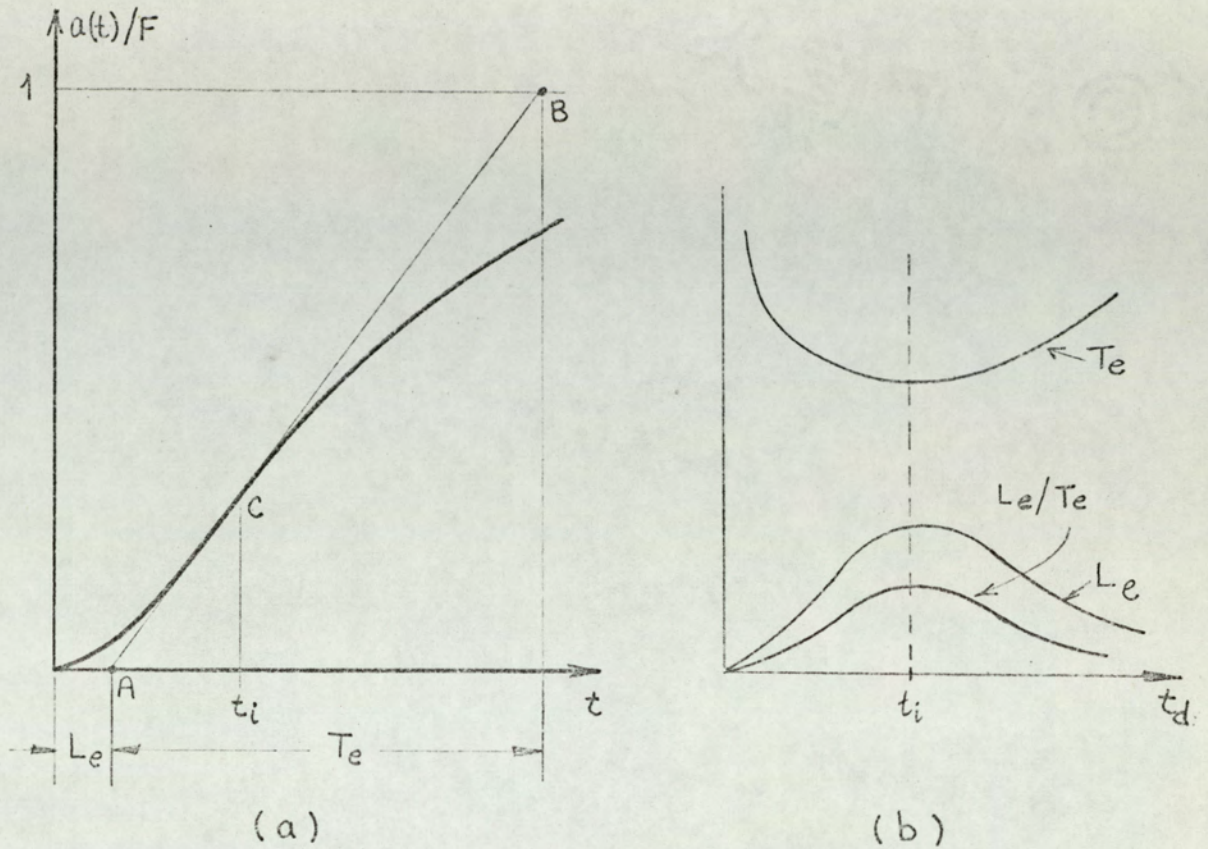


Fig. 2.1

- (a) Determination of L_e and T_e from the step response of the process. C is the inflection point of $a(t)$.
- (b) L_e and T_e which would result from a tangent drawn to the step response curve at a point $[t_d, a(t_d)]$.

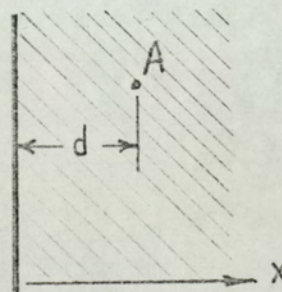


Fig. 2.2

Heat conduction through a semi-infinite solid.

One approximation method is Strejc's method⁴¹. Strejc proposed an approximate model with the transfer function:

$$F \exp(-sL_s) / (1 + sT_s)^n, \quad n \text{ integer} \quad (2.2)$$

The equivalent model parameters L_s , T_s and n are found from the L_e/T_e ratio (L_e and T_e as shown in fig. 2.1a) of the step response of the actual process, by using tables^{7,41}. This method will not be elaborated here. From the tables given by Strejc it is seen that for L_e/T_e smaller than 0.104 this method results in a first order system with lag, with parameters equal to L_e and T_e . Therefore, for $L_e/T_e < 0.104$ (which is the case for many electroheat processes), Strejc's model and Ziegler-Nichols model are identical.

Another approximation method was proposed recently by Chaussard⁸. Chaussard's model has the following transfer function:

$$F / (1 + sT_c)^c \quad (2.3)$$

As is seen from eqn. 2.3 Chaussard's model is a generalisation of Strejc's method to include non-integer values of n . Chaussard gave nomograms⁷, instead of tables, to determine T_c and c from T_e and L_e . In the following section we shall give an example of Chaussard approximation.

2.4 TYPICAL ELECTROHEAT PROCESSES

This section is a brief presentation of the time properties of some basic electroheat processes. First, we consider the distributed lag. A salient feature of thermal processes, where heat transfer is mainly due to conduction, is the distributed

lag property^{3,6,9}. The heat conduction through a semi-infinite solid (fig. 2.2) is a typical example of distributed lag. For most practical applications, a furnace wall can be represented by a semi-infinite solid. If the surface at $x = 0$ is kept at constant temperature F and if the initial temperature of the solid is zero, then the temperature at point A is given by⁶

$$\theta = F \left[1 - \operatorname{erf} \frac{d}{2\sqrt{kt}} \right] \quad (2.3)$$

where k is the diffusivity of the solid (cm^2/sec).

If we call

$$T = d^2/k \quad (\text{sec})$$

then eqn 2.3 becomes

$$\theta = F \left[1 - \operatorname{erf} \frac{1}{2} \sqrt{\frac{T}{t}} \right] \quad (2.4)$$

We know that

$$\mathcal{L}^{-1} \left[F \frac{\exp(-\sqrt{sT})}{s} \right] = F \left(1 - \operatorname{erf} \frac{1}{2} \sqrt{\frac{T}{t}} \right)$$

Therefore eqn. 2.4 represents the step response of a system with the following transfer function:

$$F \exp(-\sqrt{sT})$$

The system with the above transfer function is called a distributed lag system. Note that the time constant T for a

particular point A is proportional to the square of its distance from the heating surface.

One notes that the step response of an infinite leakage-free non-inductive transmission line has the same form.⁸ This gives rise to the possibility of simulating some electroheat processes by using ladder networks of the type of series resistance-shunt capacitance. This type of simulation has the drawback of introducing errors due to the use of the ladder (lumped) networks instead of distributed parameter line, and also due to the finite "length" of the simulated line²¹.

The Ziegler-Nichols model for the distributed lag system can be easily found by noting that the coordinates of the inflection point of the step response are:

$$t_i = T/6 \quad (2.7a)$$

$$a(t_i) = 0.085 \quad (2.7b)$$

By using these values the equivalent time constant and delay are found to be:

$$T_e = 1.08 T \quad (2.8a)$$

$$L_e = 0.075 T \quad (2.8b)$$

Hence we establish the following approximate model for the distributed lag, $\exp(-\sqrt{sT})$:

$$\exp(-0.075 Ts)/(1 + 1.08 Ts) \quad (2.9)$$

In fig. 2.3 a distributed lag system with $T = 200$ min and its approximate model (found from eqn. 2.9) are compared by their

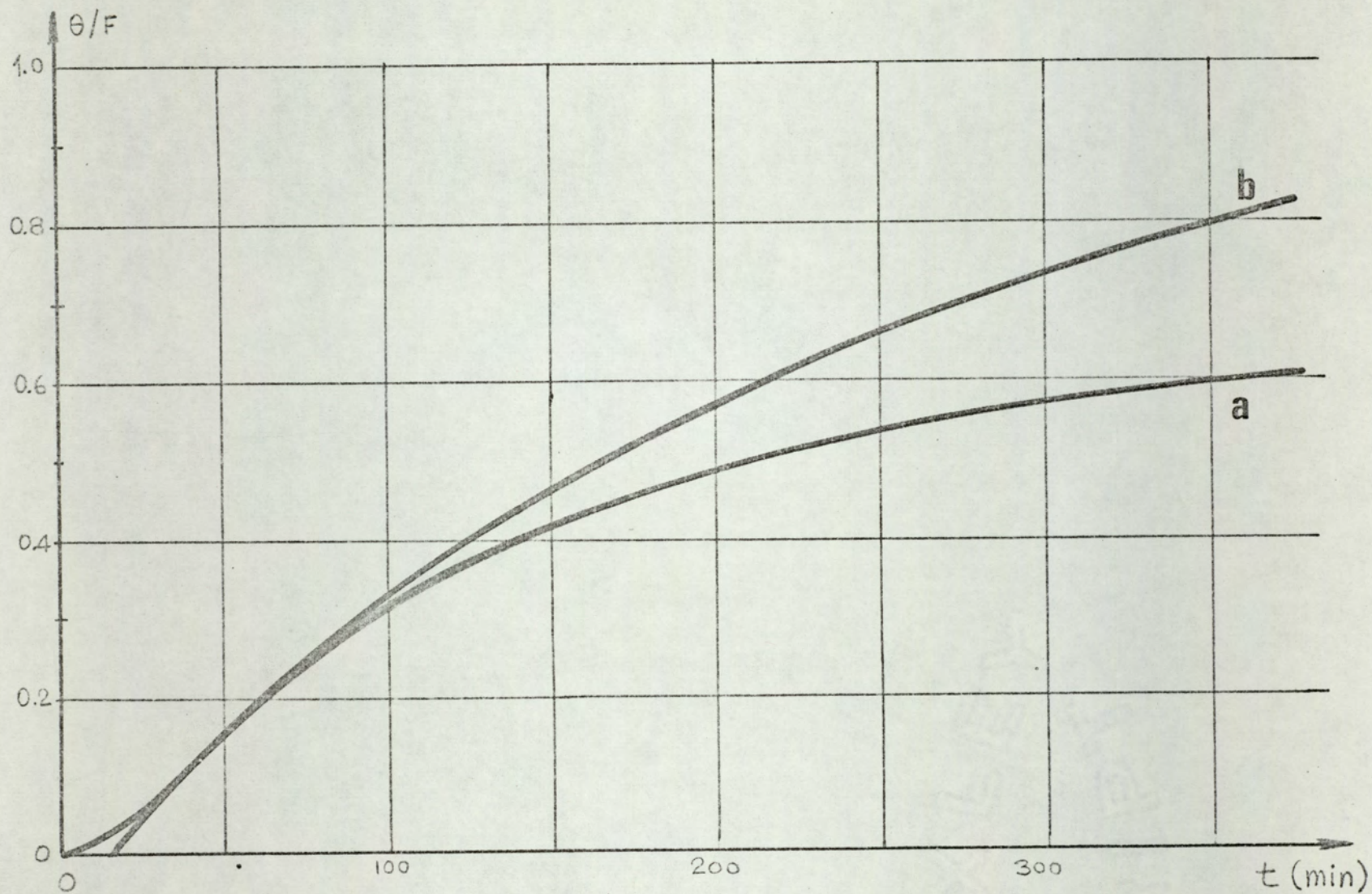


Fig. 2.3

Step response of a distributed lag system (a), and its Ziegler-Nichols approximation (b).
 a-step response of $\exp(-\sqrt{200s})$ b-step response of $\exp(-15s)/(1+216s)$

step response curves*. It can be seen that the approximation is satisfactory for values of time up to about T . Since in most of the discontinuous control systems the cycling period is considerably shorter than the time constants the above approximation will give satisfactory results for the steady state dec conditions.

As stated above, the L/T ratio is an important index for a control system. For the Ziegler-Nichols model corresponding to the distributed lag, this ratio is

$$L_e/T_e = 0.07 \quad (2.10)$$

Strejc's approximation method applied to the distributed lag system of eqn. 2.6 yields the approximate model of eqn. 2.11.

$$1/(1 + 0.43 T_s)^{1.6} \quad (2.11)$$

In order to check the applicability of this approximation method in case of a distributed lag, the step response of a transfer function of the type

$$1/(1 + T'_s)^{1.5} \quad (2.12)$$

is found and given in eqn. 2.13

$$a_1(t) = \operatorname{erf} \sqrt{\frac{t}{T'}} - \frac{2}{\sqrt{\pi}} \sqrt{\frac{t}{T'}} \exp(-t/T') \quad (2.13)$$

This transfer function is plotted for three values of

*This response corresponds to a point 6.7 cm away from the heating surface of a brick wall ($k=0.0038 \text{ cm}^2/\text{sec}$ for brick⁶).

T'/T ratio in fig. 2.4. In fig. 2.4 curve d corresponds to the actual Chaussard model ($T' = 0.43T$). From fig. 2.5 it is clear that a model with $T' = 0.8T$ is certainly a better approximation to the actual process (curve a) compared to the Chaussard model.

Some of the transfer functions which arise in electroheat process control lead to cumbersome calculations. In these instances the use of approximate models often becomes the only practical way to deal with the system. One such transfer function is given by Svenchanski⁴² and Treizon⁴⁵. This function is found as the transfer function of an electric resistance furnace and is given in eqn. 2.15.

$$\frac{K}{(1 + \sqrt{sT_1})(1 + sT_2) + K} \quad (2.14)$$

This transfer function and its step response were first analysed by Kilomeitseva and Netushil¹².

As an example of the complicated nature of calculations which can arise in the analysis of electroheat control systems we shall investigate the time properties of a simple system. In electric resistance heating the heating element generally possesses a transfer function of the form $1/(1 + sT_1)$. The receiver (walls of the furnace, body of the fluidised bed, etc.) usually exhibits a distributed lag $\exp(-\sqrt{sT_2})$. If the interaction between the heating element and the receiver is negligible then the process transfer function can be written as

$$H(s) = F \frac{\exp(-\sqrt{sT_2})}{1 + sT_1} \quad (2.15)$$

*Since an exponent of 1.6 leads to very long calculations, an exponent of 1.5 is taken.

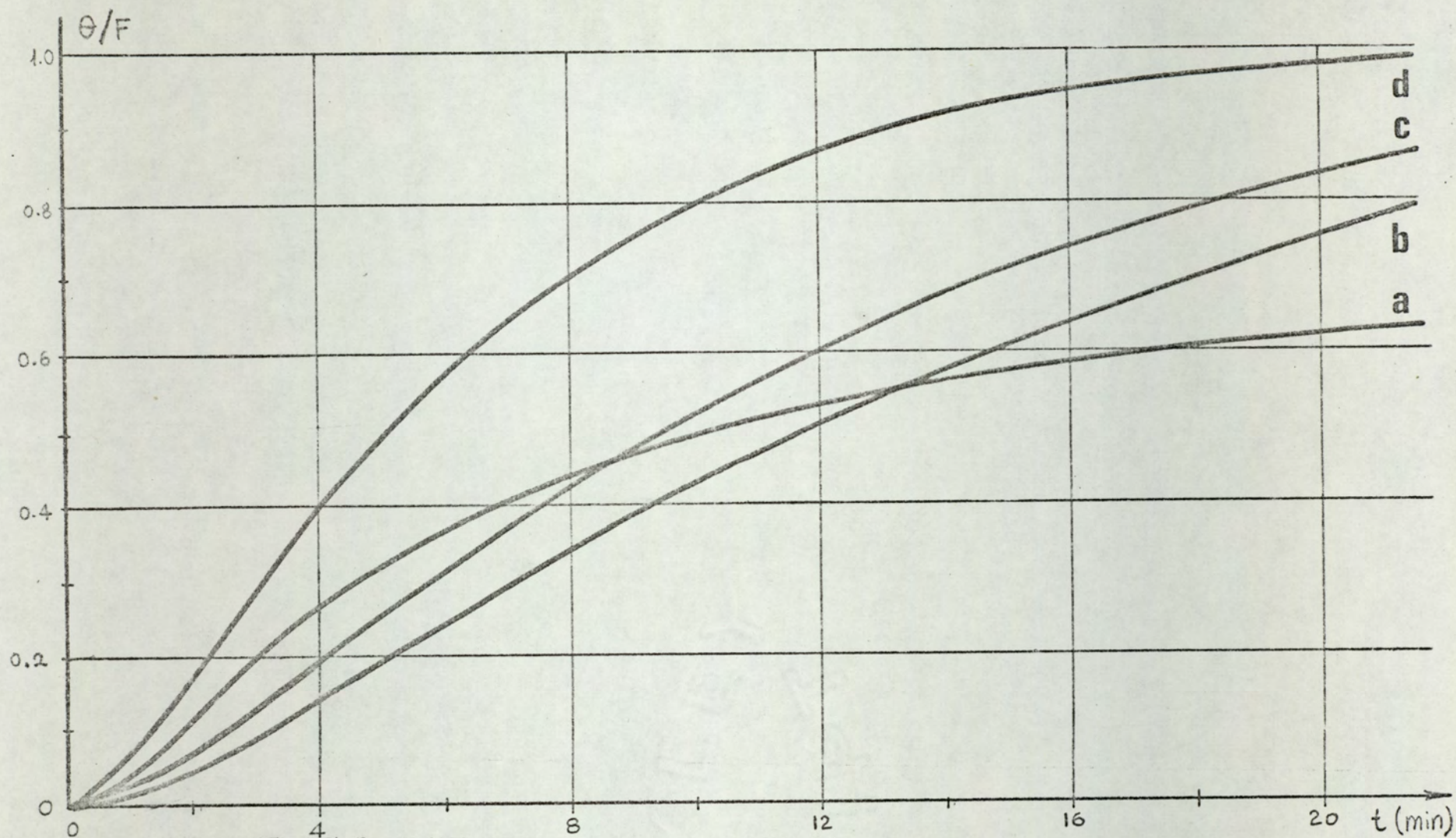


Fig. 2.4

Approximate model of the form $F/(1 + sT')^{1.5}$ of a distributed lag system (comparison of the step response curves.)

- (a) $\exp \sqrt{-sT}$, $T=10$ min. (b) approximate model, $T' = T = 10$ min.
(c) approximate model, $T' = 0.8T = 8$ min. (d) approximate model, $T'=0.43T=4.3$ min. (Chaussard model)

This process is equivalent to the transfer of heat from a heating surface into a semi-infinite solid (fig. 2.2), where the temperature at the surface ($x = 0$) varies exponentially. T_2 corresponds⁶ to d^2/k where d is the distance of temperature measuring point from the surface and k is the diffusivity of the material. T_1 corresponds to the time constant of the exponential change of temperature at the heating surface.

The inverse Laplace transform of $H(s)$ given in eqn. 2.15 is found¹³ to be

$$h(t) = \frac{F}{2T_1} e^{-t/T_1} \left[e^{-j\sqrt{T_2/T_1}} \operatorname{erfc} \left(\frac{1}{2} \sqrt{\frac{T_2}{t}} - j \sqrt{\frac{t}{T_1}} \right) + e^{j\sqrt{T_2/T_1}} \operatorname{erfc} \left(\frac{1}{2} \sqrt{\frac{T_2}{t}} + j \sqrt{\frac{t}{T_1}} \right) \right] \quad (2.16)$$

Although the error functions of complex arguments are very difficult to handle, with the introduction of the function

$$w(z) = \exp(-z^2) \operatorname{erfc}(-jz) \quad (2.17)$$

(which has recently been tabulated) this difficulty can be overcome.

From eqn. 2.17 one can write:

$$\operatorname{erfc}(z) = \exp(-z^2) w(jz) \quad (2.18)$$

or

$$\operatorname{erfc}(x \pm jy) = \exp \left[-(x \pm jy)^2 \right] w(\mp y + jx) \quad (2.19)$$

By using the following property

$$w(z^*) = w^*(-z)$$

where * denotes complex conjugate, one can write

$$\operatorname{erfc}(x + jy) = \exp [-(x + jy)^2] \cdot w^*(y + jx) \quad (2.21a)$$

$$\operatorname{erfc}(x - jy) = \exp [-(x - jy)^2] \cdot w(y + jx) \quad (2.21b)$$

Equation 2.16 can be reduced to eqn. 2.22 by using eqn.

2.21:

$$h(t) = \frac{F}{T_1} \exp(-v^2) \operatorname{Re} [w(u + jv)] \quad (2.22)$$

where $u = \sqrt{t/T_1}$ and $v = 0.5\sqrt{T_2/t}$

Then, by using the tables¹ for $w(u + jv)$, the impulse response of the plant, $h(t)$, is calculated and plotted in fig. 2.5a, for $T_1 = 5$ and $T_2 = 10$ min. By integrating the curve in fig. 2.5a numerically, the step response, $a(t)$ is obtained (fig. 2.5b).

Let $h(t)$ and $a(t)$ denote the impulse and step response of a plant. For the parameters of the Ziegler-Nichols model one can write

$$T_e = \frac{1}{\frac{da(t_i)}{dt}} = \frac{1}{h(t_i)} \quad (2.23a)$$

$$L_e = t_i - \frac{a(t_i)}{h(t_i)} \quad (2.23b)$$

where time t_i corresponds to the maximum of $h(t)$ curve or,

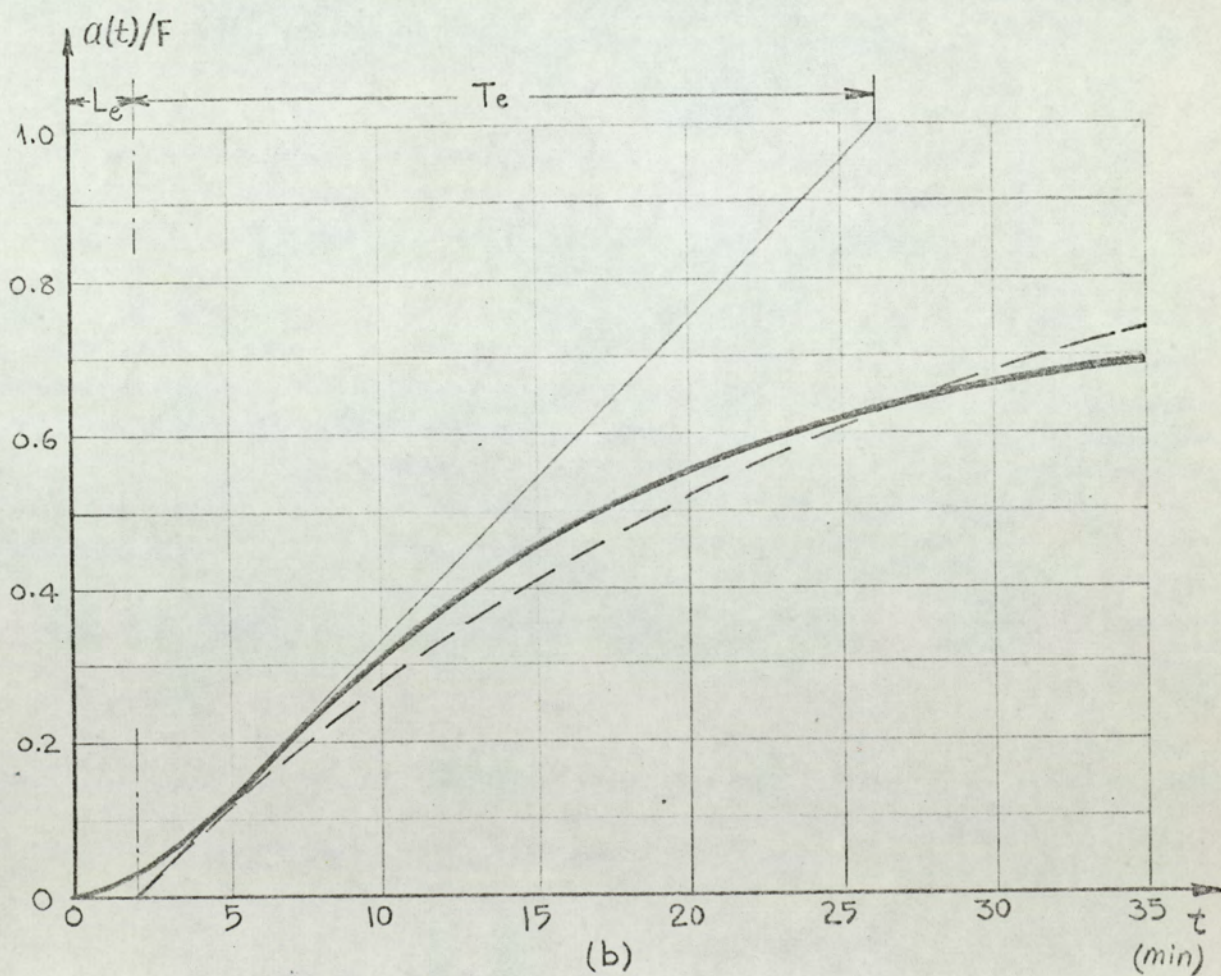
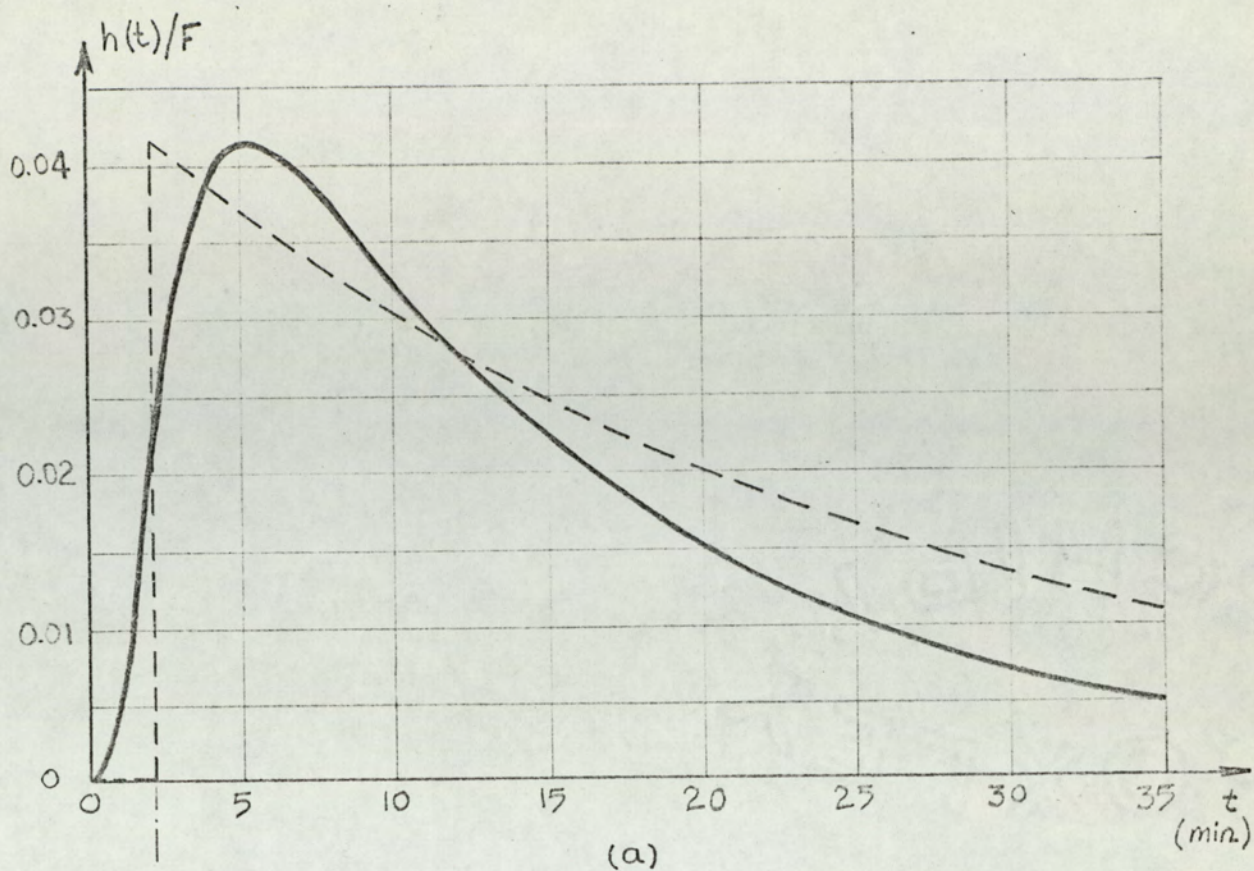


Fig. 2.5

(a) Impulse response of the transfer function given in eqn. 2.15, for $T_1 = 5$ min, $T_2 = 10$ min.

(b) Step response of the same function.

———— actual process; - - - - Ziegler-Nichols equivalent.

equivalently, to the inflection point of $a(t)$ curve.

For the process given in eqn. 2.15 and for the values of $T_1 = 5$ min. and $T_2 = 10$ min., L_e and T_e are found from fig. 2.5.

$$T_e = 24.1 \text{ min} \quad (2.24a)$$

$$L_e = 2.2 \text{ min} \quad (2.24b)$$

The impulse response and the step response of the Ziegler-Nichols model are shown by dotted lines in fig. 2.5. The L_e/T_e ratio for this plant is found to be:

$$L_e/T_e = 0.0915$$

2.5 DISCUSSION

The following comments can be made as a result of the above analysis.

1. Since most of the electroheat processes possess irrational transfer functions, their time domain investigation is rather complicated.
2. For the same reason the behaviour of electroheat control systems is very difficult to analyse exactly.
3. Therefore it is necessary to use approximate models.
4. The Ziegler-Nichols approximate model is used extensively to represent electroheat processes. The main advantages of the Ziegler-Nichols model over other approximations are its simplicity and its inherent property of giving conservative design values.
5. For most electroheat processes Strejc's approximation yields the Ziegler-Nichols model.
6. Chaussard's approximation complicates the calculations

without improving the accuracy of the approximation achieved.

7. The investigation of simple or distributed lags in the s plane is much simpler with this model than for the transfer functions which result from Chaussard's approximation. Therefore, at least for electroheat systems, the practical advantages of the Chaussard method is rather questionable.

8. For process having distributed time lag an L/T ratio of approximately 0.1 can be assumed.

2.6 SUMMARY

In this chapter some approximate models are discussed. The Ziegler-Nichols model is shown to be the most suitable approximation to electroheat processes.

3

ON-OFF CONTROL OF ELECTROHEAT PROCESSES

3.1 INTRODUCTION

In this chapter a general analysis of on-off electroheat systems is given. On-off control methods are widely used to control industrial electroheat processes since these methods often represent the simplest and most economical means of control³⁸. Such control methods are particularly important for resistance and arc furnaces, ovens, plasma torches, boilers, tanks, fluidised beds, space heating, etc.

Fig. 3.1 shows a block diagram representation of a typical on-off controlled process. One should note that this model is valid when changes in the disturbance are slow compared with the equivalent time constant of the plant. This is the case for most industrial electroheat systems³⁸.

3.2 THE ON-OFF CONTROLLER

A typical characteristic of an on-off controller is shown in fig. 3.2. It is well known that almost every on-off controller has the hysteresis effect (memory) shown in fig. 3.2. It will be shown that hysteresis has an adverse effect on the performance characteristics of the control system. For this

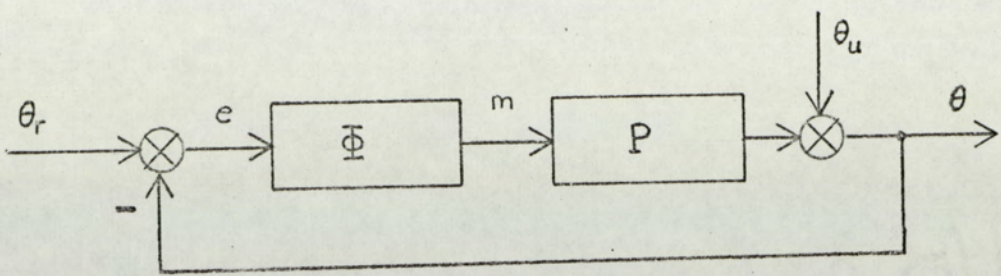


Fig. 3.1

Block diagram for a typical on-off control system

- Φ : controller
- P : plant
- θ_r : command
- θ_u : disturbance
- θ : output temperature

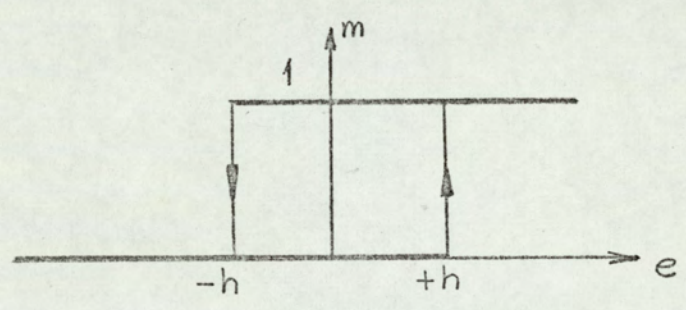


Fig. 3.2

Characteristic of the on-off controller

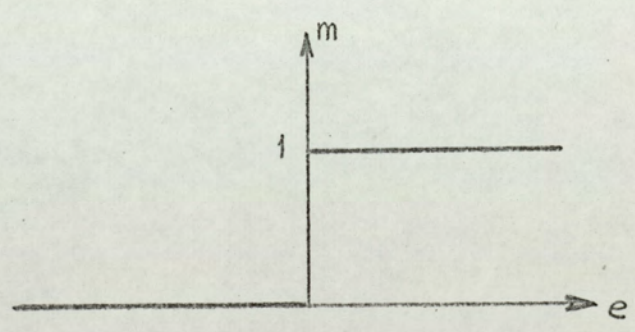


Fig. 3.3

Characteristic of the ideal (memoryless) on-off controller

reason, its reduction, or elimination is generally desirable. Hysteresis can be reduced (or eliminated) by suitable controller designs or by secondary feedback³⁷. Figure 3.3 shows the ideal on-off controller characteristic where hysteresis is not present. This characteristic is represented as:

$$m = \frac{1}{2} [1 + \text{sgn } e] \quad (3.1)$$

where $\text{sgn } e = |e| / e \quad (e \neq 0)$

3.3 ON-OFF CONTROL

In the following analysis, the controller is assumed to have memory, as in fig. 3.2. The plant is taken as a Ziegler-Nichols approximate model⁴⁰, i.e. one with a transit delay and a single pole. Hence the plant transfer function is:

$$P(s) = F \exp(-sL)/(1 + sT) \quad (3.2)$$

where F corresponds to the runaway temperature, $^{\circ}\text{C}$. If the thermal gain of the plant is $G(^{\circ}\text{C}/\text{watt})$, and the power input to the plant is $W(\text{watt})$, then $F = WG$.

The disturbance θ_u is considered to be constant or slowly varying, therefore it can be taken as a reference level, and the controlled temperature θ is the excess temperature over θ_u . The command θ_r is also taken as constant, since for the majority of electroheat systems encountered in practice, θ_r is either constant or programmed to have constant values over fixed time intervals.

The general case, where the plant has the property of mode dependence and the controller is hysteretic, has not been

analysed so far*. A brief analysis for this general case is given below.

The term mode dependence implies that in the active mode (i.e. when heating), the process time constant(s) can assume values significantly different (usually smaller) than their values in the passive mode (i.e. when cooling)^{5,33}. It is usual to express this dependence by writing the time constant as $T(m)$, but this is not justified because, for systems with time lags, the time interval in which $m = 0$ and the cooling period are not the same, one being shifted by L with respect to the other. Actually, the time constant depends on the sign of $\dot{\theta}$, hence we show this dependence by writing** $T = T(\text{sgn } \dot{\theta})$.

The active and passive time constants, T_A and T_p are defined as:

$$T_A = T(\text{sgn } \dot{\theta}) \Big|_{\text{sgn } \dot{\theta} = +1} \quad (3.3.a)$$

$$T_p = T(\text{sgn } \dot{\theta}) \Big|_{\text{sgn } \dot{\theta} = -1} \quad (3.3.b)$$

The dynamic equilibrium cycling (dec) performance of the process is shown in fig. 3.4. The dec curve rises with time constant T_A (from A to B, fig. 3.4) and decays with time constant T_p (from B to C, fig. 3.4).

From fig. 3.4 one can write:

$$\theta_r + h = \theta_{\min} e^{-t_1/T_A} + F (1 - e^{-t_1/T_A}) \quad (3.4)$$

*Roots and Woods³⁸ gave the analysis only for the special case where the controller is ideal.

**It seems that the value of the time constant depends not only on the sign of $\dot{\theta}$, but also on the temperature itself: $T = T(\theta, \text{sgn } \dot{\theta})$. No mention of this kind of dependence is given in the literature.

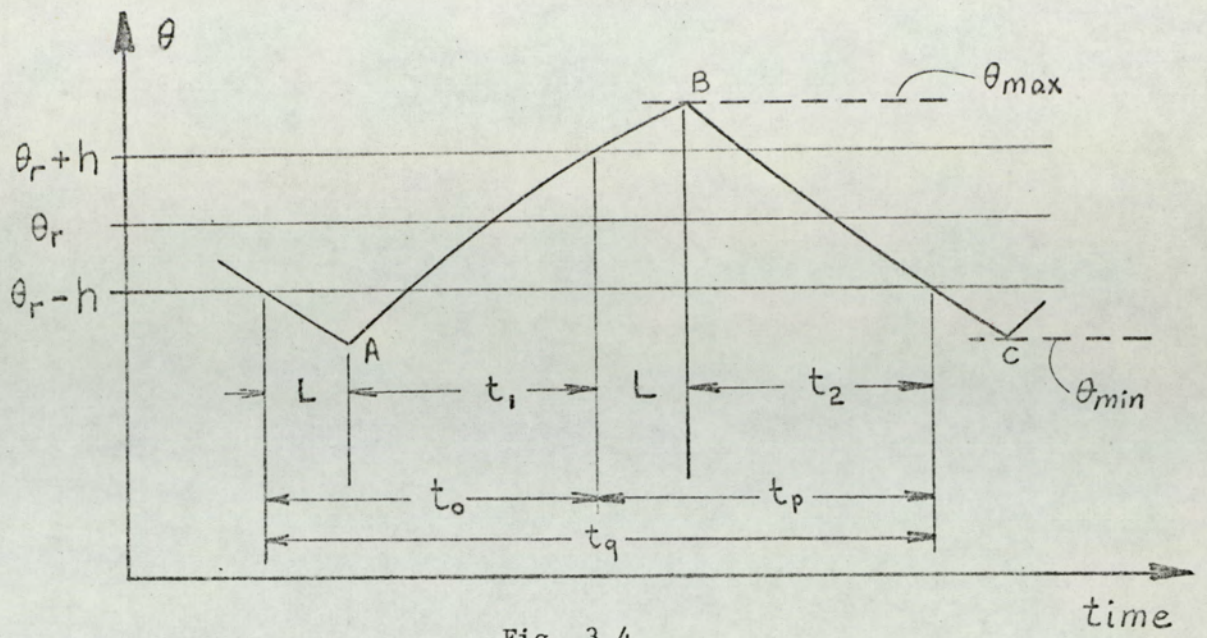


Fig. 3.4

The dec performance of the on-off system

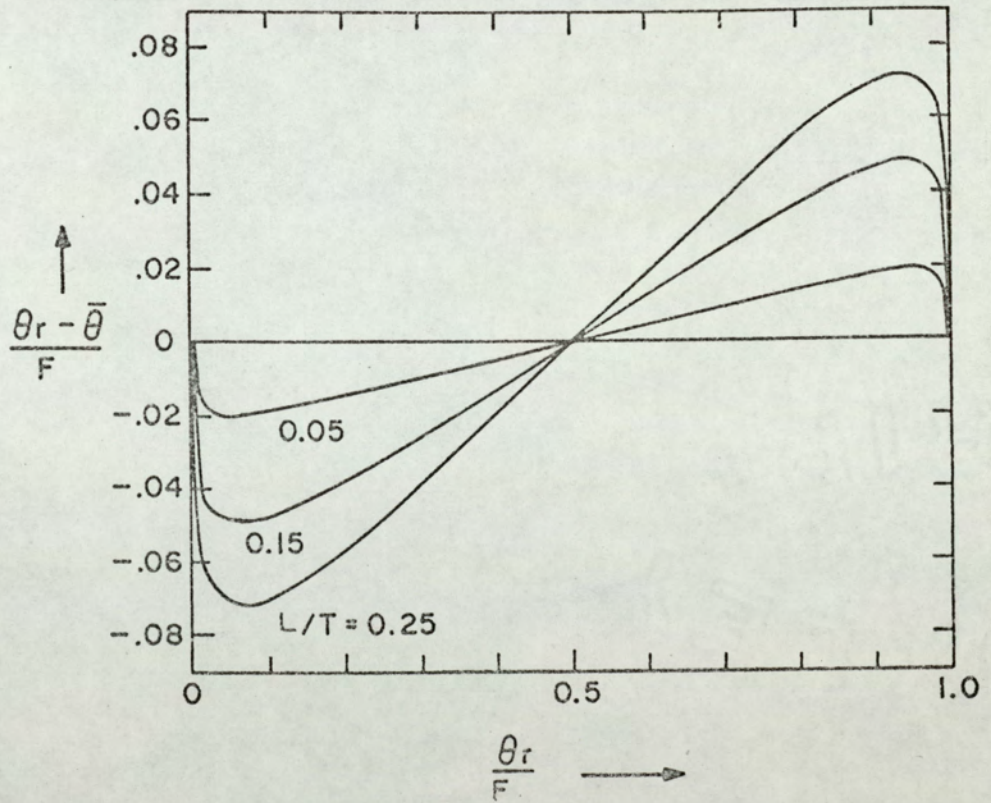


Fig. 3.5

Relative offset as a function of β (θ_r/F) and L/T
(mode independent processes)

$$\theta_{\max} = (\theta_r + h) e^{-L/T_A} + F(1 - e^{-L/T_A}) \quad (3.5)$$

$$\theta_r - h = \theta_{\max} e^{-t_2/T_P} \quad (3.6)$$

$$\theta_{\min} = (\theta_r - h) e^{-L/T_P} \quad (3.7)$$

The most significant dec performance indices are the period, t_q , the amplitude of the dec, θ_d , and the offset, $\theta_r - \bar{\theta}$.

The dec amplitude

The amplitude of dec can be found from eqns. 3.5 and 3.7:

$$\theta_d = \theta_{\max} - \theta_{\min} = F \frac{a(\beta + H) + a(\gamma - 1) - \gamma(\beta - H)}{a\gamma} \quad (3.8)$$

where

$$a = \exp(L/T_P)$$

$$\beta = \theta_r/F$$

$$\gamma = \exp(L/T_A)$$

$$H = h/F$$

For the special case of $T_A = T_P$ (mode independence) θ_d is given by:

$$\theta_d = F(2H + a - 1)/a \quad (3.9)$$

On the other hand, for the special case $h = 0$ (memoryless controller), eqn. 3.8 becomes:

$$\theta_d = F \left[\frac{\beta + \gamma - 1}{\gamma} - \frac{\beta}{a} \right] \quad (3.10)$$

For the case where $a = \gamma$ and $h = 0$:

$$\theta_d = F (a - 1) / a \quad (3.11)$$

If we use the following approximation*:

$$a = \exp (L/T) \approx 1/(1 - L/T), \quad L/T < 0.5 \quad (3.12)$$

equation 3.11 simplifies to:

$$\theta_d \approx F \frac{L}{T} \quad (3.13)$$

The equation given by Tüdös⁴⁷ for the amplitude is eqn. 3.13, which is only an approximate one, whereas the exact value of θ_d is given by eqns. 3.8 - 3.11.

From eqn. 3.9 it is seen that θ_d is strongly affected by the hysteresis. Since one of the control objectives is to decrease the dec amplitude, reduction or elimination of the hysteresis becomes one of the goals of the designer.

From the approximate eqn. 3.13, the effect of L/T ratio on amplitude is evident: the amplitude is directly proportional to L/T. As it is shown in Chapter 2, L/T ratio is in the range of 0.07 - 0.1 for most electroheat processes. If we take L/T = 0.1 then the amplitude is approximately given by

$$\theta_d \approx F (1.81 H + 0.1) \quad (3.14)$$

Equation 3.14 can be used as a rule of thumb for design when $T_A \approx T_P$.

*The approximations used in the text are explained in Appendix B.

The average output temperature $\bar{\theta}$, and offset $\theta_r - \bar{\theta}$

The average value of the output temperature, $\bar{\theta}$, is defined as:

$$\bar{\theta} = \frac{1}{t_q} \int_0^{t_q} \theta(t) dt \quad (3.15)$$

where $\theta(t)$ is the output temperature at dec. An approximate expression for $\bar{\theta}$ can be written as:

$$\bar{\theta} = (\theta_{\max} + \theta_{\min})/2 \quad (3.16)$$

$\bar{\theta}$ values obtained from eqns. 3.15 and 3.16 are approximately equal when the amplitude θ_d is small compared to F , which is the case in all of the electroheat applications.

The average value of output, obtained from eqns. 3.16, 3.5, and 3.7 is:

$$\bar{\theta} = F \frac{\alpha(\gamma - 1) + \beta(\alpha + \gamma) + H(\alpha - \gamma)}{2\alpha\gamma} \quad (3.17)$$

For the mode independent processes ($T_A = T_P$) we have:

$$\bar{\theta} = F(2\beta + \alpha - 1)/2\alpha \quad (3.18)$$

For mode dependent processes with memoryless controller ($T_A \neq T_P$, $h = 0$):

$$\bar{\theta} = F \frac{\alpha(\gamma - 1) + \beta(\alpha + \gamma)}{2\alpha\gamma} \quad (3.19)$$

Since the width of hysteresis extends symmetrically about the origin, $\bar{\theta}$ is not dependent on h for mode independent processes. Hence eqn. 3.18 holds for controllers with or without memory. However, for mode dependent processes $\bar{\theta}$ is dependent on h , as it is seen from eqn. 3.17.

One of the important performance indices is the offset $\theta_r - \bar{\theta}$:

$$\theta_r - \bar{\theta} = \theta_r - F(2\beta + \alpha - 1)/2\alpha \quad (3.20)$$

Equation 3.20 holds for mode independent processes. Relative offset is shown^{34,38} in fig. 3.5 as a function of θ_r/F , and L/T .

If we use the approximation of eqn. 3.12 in eqn. 3.18, the offset is found to be:

$$\theta_r - \bar{\theta} \approx \frac{L}{T} \left(\theta_r - \frac{F}{2} \right) \quad (3.21)$$

The approximation in eqn. 3.21 is given by Tüdös⁴⁷. The exact value of the offset (for $\theta_d \ll F$) is given by eqn. 3.20 for mode independent processes, and can be found from eqn. 3.17 for mode dependent processes.

For most electroheat processes ($L/T \approx 0.1$) one can write:

$$\theta_r - \bar{\theta} \approx 0.1(\theta_r - 0.5 F) \quad (3.22)$$

Equation 3.22 can be used as a first approximation for design, for the case where $T_A \approx T_P$.

Period of dec

From eqns. 3.4 - 3.7, on and off times are found as:

$$t_o = T_A \ln \frac{\gamma(\alpha - \beta + H)}{\alpha(1 - \beta - H)} \quad (3.23)$$

$$t_p = T_P \ln \frac{\alpha(\beta + H + \gamma - 1)}{\gamma(\beta - H)} \quad (3.24)$$

And we have

$$t_q = t_o + t_p \quad (3.25)$$

For the special case of mode independence the on and off times become:

$$t_o = T \ln \left\{ (\alpha - \beta + H) / (1 - \beta - H) \right\} \quad (3.26)$$

$$t_p = T \ln \left\{ (\beta + H + \alpha - 1) / (\beta - H) \right\} \quad (3.27)$$

On the other hand, for the special case of memoryless controller:

$$t_o = T_A \ln \left\{ \gamma(\alpha - \beta) / \alpha(1 - \beta) \right\} \quad (3.28)$$

$$t_p = T_P \ln \left\{ \alpha(\beta + \gamma - 1) / \beta\gamma \right\} \quad (3.29)$$

The period t_q , obtained from eqns. 3.28 and 3.29 is shown³⁴ as a function of $1/\beta$ in fig. 3.6.

For the mode independent process with memoryless controller we have:

$$t_q = T \ln \left\{ 1 - \left[\alpha(\alpha - 1) / \beta(\beta - 1) \right] \right\} \quad (3.30)$$

From eqn. 3.30 an approximate equation for t_q can be found as:

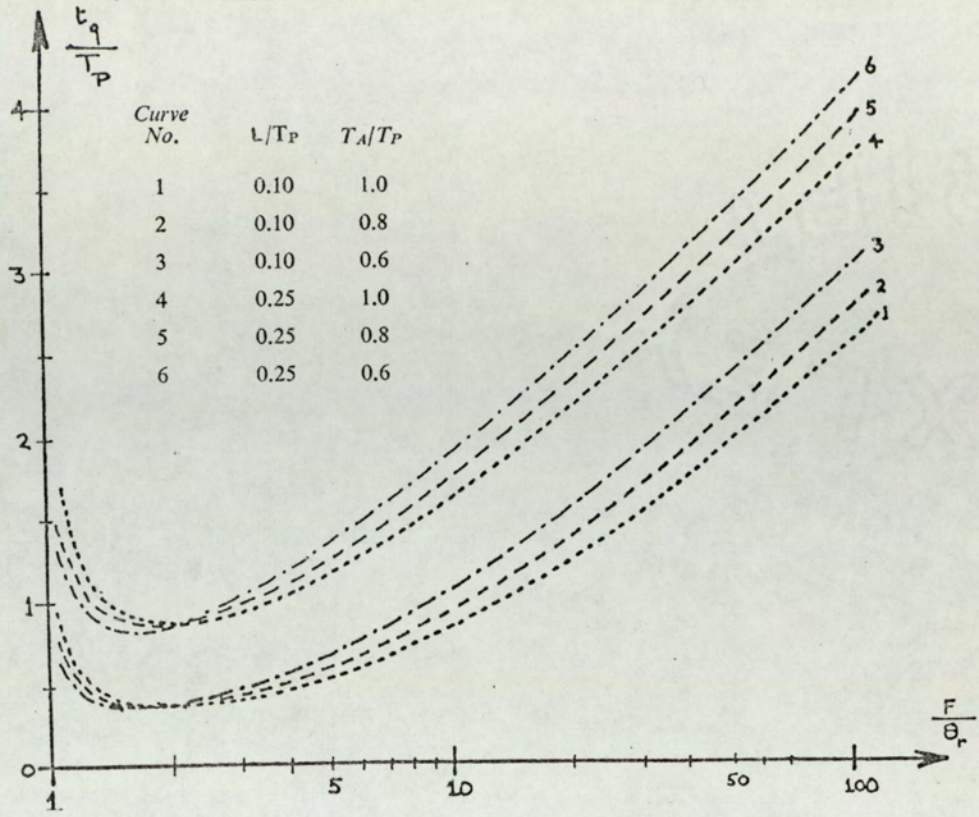


Fig. 3.6

Display of t_q/T_P as a function of F/θ_r in a mode dependent process control system

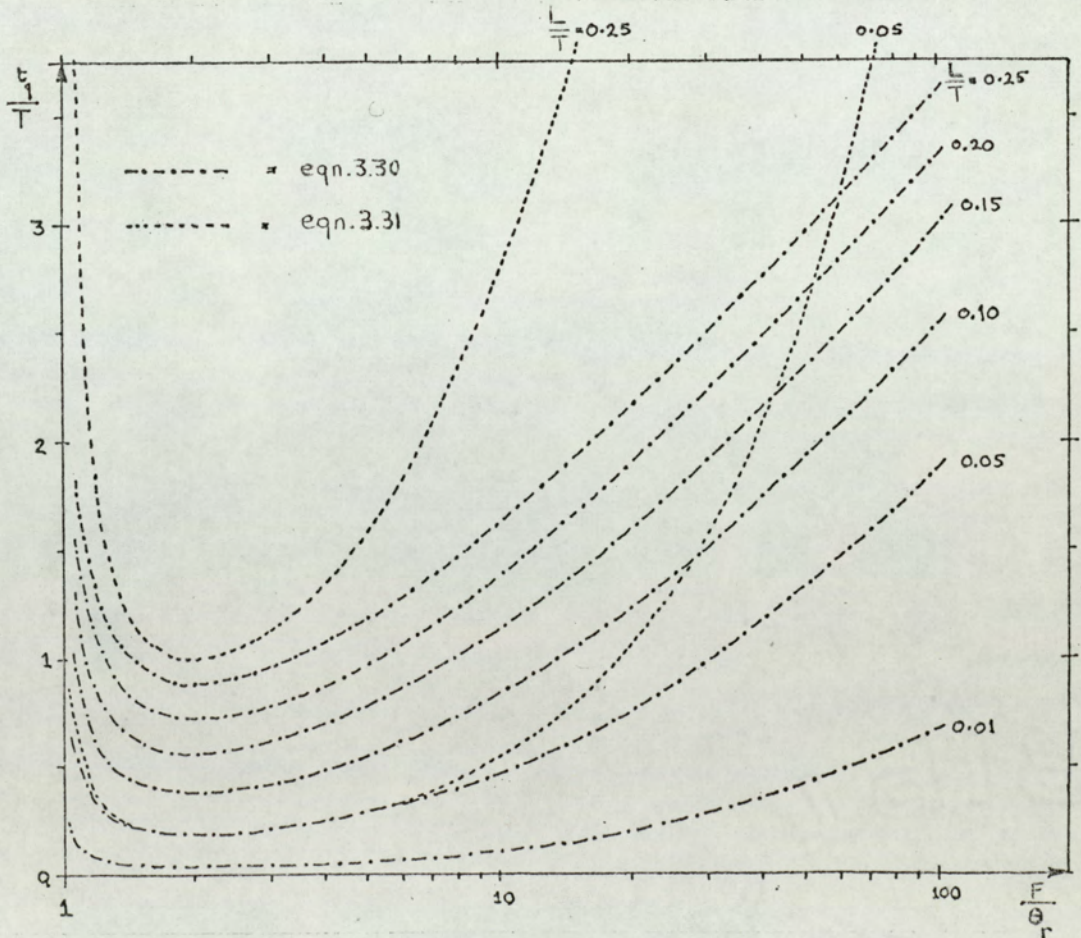


Fig. 3.7

Display of t_q/T as a function of F/θ_r ($H=0$)

$$t_q \approx T \left[\frac{1}{\beta} \cdot (\beta - 1) \right] \quad (3.31)$$

Using the approximations*:

$$\ln x \approx x - 1, \quad 0.8 < x < 1.25 \quad (3.32)$$

$$a = \exp(L/T) \approx 1 + L/T, \quad L/T < 0.4 \quad (3.33)$$

Equations 3.30 and 3.31 are found by Roots and Woods³⁸, and Tüdös⁴⁷ respectively. These equations apply for the special case where $H = 0$. Equations 3.30 and 3.31 are displayed³⁴, in fig. 3.7, where normalized period (t_q/T) is shown as a function of $1/\beta = F/\theta_r$, for varying values of L/T .

Since one of the objectives of the design is to reduce the period³⁸, the minimum value assumed by t_q has a significance. It can be shown that for mode independent processes t_q attains its minimum value for $\beta = 0.5$ (i.e. for $\theta_r = F/2$). When $\beta = 0.5$, on and off times are equal, offset is zero (as shown in fig. 3.5), and period is minimum. The value of this minimum is found to be:

$$t_{qmin} = 2T \ln \frac{a + H - 0.5}{0.5 - H} \quad (3.34)$$

From eqn. 3.34 an approximate equation can be obtained for t_{qmin}

$$t_{qmin} \approx 4T \left[2H + \frac{L}{T} (1 - 2H) \right] \quad (3.35)$$

*The approximations used in the text are explained in appendix B.

For memoryless controller case, t_{qmin} (at $\beta = 0.5$) is found from eqn. 3.34:

$$t_{qmin} = T \ln [1 + 4 \alpha (\alpha - 1)] \quad (3.36)$$

By using eqns. 3.35 and 3.36, the value of the minimum period for memoryless controller can be estimated: Substituting $H = 0$ in eqn. 3.35 or by taking $\alpha \approx 1 + L/T$ in eqn. 3.36 we get:

$$t_{qmin} \approx 4L \quad (3.37)$$

Tüdös⁴⁷ gives approximation in eqn. 3.37 for the minimum period. On the other hand, in Shapiro³⁹ it is asserted that

$$t_q \geq 2L \quad (3.38)$$

However, from the above analysis it is clear that t_q cannot be equal to $2L$.

As a rule of thumb, the following equation can be given for most of the electroheat processes:

$$t_{qmin} \approx 0.36 T \quad (3.39)$$

For mode dependent processes, the minimum of t_q no longer occurs at $\beta = 0.5$, but at a value very near to 0.5. It can be shown that, for $H = 0$, the minimum of t_q occurs at

$$\beta \approx T_P / (T_A + T_P) \quad (3.40)$$

and

$$t_{qmin} \approx 4L \quad (3.41)$$

Start-up time

It can be shown that for a cold start, the time required for the cycling to start is given by:

$$t_w = L + T_A \ln \frac{1}{1 - \beta} \quad (3.42)$$

In fig. 3.8, normalized start-up time, t_w/T_A , is displayed as a function of β ; for $L/T_A = 0.1$ (curve 1), and for $L/T_A = 0.07$ (curve 2).

For comparison, normalised start-up time, t_w/T , for a distributed lag system $\exp(-\sqrt{sT})$ is also shown in fig. 3.8 (curve 3). A comparison of the two curves reveals that when β is larger than 0.4, the start-up time for distributed lag system becomes substantially larger. It is also seen that β values larger than about 0.6 are impractical for distributed lag systems because of very large start-up times.

Choice of β

The choice of β depends mainly on three factors:

1. In terms of offset and cycling period, $\beta = 0.5$ gives optimum results. Since, for $\beta = 0.5$ offset is zero, and cycling period is minimum.
2. In terms of start-up time, lower β values are preferred, as is shown above.
3. In terms of input power, larger β values are preferred. For a given output temperature F increases with decreasing β . Hence, if the available power is limited, larger β values should be chosen. The energy input does not change with β and this is reflected in

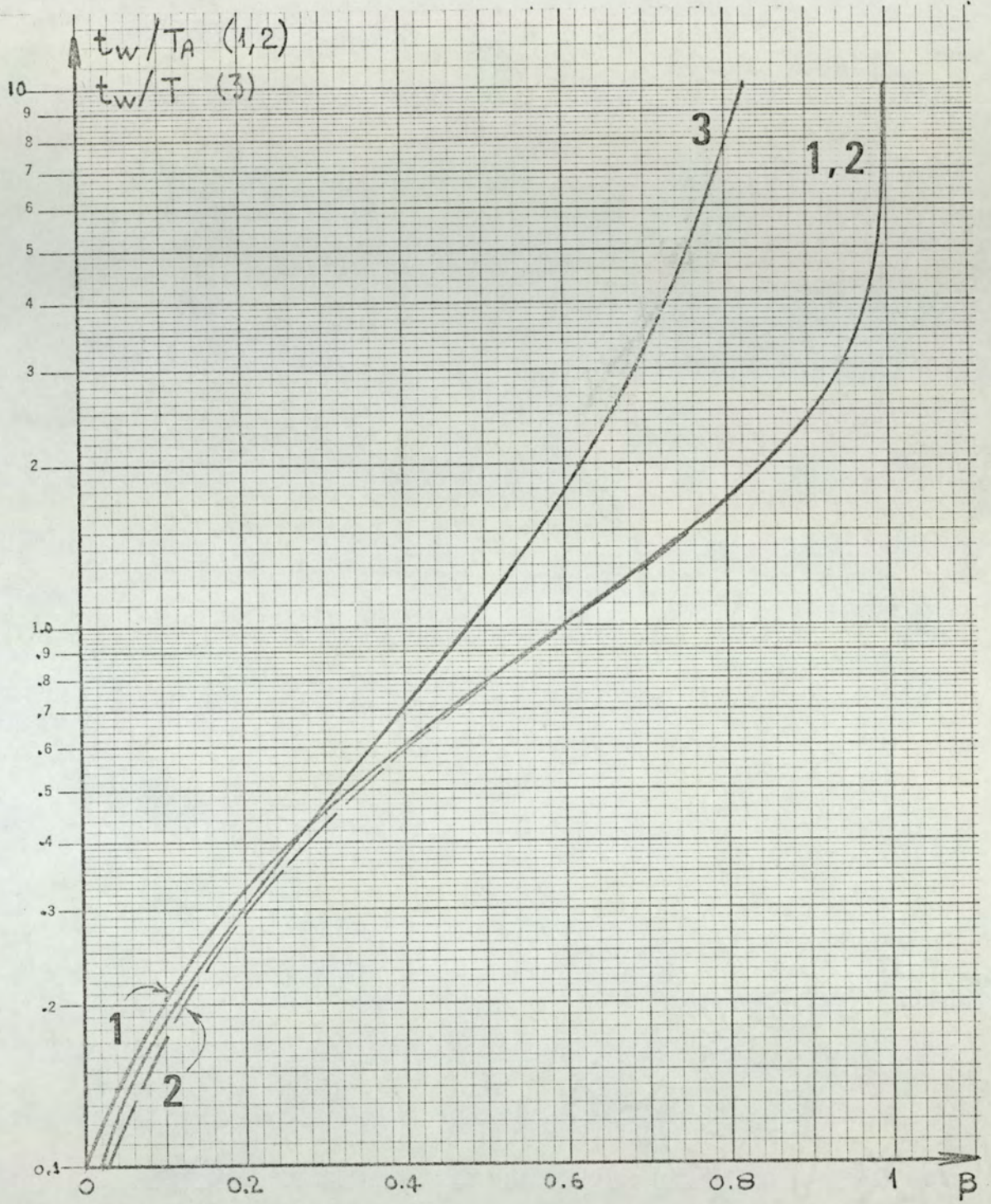


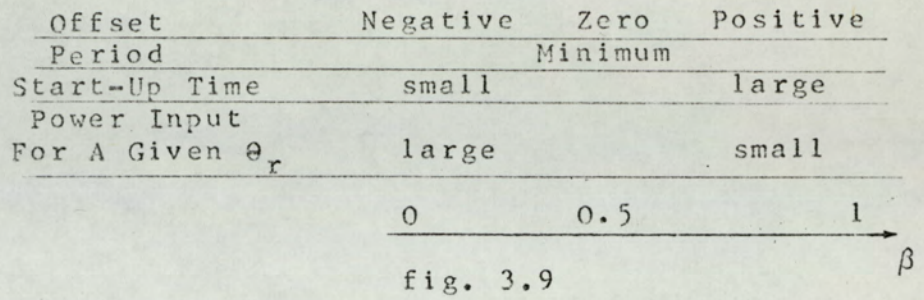
Fig. 3.8

Start-up times for first order and distributed lag systems

- 1 first order system, $L = 0.1 T_A$
- 2 first order system, $L = 0.07 T_A$
- 3 distributed lag, $\exp(-\sqrt{sT})$

the fact that the t_o/t_p ratio becomes larger for smaller β values.

The above comments on the choice of β are summarized in fig. 3.9.



Factors having a role in the choice of β

3.4 ILLUSTRATIVE EXAMPLE

Various electroheat processes possess largely varying time constants and lags. As an example, characteristic values for three different types of furnaces are given below²⁵:

	time constant of Ziegler-Nichols model (sec)	transit delay of Ziegler-Nichols model (sec)	G ($^{\circ}C/W$)
Chamber furnace (oven)	1500 - 3000	10 - 20	0.2 - 2
Muffle furnace	4000 - 1000	200 - 300	~ 1
Tubular furnace	600 - 4000	120 - 200	0.5 - 2

One notes that for the furnaces with covered heating elements L/T ratio is larger. In fact these furnaces exhibit approximately second-order characteristics*²⁶. For a second-order system, the largest value of L/T ratio, where L and T are

*The same is true for thermometers and thermocouples; coated thermometers exhibit second order characteristics

Ziegler-Nichols model parameters, is about 0.10; and it occurs when the two time constants are equal²⁶.

If the process to be controlled is a muffle furnace with $T = 5000$ sec and $L = 300$ sec, with a gain of $1^\circ\text{C}/\text{w}$; and a temperature of $200 \pm 15^\circ\text{C}$ is required, then using the notation given in sec. 3.3, we have:

$$\bar{\theta} = 200^\circ\text{C}$$

$$\theta_d = 30^\circ\text{C}$$

$$a = \exp(L/T) = \exp(0.06) = 1.062$$

$$G = 1^\circ\text{C}/\text{w}$$

If we choose a β value of 0.5:

$$F = 400^\circ\text{C}$$

$$W = F/G = 400 \text{ W}$$

From eqn. 3.9:

$$\theta_d = 400 \frac{2H + 0.062}{1.062} \leq 30$$

or

$$h \leq 0.64^\circ\text{C}$$

With $h = 0.64^\circ\text{C}$ or $H = 0.0016$, we have

$$t_o = t_p = 5000 \ln \frac{1.062 - 0.5 + 0.0016}{1 - 0.5 - 0.0016} = 600 \text{ sec}$$

$$t_q = 1200 \text{ sec.} = 20 \text{ min.}$$

From eqn. 3.42:

$$t_w = 300 + 5000 \ln 2 = 300 + 3465 = 3765 = 62.7 \text{ min.}$$

For this furnace, which has an L/T ratio of 0.06, the minimum cycling amplitude (which can be obtained with an ideal controller) is:

$$\theta_d = 400 \frac{0.062}{1.062} = 23.4^\circ\text{C}$$

Hence the regulated temperature cannot be better than $200 \pm 11.7^\circ\text{C}$. This suggests other types of control (open loop, indirect, or PWM control).

Figure 3.10 shows the digital simulation result for the above example, for $h = 0$ case.

3.5 DIGITAL SIMULATION OF ON-OFF CONTROL SYSTEMS

3.5.1 Method used for simulation

The input to the plant, $m(t)$, can be taken as the sum of unit step functions appropriately shifted in time:

$$m(t) = \sum_{i=0}^n (-1)^i u(t - \lambda_i), \quad \lambda_n < t < \lambda_{n+1} \quad (3.43)$$

where λ_i are switching instants, and $u(t)$ is the unit step function (fig. 3.11)

Then, by superposition, the output temperature is found

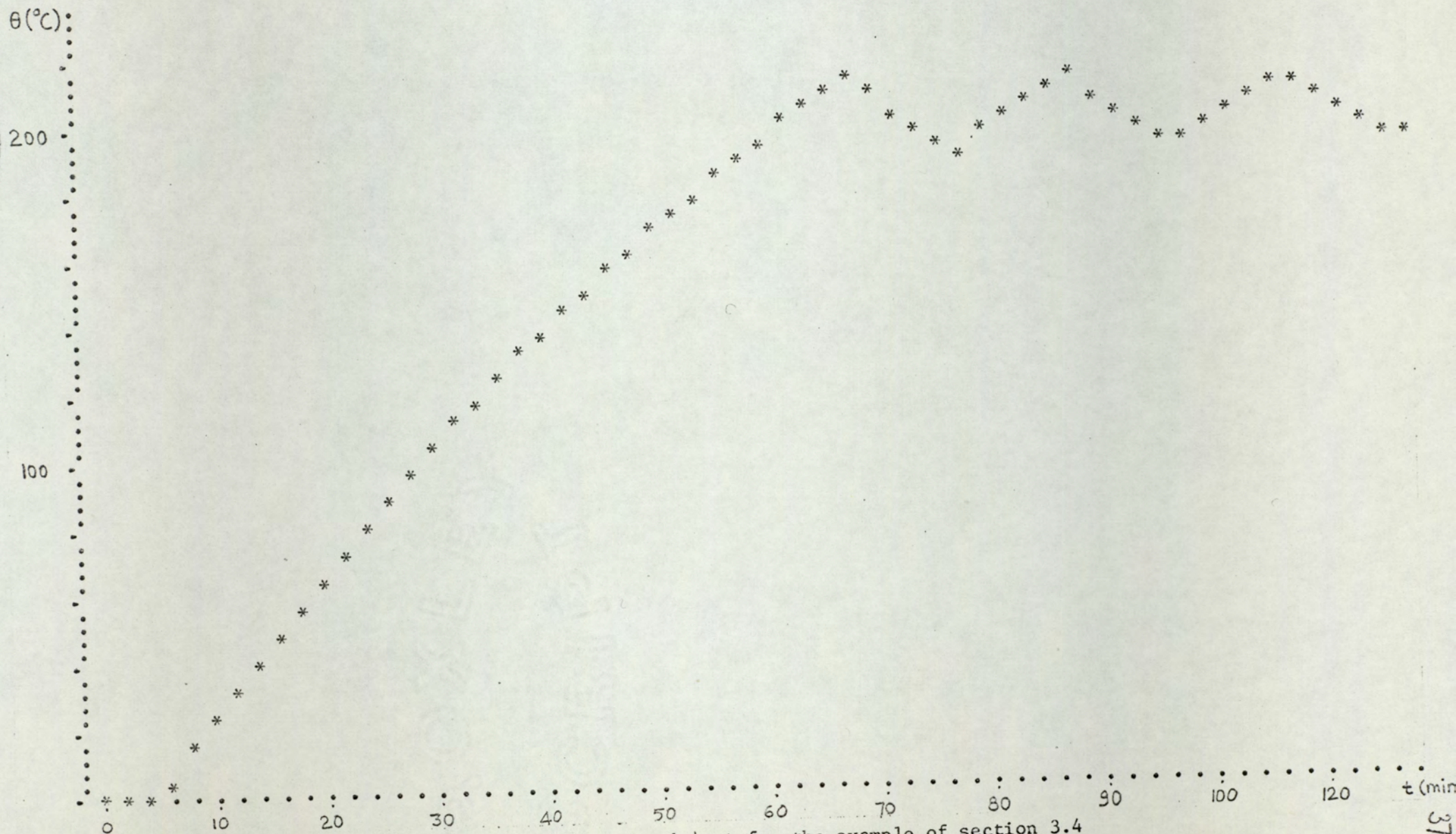


Fig. 3.10 - Digital simulation printout for the example of section 3.4

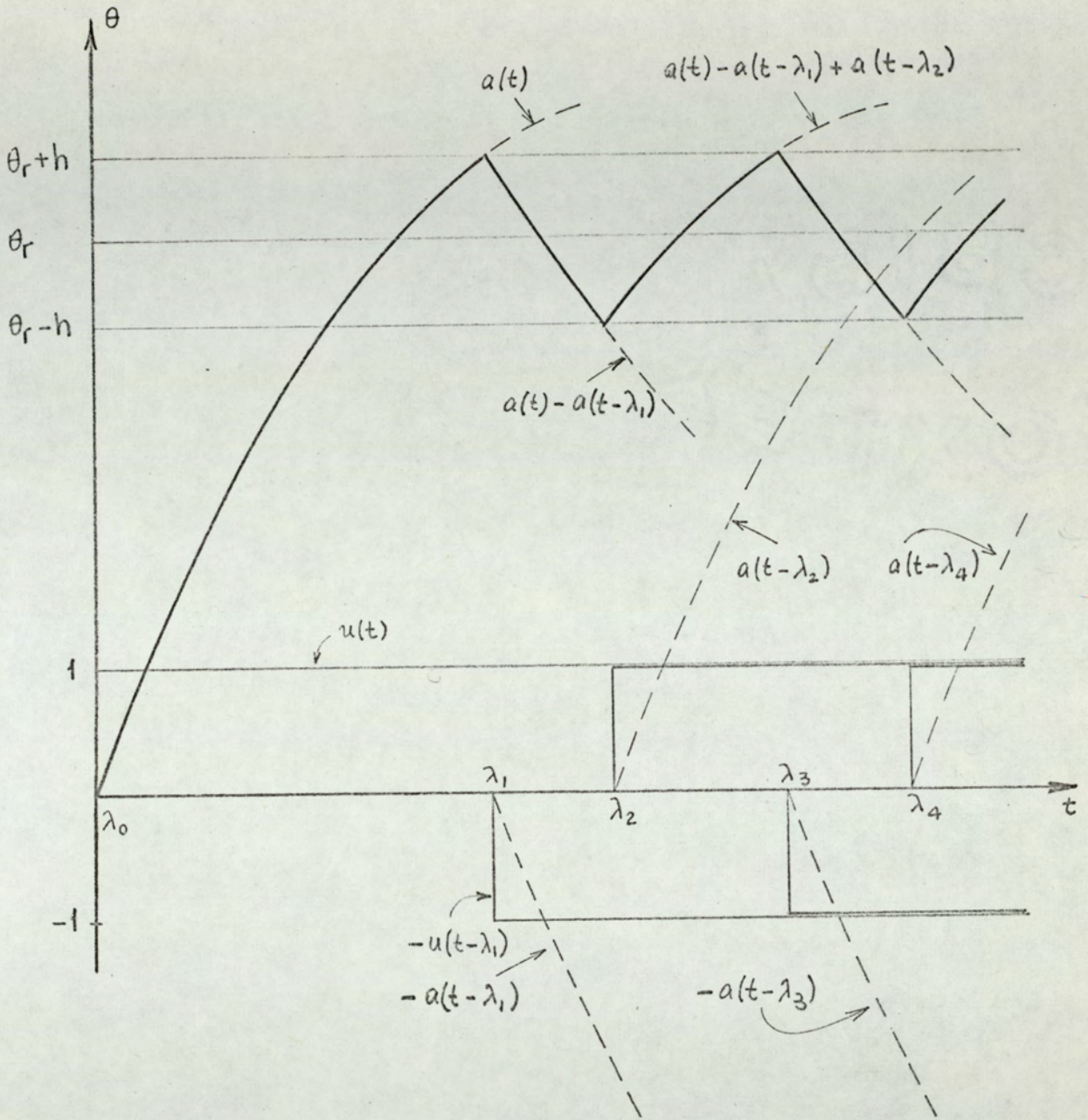


Fig. 3.11

System output for on-off control

to be:

$$\theta(t) = \sum_{i=0}^n (-1)^i a(t - \lambda_i), \quad \lambda_n < t < \lambda_{n+1} \quad (3.44)$$

where $a(t)$ is the step response of the plant.

The problem here is to find the switching instants λ_i . As seen from fig. 3.11, λ_i can be found from:

$$\left. \begin{aligned} \theta(\lambda_i) &= \theta_r(\lambda_i) + h, & i \text{ odd } (\dot{\theta} > 0) \\ \theta(\lambda_i) &= \theta_r(\lambda_i) - h, & i \text{ even } (\dot{\theta} < 0) \end{aligned} \right\} \lambda_{i-1} < t < \lambda_i \quad (3.45)$$

We note that this method is a general one, i.e. it is valid for all types of plant transfer functions, for hysteretic controllers, and for time varying commands. One of the advantages of this method of calculation is that there is no need to carry along the initial conditions for every interval¹⁰.

3.5.2 Simulation programme

The digital simulation programme for the on-off control systems, called ONOFF, is based on the method given in section

3.5.1. This programme has the following features:

1. Possibility of simulation of any type of linear, time invariant plant, provided that the step response of the plant can be expressed analytically (either exactly, or approximately).
2. Possibility of selecting various sampling intervals, command value, and hysteresis width.
3. Possibility of printing or plotting the output temperature and $m(t)$.

4. In order to avoid long printing times which are required when the sampling interval is small, a skipping possibility is included in the programme. For a skipping factor of, say 10, every other tenth value of time/output-temperature pair is printed (or plotted); the intermediate values being internally calculated, but not printed.

The programme ONOFF requires two subprogrammes;

1. Subroutine SPLOT4
2. A function subprogramme from STEP series.

Subroutine SPLOT4 is the printing-plotting subprogramme. Subprogrammes STEP define the step response of the plant. The following STEP subprogrammes are used:

1. STEP 1 - step response of a first order plant with or without time lag
2. STEP 2 - step response of a second order plant
3. STEP 3 - step response of distributed lag $\exp(-\sqrt{sT})$.

This subprogramme requires another subprogramme, SUBERF, which calculates the error function of real arguments. This calculation is based on a polynomial approximation.

All the above programmes are given in appendix A, along with the relevant information about them.

3.5.3 Simulation results

Some results obtained from the digital simulation programme ONOFF will be given in this subsection.

First order system with lag

In fig. 3.10, output temperature of the system given in the example of section 2.4 is given. The parameters of the system are:

$$\begin{aligned}
 F &= 400^{\circ}\text{C} & T &= 83.3 \text{ min} & h &= 0 \\
 \theta_r &= 200^{\circ}\text{C} & L &= 5 \text{ min}
 \end{aligned}$$

The maximum, minimum, and average values of the output temperature, found from eqns 3.5, 3.7 and 3.16 are

$$\begin{aligned}
 \theta_{\max} &= 211.6^{\circ}\text{C} \\
 \theta_{\min} &= 188.4^{\circ}\text{C} \\
 \bar{\theta} &= 200.0^{\circ}\text{C}
 \end{aligned}$$

The start-up time t_w , and the period t_q were found in sect. 3.4 as:

$$\begin{aligned}
 t_w &= 62.7 \text{ min} \\
 t_q &= 20 \text{ min}
 \end{aligned}$$

From fig. 3.10, the corresponding values are seen to be:

$$\begin{aligned}
 \theta_{\max} &= 212^{\circ}\text{C} \\
 \theta_{\min} &= 188^{\circ}\text{C} \\
 \bar{\theta} &= 200^{\circ}\text{C} \\
 t_w &= 60 \text{ min} \\
 t_q &= 20 \text{ min}
 \end{aligned}$$

Therefore, we conclude that the simulation results confirm the analysis presented in 3.3.

Distributed lag systems and their equivalent first order models.

The on-off control of a distributed lag system with transfer function

$$100 \exp(-\sqrt{200} s)$$

and its equivalent first order system

$$100 \exp(-15 s)/(1 + 216 s)$$

are simulated for a command of $\theta_r = 50^\circ\text{C}$ and the printouts are shown in figs. 3.12, 3.13, 3.14, and 3.15.

Fig. 3.12 shows the output temperature of first order system, controlled by the ideal controller, fig. 3.13 shows the output temperature of the distributed lag under the same conditions. Whereas fig. 3.14 and 3.15 are outputs of the first order system and the distributed lag system, controlled by a controller with $h = 10^\circ\text{C}$.

The results are summarised in table 3.1.

figure	plant	h $^\circ\text{C}$	θ_{\max} $^\circ\text{C}$	θ_{\min} $^\circ\text{C}$	$\bar{\theta}$ $^\circ\text{C}$	t_q min	t_w min
3.12	first order	0	54	46	50	60	170
3.13	dist. lag	0	52	46	49	70	210
3.14	first order	10	62	38	50	225	170
3.15	dist. lag	10	60	38	49	235	210

Table 3.1

The following comments can be made on the results summarised in table 3.1.

1. For the first order plant with $h = 0$, equations 3.5, 3.7 and 3.30 gives $\theta_{\max} = 53.4^\circ\text{C}$ and $\theta_{\min} = 46.6^\circ\text{C}$, $t_q = 58.5$ min; and curve 2 of fig. 3.8 gives $t_w = 165$ min, hence calculated and simulated results are very close.

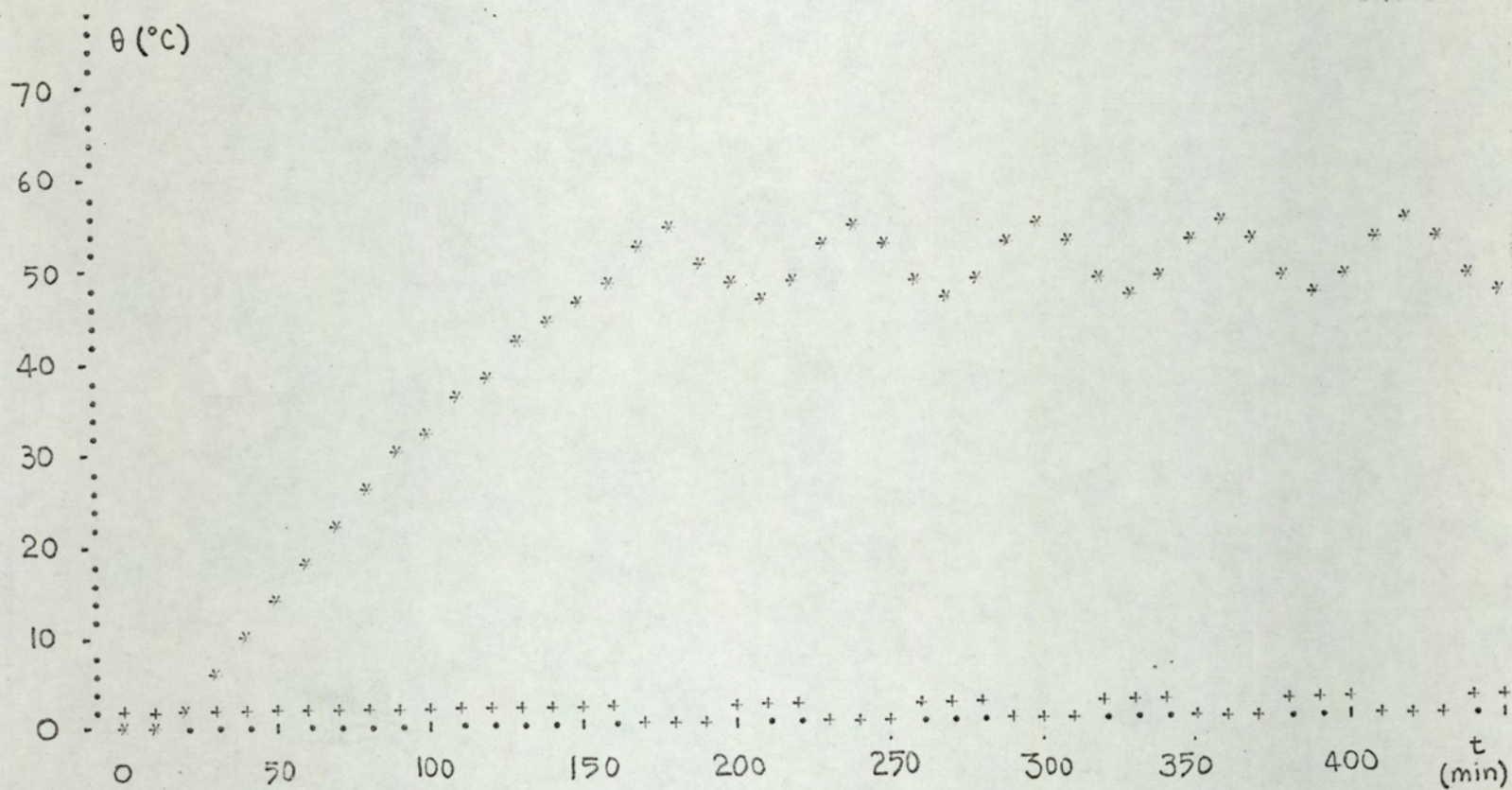


Fig. 3.12

Computer plot of the output temperature (*) and m (+) for a first order system. The parameters of the system are: $F = 100^{\circ}\text{C}$, $T = 216 \text{ min}$, $L = 15 \text{ min}$, $h = 0$, $\theta_r = 50^{\circ}\text{C}$.

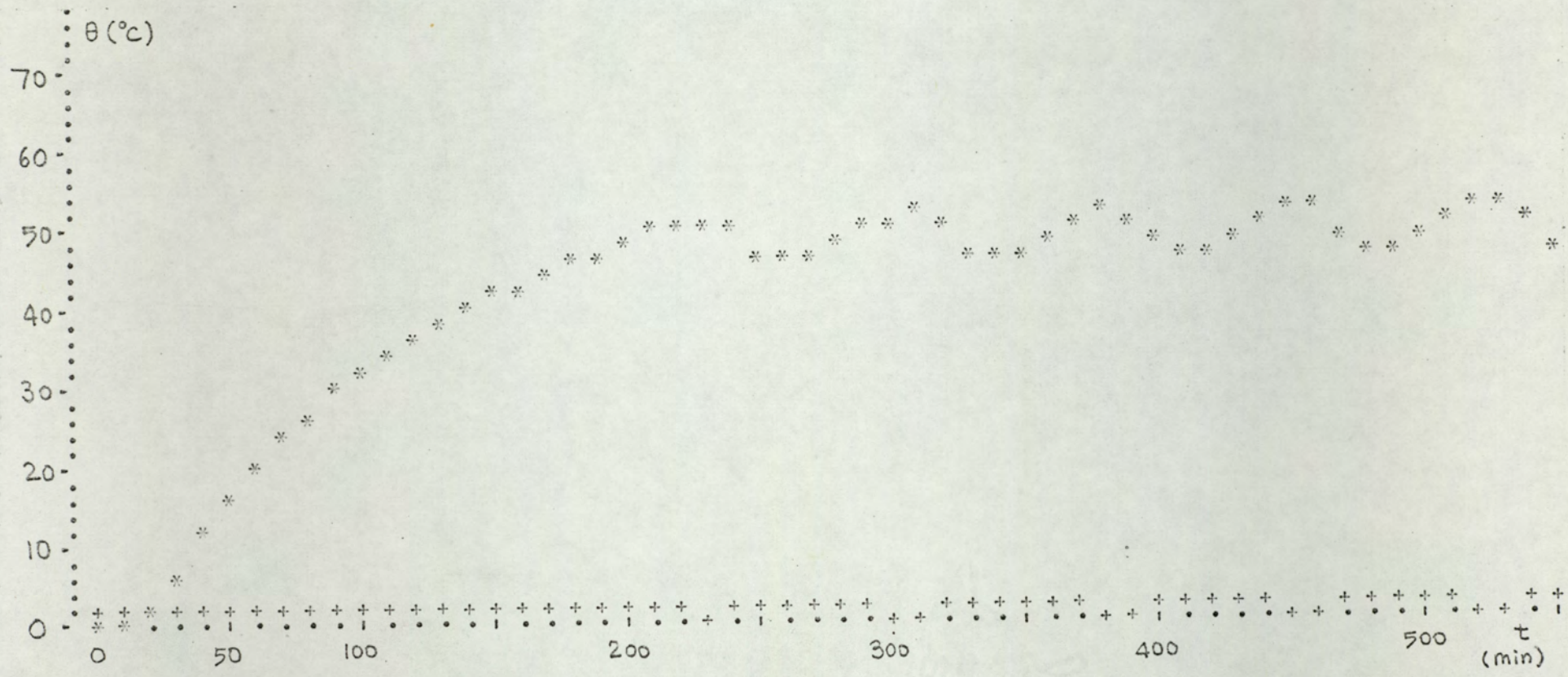


Fig. 3.13

Computer plot of the output temperature (*) and m (+) for the distributed lag system $[100 \exp(-\sqrt{sT})]$, where $T = 200$ min., $\theta_r = 50^\circ$ C, $h = 0$. This figure is to be compared with fig. 3.12.

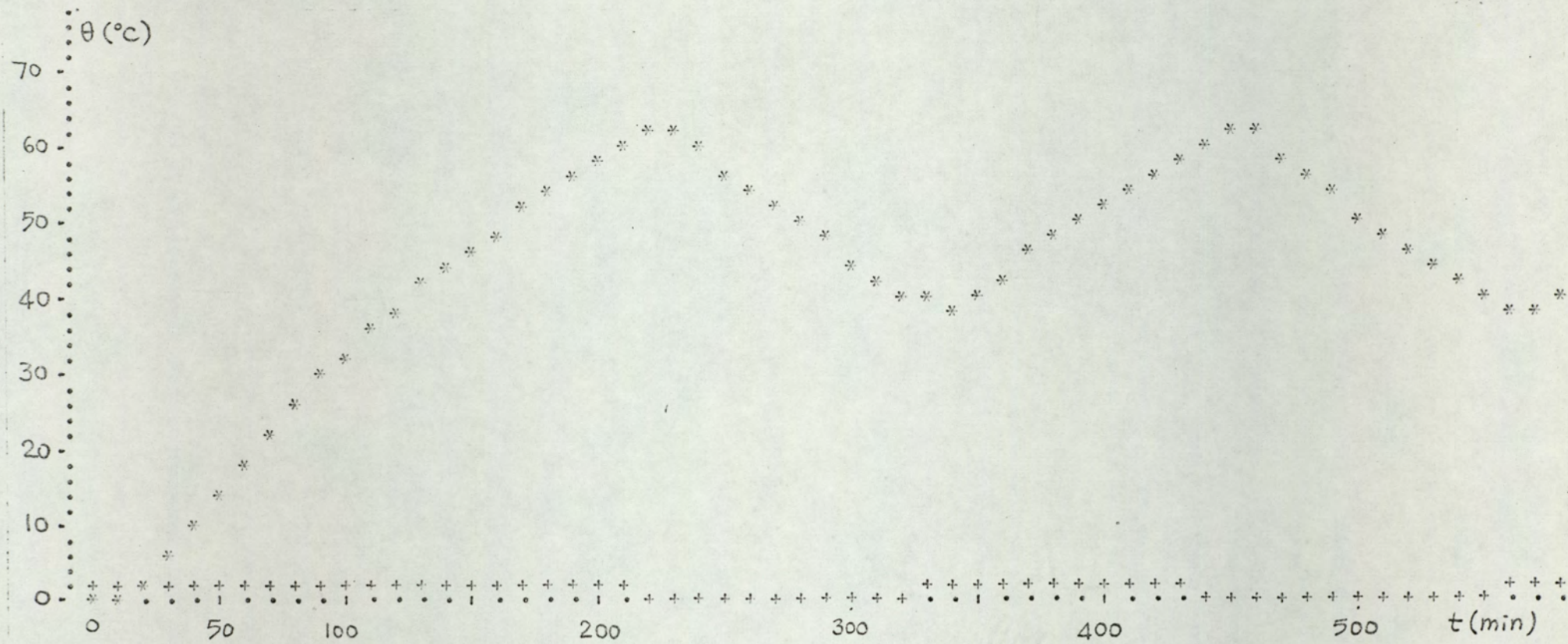


Fig. 3.14

Computer plot of the output temperature (*) and $m(t)$ for a first order system with hysteresis. The parameters of the system are: $F = 100^{\circ}\text{C}$, $T = 216\text{ min}$, $L = 15\text{ min}$, $h = 10^{\circ}\text{C}$, $\theta_r = 50^{\circ}\text{C}$.

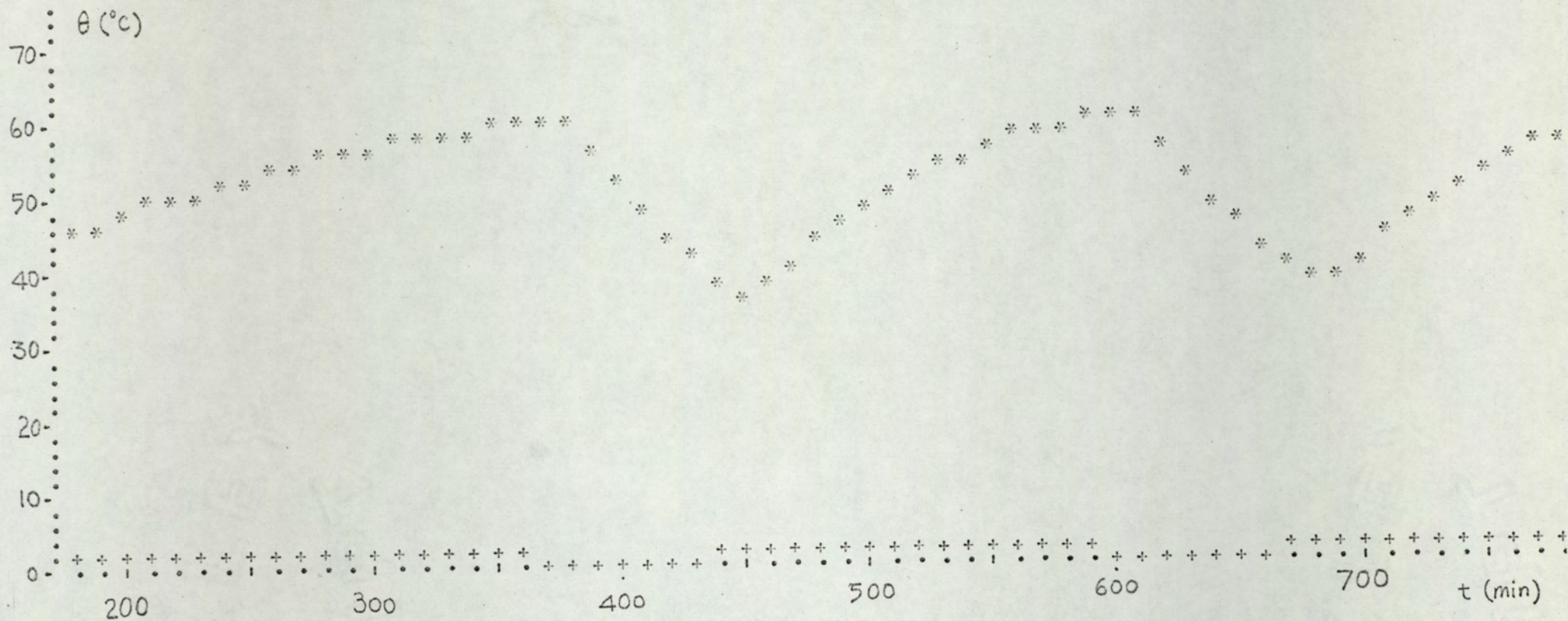


Fig. 3.15

Computer plot of the output temperature (*) and m (+) for the distributed lag system $[100 \exp(-\sqrt{sT})]$ with hysteresis. The system parameters are: $T = 200$ min, $\theta_r = 50^{\circ}\text{C}$, $h = 10^{\circ}\text{C}$. This figure is to be compared with fig. 3.14.

2. For the distributed lag with $h = 0$, curve 3 of fig. 3.8 gives $t_w = 220$ min, whereas simulation gives 210 min.
3. Comparison of figs. 3.12 and 3.13 shows that apart from the difference in start-up times, the first order model as given in eqn. 2.9 represents a close approximation to the distributed lag. As stated in 3.3, the difference in start-up times becomes negligible for $\beta < 0.4$ and large for $\beta > 0.6$ (fig. 3.8)
4. Note that, for the distributed lag system, the output temperature takes very long time to reach its steady state, because of the nature of error function. The period of dec will decrease and temperatures will increase slightly when the system reaches its steady state. This explains the differences in $\bar{\theta}$ and t_q as shown in fig. 3.12 and fig. 3.13.
5. For the first order plant with $h = 10^\circ\text{C}$, equations 3.5, 3.7, 3.26 and 3.27 gives:

$$\theta_{\max} = 62.7^\circ\text{C}, \quad \theta_{\min} = 37.3^\circ\text{C}, \quad t_q = 224 \text{ min.}$$

These values are very close to those found by simulation (3rd line, table 3.1).

6. Comparison of figs. 3.14 and 3.15 again shows the validity of the approximate model, this time for on-off control with hysteretic controller. The difference in start-up times is the same as it is for ideal controller case.

Varying commands

It is not possible to include time varying commands in the programme ONOFF; because ONOFF, with its subprogrammes,

worked on the verge of the memory capabilities of the computer used (PDP 9 with 8K memory). For this reason another computer programme was written, whose listing is not included in this investigation, for varying commands. One of the printouts of this programme is displayed in fig. 3.16. The parameters for the control system are:

$$F = 100^{\circ}\text{C}, \quad L/T = 0.1, \quad H = 0$$

$$\theta_r = 25 + 7.5 \sin (t/T) ^{\circ}\text{C}$$

Since the period of the command is about twelve times greater than the period of dec, the analysis of sec. 3.3 must still be valid. From fig. 3.16 it is seen that this is the case.

3.5.4 Discussion

Since digital simulation, by its nature, works on sampling principle, a systematic error is introduced in simulation. When the step length, Δt , is not very small compared with the time constant involved, the determination of switching instants (λ_i) becomes somewhat erroneous. If we denote the actual value of the i -th switching instant by λ_i , computer determines this instant as λ_i^* , where

$$\lambda_i^* = (k + 1) \Delta t \quad (3.46)$$

where k is such that

$$\theta(k \Delta t) < \theta_r \pm h < \theta \{(k + 1) \Delta t\}$$

whereas the actual value of λ_i is given by

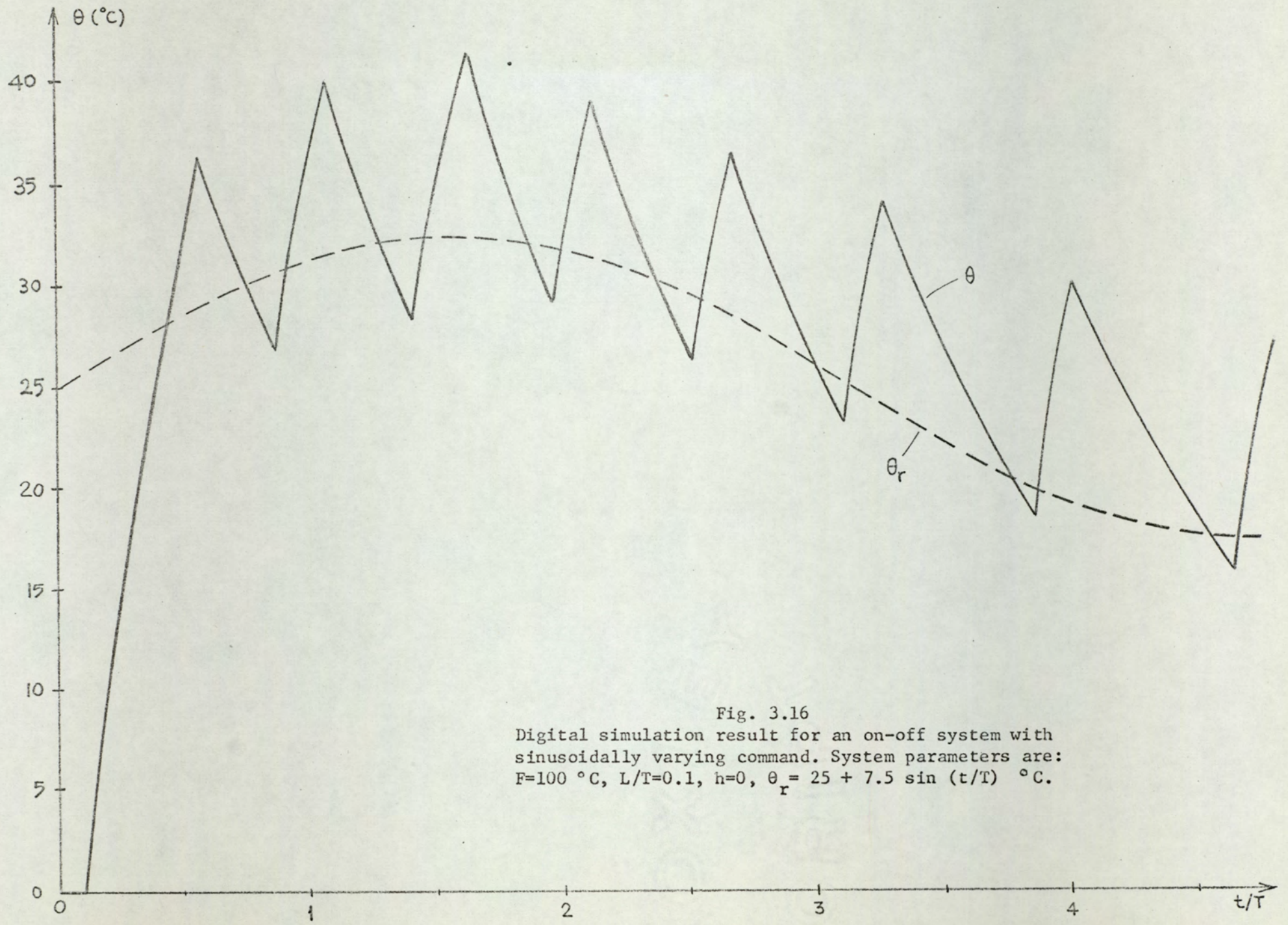


Fig. 3.16
 Digital simulation result for an on-off system with sinusoidally varying command. System parameters are: $F=100$ °C, $L/T=0.1$, $h=0$, $\theta_r = 25 + 7.5 \sin (t/T)$ °C.

$$\theta(\lambda_i) = \theta_r \pm h$$

(3.47)

The plus and minus signs in eqns 3.46 and 3.47 correspond to odd and even values of i , respectively.

The following four strategies suggest themselves as a remedy for these kinds of errors:

1. Choice of small values for Δt

By choosing small values for step-length better simulation is obtained up to a point. For very small values of Δt , another kind of error, the roundoff error attains importance and tends to impair the accuracy of calculation. Roundoff errors arise from the limited precision with which arithmetic operations are carried out in the computer⁴. There is also the problem of computing time, which becomes very large with very small values of Δt . Therefore, there is an optimum range of values for Δt . In fig. 3.17 the results obtained by simulation, by using three different values of Δt , are shown. The parameters of the system are:

$$F = 100^{\circ}\text{C}, \quad \theta_r = 25^{\circ}\text{C}, \quad T = 1 \text{ min}, \quad L = 0.1 \text{ min},$$

$$h = 0$$

The values of the step-length, Δt , and the skipping ratio, JJ, are as follows:

curve no.	Δt	JJ
1	0.050 min	1
2	0.005 min	10
3	0.001 min	50

Curve 1 is wrong, due to the errors in determination of

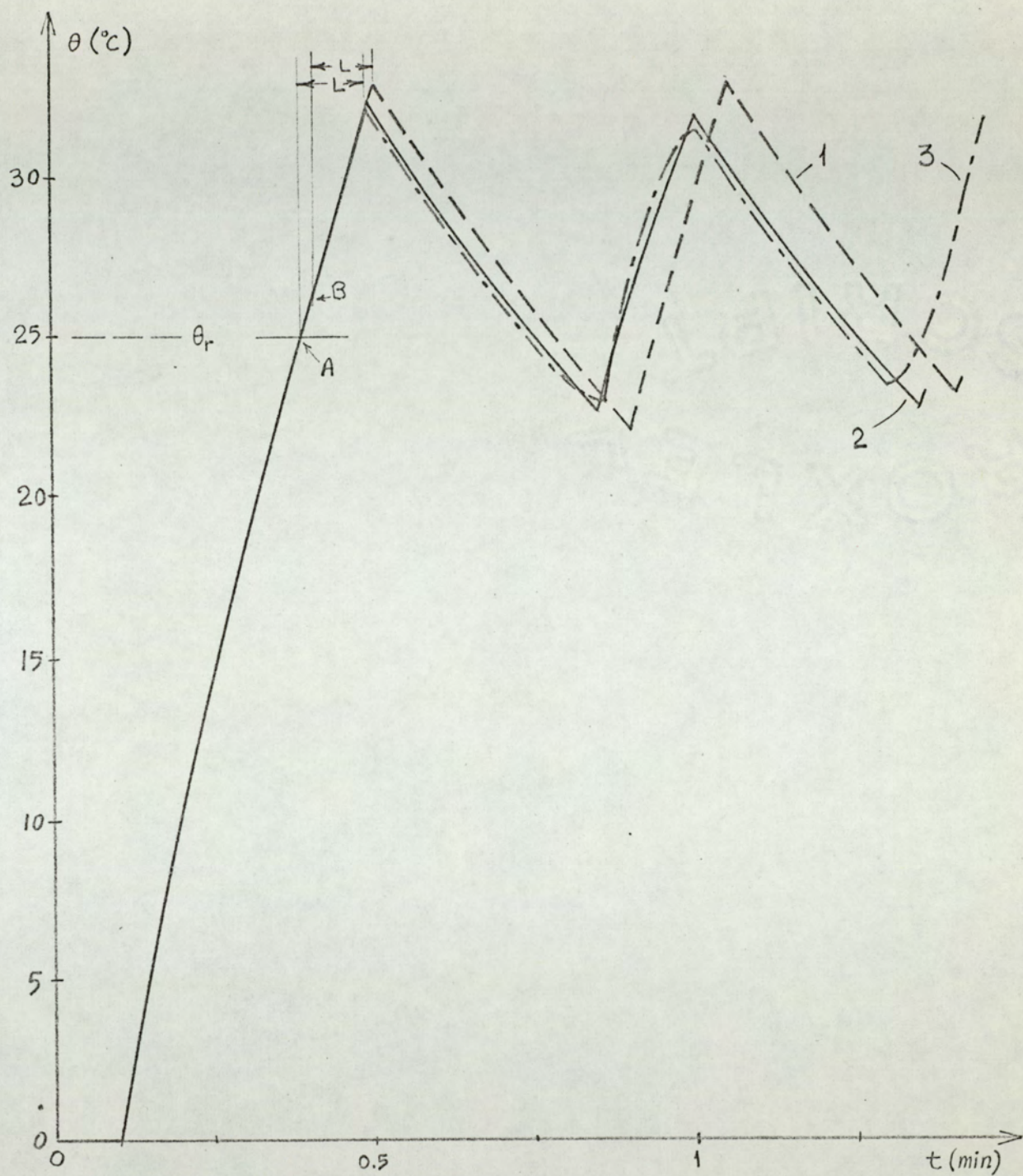


Fig. 3.17

The effect of step length on the accuracy of the calculation
 $F = 100^\circ \text{C}$, $\theta_r = 25^\circ \text{C}$, $T = 1 \text{ min}$, $L = 0.1 \text{ min}$, $h = 0$

curve 1 : $\Delta t = 0.050 \text{ min}$
 curve 2 : $\Delta t = 0.005 \text{ min}$
 curve 3 : $\Delta t = 0.001 \text{ min}$

the crossing points, λ_1 . For example, the simulation programme takes point B (the first sampling instant after the actual crossing point) as λ , whereas actual λ corresponds to point A. On the other hand, curve 3 shows the effect of round-off errors. For practical applications curve 2 is the best of the three, and corresponds to an optimum value of the step length.

2. The use of double precision arithmetic

Another remedy would be the use of double precision arithmetic throughout or in some parts of the programme, in addition to using small step lengths. The double precision version of the programmes ONOFF and STEP can be obtained very easily from the standard ones given in appendix A. Clearly, the double precision programmes will require more memory space.

3. The use of variable step lengths

Another possible scheme is to use variable step lengths. When the output temperature is not close to the command value (i.e. when the error is large) Δt is chosen large. When the error becomes smaller, Δt is decreased, so that more frequent sampling is performed. In this way it is possible to avoid the piling of the roundoff errors and to find the switching instances more accurately since Δt becomes small when the temperature approaches a crossing point. A variable step-length programme, VARDEL has been written and run, for which the step length is calculated by the computer as:

$$\Delta t = 0.475 \left| F - \theta_r \right| + 0.005, \quad \left| F - \theta_r \right| < 0.2$$

$$\Delta t = 0.1, \quad \left| F - \theta_r \right| \geq 0.2$$

The results, which are not included in this investigation show a considerable increase in the accuracy of calculation.

Another approach is the use of an iterative algorithm to calculate the crossing points. In this case there is no need to choose the step length very small. In this method, as the temperature approaches the command value, the actual intersection of the output curve and the command curve is found by an iterative root solving algorithm. The exact switching instant λ_i found by root solving is taken as a sampling instant, and next sampling times continue to be:

$$\lambda_i + \Delta t, \quad \lambda_i + 2 \Delta t, \quad \lambda_i + 3 \Delta t, \dots$$

until the next switching instant. One simple algorithm which can be used is the Newton-Raphson iteration method. In this method, due to the continuous correction in sampling instants, teletype plotting of the output temperature becomes impossible. However, this method seems to be the best solution to overcome the systematic and/or roundoff errors in the simulation.

3.6 SUMMARY

In this chapter an analysis of on-off electroheat control systems is presented. In sec. 3.2 the characteristics of on-off controllers are described. In sec. 3.3 an analytical investigation of on-off systems is given. The general case, where a mode dependent plant with time-lag which is controlled by a controller with memory is analysed. The displays which are intended to be used for the design of on-off control systems are included. In sec. 3.4 numerical examples to illustrate the use of the material presented in sec. 3.3 are given. In sec. 3.5 digital simulation methods of on-off systems are discussed. A digital computer programme to simulate on-off

control systems is given. The analytical results of sec. 3.4 are found to be in agreement with the simulation results. The effects of the model approximations on the overall systems response are shown. Possibilities for more elaborate simulation schemes are discussed.

4

OPEN-LOOP AND INDIRECT ELECTROHEAT CONTROL

4.1 INTRODUCTION

In this chapter two control schemes are investigated: Open loop control, and indirect control.

In sec. 4.2 an analysis of open loop electroheat control systems is given. This analysis is important for the following reasons:

1. Open loop control can be used in systems where the disturbance is constant (or predictable). This restriction does not apply to a large number of electroheat systems but, nevertheless, open loop control finds its place in control practice. The analysis presented in sec. 4.2 will be useful for the design of open-loop control systems.

2. The results obtained from the analysis of open-loop control systems will be used in the second half of this chapter where indirect electroheat control is presented.

3. Open loop control constitutes a basis for the investigation of pulse width modulation control systems, which is presented in Chapter 5.

In sec. 4.3, indirect electroheat control is presented. Indirect control has certain advantages over conventional on-off control. These advantages are discussed, and design

criteria for indirect electroheat control systems are presented.

4.2 OPEN-LOOP CONTROL

A block diagram of a typical open-loop control system is shown in fig. 4.1. The control element (switch, relay, thyristor, etc..) operates with a constant period t_q , and a preset on-off ratio $\psi = t_o/t_p$. Φ represents the control element. P is the electroheat process. The transit delay L which P may possess has no influence on the output temperature waveshape, since its only effect is to retard the output temperature cycle.

4.2.1 First order systems

In this section, P is assumed as being a mode dependent first order system, with heating and cooling time constants, T_A and T_p , respectively. In fig. 4.2, the output temperature for heating and cooling intervals are shown.

From fig. 4.2 one can write:

$$\theta_2 = (1 - p)F + p \theta_1 \quad (4.1)$$

$$\theta_3 = q \theta_2 \quad (4.2)$$

where

$$p = \exp(-t_o/T_A)$$

$$q = \exp(-t_p/T_p)$$

Since the only periodic change in the system has the period t_q θ will also be periodic in the dec with period t_q , and:

$$\theta_2 = \theta_{\max} \quad (4.3)$$

$$\theta_1 = \theta_3 = \theta_{\min} \quad (4.4)$$

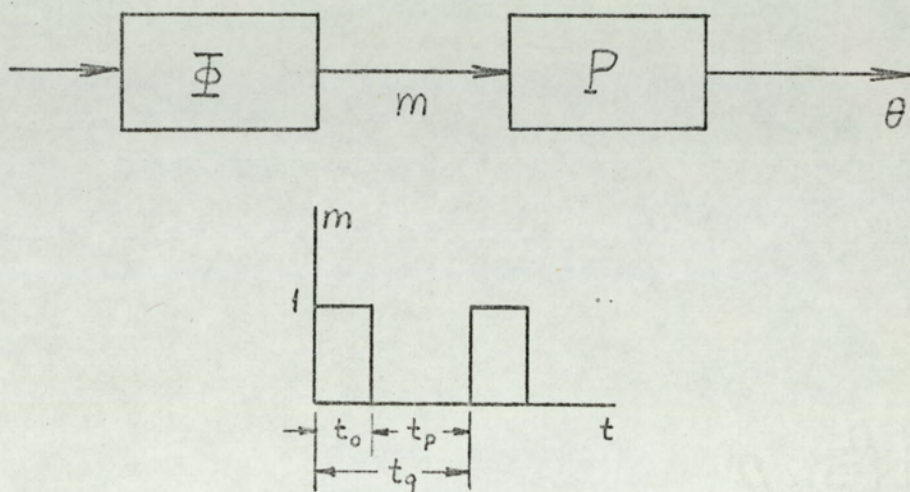


Fig. 4.1

Open-loop control

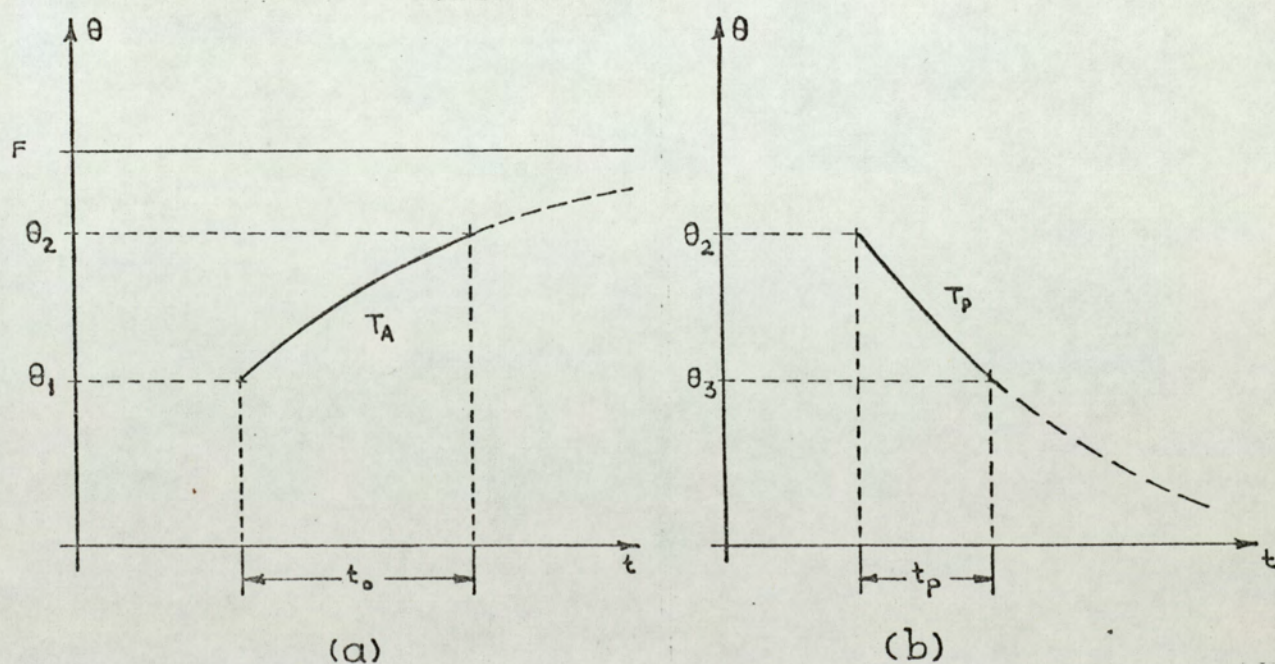


Fig. 4.2

Heating and cooling intervals for the open-loop control system

(a) heating interval

(b) cooling interval

Substituting eqns. 4.3 and 4.4 into eqns. 4.1 and 4.2:

$$\theta_{\max} = F \frac{1 - p}{1 - pq} \quad (4.5)$$

$$\theta_{\min} = \frac{q(1 - p)}{1 - pq} F \quad (4.6)$$

From eqns. 4.5 and 4.6:

$$\theta_d = \theta_{\max} - \theta_{\min} = F \frac{(1 - p)(1 - q)}{1 - pq} \quad (4.7)$$

Figure 4.3 displays θ_d/F as a function of t_o/T_A and t_p/T_p .

An approximate equation can be obtained by using the approximation* $\exp(-x) \approx 1 - x$

$$\theta_d \approx \frac{t_o t_p}{t_o T_p + t_p T_A} \quad t_o < T_A, t_p < T_p \quad (4.8)$$

The average value of the output temperature can be found from:

$$\bar{\theta} = \frac{1}{t_q} \int_0^{t_o} \left[F + (\theta_{\min} - F) \exp(-t/T_A) \right] dt + \frac{1}{t_q} \int_{t_o}^{t_p} \theta_{\max} \exp(-t/T_p) dt \quad (4.9)$$

*See appendix B for the explanation and validity ranges of this approximation.

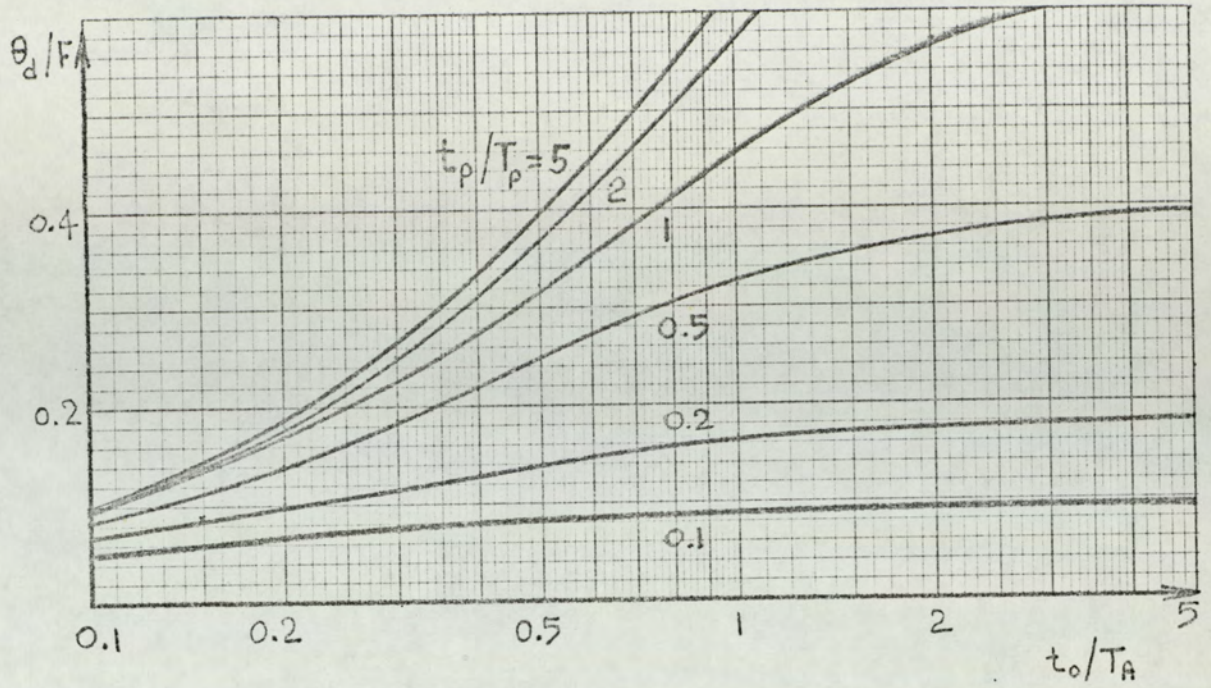


Fig. 4.3

Normalized dec amplitude as a function of t_o/T_A and t_p/T_p (mode dependent system)

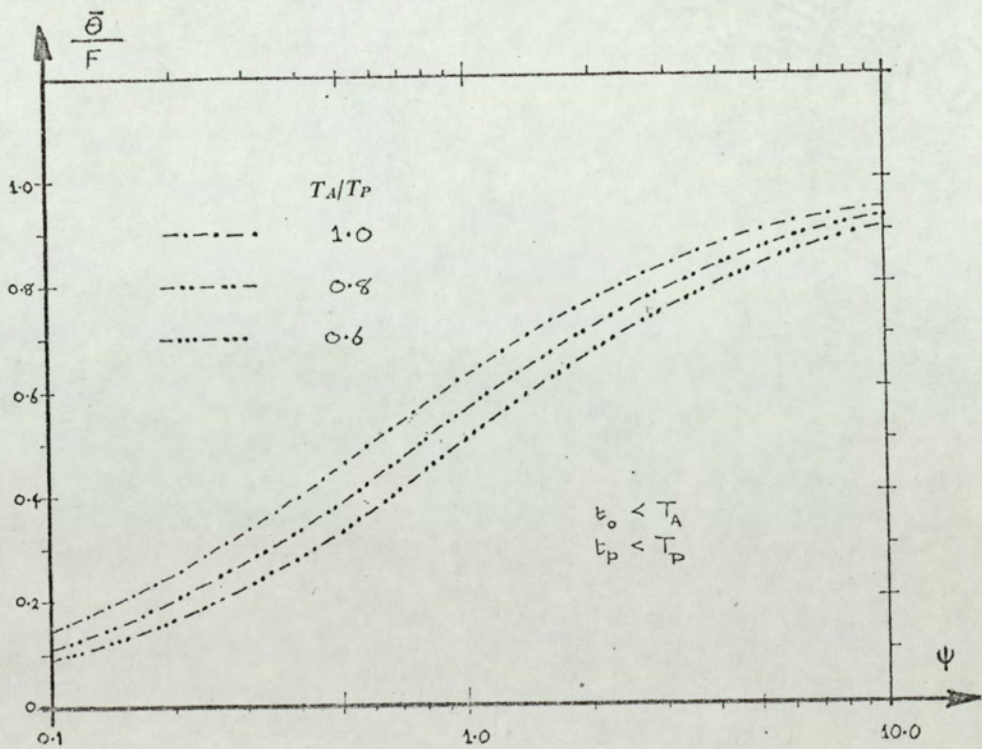


Fig. 4.4

$\bar{\theta}/F$ as a function of ψ in an open-loop-controlled mode-dependent electroheat process in which $t_o < T_A$ and $t_p < T_P$.

Combining eqns. 4.9, 4.5, and 4.6 one obtains*

$$\bar{\theta} = F \cdot \frac{1}{t_q} \left[t_o + (T_p - T_A) \frac{(1-p)(1-q)}{1-pq} \right] \quad (4.10)$$

Figure 4.4 displays the normalized average output temperature, $\bar{\theta}/F$, as a function of ψ . This figure is valid for the common constraints $t_o < T_A$ and $t_p < T_p$. For cases where these do not apply, fig. 4.5 can be used to evaluate $\bar{\theta}/F$ for a wider range of t_o/T_A and t_p/T_p values.

For the special case of mode independence, eqn. 4.10 becomes:

$$\bar{\theta} = F \frac{t_o}{t_q} = F \frac{\psi}{1 + \psi} \quad (4.11)$$

On the other hand, if $t_o < T_A$ and $t_p < T_p$, which is a common case for electroheat processes, the approximation $\exp(-x) \approx 1 - x$ yields

$$\bar{\theta} \approx F \frac{t_o T_p}{t_o T_p + t_p T_A} = F \frac{\psi}{\psi + \delta} \quad (4.12)$$

*Shapiro³⁹ gives the following equation for $\bar{\theta}$:

$$\bar{\theta} = \frac{F}{t_q} \left[t_o + (T_p - T_A)(1-p) \right]$$

It can be shown that this equation gives errors of the order of several hundred percent, especially when T_A and T_p differ significantly. For a comparison of Shapiro's formula with eqn. 4.10, see Roots and Gönenc³⁴.

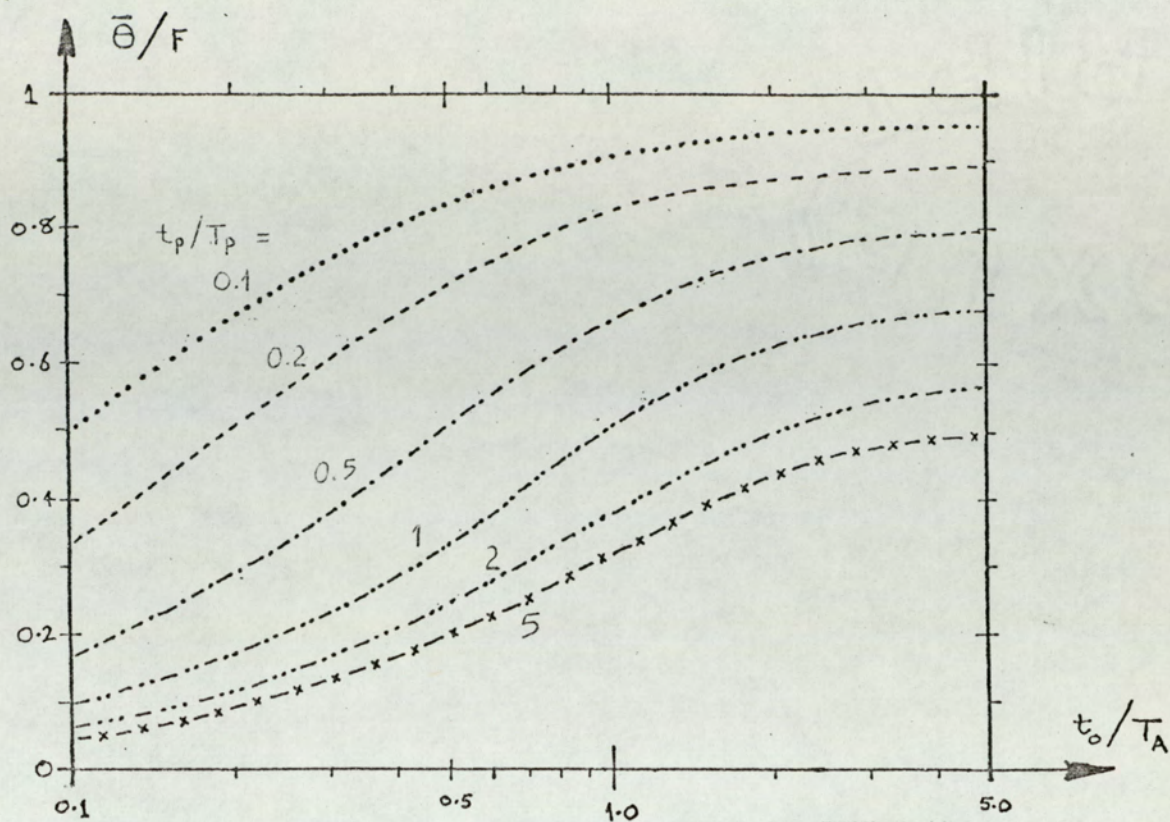


Fig. 4.5

Normalized average output temperature in an open-loop-controlled mode-dependent process without constraints on t_0 or t_p .

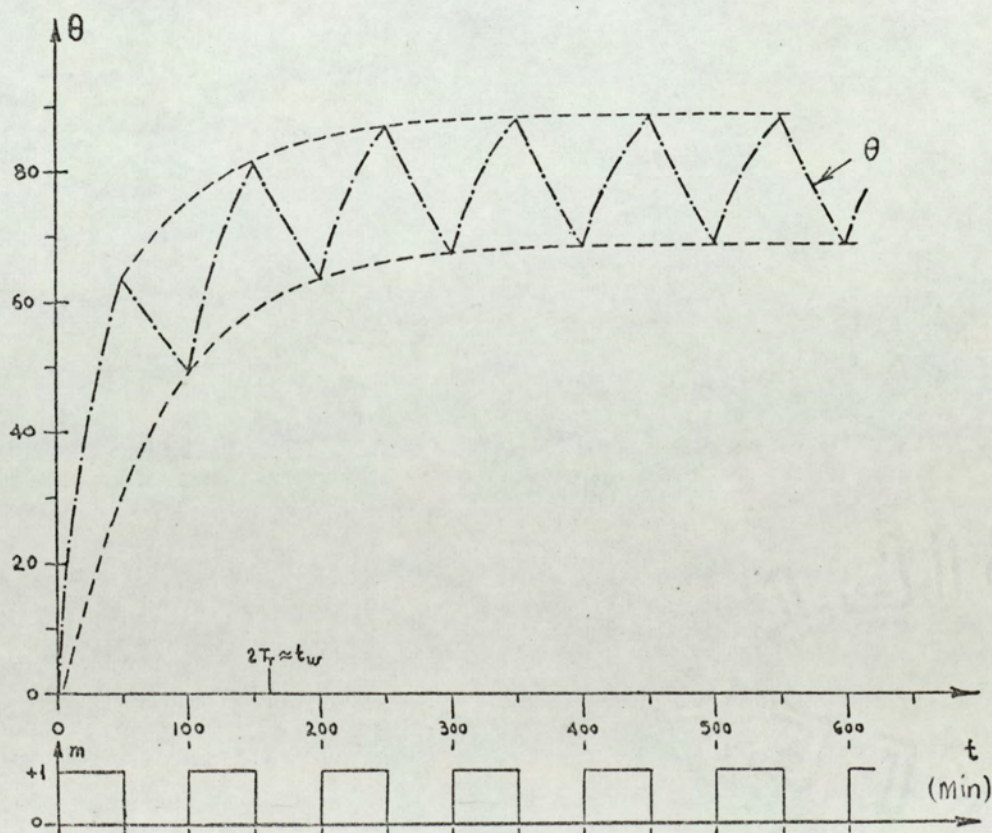


Fig. 4.6

Typical cold start in an open-loop-controlled mode dependent electroheat process when $F=100$ °C, $\psi=1$, $T_A/T_P=0.25$, $T_A=50$ min.

where $\delta = T_A/T_p$

The equations given above are for steady-state dec. On the other hand, when transients occur (on start-up, shut-down, change of ψ , etc..) the transient will respond to an equivalent time constant T_T as shown in the open-loop start-up operation in fig. 4.6. To find this equivalent time constant one compiles the following difference equation from eqns. 4.1 and 4.2:

$$\left. \begin{aligned} \theta_{2k+1} &= q \theta_{2k} \\ \theta_{2k} &= F(1-p) + p\theta_{2k-1} \end{aligned} \right\} k = 1, 2, \dots \quad (4.13)$$

with the initial condition:

$$\theta_1 = 0 \quad (4.14)$$

where $\theta_{2k+1} = \theta(t = kt_q)$ and $\theta_{2k+2} = \theta(t = kt_q + t_o)$

$$\theta_{2k+1} = \theta(t = kt_q) \text{ and } \theta_{2k+2} = \theta(t = kt_q + t_o)$$

Solving eqn. 4.13 for the minima and maxima:

$$\theta_{2k+1} = F \frac{q(1-p)}{1-pq} - F(pq)^k \frac{q(1-p)}{1-pq}, k = 1, 2, \dots \quad (4.15)$$

$$\theta_{2k+2} = F \frac{(1-p)}{1-pq} - (pq)^k \left[F \frac{1-p}{1-pq} - \theta_2 \right], k = 1, 2, \dots \quad (4.16)$$

In eqns. 4.15 and 4.16 the first terms are the steady-state, and the second terms, the transient, solutions.

Equating θ_{2k+1} and θ_{2k+2} to the values of a continuous exponential function at $t = kt_q$ and $t = kt_q + t_o$, respectively; one obtains:

$$\theta_{2k+1} = \theta(t = kt_q) = F \frac{q(1-p)}{1-pq} \left[1 - \exp(-kt_q/T_T) \right] \quad (4.17)$$

$$\theta_{2k+2} = \theta(t = kt_q + t_o) = F \frac{1-p}{1-pq} - \left[F \frac{1-p}{1-pq} - \theta_2 \right] \exp(-kt_q/T_T) \quad (4.18)^*$$

By comparing eqn. 4.15 with 4.17, and eqn. 4.16 with 4.18 one obtains**

$$T_T = t_q \frac{T_A T_P}{t_o T_P + t_p T_A} = T_A \frac{\psi + 1}{\psi + \delta} \quad (4.19)$$

In the mode independent case ($T_A = T_P = T$, $\delta = 1$), eqn. 4.19 becomes:

$$T_T = T$$

Graphical solution

A graphical solution¹⁵ of the difference equation governing open loop control of first order systems can be devised.

If we denote:

$$\theta_n = \theta(nt_q), \theta_{n+1} = \theta[(n+1)t_q], \theta_m = \theta(nt_q + t_o)$$

*The right hand side of the eqn. 4.18 involves a shift of time by t_o .

** T_T is evaluated for the maxima and minima during the transient. It follows that the average temperature during the transient will follow the same time constant T_T .

we have

$$\theta_m = p\theta_n + F(1 - p) \quad (4.20)$$

$$\theta_{n+1} = q\theta_m \quad (4.21)$$

If the initial temperature $\theta_0 = \theta(0)$ is known, successive maxima and minima can be found from eqns. 4.20 and 4.21. Note that eqns. 4.20 and 4.21 represent straight lines, in the θ_m, θ_n and θ_{n+1}, θ_m planes, successively. To illustrate the solution of the above equations by the graphical method, let us consider a numerical example. A plant with active and passive time constant of $T_A = 50$ min., and $T_p = 200$ min. is assumed. Also let $L = 0$, $F = 100^\circ\text{C}$, $t_o = t_p = 50$ min. Therefore we have:

$$p = \exp(-t_o/T_A) = 0.368$$

$$q = \exp(-t_p/T_p) = 0.779$$

Equations 4.20 and 4.21 become:

$$\theta_m = 0.368 \theta_n + 63.2$$

$$\theta_{n+1} = 0.779 \theta_m$$

Two straight lines corresponding to these two equations are shown in fig. 4.7. A third straight line which passes through the origin with slope 1 serves as a link between successive values of n . Assuming an initial temperature of $\theta_0 = 0$ (cold start), successive maxima and minima are found as shown in fig. 4.7. The parameter values are the same as those of fig. 4.5, making a comparison possible. It is clear that the "cobweb" pattern, as it is usually called in econo-

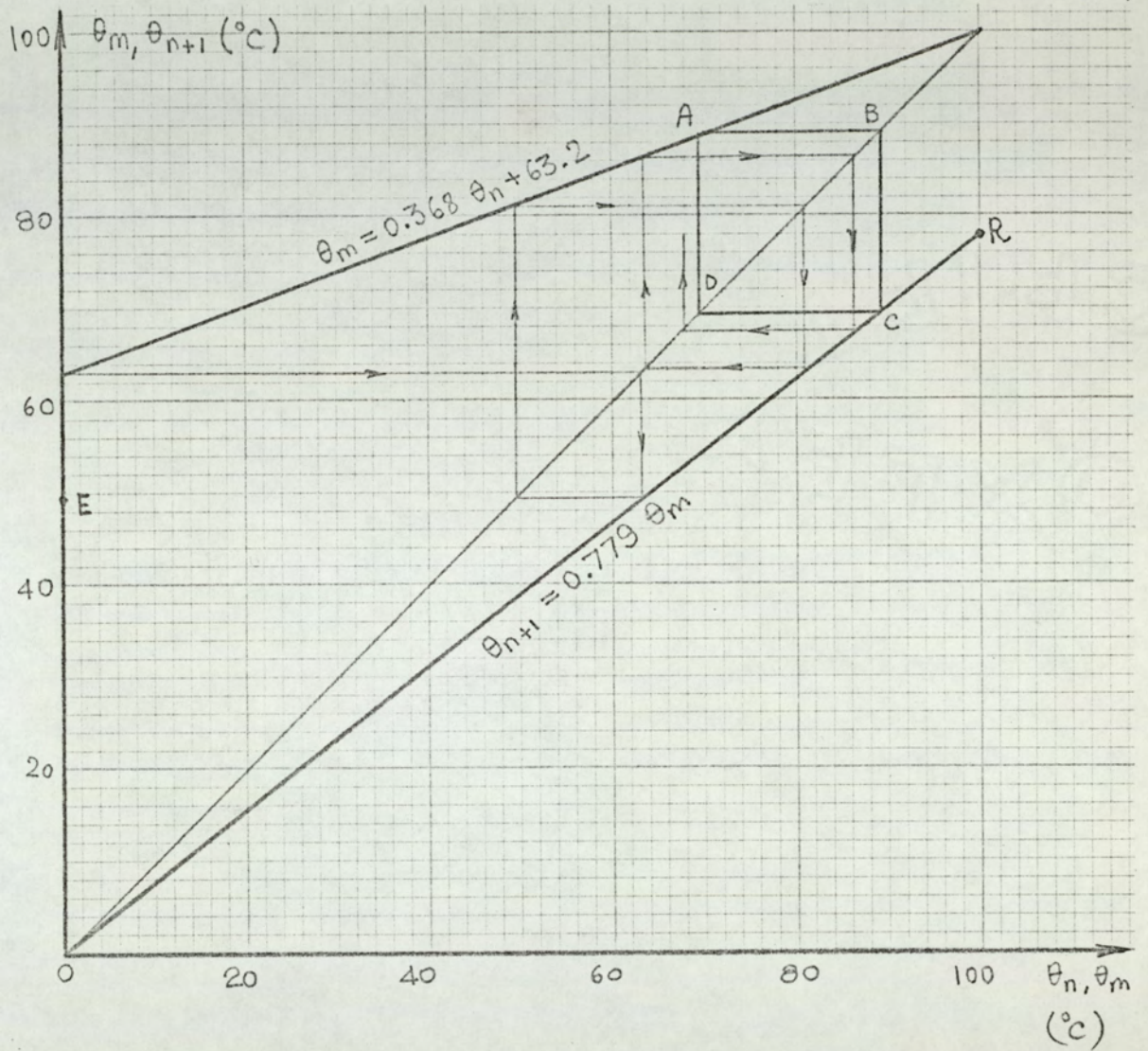


Fig. 4.7

Graphical solution for the open loop control. (mode dependent process). ABCD is the dec trajectory.

mical analysis, approaches the square ABCD, which corresponds to the dec.

Another approach to the graphical solution would be to combine eqns. 4.20 and 4.21, by eliminating θ_m :

$$\theta_{n+1} = pq \theta_n + F(1-p)q \quad (4.22)$$

From eqn. 4.22, the minima of the output temperature can be found, for $n = 0, 1, 2, \dots$. In terms of the above parameter values, eqn. 4.22 becomes:

$$\theta_{n+1} = 0.286 \theta_n + 49.1$$

This equation corresponds to a straight line passing through the points E, D, and R in fig. 4.7. In this case, the trajectory will approach point D.

Since the control is open loop, the delay which the plant may possess does not affect the method.

4.2.2 Higher order systems

For a second order plant, P is given by

$$P(s) = \frac{F}{(1 + T_1 s)(1 + T_2 s)} \quad (4.23)$$

The step response of the plant is:

$$a(t) = F \left[1 + \frac{1}{T_1 - T_2} \left(T_2 e^{-t/T_2} - T_1 e^{-t/T_1} \right) \right] u(t) \quad (4.24)$$

$T_1 \neq T_2$

where $u(t)$ is the unit step function.

Since $m(t)$, the input to the plant is periodic, its Laplace transform is given by:

$$M(s) = \frac{1 - e^{-t_0 s}}{s(1 - e^{-t_q s})} \quad (4.25)$$

Therefore, the transform of the output is:

$$\Theta(s) = \frac{1 - e^{-t_0 s}}{s(1 - e^{-t_q s})} \cdot \frac{F}{(1 + sT_1)(1 + sT_2)} \quad (4.26)$$

Obtaining the inverse transform of eqn. 4.26

$$\theta(t) = \frac{F}{T_1 - T_2} \left[T_2 \left(e^{-t/T_2} - e^{-(t-t_0)/T_2} \right) \frac{e^{nt_q/T_2} - 1}{e^{t_q/T_2} - 1} - T_1 \left(e^{-t/T_1} - e^{-(t-t_0)/T_1} \right) \frac{e^{nt_q/T_1} - 1}{e^{t_q/T_1} - 1} \right] \quad (4.27)$$

for $t_0 + (n-1)t_q < t < nt_q$

and

$$\theta(t) = F + \frac{F}{T_1 - T_2} \left[T_2 \left(e^{-t/T_2} \frac{e^{(n+1)t_q/T_2} - 1}{e^{t_q/T_2} - 1} - e^{-(t-t_0)/T_2} \frac{e^{nt_q/T_2} - 1}{e^{t_q/T_2} - 1} \right) - T_1 \left(e^{-t/T_1} \frac{e^{(n+1)t_q/T_1} - 1}{e^{t_q/T_1} - 1} - e^{-(t-t_0)/T_1} \frac{e^{nt_q/T_1} - 1}{e^{t_q/T_1} - 1} \right) \right] \quad (4.28)$$

for $nt_q < t < (n+1)t_q$

In eqns. 3.27 and 3.28, the terms containing n will give steady state solutions. Taking the terms containing n , and substituting $n = 1$ in eqn. 3.27 and $n = 0$ in eqn. 3.28, we obtain:*

$$\theta_{\text{off}}(t) = \frac{F}{T_1 - T_2} \left[T_2 \frac{1 - p_2}{p_2(1 - q_2)} e^{-t/T_2} - T_1 \frac{1 - p_1}{p_1(1 - q_1)} e^{-t/T_1} \right] \quad (4.29)$$

$$\theta_{\text{on}}(t) = F + \frac{F}{T_1 - T_2} \left[T_2 \frac{1 - q_2}{1 - p_2 q_2} e^{-t/T_2} - T_1 \frac{1 - q_1}{1 - p_1 q_1} e^{-t/T_1} \right] \quad \begin{matrix} t_o < t < t_q \\ o < t < t_o \end{matrix} \quad (4.30)$$

where $p_i = e^{-t_o/T_i}$ and $q_i = e^{-t_p/T_i}$, $i = 1, 2$.

The maximum and minimum values of the output temperature can be found by differentiating eqns. 4.29 and 4.30 with respect to time.

1. The maximum value of the output temperature:

Output temperature attains its extremum value in the off interval at $t = t_M$, where

$$\frac{d}{dt} \theta_{\text{OFF}}(t_M) = 0 \quad (4.31)$$

From eqns. 4.31 and 4.29 one obtains

$$t_M = \frac{T_1 T_2}{T_1 - T_2} \ln \frac{p_1(1 - p_2)(1 - p_1 q_1)}{p_2(1 - p_1)(1 - p_2 q_2)} \quad (4.32)$$

*Note that eqns. 4.29 and 4.30 are the steady-state solutions for the output temperature; reduced, for the sake of simplicity, to the first period

and the value of this extremum can be found by substituting the value of t_M given by eqn. 4.31 in eqn. 4.29:

$$\theta_{\max} = \theta_{\text{OFF}}(t_M) = F \frac{1 - p_1}{p_1(1 - p_1 q_1)} \left[\frac{p_2(1 - p_1)(1 - p_2 q_2)}{p_1(1 - p_2)(1 - p_1 q_1)} \right]^{T_2 / (T_1 - T_2)}$$

(4.33)

To show that the extremum given in eqn. 4.33 is a maximum, we find $d^2 \theta_{\text{off}}(t)/dt^2$ at $t=t_M$:

$$\frac{d^2}{dt^2} \theta_{\text{OFF}}(t_M) = F \left[\frac{1}{(T_1 - T_2) T_1} \frac{1 - p_1}{p_1(1 - p_1 q_1)} e^{-t/T_1} - \frac{1}{(T_1 - T_2) T_2} \frac{1 - p_2}{p_2(1 - p_2 q_2)} e^{-t/T_2} \right]$$

(4.34)

It can be shown that:

$$\frac{e^{t_M/T_2}}{F} \frac{p_2(1 - p_2 q_2)}{1 - p_2} \cdot \frac{d^2}{dt^2} \theta_{\text{OFF}}(t_M) = -\frac{1}{T_1 T_2} < 0$$

(4.35)

Since the coefficient of $d^2 \theta_{\text{OFF}}(t_M)/dt^2$ is positive in the above equation, one concludes that t_M corresponds to the maximum of $\theta(t)$, and eqn. 4.33 gives θ_{\max} . Since there is one extremum in the off interval and one extremum in the on interval, one concludes that the extremum in the on interval corresponds to a minimum.

2. The minimum value of the output temperature:

Proceeding exactly as above, it can be shown that the minimum of $\theta(t)$ occurs in the on interval, for $t = t_m$, where:

$$t_m = \frac{T_1 T_2}{T_1 - T_2} \ln \frac{(1 - p_1 q_1)(1 - q_2)}{(1 - q_1)(1 - p_2 q_2)} \quad (4.36)$$

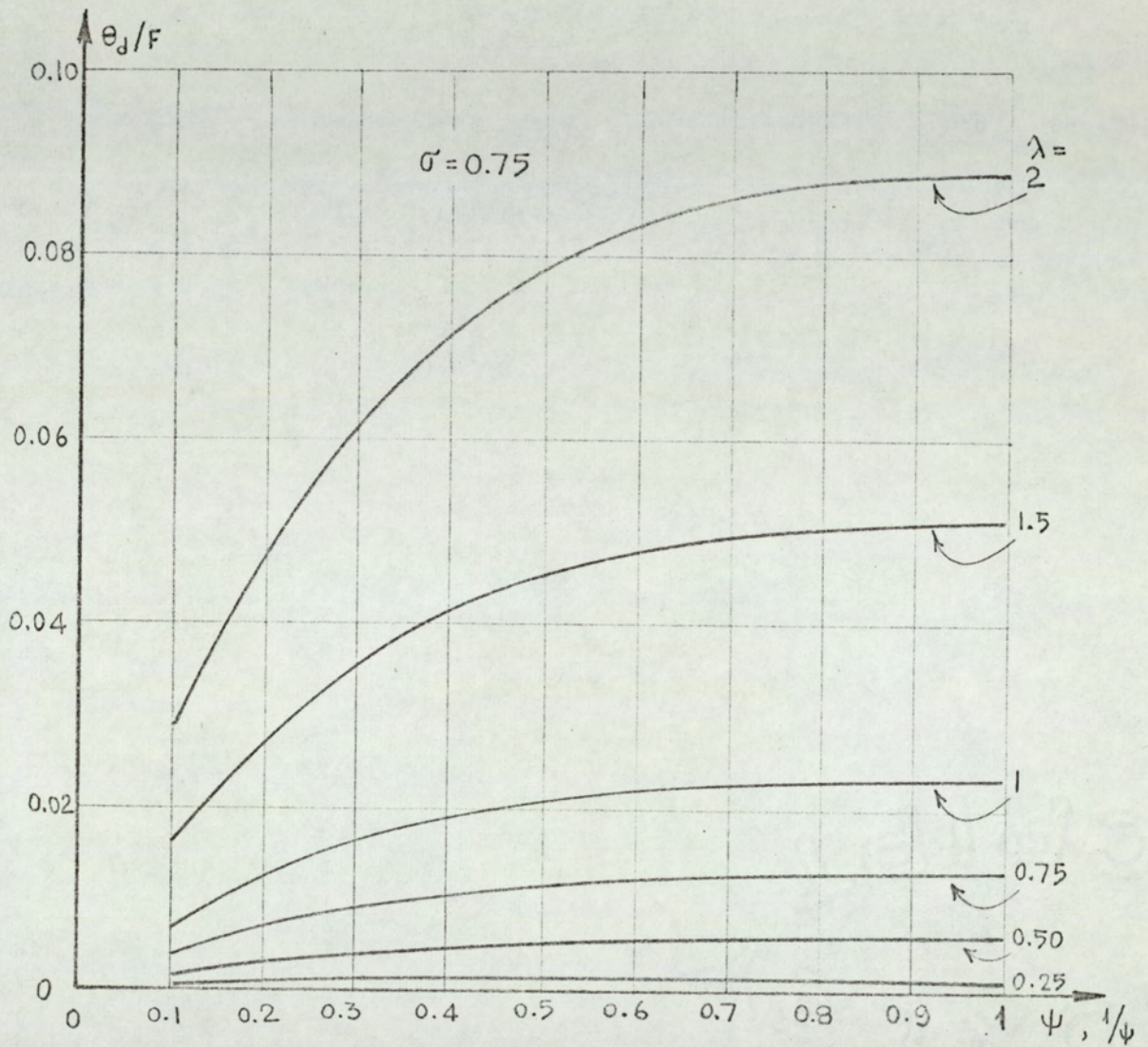
The value of this minimum is given by:

$$\theta_{\min} = \theta_{\text{on}}(t_m) = F \left[1 - \frac{1 - q_1}{1 - p_1 q_1} \left(\frac{(1 - q_1)(1 - p_2 q_2)}{(1 - q_2)(1 - p_1 q_1)} \right)^{T_2 / (T_1 - T_2)} \right] \quad (4.37)$$

The dec amplitude, θ_d , can be found as $\left[\theta_{\max} - \theta_{\min} \right]$ from eqns. 4.37 and 4.33.

Since eqns. 4.33 and 4.37 are rather involved, normalized dec amplitude, θ_d/F , calculated from eqns. 4.33 and 4.37 is displayed in figure 4.8a-d. In these figures, θ_d/F is plotted as a function of $\psi = t_o/t_p$, for various values of $\lambda = t_q/T_1$ and $\sigma = T_1/T_2$. One notes that, as expected, the dec amplitude is very much smaller than it is for first order systems. The dec amplitude passes through a maximum for $\psi = 1$, i.e. $t_o = t_p$. One also notes that θ_d increases when the period of the input becomes larger with respect to the time constants. The amplitude also increases as the two time constants approach a common value. In fact, as stated in sect. 3.4, the value of the equivalent lag for the Ziegler-Nichols model becomes maximum when the two time constants are equal²⁶, therefore the dec amplitude attains a maximum when $T_1 = T_2$ ($\sigma = 1$).

Since we assume a mode independent process, the average value of the dec output temperature is simply:

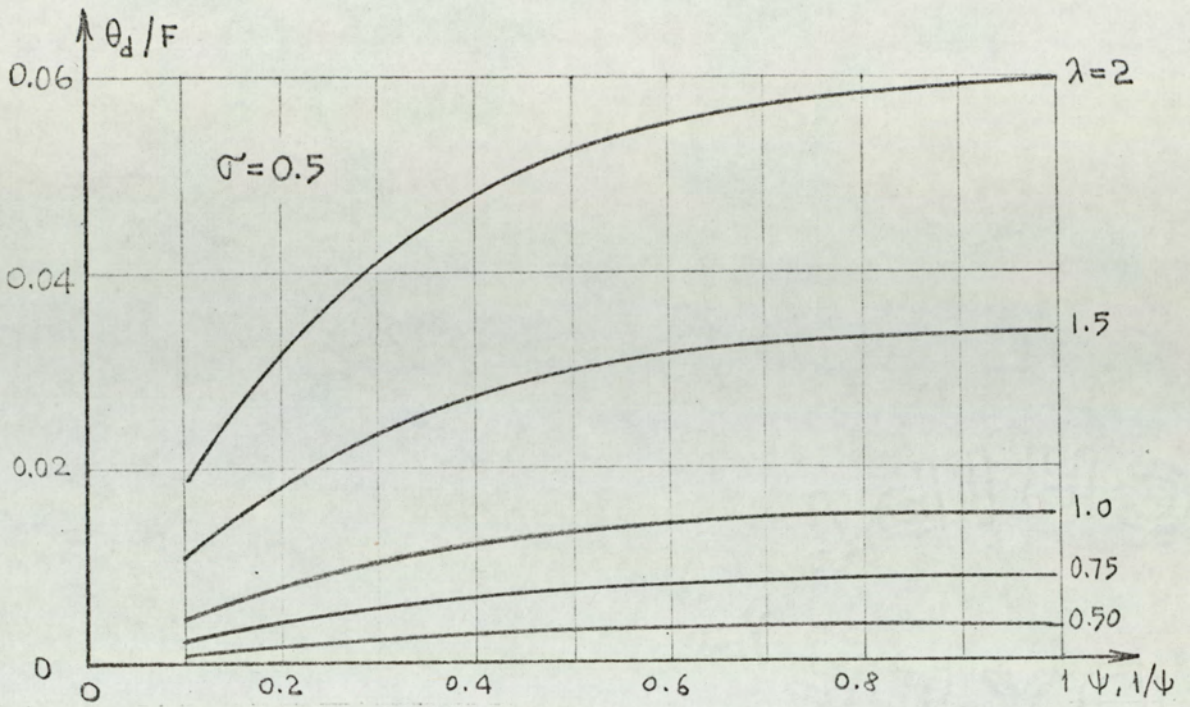


(a)

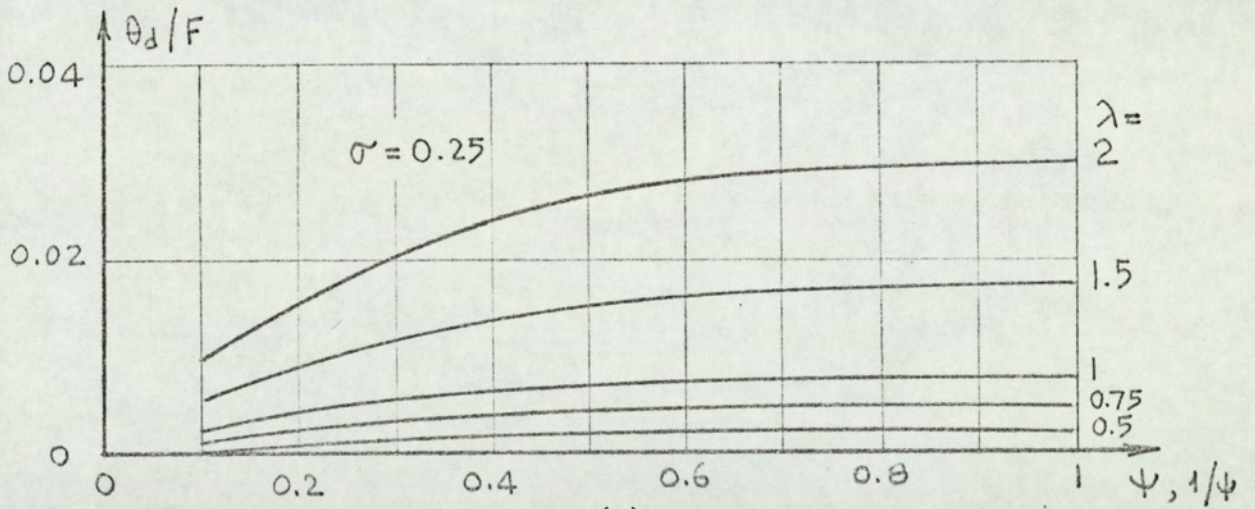
Fig. 4.8

Normalized dec amplitude for the open loop control of second order plants.

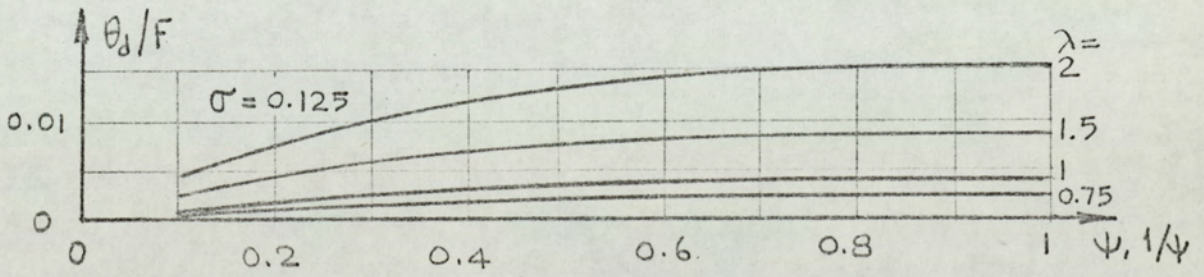
$$\psi = t_o/t_p, \quad \lambda = t_q/T_1, \quad \sigma = F_1/T_2$$



(b)



(c)



(d)

Fig. 4.8 , continued.

$$\bar{\theta} = F \frac{t_o}{t_q} = F \frac{\psi}{\psi + 1} \quad (4.38)$$

In fact, eqn. 4.38 is valid for all types of transfer functions, provided that they are mode independent. For any type of plant, the average value of the output temperature for transients will follow the curve:

$$f(t) = \frac{t_o}{t_q} a(t) \quad (4.39)$$

where $a(t)$ is the step response of the plant. Therefore, the start-up time for open loop control can be found by solving the equation

$$\theta_r = \frac{t_o}{t_q} a(t_w) \quad (4.40)$$

for t_w .

On the other hand, for on-off control the start-up time is found by solving

$$\theta_r = a(t_w) \quad (4.41)$$

for t_w .

Generally, start-up time for open loop control is considerably longer than the start-up time for on-off control, for the same plant. The difference between the two is larger for slow rising systems, such as a plant with distributed lag. The analogue computer plot given in fig. 7.10 provides an example for the start-up operation. Curve a in fig. 7.10 corresponds to PWM control, which operates on on-off basis in the start-up. Curve b corresponds to open-loop control.

4.2.3 Digital simulation of open-loop control systems

4.2.3.1 Method used for simulation

Input to the plant, $m(t)$, can be expressed as:

$$m(t) = u(t) \quad \left. \begin{array}{l} 0 < t < t_0 \\ \\ \\ \\ \end{array} \right| \begin{array}{l} \\ \\ \\ \\ \end{array}$$

$$m(t) = \sum_{k=0}^n u(t - kt_q) - \sum_{k=0}^{n-1} u(t - t_0 - kt_q) \quad \left. \begin{array}{l} nt_q < t < (n+1)t_q \\ \\ \\ \end{array} \right| \begin{array}{l} \\ \\ \\ \end{array}$$

(4.42)

$$m(t) = \sum_{k=0}^n u(t - kt_q) - \sum_{k=0}^n u(t - t_0 - kt_q) \quad \left. \begin{array}{l} nt_q + t_0 < t < (n+1)t_q \\ \\ \\ \end{array} \right| \begin{array}{l} \\ \\ \\ \end{array}$$

(4.43)

where $u(t)$ is the unit step function, and $n = 0, 1, 2, \dots$

The system output is found using the superposition principle; therefore the equations for the output have the same form as eqns. 4.42 and 4.43, with the following changes:

$$m(t) \rightarrow \theta(t) \quad \text{and} \quad u(t) \rightarrow a(t)$$

One notes that this method is similar to the one used for the simulation of on-off control systems, except that, for open-loop systems the switching instants are periodic.

This method is valid for all linear, time invariant systems.

4.2.3.2 Simulation programme

The digital simulation programme, called OPLOOP, is based on the above method. This programme requires two subprogrammes.

a. Subroutine SPL04.

Subroutine SPLOT4 is for plotting (and printing) and subprogramme STEP supplies the step response of the plant. Data to be supplied are t_o , t_p , step length, and the parameters of the plant. Note that the subprogrammes used with OPLOOP are the same as those used with ONOFF.

All the above programmes are given in appendix A.

4.2.3.3. Simulation results

Four examples are given on digital simulation.

1. Figure 4.9 shows the start-up operation for the exponential lag plant whose transfer function is $F \exp(-\sqrt{sT})$ where $F = 100^\circ\text{C}$ and $T = 100 \text{ min} = 6000 \text{ sec}$. The control parameters are $t_o = 10 \text{ min}$, and $t_p = 20 \text{ min}$.

2. Figure 4.10 shows the start-up operation for the Ziegler-Nichols approximation to the exponential lag of example (1). This model has the transfer function $F \exp(-sL)/(1 + sT')$, where $F = 100^\circ\text{C}$, $L = 7.5 \text{ min} = 450 \text{ sec}$, and $T' = 108 \text{ min} = 6480 \text{ sec}$. Both curves in fig. 4.9 and 4.10 have an average dec. temperature of

$$\frac{t_o}{t_o + t_p} F = \frac{1}{3} 100 = 33.3^\circ\text{C}$$

The steady state (dec) performances are not shown due to reasons of space.

A comparison of the two curves shows that the Ziegler-Nichols equivalent model is a good approximation for the exponential lag in open-loop control systems. Note that the same two plants have been compared for on-off control, in figs. 3.12 and 3.13.

From eqns. 4.5, 4.6 and 4.7, one obtains; for the first

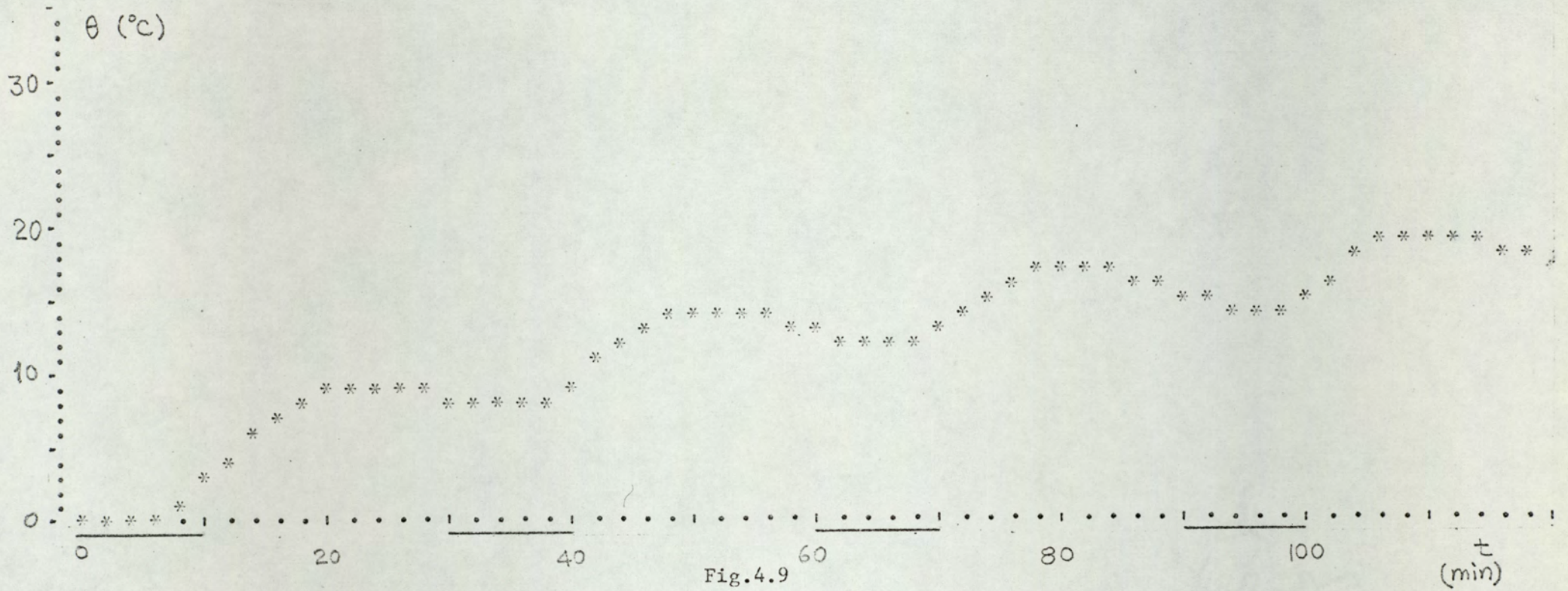


Fig.4.9

Computer plot of the output temperature for start-up. The plant transfer function is $[F \exp(-\sqrt{T}s)]$ where $F=100^\circ\text{C}$ and $T=100$ min. Control parameters are: $t_o=10$ min., $t_p=20$ min.

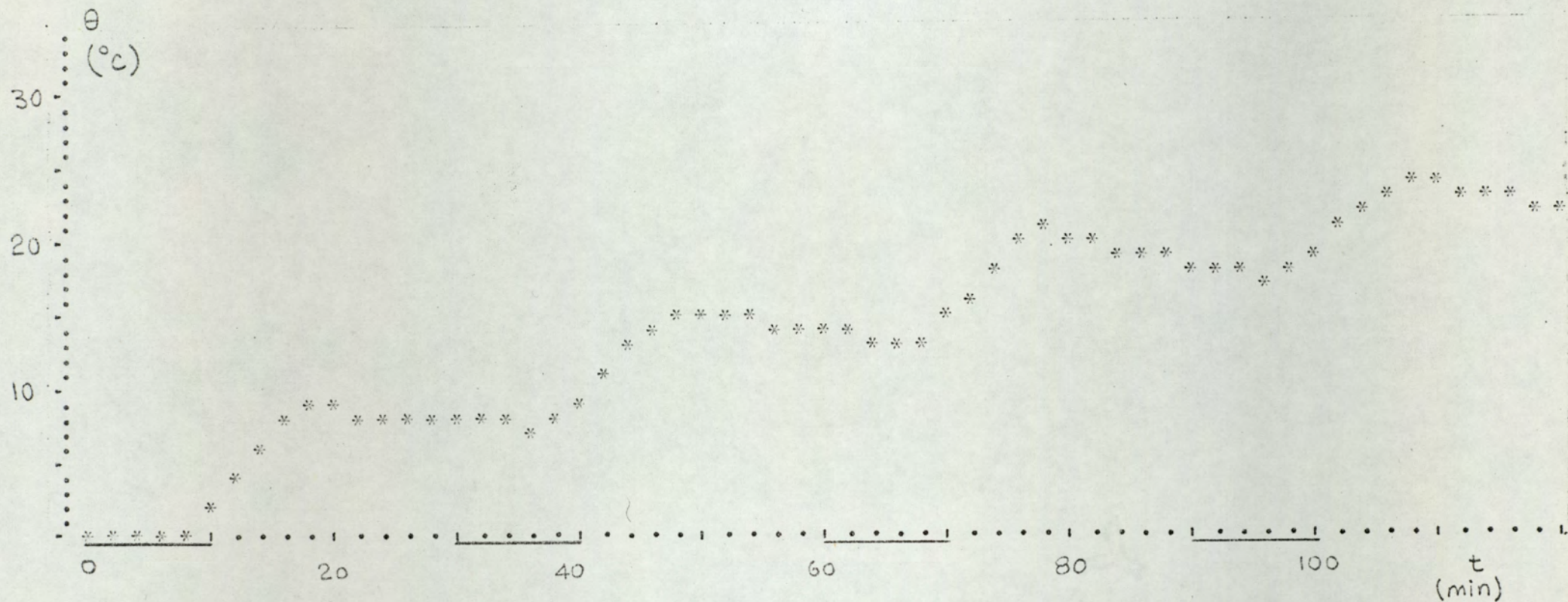


Fig. 4.10

Computer plot of the output temperature for the start-up. The plant transfer function is $[f \exp(-sL)/(1 + sT')]$ where $f=100$ C, $L=7.5$ min, $T'=108$ min. This plant is the Ziegler-Nichols equivalent of the plant of fig. 4.9. Since the control parameters have the same values ($t_o=10$ min, $t_p=20$ min) a comparison is possible.

order system $100 \exp(-450 s)/(1 + 6480 s)$:

$$\theta_{\max} = 35.4^{\circ}\text{C}, \quad \theta_{\min} = 29.4^{\circ}\text{C}, \quad \theta_d = 6^{\circ}\text{C}$$

(This value of θ_d can also be found from fig. 4.3.) The simulation curve in fig. 4.10 has an amplitude of approximately 6°C , so it agrees with the analytical result.

3. Figure 4.11 shows the simulation result for the open-loop control system, with a plant transfer function

$$F/(1 + sT_1)(1 + sT_2)$$

where $F = 100^{\circ}\text{C}$, $T_1 = 100 \text{ min}$, $T_2 = 200 \text{ min}$, and $t_o = 20 \text{ min}$, $t_p = 80 \text{ min}$. Average value of the dec temperature is $\bar{\theta} = F t_o/t_q = 20^{\circ}\text{C}$. The dimensionless parameters which are previously described are:

$$\sigma = T_1/T_2 = 0.5, \quad \lambda = t_q/T_1 = 1 \quad \text{and} \quad \psi = t_o/t_p = 0.25$$

Using these values, from fig. 4.8b, the value of the dec amplitude can be found as:

$$\theta_d/F = 0.01 \quad \text{or} \quad \theta_d = 1^{\circ}\text{C}$$

Equations 4.33 and 4.37 gives θ_{\max} and θ_{\min} as:

$$\theta_{\max} = 20.4^{\circ}\text{C}, \quad \theta_{\min} = 19.4^{\circ}\text{C}, \quad \theta_d = 1^{\circ}\text{C}$$

From the printouts of OPLOOP programme we have,

$$\theta_{\max} = 20.39^{\circ}\text{C}, \quad \theta_{\min} = 19.42^{\circ}\text{C}, \quad \theta_d = 0.97^{\circ}\text{C}$$



Fig. 4.11

Simulation result for the open loop control of a second order system. $T_1 = 100$ min, $T_2 = 200$ min, $F = 100$ C, $t_o = 20$ min, $t_p = 80$ min.

Hence the simulation results are in close agreement with the analytical results.

4. Figure 4.12 shows simulation results for the same plant in (3) above (i.e. $F = 100^{\circ}\text{C}$, $T_1 = 100$ min, $T_2 = 200$ min), but this time with $t_o = 100$ min, and $t_p = 400$ min. For this case one has:

$$\sigma = 0.5, \quad \lambda = 5, \quad \psi = 0.25$$

Since t_o and t_p values are of the same order of time constants, this example shows a bad choice of control parameters. For this reason, the value of λ , which is very high, is out of the range of fig. 4.8. Equations 4.33 and 4.37 give:

$$\theta_{\max} = 29.5^{\circ}\text{C}, \quad \theta_{\min} = 10.5^{\circ}\text{C}, \quad \theta_d = 19^{\circ}\text{C}$$

The average value is:

$$\bar{\theta} = F t_o / t_q = 20^{\circ}\text{C}$$

Simulation gives (from fig. 4.12):

$$\theta_{\max} = 29^{\circ}\text{C}, \quad \theta_{\min} = 10.5^{\circ}\text{C}$$

4.3 INDIRECT CONTROL

In some on-off regulation systems, it is suitable to have the feedback loop not around the main process itself, but around an auxiliary process. The main process is then controlled on an open-loop basis by the same controller which is included in the feedback loop. This regulation scheme can be

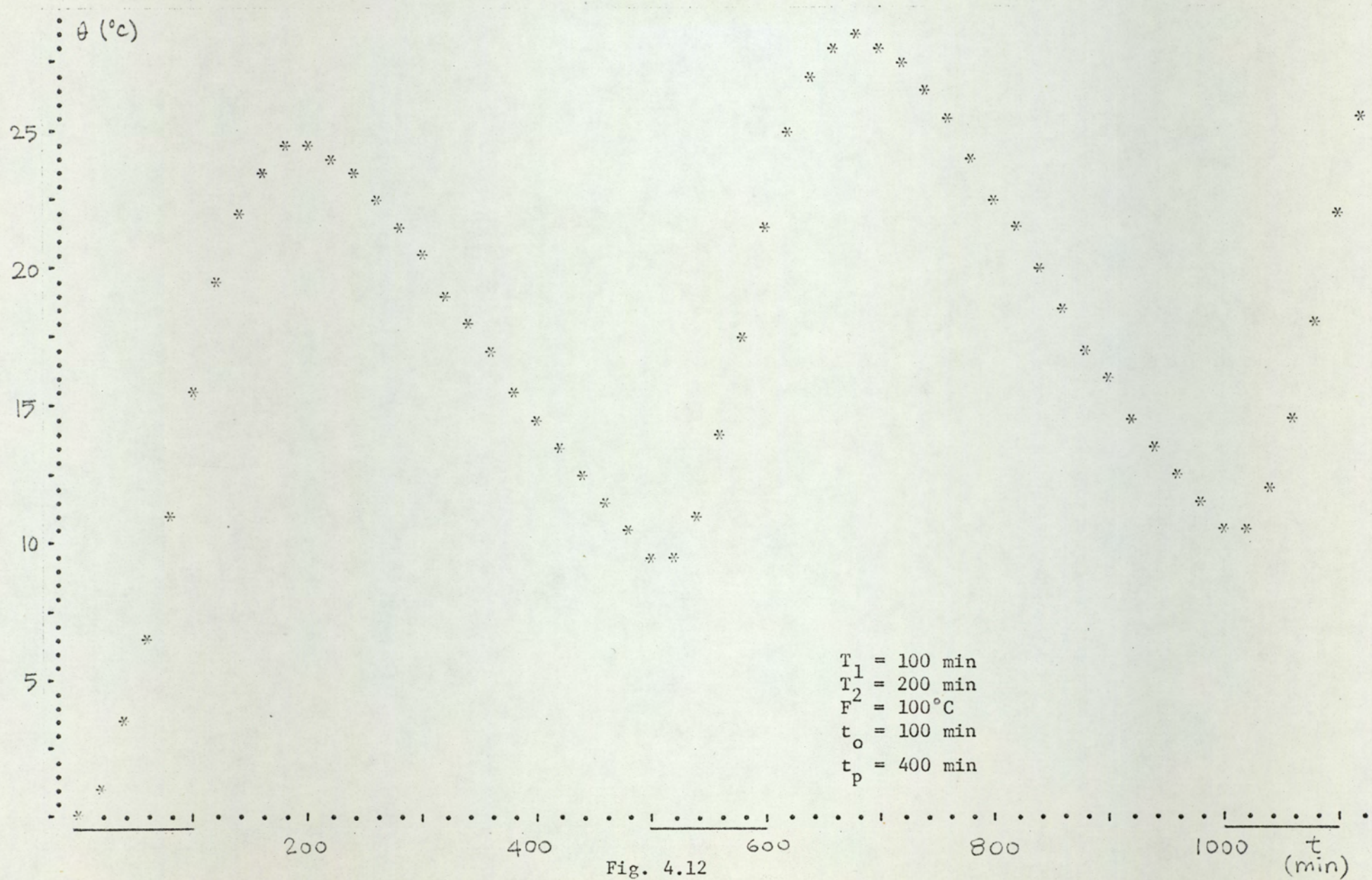


Fig. 4.12

Computer plot of the output temperature for the open loop control of a second order system.

useful when

1. it is undesirable or physically impossible to have the location of prime importance (temperature sensing point) at the output of the process,
2. the process to be controlled has a large delay.

The auxiliary process may be an electrical analogue or it may be another thermal process. In both cases its parameters can deliberately be made different than those of the main process.

In the following section some design criteria are developed for this type of regulation and it is shown that, in some cases, the use of this scheme results in better performance criteria than the conventional on-off regulation³⁵.

4.3.1 Description and design criteria

In fig. 4.13 an indirect regulation scheme is shown. Both processes are assumed to be of first order and with inherent time lags. The limit cycling performance of the process is given in fig. 4.14

From the closed-loop part, on and off times are found as (from eqns. 3.26 and 3.27):

$$t_o = T \ln \frac{\alpha - \beta + H}{1 - \beta - H} \quad (4.44)$$

$$t_p = T \ln \frac{\beta + H + \alpha - 1}{\beta - H} \quad (4.45)$$

The pulse train, with t_o and t_p as given in eqns. 4.44 and 4.45, is applied to the main thermal process.

The average value of the output temperature, $\bar{\theta}_1$, can be found from eqn. 4.11, with t_o and t_p as given in eqns. 4.44 and

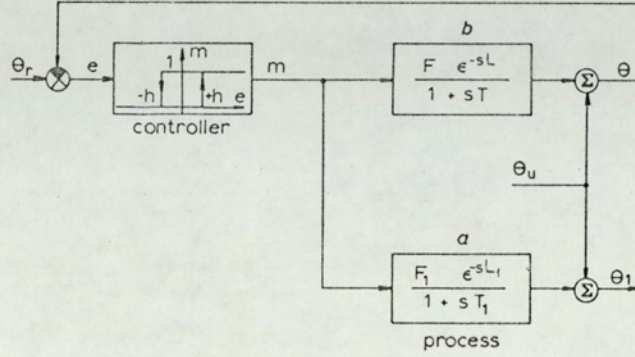


Fig 4.13

Control by means of an auxiliary process
 a - main process to be controlled
 b - auxiliary process (model)

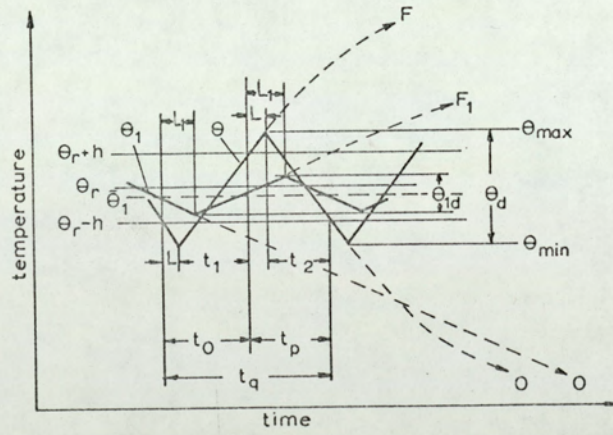


Fig. 4.14

Dynamic equilibrium cycling for system in fig. 4.13

4.45. The amplitude, θ_{1d} , of the limit cycling can be found from eqn. 4.7, with t_o and t_p again as given by eqns. 4.44 and 4.45.

The transit delay, L_1 , of the main process has no influence on these indexes since control is open-loop; the only effect of this delay is to retard the output waveshape.

Two cases are investigated:

1. zero delay in the closed loop ($L = 0, h > 0$)
2. memoryless controller ($L > 0, h = 0$)

1. zero delay in the closed loop

Substitution of $\alpha = 1$ and $\gamma = 1$ in eqns. 3.23 and 3.24 gives t_o and t_p , and with these values of t_o and t_p , one obtains from eqn. 4.11

$$\frac{\bar{\theta}_1}{F} = \frac{\ln \frac{1 - \beta + H}{1 - \beta - H}}{\ln \frac{1 - \beta + H}{1 - \beta - H} + \ln \frac{\beta + H}{\beta - H}} \quad (4.46)$$

Using the approximation*

$$\ln x \approx 2(x-1)/(x+1) \quad (4.47)$$

One can obtain from eqn. 4.46 an approximate equation

$$\frac{\bar{\theta}_1}{F_1} \approx \beta = \frac{\theta_r}{F}, \quad h \ll F \quad (4.48)$$

It must be noted that one has always

$$\theta_r + h < F \quad \text{or} \quad H < 1 - \beta \quad (4.49)$$

*See appendix B.

Moreover, it is logical to put a limit on the value of h/θ_r since, in practice, h is generally a fraction of θ_r .

The exact result of eqn. 4.46 is displayed in fig. 4.15 where the average output temperature is plotted as a function of h_F . An upper limit of 0.3 is taken for h/θ_r , hence

$$h < 0.3 \theta_r \quad \text{or} \quad H < 0.3 \beta \quad (4.50)$$

From fig. 4.15 it can be seen that for small values of h the approximation given by eqn. 4.48 is in fact valid.

The dec amplitude θ_{1d} is found from eqn. 4.50, with p and q having the values:

$$p = \exp(-t_o/T_1) = \exp\left(-\frac{T}{T_1} \ln \frac{1-\beta+H}{1-\beta-H}\right) = \left(\frac{1-\beta-H}{1-\beta+H}\right)^\rho \quad (4.51)$$

$$q = \exp(-t_p/T_1) = \exp\left(-\frac{T}{T_1} \ln \frac{\beta+H}{\beta-H}\right) = \left(\frac{\beta-H}{\beta+H}\right)^\rho \quad (4.52)$$

where $\rho = T/T_1$

In fig. 4.16 normalized dec amplitude is shown as a function of h . The amplitude is dependent on ρ but shows very little dependence on β . For small h , the amplitude is approximately a linear function of h . This can be shown as follows. For small h , both p and q and $1-pq$ can be expressed as:

$$p = (1-v)^\rho = \left(1 - \frac{2H}{1-\beta+H}\right)^\rho \approx 1 - \rho v = 1 - \frac{2H\rho}{1-\beta+H} \quad (4.53)$$

$$q = (1-w)^\rho = \left(1 - \frac{2H}{\beta+H}\right)^\rho \approx 1 - \rho w = 1 - \frac{2H\rho}{\beta+H} \quad (4.54)$$

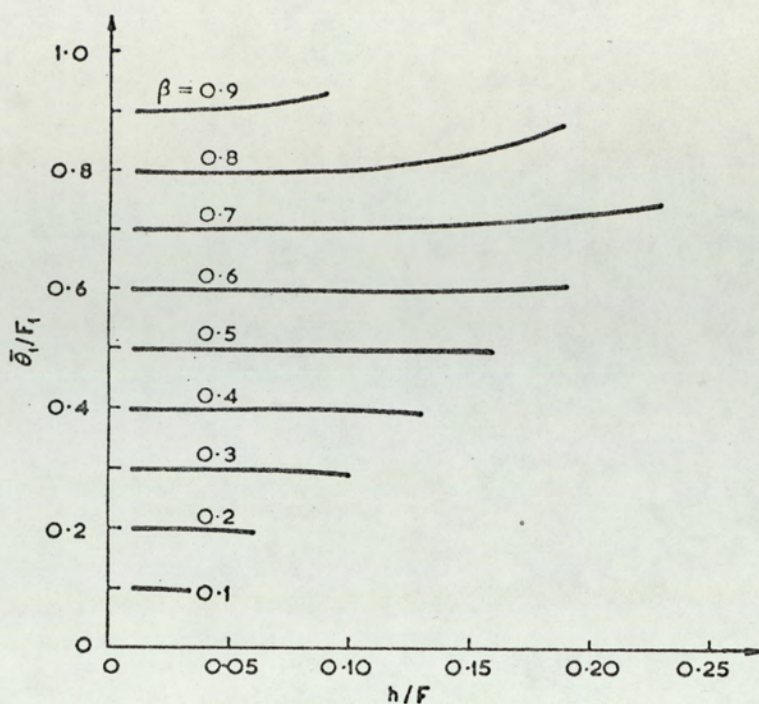


Fig. 4.15

Average output temperature vs hysteresis width (both normalized) for $\tau = 0$.

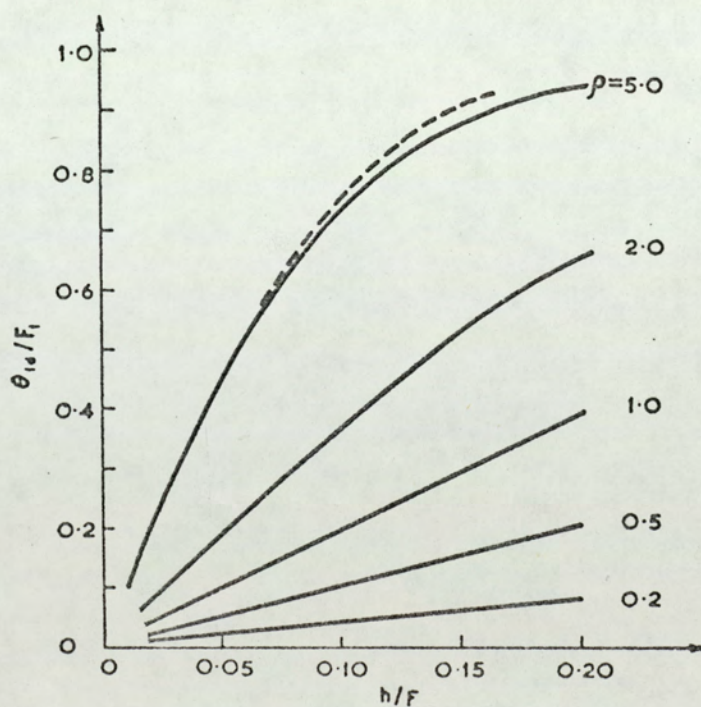


Fig. 4.16

Cycling amplitude vs hysteresis width (both normalized) for $\tau = 0$.

ρ ($=T/T_1$) is the parameter. For small ρ , β has negligible effect.

———— $\beta = 0.7$ - - - - $\beta = 0.5$

$$1 - pq = 1 - [(1 - v)(1 - w)]^\rho \approx 1 - (1 - v - w)^\rho$$

$$\approx \rho (v + w) = 2H\rho \left(\frac{1}{1 - \beta + H} + \frac{1}{\beta + H} \right) \quad (4.55)$$

Substituting these approximate values of p, q and $(1-pq)$ in eqn. 4.50, one obtains:

$$\frac{\theta_{1d}}{F_1} \approx 2H\rho = 2 \frac{h}{F} \frac{T}{T_1} \quad h \ll F \quad (4.56)$$

On the other hand, it can be shown that, for $\rho = 1$,

$$\frac{\theta_{1d}}{F_1} = 2H = 2 \frac{h}{F} \quad (4.57)$$

This linear dependence of θ_{1d} on h is clear from fig. 4.16.

2. Memoryless controller

In this case ($h = 0$ and $L > 0$) from eqns. 3.23, 3.24 and 4.11:

$$\frac{\bar{\theta}_1}{F_1} = \frac{\ln \frac{\alpha - \beta}{1 - \beta}}{\ln \frac{\alpha - \beta}{1 - \beta} + \ln \frac{\alpha + \beta - 1}{\beta}} \quad (4.58)$$

Using the approximation of eqn. 4.47 in eqn. 4.58, one obtains

$$\frac{\bar{\theta}_1}{F_1} \approx \frac{\alpha + 2\beta - 1}{2\alpha} \quad L \ll T \quad (4.59)$$

The exact values of average temperature are displayed as a function of L/T in fig. 4.17.

The dec amplitude is found from eqns. 3.23, 3.24 and 4.7 as:

$$\frac{\theta_{1d}}{F_1} = \frac{(1-p)(1-q)}{1-pq} \quad (4.60)$$

where p and q are now given by

$$p = \left(\frac{1-\beta}{\alpha-\beta} \right)^{\rho} \quad (4.61)$$

$$q = \left(\frac{\beta}{\beta+\alpha-1} \right)^{\rho} \quad (4.62)$$

With the same type of approximation used to find eqns 4.53-4.55, one obtains

$$\frac{\theta_{1d}}{F_1} \approx \frac{T}{T_1} \frac{\alpha-1}{2\alpha-1} \quad L \ll T \quad (4.63)$$

The exact values of dec amplitude are displayed in fig. 4.18.

4.3.2 Applications

In conventional on-off control, large time lags cause long periods and large values of cycling amplitude. For obvious reasons, among the control objectives is the reduction of the period and cycling amplitude. But the approximate minimum value of the period equals four times the inherent time lag (eqn. 3.37); and the cycling amplitude is roughly proportional to the lag (eqn. 3.13).

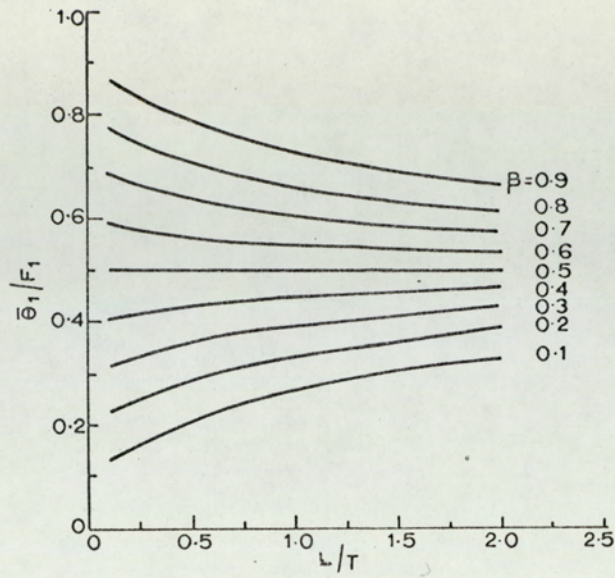


Fig. 4.17

Average output temperature vs delay, where hysteresis is not present

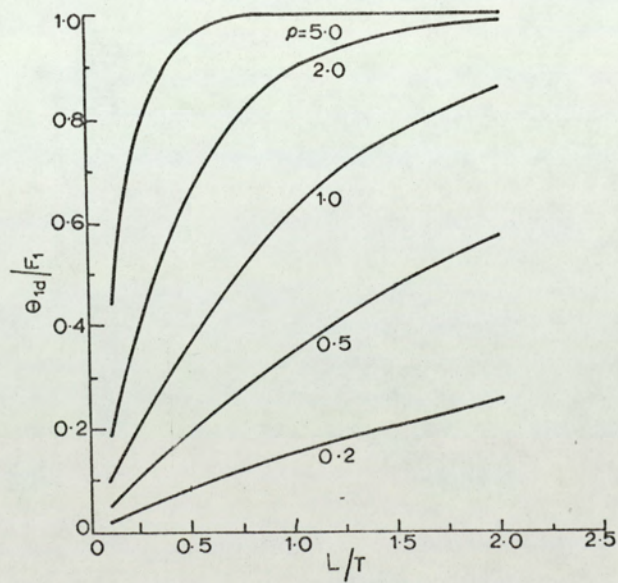


Fig. 4.18

Cycling amplitude vs delay, where hysteresis is not present
 These curves are for $\beta = 0.5$ but β has negligible effect

By having a modified model of the process in the closed loop one can eliminate these effects. The following example makes this idea clear.

Example: The process to be controlled has a time constant of $T_1 = 10$ min. and a large transit delay of $L_1 = 5$ min. The command is $\theta_r = 50^\circ\text{C}$. A controller with negligible hysteresis is used.

For the conventional on-off system, in order to obtain the minimum value of the period, one chooses $\beta = 0.5$ hence $F_1 = 100^\circ$. The period is then, from eqn. 3.30

$$t_q = T_1 \ln [1 + 4\alpha(\alpha - 1)]$$

and since $\alpha = \exp(L_1/T_1) = 1.65$

$$t_q = 10 \ln [1 + 4.3] = 10 \ln 5.3 = 16.7 \text{ min}$$

The amplitude is found from eqn. 3.11, or

$$\theta_{1d} = F_1 \frac{\alpha - 1}{\alpha} = 100 \frac{0.65}{1.65} = 39.4^\circ\text{C}$$

This is a very high value, and it renders the control system useless.

For control by the auxiliary model, if one uses a model with $T = 2$ min and $L = 1$ min in the feedback loop and control the process on an open loop basis (still with $\theta_r = 50^\circ\text{C}$ and $F = F_1 = 100^\circ\text{C}$), one has $L/T = 0.5$, and $\rho = T/T_1 = 0.2$. Hence from fig. 4.18

$$\theta_{1d}/100 = 0.08 \quad \text{or} \quad \theta_{1d} = 8^\circ\text{C}$$

which is very much smaller than the result obtained above. Average of the output temperature can be found from fig. 4.17:

$$\bar{\theta}_1/100 = 0.5 \quad \text{or} \quad \theta_1 = 50^\circ\text{C}$$

The period can be found from eqn. 3.30, with $\alpha = 1.65$,

$$t_q = T \ln [1 + 4\alpha(\alpha - 1)] = 2 \ln 5.3 = 3.33 \text{ min}$$

Hence the period is reduced from 16.7 min to 3.33 min.

When the lag in the process is caused by a gas or fluid column between the heater and the location of prime importance^{32,35} (l.p.i.), the above example corresponds to shifting the temperature sensing point from the l.p.i. towards the heater (fig. 4.19). In this way the portion of the process included in the feedback loop (A in fig. 4.19) becomes shorter, hence the time constant of this portion becomes smaller, even though L/T ratio remains constant. As is shown in the above example, better performance criteria (smaller dec amplitude, smaller periods) are obtained. The disadvantage of this scheme is that the disturbances which affect only the open-loop part of the process (B in fig. 4.19) will not be sensed and, therefore, their effects will not be corrected. It is clear that dec amplitude and period will become smaller, hence the performance will be better if we shift the temperature sensing point nearer to the heater, but at the same time the region for which the disturbance is not sensed becomes larger. This confronts the designer with the necessity of a compromise.

The process which is included in the feedback loop can be an electrical analogue of the main process. In this case, the parameters of this model must be different than those of the main process, in order to obtain better performance. When

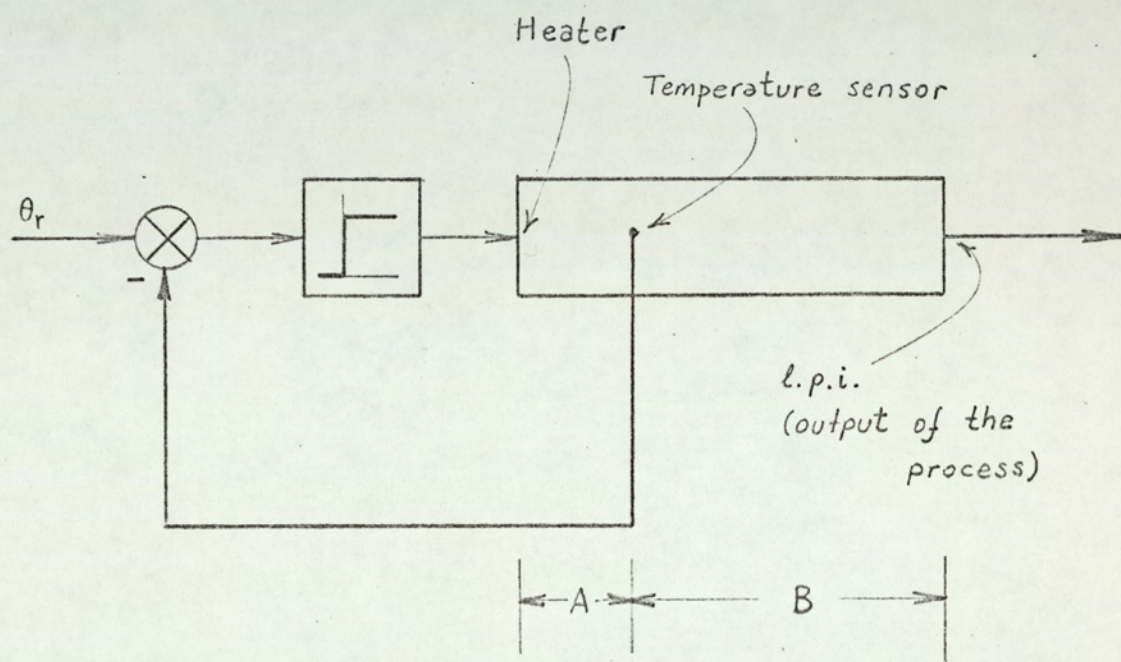


Fig. 4.19

Shifting the temperature sensing point from l.p.i. towards the heater.

using such a model, it is important to ensure that both the model and the process are subjected to the same disturbances, as in fig. 4.13. If the model is energised from the ^{same} voltage supply as the electroheat, disturbances due to supply-voltage variation are catered for. Disturbances arising from the change of ambient temperature, and from the quantity, quality and initial temperature of the charge will require special instrumentation to feed corresponding signals to the model.

The indirect-control approach presented in this chapter can also be applied to a wide variety of control problems.

4.4. SUMMARY

In this chapter open-loop control and indirect control (control by model) are investigated. The advantages and disadvantages of both are discussed. It is shown that, by using indirect control, with a suitable choice of the model parameters, performance criteria can be substantially improved.

Computer programmes for the digital simulation of open loop control systems are given, and examples are included.

5

PULSE WIDTH MODULATION CONTROL

5.1 INTRODUCTION

Pulse width modulation (PWM) found many applications in the field of communications and control since its theoretical investigation started 13 years ago. PWM has some definite advantages over the conventional sampled data systems. But on the other hand it is an inherently nonlinear process. Because of this, analysis of PWM systems are more difficult than, for example, pulse amplitude modulation (PAM) systems which are basically linear.

The first PWM system was described by Gouy in an historic paper 72 years ago¹⁶. His system was actually a PWM electroheat regulation scheme. This regulation system (fig. 5.1) consists of a resistively heated oven, a relay, a mercury thermometer and an electrical contact mounted on a motor driven eccentric. From fig. 5.1 it is clear that the sequence of current pulses passing through the resistive heating element has a constant period set by the speed of the motor. The duration of the pulses, however, depends on the time that the contact is immersed in the mercury, i.e. the level of the mercury in the thermometer. Since the level of the mercury is a function of

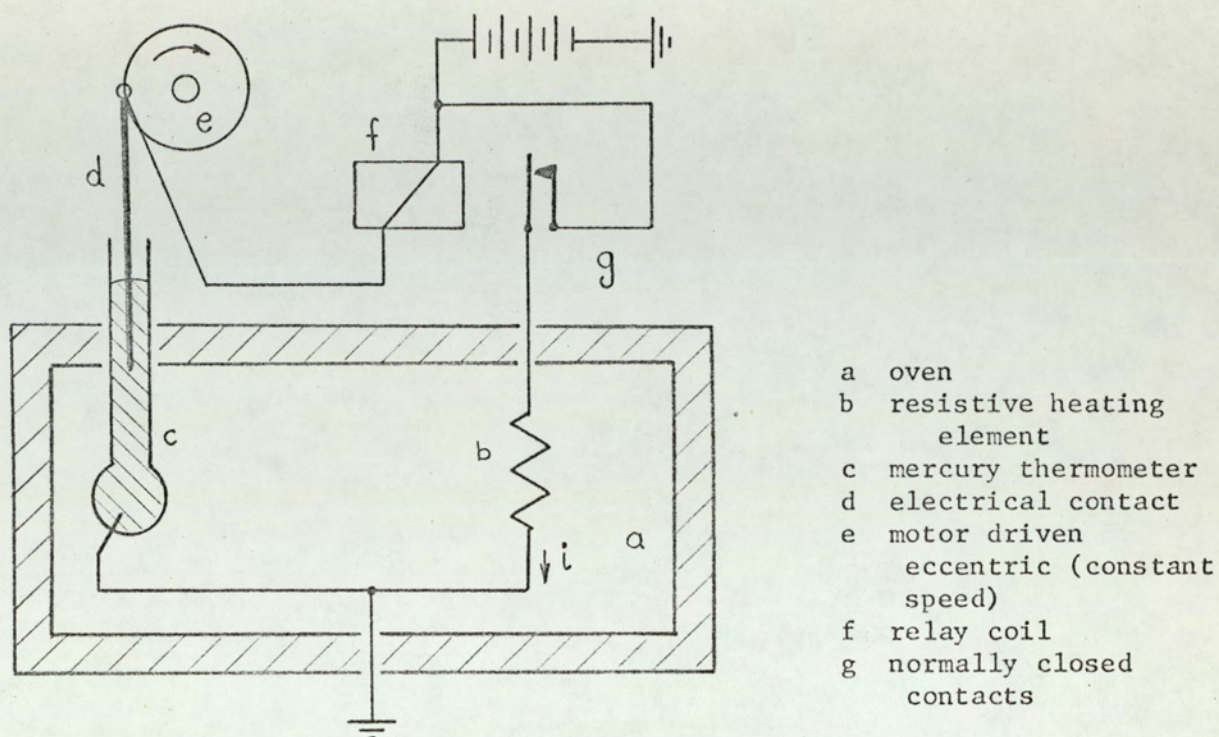


Fig. 5.1 Gouy temperature regulator

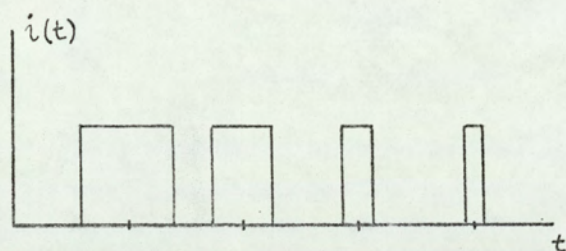


Fig. 5.2

Typical pulse train through the heating element of Gouy temperature regulator

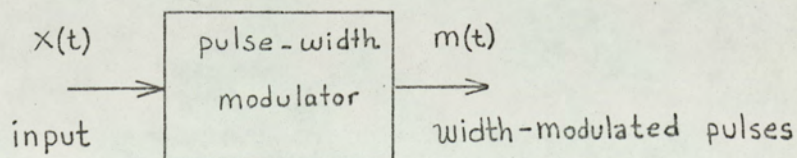


Fig. 5.3

Block diagram of pulse width modulator

the oven temperature, a closed loop control is achieved in this way. In fig. 5.2 a typical pulse train through the heating element is shown. This waveshape will be compared with today's standard PWM outputs in the next section.

PWM remained one of the unexplored topics in control-theory until 1956. Starting with Shnaidman⁴⁰ in U.S.S.R. (1956) and Nease²⁸ in U.S.A. (1957) investigators began to publish papers in this field. Since PWM systems are described by nonlinear equations, an exact analysis is very difficult. Approximate methods of analysis generally depend on either linearization or describing function techniques. Andeen² used linearization, and assumed non-saturating PWM systems only. Delpheld and Murphy¹² resorted to describing function analysis. Gelb and Vander Velde¹⁴ also presented a short account on the describing function analysis of PWM systems. Stability conditions can be investigated by using Lyapunov's second method. Nelson²⁹ and Kadota and Bourne²⁰ are among the authors who used Lyapunov's method for stability analysis.

Approximation methods like linearization and describing function analysis can only be used for the investigation of local stability and small deviations³⁰. Linearization methods overlook the inherent nonlinearities in the system. Describing function analysis fails to give correct results when it is applied to first order systems. On the other hand, results obtained by Lyapunov's second method are, in general, conservative; since this method yields only sufficient conditions for stability, but not necessary and sufficient conditions.

Because of the reasons mentioned above, an exact analysis of the limit cycling behaviour and stability of PWM control of electroheat systems is presented in this study. Another reason for this analysis is the fact that although PWM is first

presented as a means of electroheat regulation (by Gouy), later papers overlook the possible applications of PWM to electroheat control. Emphasis has been mainly on communication systems and control of mechanical quantities.

In general, PWM has the following advantages^{2,27}:

1. PWM systems are less susceptible to noise, since noise affects the amplitude of the signal, whereas in PWM, information is conveyed by the duration of pulses.
2. The output stage of the PWM can be a simple relay. As a result of this, large amounts of power can be handled with low cost equipment.
3. Compared to on-off control, PWM has the following advantages:
 - a. For on-off control, the cycling period depends on the time lag of the plant and the controller hysteresis and, thus, may attain undesirably large values. On the other hand, for PWM control the period is under the command of the designer.
 - b. For on-off control, cycling amplitude may attain large values. Especially if the L/T ratio of plant is large, large values of the cycling amplitude render the control system useless. On the other hand the cycling amplitude for the PWM control system can be reduced to a low level by choosing small sampling intervals.
 - c. The effects of hysteresis can be eliminated in PWM systems.
4. Compared to open-loop control, PWM has the following advantages:
 - a. Since PWM control is a closed-loop control, the

effects of disturbance are greatly reduced, or eliminated.

- b. Start up time for open-loop control systems is large. On the other hand, start up time is optimal for PWM systems, since the control is on-off until the output reaches the command.
5. With PWM a continuously varying control parameter (t_o/t_p) can be obtained by using on-off devices (relays, thyristors, etc). Therefore many of the advantages of continuous control is achieved with low cost elements.
6. One point which is regarded² as a disadvantage of the PWM is that PWM can only be used where the control object has a low pass characteristic. (To filter down the ripple caused by the pulsed nature of the control the plant should have low pass characteristic. The same requirement also applies to on-off and open-loop control systems of chapters 2 and 3). Since the characteristics of all electroheat processes are low pass in nature the application of PWM creates no problem.

In this chapter an analysis of PWM electroheat control systems is presented. In section 5.2 PWM is defined, and various types of PWM are discussed. A PWM system with only positive going output pulses is defined. This is necessary, since most electroheat control systems use the on-off (heat-off)^{30,32} principle. In section 5.3, after a brief introduction to the solution of system differential equations for sampled data systems, a state variable formulation of the PWM control system is presented. Some numerical examples are included. Since the calculation of system behaviour is rather cumbersome,

a digital computer programme for the simulation of PWM control systems is developed and the results are discussed. This programme is also used to check and verify the analysis of limit cycle behaviour of PWM systems, which is the main topic of chapter 6.

5.2 PULSE WIDTH MODULATION AS A SAMPLING PROCESS

Sampling processes can be divided in three categories²⁷:

1. Fixed-pattern sampling
2. Signal dependent sampling
3. Random sampling

In the first category the sampling period and the duration of the pulses are independent of the signals flowing in the system. Therefore sampling processes of this category are linear in the sense that inputs and outputs are governed by the superposition principle. This category can be divided into many types, the simplest and well-known one being the classical sampling scheme, where the pulses are periodic with a fixed period t_q , and the pulse duration is sufficiently short, so that the pulses may be regarded as impulses. The information is carried through the changes in the pulse amplitude, hence this category is called pulse amplitude modulation (PAM). Cyclic variable rate, multirate, and finite pulse width sampling schemes are in this category^{27,44}.

In the second category, the sampling period and/or the duration of the pulses are dependent on the signals flowing in the system. This type of sampling, therefore, is basically non-linear; hence linear system theory is no longer applicable to these systems. Among these systems are pulse width modulation (or as it is sometimes called variable pulse width sampling, or

pulse duration modulation), pulse frequency modulation and double (pulse frequency-pulse width) modulation²² systems.

In the third category, sampling instances are random. This type of sampling can only be treated by statistical methods.

PWM schemes can be divided into four types^{20,27}:

1. lead type
2. lag type
3. lag-delay type
4. lag-delay-integrator type

A block diagram of a pulse width modulator is shown in fig. 5.3

The input signal is sampled with a constant period, denoted by t_s . The width of the pulse is proportional to the absolute value of (1) the input signal for the lead, lag, and lag-delay type, and (2) the integral of the input signal for the lag-delay-integrator type. Since the pulse width cannot be larger than t_s , saturation occurs for large values of the input voltage. The height of the pulses are +1 or -1 according to the polarity of the input signal (or the polarity of the integral of the input signal, for the integrator type). A typical input signal and the output waveforms for PAM (finite pulse width type) and four different types of PWM are shown in fig. 5.4. The modulation type for the Gouy regulator, shown in fig. 5.2 does not correspond to any of the types shown in fig. 5.4. But when the sampling period is small compared to the smallest time constant in the system; lead, lag and Gouy types of PWM yield approximately same behaviour. Types of PWM shown in fig. 5.4 have been extensively used in communication systems. Note that for all these types, the output signal can assume positive or negative values. For electroheat control, a positive input to the plant means heating, while a negative input means cooling. A controller with -1, 0, +1 outputs is

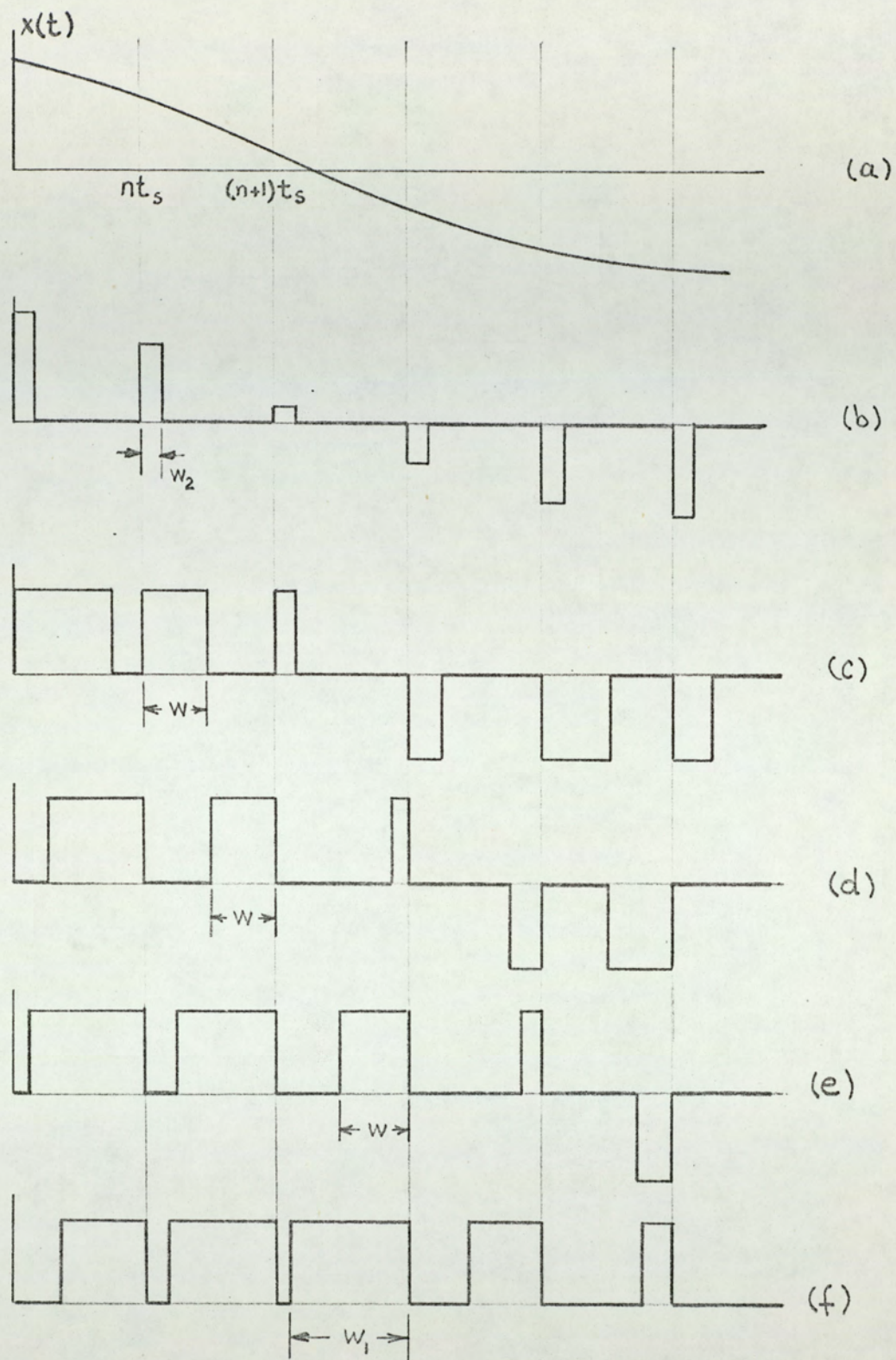


Fig. 5.4

PAM, and various types of PWM. a: input signal, b: PAM, c: lead type PWM, d: lag type PWM, e: lag-delay type PWM, f: lag-delay-integrator type PWM. w is proportional to $|x(nt_s)|$, w_1 is proportional to the integral of $x(t)$ up to $t=nt_s$, w_2 is constant.

not suitable for the control of electric heating. Because of this a modified version of PWM is adapted in this work. This version has only positive going pulses at the output. It is clear that four types of PWM, as shown in fig. 5.4, also exist for this version. Since the lead type PWM is especially suitable for dc thyristor (SCR) control²³ (and easier to implement, in general) this type of PWM will be considered in this study. Lead type PWM with positive pulses is shown in fig. 5.5. The output of the modulator is given by:

$$m(t) = \begin{cases} 1 & \text{for } nt_s \leq t \leq nt_s + \gamma_n t_s \\ 0 & \text{for } nt_s + \gamma_n t_s \leq t \leq (n+1)t_s \end{cases} \quad (5.1)$$

where $\gamma_n = f [x(nt_s)]$

The function f defines the modulation law. Generally the modulation law is a linear relationship between two saturation limits, in this case f is the saturation function:

$$\gamma_n = \text{sat} [x(nt_s)] \quad (5.2)$$

where

$$\text{sat}(x) = \begin{cases} 0 & \text{for } x < 0 \\ x & \text{for } 0 \leq x \leq 1 \\ 1 & \text{for } x > 1 \end{cases}$$

Saturation function is shown in fig. 5.6.

If the modulation law is the saturation function, then the upper saturation limit is 1 and the lower saturation limit is 0, i.e. if the input signal at $t = nt_s$ is negative, there

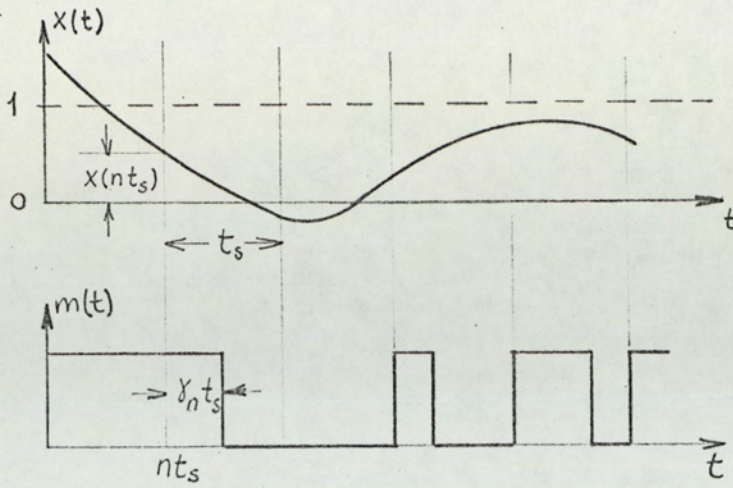


Fig. 5.5

Lead type PWM with positive pulses.

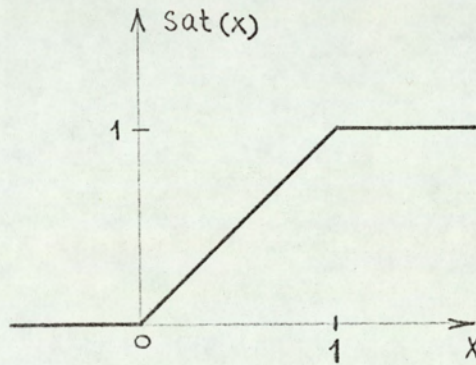


Fig. 5.6

Saturation function.

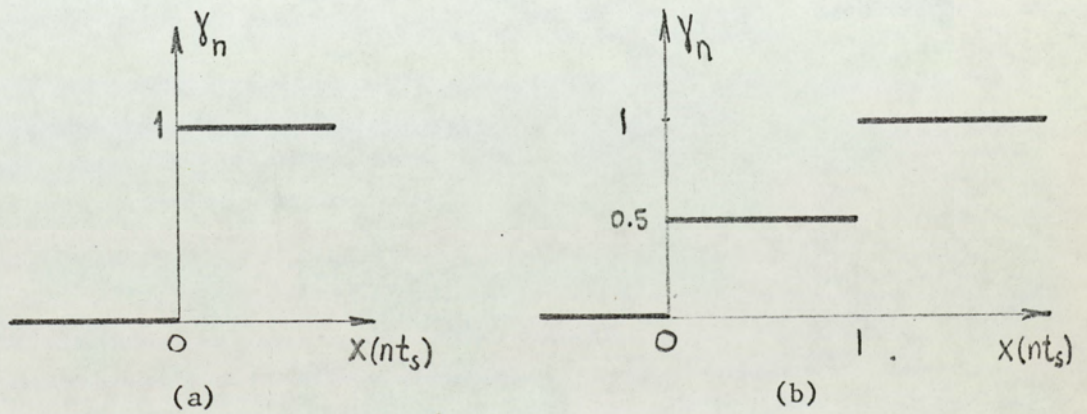


Fig. 5.7

- (a) Modulation law of eqn. 5.3.a
- (b) Modulation law of eqn. 5.3.b.

is no pulse in the n th period; if, on the other hand, the input signal at $t = nt_s$ is larger than 1, pulse duration in the n th period is t_s , so that $m = 1$ for the whole period. If the value of the input signal is between 0 and 1, the pulse duration in the n th period is proportional to the input.

Modulation laws other than the saturation function can be used. An interesting approach is the choice of the following functions:

$$\gamma_n = \frac{1}{2} \left\{ 1 + \operatorname{sgn} [x(nt_s)] \right\} \quad (5.3.a)$$

$$\gamma_n = 0.5 + 0.25 \left\{ \operatorname{sgn} [x(nt_s)] + \operatorname{sgn} [x(nt_s) - 1] \right\} \quad (5.3.b)$$

With the modulation law of the form of eqn. 5.3.a, the PWM system becomes an on-off control system, whereas with a modulation law as in eqn. 5.3.b it becomes a three-level control system. The control laws given in eqns. 5.3.a and 5.3.b are shown in fig. 5.7. In fact, by choosing appropriate modulation laws, nearly all types of conventional control can be investigated as special cases of PWM.

5.3 ANALYSIS OF PWM CONTROL SYSTEMS

5.3.1 Description of the system

The modulator is assumed lead type, with positive going pulses, as described by equations 5.1. The plant is assumed a Ziegler-Nichols model:

$$F \exp(-sL)/(1 + sT)$$

where the only restriction is that L is assumed an integer

multiple of the sampling period:

$$L = u t_s, \quad u \text{ non-negative integer}$$

The block diagram of the control system is shown in fig. 5.8. In fig. 5.8, k is the actual modulator gain. In fact, the block shown dotted in fig. 5.8 is the actual modulator. The quantity b is a bias to shift the PWM characteristic. The block labelled PWM is the modulator defined by eqn. 5.1. The value of the bias depends on T , t_s , and θ_r ; and will be kept constant at a set value depending on T , t_s , and θ_r . This point will be made clear later. If one incorporates the gain k , and the bias b in the modulator, as it is shown dotted in fig. 5.8, the modulator equations become:

$$m = \begin{cases} 1 & \text{for } nt_s \leq t \leq nt_s + \gamma_n t_s \\ 0 & \text{for } nt_s + \gamma_n t_s \leq t \leq (n+1)t_s \end{cases} \quad (5.4)$$

$$\text{where } \gamma_n = f [b + ke(nt_s)] \quad (5.5)$$

or, if f is the usual saturation function law:

$$\gamma_n = \text{sat} [b + ke(nt_s)] \quad (5.6)$$

Equation 5.6 is displayed in fig. 5.9, which shows the overall characteristic of the modulator. From fig. 5.9, one can see that b is actually the (pulse duration/sampling period) ratio for zero error in the system. Then, from fig. 5.8, and for $u \approx 0$, $e = 0$:

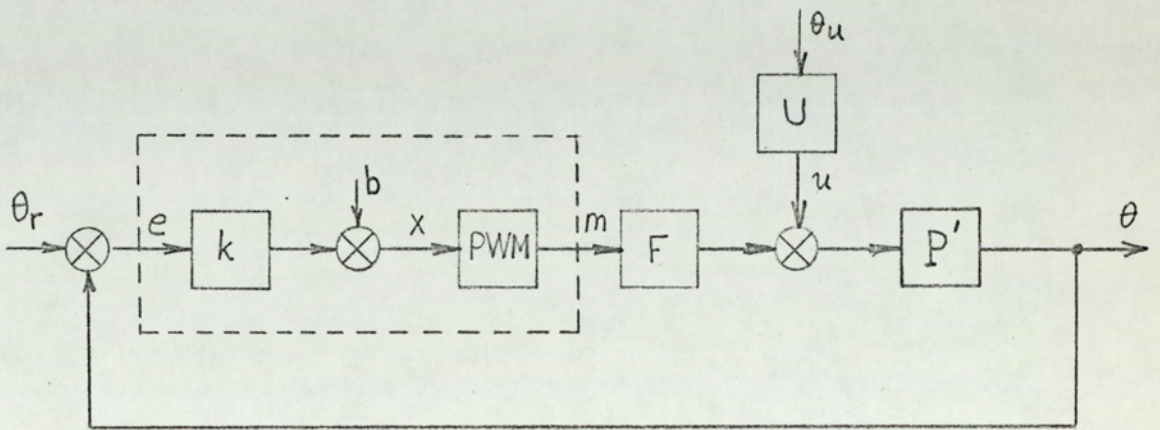


Fig. 5.8

PWM control system

- θ_r = command [$^{\circ}\text{C}$]
- k = gain [$1/^{\circ}\text{C}$]
- b = bias [-]
- θ_u = disturbance temperature [$^{\circ}\text{C}$]
- u = disturbance [-]
- F = plant gain (runaway temperature) [$^{\circ}\text{C}$]
- θ = output temperature [$^{\circ}\text{C}$]
- e = error [$^{\circ}\text{C}$]
- m = modulator output (0 or 1) [-]
- x = modulator input [-]
- U = disturbance transmittance [$1/^{\circ}\text{C}$]
- P' = $\exp(-sL)/(1 + sT)$

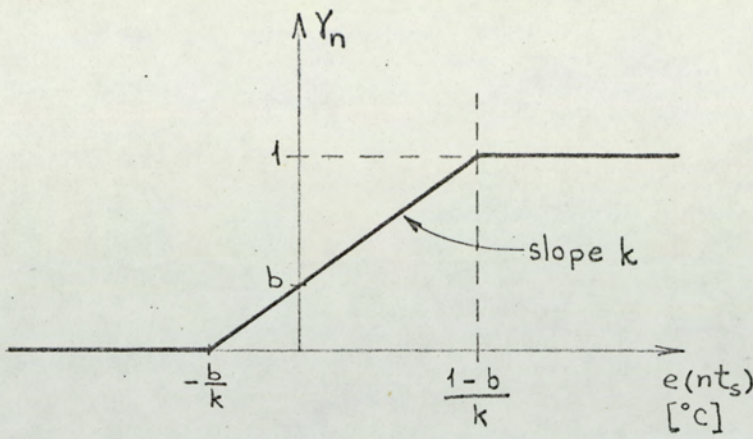


Fig. 5.9
Overall characteristic of the modulator.

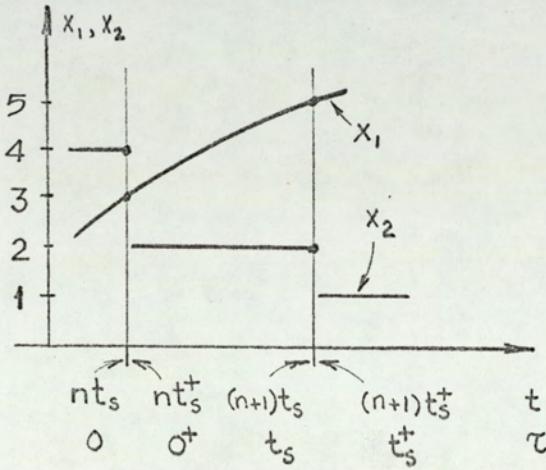


Fig. 5.10
Continuous and discontinuous state variables.

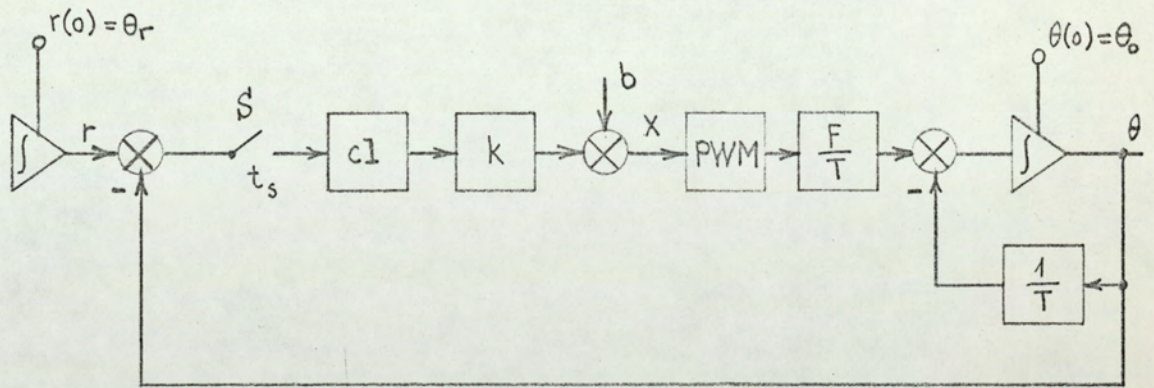


Fig. 5.11
State variable diagram of the PWM control system. Cl: zero order hold (clamp), S: sampler with period t_s , θ_0 : initial value of the temperature.

$$b \approx \theta_r / F$$

(5.7)

5.3.2 Solution of system differential equation for sampled-data systems⁴⁴

Let v denote the state vector of the system. Actually, v consists of the inputs and the proper state variables of the system. The n -th sampling interval, $nt_s < t \leq (n+1)t_s$, is shown in fig. 5.10, with two types of state variables: x_1 , a continuous state variable, such as, for example, the output of an integrator; and x_2 , a discontinuous state variable, such as the output of a sampler-clamp. One can define a new variable, τ , which denotes the time elapsed since the start of the interval, hence $\tau = t - nt_s$. The time instant just before the n -th sampling interval starts is denoted as $t = nt_s$ or $\tau = 0$, whereas the instant just after the n -th interval starts (just after the sampler switch is closed and opened) is denoted as $t = nt_s^+$ or $\tau = 0^+$. For example, referring to fig. 5.10:

$$x_1(nt_s) = x_1(nt_s^+) = 3, \quad x_1 \left[(n+1)t_s \right] = x_1 \left[(n+1)t_s^+ \right] = 5$$

$$x_2(nt_s) = 4, \quad x_2(nt_s^+) = x_2 \left[(n+1)t_s \right] = 2, \quad x_2 \left[(n+1)t_s^+ \right] = 1$$

The system is described by the matrix differential equation:

$$\frac{d}{dt} v(t) = A v(t), \quad nt_s < t \leq (n+1)t_s \quad (5.8)$$

where A is a square coefficient matrix. The initial conditions for the above differential equation can be found from the value

of the state vector at the end of the previous sampling interval:

$$v(nt_s^+) = B v(nt_s) \quad (5.9)$$

This equation describes the transition of the state variables at the sampling instances. B is a square matrix defining this transition. The solution of the scalar differential equation

$$\frac{d}{dt} x(t) = a x(t) \quad (5.10)$$

is given by

$$x(t) = e^{at} x(0^+) \quad (5.11)$$

By analogy to this solution, the solution to the matrix equation 5.8 can be written as:

$$v(t) = e^{At} v(0^+) \quad (5.12)$$

where e^{At} is a matrix defined as:

$$e^{At} = \sum_{k=0}^{\infty} A^k \frac{t^k}{k!}$$

The values of the vector v at two different instants of time can be related to each other in the following way.

From eqn. 5.12:

$$v(0^+) = e^{-At} v(t) \quad (5.13)$$

for $t = t_1$:

$$v(0^+) = e^{-At_1} v(t_1) \quad (5.14)$$

Substituting this value of $v(0^+)$ back into eqn. 5.12, and for $t = t_2$:

$$v(t_2) = e^{At_2} e^{-At_1} v(t_1) = e^{A(t_2-t_1)} v(t_1) \quad (5.15)$$

Equation 5.15 relates the values of vector v at t_2 and t_1 . Note that both t_1 and t_2 should be in the same sampling interval. It is usual to denote the matrix e^{At} by $\Phi(t)$, and call it the overall transition matrix. With this new notation; and with $t_2 = t$, $t_1 = nt_s^+$ (initial time for the n th sampling interval):

$$v(t) = \Phi(t - nt_s) v(nt_s^+) \quad nt_s < t \leq (n+1)t_s \quad (5.16)$$

Equation 5.16 gives the values of v for any time in the n th sampling interval, provided that its initial value for that interval, $v(nt_s^+)$, is known. Equations 5.9 and 5.16 can be combined together:

$$v(t) = \Phi(t) B v(nt_s), \quad nt_s < t \leq (n+1)t_s \quad (5.17)$$

Equation 5.17 can be used successively ($n = 0, 1, 2, \dots$) to find the behaviour of the system.

Matrices A and B can be written from the state-variable diagram of the system by inspection. The matrix Φ can be found from the equation $\Phi(t) = e^{At}$. A simpler method to find Φ can

be obtained by solving eqn. 5.8 by the Laplace transform method:

$$sV(s) = AV(s) + v(0^+) \quad (5.18)$$

or

$$V(s) = [sI - A]^{-1} v(0^+) \quad (5.19)$$

where I is the unit matrix of the same order as A . Taking inverse Laplace transform;

$$v(\tau) = \mathcal{L}^{-1} [(sI - A)^{-1}] v(0^+) \quad (5.20)$$

where \mathcal{L}^{-1} denotes inverse Laplace transformation. By comparing eqns. 5.20 and 5.12

$$\Phi(\tau) = \mathcal{L}^{-1} [(sI - A)^{-1}] \quad (5.21)$$

Equation 5.21 provides an easier way of finding the matrix Φ .

5.3.3 Analysis of the PWM system

The state variable diagram of the PWM system of fig. 5.8 is shown in fig. 5.11. The delay in the plant and the disturbance are taken zero for the time being. The constant input θ_r is taken as an element of the state vector v , and it is denoted by r . Clamp and integrator outputs are to be taken as state variables. Therefore, a suitable choice for state variables is the pair θ, x . The state vector, and its initial value is:

$$v = \begin{bmatrix} r \\ \theta \\ x \end{bmatrix} \quad v(0) = \begin{bmatrix} r \\ \theta_0 \\ b \end{bmatrix} \quad (5.22)$$

On interval

$$nt_s < t \leq nt_s + \gamma_n t_s, \quad \gamma_n = f [x(nt_s^+)] , m = 1$$

The system differential equations for this interval are:

$$\dot{r} = 0 \tag{5.23 a}$$

$$\dot{\theta} = \frac{F}{T} m - \frac{1}{T} \theta = - \frac{1}{T} \theta + \frac{F}{T \cdot x(nt_s^+)} x(nt_s^+) \tag{5.23 b}$$

$$\dot{x} = 0 \tag{5.23 c}$$

From eqns. 5.23 a, b, and c, the matrix A_1 which is the coefficient matrix for the on interval can be written as:

$$A_1 = \begin{bmatrix} 0 & 0 & 0 \\ 0 & -\frac{1}{T} & \frac{F}{T \cdot x} \\ 0 & 0 & 0 \end{bmatrix} \tag{5.24}$$

where x denotes $x(nt_s^+)$

From eqn. 5.24:

$$sI - A_1 = \begin{bmatrix} s & 0 & 0 \\ 0 & s + \frac{1}{T} & -\frac{F}{Tx} \\ 0 & 0 & s \end{bmatrix} \tag{5.25}$$

Taking inverse:

$$(sI - A_1)^{-1} = \begin{bmatrix} \frac{1}{s} & 0 & 0 \\ 0 & \frac{T}{1+sT} & \frac{F}{x \cdot s \cdot (1+sT)} \\ 0 & 0 & \frac{1}{s} \end{bmatrix} \quad (5.26)$$

Finally, taking the inverse Laplace transform of eqn. 5.26, Φ_1 , the overall transition matrix for the on period is found:

$$\Phi_1(\tau) = \mathcal{L}^{-1} (sI - A)^{-1} = \begin{bmatrix} 1 & 0 & 0 \\ 0 & e^{-\tau/T} & \frac{F}{x}(1 - e^{-\tau/T}) \\ 0 & 0 & 1 \end{bmatrix} \quad (5.27)$$

The state transition equations are:

$$r(nt_s^+) = r(nt_s) \quad (5.28a)$$

$$\theta(nt_s^+) = \theta(nt_s) \quad (5.28b)$$

$$\begin{aligned} x(nt_s^+) &= b(nt_s) + k [r(nt_s) - \theta(nt_s)] \\ &= kr(nt_s) - k\theta(nt_s) + \frac{b}{x(nt_s)} \cdot x(nt_s) \end{aligned} \quad (5.28c)$$

The state transition matrix for the on period, B_1 , can be written from eqns. 5.28a, b, and c:

$$B_1 = \begin{bmatrix} 1 & 0 & 0 \\ 0 & 1 & 0 \\ k & -k & \frac{b}{x(nt_s)} \end{bmatrix} \quad (5.29)$$

The value of the state vector v can be calculated from eqns. 5.9 and 5.16, with $\Phi_1(\tau)$ and B_1 as given in eqns. 5.27 and 5.29, for any time instant in the on interval of the n th sampling period. In particular, for $t = nt_s + \gamma_n t_s$, i.e. for the end of the on interval, the state vector is given by:

$$v(nt_s + \gamma_n t_s) = \Phi_1(\gamma_n t_s) v(nt_s^+) \quad (5.30a)$$

$$v(nt_s^+) = B_1 v(nt_s) \quad (5.30b)$$

Off interval

$$nt_s + \gamma_n t_s < t \leq (n+1)t_s, \quad \gamma_n = f [x(nt_s^+)], \quad m = 0$$

The system differential equations are:

$$\dot{r} = 0 \quad (5.31a)$$

$$\dot{\theta} = -\frac{1}{T} \theta \quad (5.31b)$$

$$\dot{x} = 0 \quad (5.31c)$$

The coefficient matrix for the off interval, A_2 , is found from eqns. 5.31 a, b, and c:

$$A_2 = \begin{bmatrix} 0 & 0 & 0 \\ 0 & -\frac{1}{T} & 0 \\ 0 & 0 & 0 \end{bmatrix} \quad (5.32)$$

Therefore:

$$sI - A_2 = \begin{bmatrix} s & 0 & 0 \\ 0 & s + \frac{1}{T} & 0 \\ 0 & 0 & s \end{bmatrix} \quad (5.33)$$

and

$$(sI - A_2)^{-1} = \begin{bmatrix} \frac{1}{s} & 0 & 0 \\ 0 & \frac{T}{1+sT} & 0 \\ 0 & 0 & \frac{1}{s} \end{bmatrix} \quad (5.34)$$

Hence the overall transition matrix for the off period, Φ_2 , is:

$$\Phi_2(\tau) = \mathcal{L}^{-1} \left[(sI - A)^{-1} \right] = \begin{bmatrix} 1 & 0 & 0 \\ 0 & e^{-\tau/T} & 0 \\ 0 & 0 & 1 \end{bmatrix} \quad (5.35)$$

Since no change occurs in the sampler status while passing from the on interval to the off interval

$$B_2 = \begin{bmatrix} 1 & 0 & 0 \\ 0 & 1 & 0 \\ 0 & 0 & 1 \end{bmatrix} = I, \quad (5.36)$$

that is, the state variables are continuous at $t = nt_s + \gamma_n t_s$

The value of the state vector at any time in the off interval of the n-th sampling period is given by:

$$v(t) = \Phi_2(t - nt_s - \gamma_n t_s) \cdot v(nt_s + \gamma_n t_s) \quad (5.37)$$

In particular, at the end of the period, $t = (n + 1)t_s$:

$$v \left[(n + 1)t_s \right] = \Phi_2 (t_s - \gamma_n t_s) \cdot v(nt_s + \gamma_n t_s) \quad (5.38)$$

A similar formulation can easily be given for higher order systems, by increasing the order of v , A , B and Φ .

Numerical Example

Consider a PWM control system with the following parameter values:

plant time constant	$T = 50$ min
sampling period	$t_s = 10$ min
initial output temp.	$\theta_o = 20^\circ\text{C}$
plant runaway temp.	$F = 100^\circ\text{C}$
command	$\theta_r = 80^\circ\text{C}$
modulator gain	$k = 0.01$ $1/^\circ\text{C}$
bias	$b = 0.815$
modulation law	sat function (fig. 5.6)

In order to find the output temperature as a function of time, one proceeds as follows:

The initial value of the state vector is, from eqn. 5.22:

$$v(0) = \begin{bmatrix} 80 \\ 20 \\ 0.815 \end{bmatrix}$$

$n = 0$, on period:

From eqn. 5.29:

$$B_1 = \begin{bmatrix} 1 & 0 & 0 \\ 0 & 1 & 0 \\ 0.01 & -0.01 & 1 \end{bmatrix}$$

From eqn. 5.30.b:

$$v(0^+) = \begin{bmatrix} 1 & 0 & 0 \\ 0 & 1 & 0 \\ 0.01 & -0.01 & 1 \end{bmatrix} \begin{bmatrix} 80 \\ 20 \\ 0.815 \end{bmatrix} = \begin{bmatrix} 80 \\ 20 \\ 1.415 \end{bmatrix}$$

$$x(0^+) = 1.415 \quad \gamma_0 = \text{sat}(1.415) = 1$$

$$\gamma_0 t_s = 10$$

From eqn. 5.27:

$$\Phi_1(10) = \begin{bmatrix} 1 & 0 & 0 \\ 0 & 0.82 & 12.7 \\ 0 & 0 & 1 \end{bmatrix}$$

From eqn. 5.30.a

$$v(10) = \Phi_1(10) \begin{bmatrix} 80 \\ 20 \\ 1.415 \end{bmatrix} = \begin{bmatrix} 80 \\ 34.4 \\ 1.415 \end{bmatrix}$$

n = 1, on period:

$$x(10) = 1.415$$

$$B_1 = \begin{bmatrix} 1 & 0 & 0 \\ 0 & 1 & 0 \\ 0.01 & -0.01 & 0.576 \end{bmatrix}$$

$$v(10^+) = B_1 v(10) = \begin{bmatrix} 80 \\ 34.4 \\ 1.271 \end{bmatrix}$$

$$x(10^+) = 1.271 \quad \gamma_1 = \text{sat}(1.271) = 1$$

$$\gamma_1 t_s = 10$$

$$\Phi_1(10) = \begin{bmatrix} 1 & 0 & 0 \\ 0 & 0.82 & 14.1 \\ 0 & 0 & 1 \end{bmatrix}$$

$$v(20) = \Phi_1(10) v(10^+) = \begin{bmatrix} 80 \\ 46.2 \\ 1.271 \end{bmatrix}$$

Similarly:

$$v(20^+) = \begin{bmatrix} 80 \\ 46.2 \\ 1.153 \end{bmatrix}, \quad \gamma_2 = 1,$$

$$v(30) = \begin{bmatrix} 80 \\ 55.9 \\ 1.153 \end{bmatrix}$$

$$v(30^+) = \begin{bmatrix} 80 \\ 55.9 \\ 1.056 \end{bmatrix}, \quad \gamma_3 = 1,$$

$$v(40) = \begin{bmatrix} 80 \\ 63.8 \\ 1.056 \end{bmatrix}$$

$$v(40^+) = \begin{bmatrix} 80 \\ 63.8 \\ 0.977 \end{bmatrix}, \quad \gamma_4 = 0.977$$

Then, for $t = 40 + (0.977)(10) = 49.77$:

$$v(49.77) = \Phi_1(9.77) v(40^+) = \begin{bmatrix} 80 \\ 63.8 \\ 0.977 \end{bmatrix}$$

$n = 4$, off interval

$$v(50) = \Phi_2(0.23) v(49.77)$$

$$\Phi_2(0.23) = \begin{bmatrix} 1 & 0 & 0 \\ 0 & 0.995 & 0 \\ 0 & 0 & 1 \end{bmatrix}$$

$$v(50) = \begin{bmatrix} 80 \\ 71.5 \\ 0.977 \end{bmatrix}$$

n = 5, on interval:

$$v(50^+) = \begin{bmatrix} 80 \\ 70.2 \\ 0.913 \end{bmatrix}, \quad \gamma_5 = 0.913$$

$$v(59.13) = \begin{bmatrix} 80 \\ 75.1 \\ 0.913 \end{bmatrix}$$

n = 5, off interval

$$v(60) = \begin{bmatrix} 80 \\ 75.1 \\ 0.913 \end{bmatrix}$$

The calculation continues according to the above pattern. The result is plotted in fig. 5.12.

From fig. 5.12 the following points of interest are noted:

- a. In the start-up, output of the modulator is constantly on, this results an on-off type (short duration) start-up.
- b. Pulse duration settles at 8.15 min., which is $b \cdot t_s$.



Fig. 5.12

Output temperature corresponding to the numerical example given in the text.

As it was mentioned earlier (see fig. 5.9) the value of the bias is equal to the pulse duration/sampling period ratio for zero error in the system.

c. The value of the output temperature at sampling instants settles to 80°C (command value). In fact the value of the bias (0.815) is deliberately chosen to obtain this result. This point will be explained later, in section 6.2.3.

d. It is evident that the system is stable.

5.4 DICITAL SIMULATION OF PWM CONTROL SYSTEMS

From the numerical example given in section 4.3 it is clear that the calculation of the system response is somewhat cumbersome. In order to investigate the effects of changing various parameters, one needs a quick method of calculation. The state variable approach of section 4.3 is particularly suitable for digital programming.

The digital simulation programme for the simulation of PWM systems is called PWMSYS. The programme is for first order systems, but it can easily be converted to handle second or higher order systems.

The programme PWMSYS requires the following five subprogrammes:

- a. A subroutine for matrix multiplication: SUBMUL
- b. A subroutine for printing and plotting: SPLOT5
- c. A subroutine for introducing delay to the system:
SUBLAG
- d. A function subprogramme to define the modulation law. For this purpose, three subprogrammes are used: FUNSAT, SATN2, and SATN10. The modulation laws corresponding to these subprogrammes are defined in appendix A.
- e. A function subprogramme to define the disturbance.

For this purpose, several subprogrammes are used: FUND, for zero disturbance; FRAMP2 for ramp disturbance; FSTEP2 for step disturbances; and FSIN for sinusoidal disturbances.

Flowchart and Fortran listing for programme PWMSYS and for the subprogrammes are given in appendix A.

The programme PWMSYS follows the procedure described in section 5.3. Some important points are explained below:

1. The data to be supplied to the programme are: sampling period, time constant of the plant, modulator gain, runaway temperature of the plant, command value, the initial value of the output temperature, and the delay in the plant (as $\mu = L/t_s$ where μ is an integer). In case of step disturbance, the value of the step, and the time instant when it is applied should also be given as data. In case of sinusoidal disturbance the parameters of the sinusoid (amplitude, average value and period) are to be supplied.

2. The value of the bias is internally calculated according to the equation:

$$b = \frac{T}{t_s} \ln \left[1 + \frac{\theta_r}{F} (e^{t_s/T} - 1) \right] \quad (5.39)$$

This equation, found from the difference equation of the system will be derived and explained in section 6.2.3. This value of b results in a steady-state value of the output temperature (at sampling instances) equal to command value. Note that, for small values of t_s/T , eqn. 5.39 becomes:

$$b \approx \frac{\theta_r}{F}$$

which was given in eqn. 5.7.

This internal calculation corresponds to a forward loop in the system block diagram, considering t_s , T , and F constant (fig. 5.13).

3. The delay is introduced to the system in the following way. Since the plant is linear, the blocks representing delay and the first order parts of the plant can be separated and their order is immaterial. Hence to simulate the delay in the plant, it is sufficient to delay γ_n by an amount of $L = \mu t_s$. This delay can be achieved by a shifting algorithm as shown in fig. 5.14.

4. The disturbance is introduced as a function subprogramme. The disturbance is assumed constant during one sampling period. This is equivalent to assuming a slowly varying disturbance.

5. The use of subroutine SPLOT5 makes plotting possible. Since the teletype can plot only with equal increments along time axis, the values of the output temperature only at sampling instants are plotted. However, the values at $t = (n + \gamma_n)t_s$ can be obtained by using the printing option.

6. The value of the state vector v at $t = nt_s$ is called internally V , whereas the value at $t = nt_s^+$ is called Z , and the value at $t = (n + \gamma_n)t_s$ is called U . Using this notation, the programme, in plotting mode, plots successive values of V , on the other hand, in printing mode, it is possible to print only V values, or V and U values. These options are selected by assigning different values to NV and NU , as explained in appendix A.

7. In plotting mode, scaling of the temperature axis is obtained by furnishing a scaling factor as data. On the time axis, dimensionless time t/t_s is indicated.

8. In plotting mode the programme plots the output

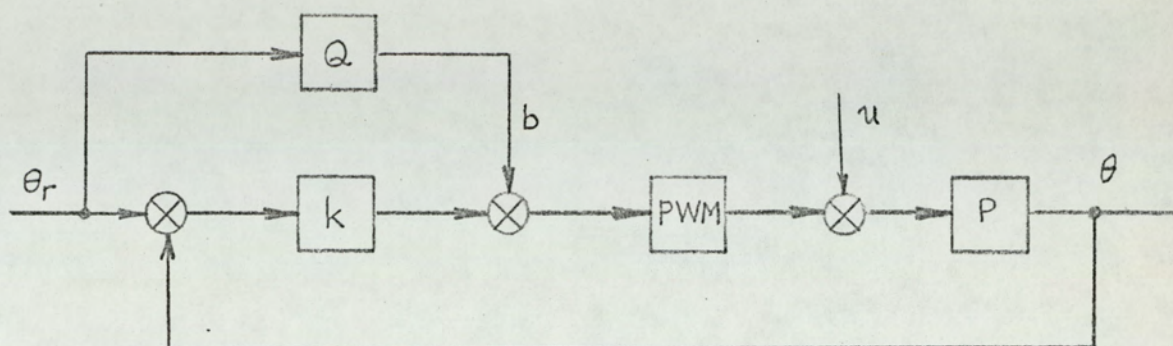


Fig. 5.13

Forward loop showing the dependence of the bias upon command. Q represents the functional relationship given in eqn. 5.39.

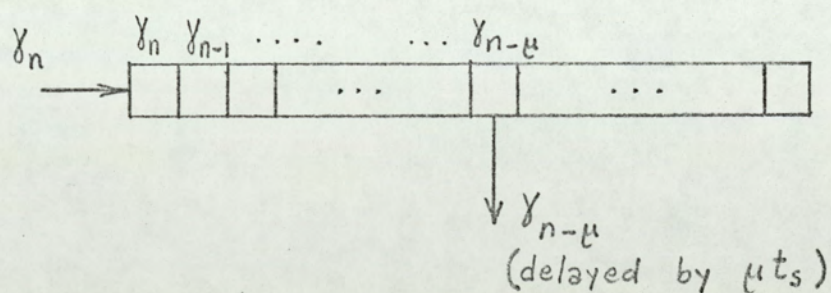


Fig. 5.14

Shifting process to simulate delay.

At each sampling instant a new value of γ is introduced from left, and all existing values are shifted to the right by one location.

temperature $\theta(nt_s)$ and disturbance $\theta_u(nt_s)$ versus $n = t/t_s$; in printing mode it prints the time ($t = nt_s$, and $t = nt_s + \gamma_n t_s$), and corresponding output temperature, modulator input $x(nt_s)$, and disturbance.

Examples

In fig. 5.15 the output temperature plot of a limit cycling PWM system is shown. Until $t = 35 t_s$ the disturbance is zero. The system settles in a 6-1 mode limit cycling. At $t = 35 t_s$ a step disturbance of 62°C is applied and the system changes its mode of limit cycling, and settles in a 1-2 mode. The limit cycling modes will be discussed in chapter 6 in detail.

In fig. 5.16 the output temperature plot of a plant with delay is shown. The output temperature follows a sinusoid whose period is about $8.5 t_s$. Limit cycling for time lag PWM systems will be discussed in chapter 6, and it will be shown that with the parameter values of fig. 5.16, solution of difference equations indicate a sinusoidal oscillation of period $8.47 t_s$. Analogue simulation result corresponding to the same parameter values is given in fig. 6.34 (curve a). From analogue simulation the period of oscillations are found as $8.4 t_s$.

Other examples to digital simulation of the PWM electroheat control system are given in Chapter 6 (figs. 6.30, 6.31, 6.35, 6.36 and 6.37). All these computer outputs are obtained from PWMSYS programmes with relevant subprogrammes.

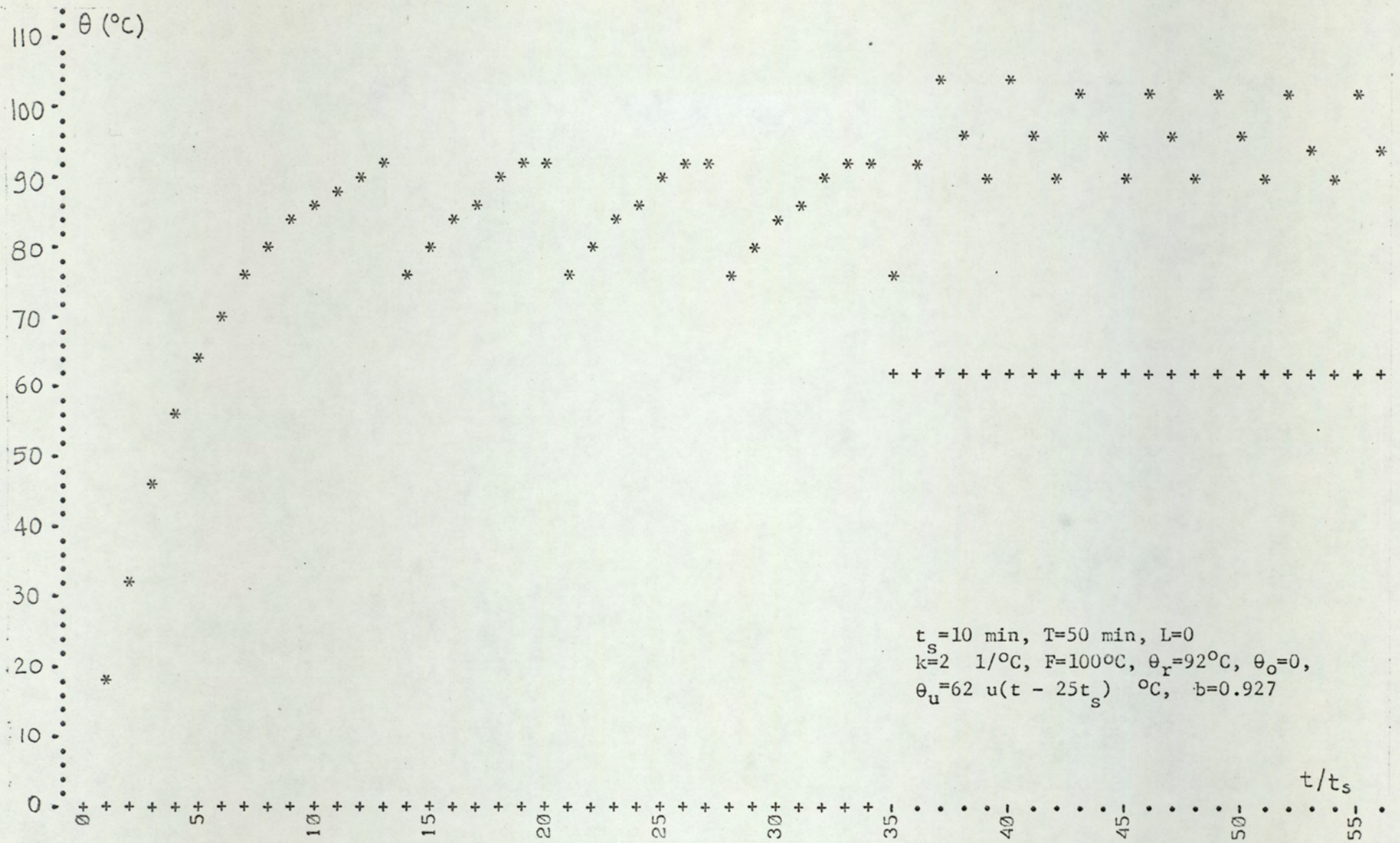


Fig. 5.15

Digital computer printout of the output temperature (*) and disturbance(+) for a PWM control system.

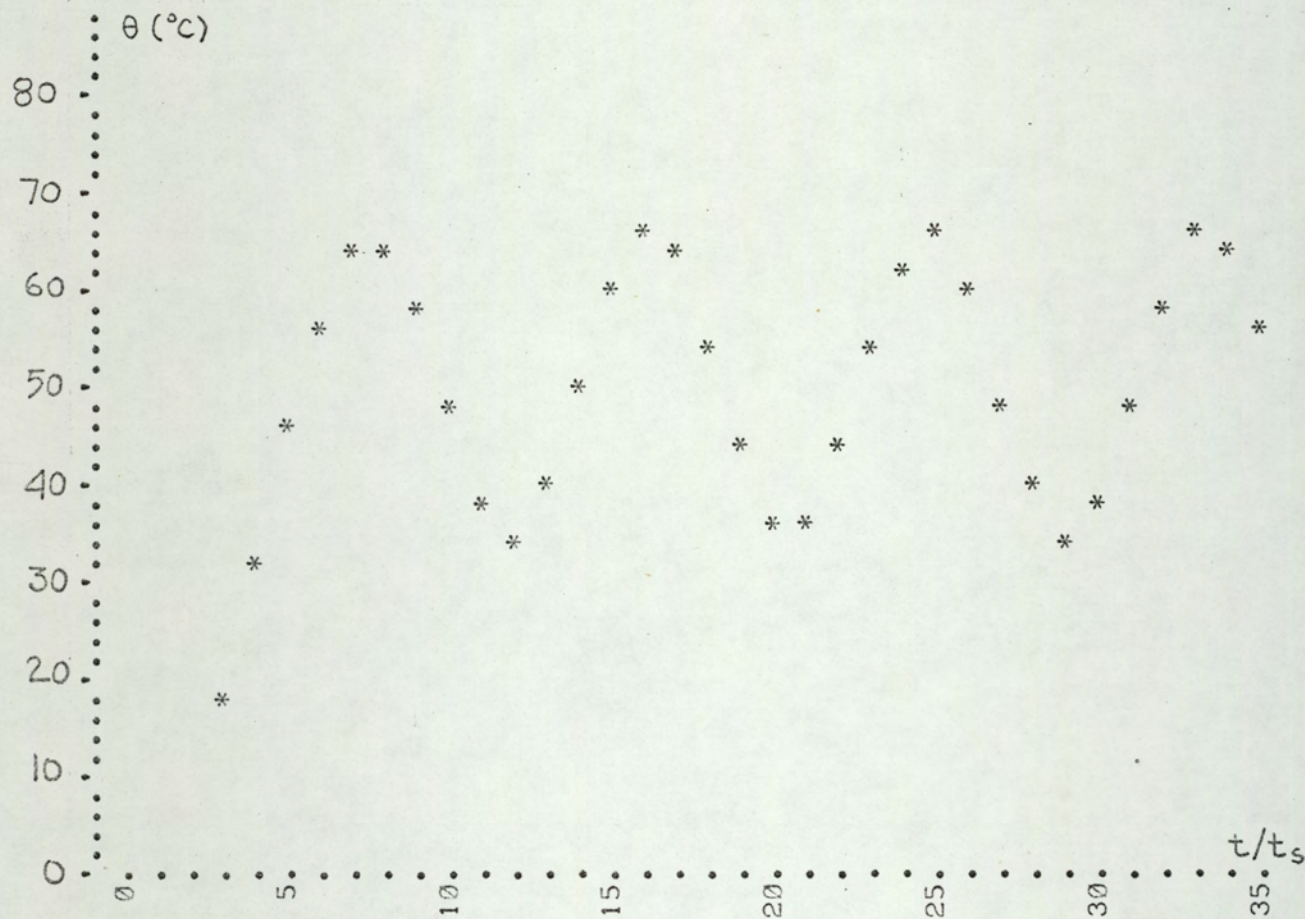


Fig. 5.16

Digital computer printout of the output temperature for a PWM control system. System parameters are: $t_s = 5$ min, $T = 25$ min, $L = 10$ min, $k = 0.045$ $1/^{\circ}\text{C}$, $F = 100^{\circ}\text{C}$, $\theta_r = 50^{\circ}\text{C}$, $\theta_o = 0$, $\theta_u = 0$, $b = 0.52$. The response is oscillatory, The period of the oscillations is about $8.5t_s$.

5.5. SUMMARY

In this chapter an analysis of PWM electroheat control systems is presented. Definitions and various types of PWM are discussed. It was shown that the PWM methods hitherto studied in the literature are not applicable to electroheat systems. Therefore, a PWM system with positive going pulses is defined.

After a brief introduction to the solution of system differential equations for sampled data systems, a state variable formulation of the PWM is presented. This formulation constitutes the basis for the digital simulation also presented in this chapter. Since the formulation of this simulation is based on the state variable technique, it can easily be extended to higher order systems. (In fact the matrix multiplication subroutine is written for matrices up to 10th order). This simulation programme serves the following basic purposes:

1. It provides the insight required for a better understanding of the system operation.
2. It is a powerful tool in the analysis and synthesis of PWM electroheat control systems.
3. It makes it possible to check the analytical results obtained for the PWM control.

This programme comprises subroutines for the simulation of:

1. processes with or without transit delay
2. systems incorporated with various PWM laws,
3. systems subjected to various forms of disturbance.

This programme has been developed in such a way that on-off, open-loop, and multiposition (quasi-continuous) control systems can be simulated by treating them as special cases of PWM control.

6

LIMIT CYCLES IN PWM CONTROL SYSTEMS

6.1 INTRODUCTION

The term "limit cycling" denotes a steady state oscillation of a system which is independent of the initial conditions¹⁴. Limit cycling occurs in almost all nonlinear systems. Terms such as "cycling" and "dynamic equilibrium cycling" (dec) are also used in the literature³² to denote limit cycling. We distinguish two types of cycling:

a. The steady state cycling of a stable system due to the pulsed nature of control. In this type of cycling the output values at sampling instants remains constant in steady state. This type of cycling, which we have called dec in previous chapters, is present even if the control is open-loop. It is an inherent property of relay control systems (or, "pulsed" systems), and is thus unavoidable.

obscure | b. The steady state cycling of the output value at sampling instants. This cycling will be called "limit cycling" in the analysis that will follow.

We call a system stable if its output (state variables at sampling instants) is either constant or approaches a constant value asymptotically. It is clear that a system which

is cycling in the sense of (a) above is stable, whereas a limit cycling system is unstable.

Limit cycling can be desirable in some control applications, especially in mechanical systems, since it provides the vibration which minimizes frictional effects¹⁴. In electroheat systems, limit cycling per se does not provide an advantage. But, since it is desirable to have larger gains for better regulation and large gains cause limit cycling, it is important to know the system performance under limit cycling conditions. Then, should limit cycling not impair system performance, it may be allowed and we may thus benefit from the advantages of higher loop gains.

Limit cycling of PWM systems was first investigated in China by Da-Chuan¹¹ (1959). Da-Chuan investigated the possibility of limit cycles with a period of $2t_s$. Pyskin³¹ used describing function technique to predict limit cycles. Jury and Nishimura¹⁸ used the equivalence of limit cycling PWM systems to the finite length pulse systems with periodically varying sampling pattern. In a further paper Jury and Nishimura¹⁹ used the same technique to find sat-sat mode limit cycles. In literature cited above, and in all other sources the type of PWM investigated was that with positive and negative going pulses, as in fig. 4.4.c. Since this type is not suitable for electroheat control for reasons stated in chapter 4, the results found so far by various authors are not applicable to electroheat control systems. For example, Jury and Nishimura¹⁹ stated that the only possible limit cycling for first order systems was the one with a period of $2t_s$. As will be shown later in this chapter, this is not true for positive pulse PWM. Therefore an analysis of limit cycling phenomenon in PWM electroheat control systems was necessary. Since use

of describing function techniques is limited to systems of order three or more¹⁴ it is not possible to use this technique for electroheat system analysis. In Gelb and Vander Velde¹⁴ describing functions for PWM systems are given for limit cycling periods up to $8t_s$. But as is stated above, these are not applicable to electroheat systems because of the following two reasons:

- a. the different nature of PWM used (positive-negative going pulses)
- b. the inherent limitation of describing function technique (it cannot be used for first order systems).

In this chapter a complete analysis of limit cycling in PWM systems is given, for positive pulse PWM. An exact investigation method is followed, not overlooking the inherent non-linearity of the system, based on the graphical solution of difference equations. Graphical solution of difference equations is a well-known technique¹⁵ especially in economical systems analysis. First (and only) use of this method to analyse PWM systems was by Polak³⁰ who presented a brief graphical analysis of PWM control systems for first order plants (without transit delay). Polak completely overlooked the possibility of sat-sat oscillations.

6.2 GRAPHICAL ANALYSIS OF PWM CONTROL SYSTEMS

6.2.1 Difference equation formulation of the system

The following notation will be used in chapters 6 and 7:

$$\theta_n = \theta(nt_s), e_n = e(nt_s), \phi = t_s/T, A = \exp(-t_s/T)$$

For the system given in fig. 5.8, and with the modulation equations of eqns. 5.4 and 5.6, the equations relating θ_{n+1} to θ_n can be formulated in the following way:

1. Modulator saturated, $\gamma_n = 1$, power is constantly on. This occurs when

$$b + k e_n \geq 1$$

or

$$e_n \geq (1 - b)/k$$

Output of the modulator, m , is 1 for the whole period and we have:

$$\theta(\tau) = \theta_n e^{-\tau/T} + F(1 - e^{-\tau/T}) \quad (6.1)$$

Therefore, for $\tau = t_s$

$$\theta_{n+1} = A \theta_n + F(1 - A) \quad (6.2)$$

2. Modulator saturated, $\gamma_n = 0$, power is constantly off. This occurs when:

$$b + k e_n \leq 0$$

or

$$e_n \leq -b/k$$

$m = 0$ for the whole period, and we have:

$$\theta(\tau) = \theta_n e^{-\tau/T} \quad (6.3)$$

therefore for $\tau = t_s$

$$\theta_{n+1} = A \theta_n \quad (6.4)$$

3. Modulator in its linear region, $0 < \gamma_n = b + k e_n < 1$
and

$$m = 1 \text{ for } 0 < \tau < \gamma_n t_s \text{ (on interval)}$$

$$m = 0 \text{ for } \gamma_n t_s < \tau < t_s \text{ (off interval).}$$

On interval: From eqn. 6.1 and for $\tau = \gamma_n t_s$:

$$\theta(\gamma_n t_s) = \theta_n e^{-\gamma_n t_s/T} + F(1 - e^{-\gamma_n t_s/T}) \quad (6.5)$$

Off interval: From eqn. 6.3, with θ_n replaced by $\theta(\gamma_n t_s)$ as given in eqn. 6.5, and for $\tau = (1 - \gamma_n)t_s$:

$$\theta_{n+1} = \theta_n e^{-\gamma_n t_s/T} e^{-(1-\gamma_n)t_s/T} + F e^{-(1-\gamma_n)t_s/T} (1 - e^{-\gamma_n t_s/T}) \quad (6.6)$$

or

$$\theta_{n+1} = A \theta_n + FA (e^{\gamma_n t_s/T} - 1) \quad (6.7)$$

Substituting $\gamma_n = b + k e_n = b + k(\theta_r - \theta_n)$ in eqn. 6.7:

$$\theta_{n+1} = A \theta_n + FA \left[e^{[b + k(\theta_r - \theta_n)] \phi} - 1 \right] \quad (6.8)$$

The system will be said in region I when $b + k e_n \geq 1$; in region II when $0 < b + k e_n < 1$; and in region III when $b + k e_n \leq 0$. Typical output waveshapes in one sampling period are shown in fig. 6.1.

Equations 6.2, 6.4 and 6.8 are the difference equations

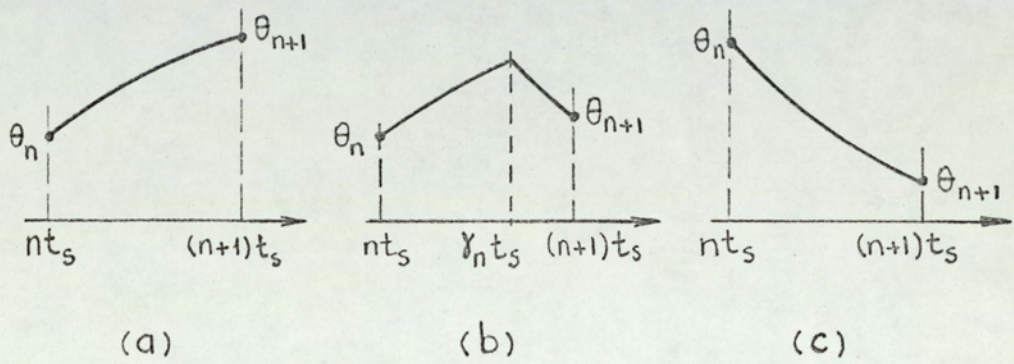


Fig. 6.1

Typical output waveforms for the PWM control system.

- (a) $e_n \geq (1 - b)/k$ (region I)
- (b) $-b/k < e_n < (1 - b)/k$ (region II)
- (c) $e_n \leq -b/k$ (region III)

which govern the system, for regions I, III, and II, respectively. Note that when the system is saturated, i.e. when it is in either region I or III, the governing difference equations are linear, whereas in the control region, i.e. in region II, the system difference equation is nonlinear.

One notes that the exponent in eqn. 6.8 has the following property:

$$[b + k(\theta_r - \theta_n)] \phi < 1 \quad (6.9)$$

The quantity in brackets is less than 1, because of the control condition for region II. $\phi = t_s/T$ is generally very much smaller than 1. Hence the inequality of 6.9 is valid. Therefore, one can use the following approximation:

$$\exp \{ [b + k(\theta_r - \theta_n)] \phi \} \approx 1 + [b + k(\theta_r - \theta_n)] \phi \quad (6.10)$$

Substituting into eqn. 6.8

$$\theta_{n+1} \approx A \theta_n + F A \phi \{ b + k(\theta_r - \theta_n) \} \quad (6.11)$$

One notes that

$$A = e^{-\phi} \approx \frac{1}{1+\phi} \quad (6.12)$$

or

$$A\phi \approx 1 - A \quad (6.13)$$

Substituting the approximate value of $A\phi$ given by eqn. 6.13 into eqn. 6.11:

$$\theta_{n+1} \approx A \theta_n + F(1 - A) \{ b + k(\theta_r - \theta_n) \} \quad (6.14)$$

or

$$\theta_{n+1} \approx \{ A - Fk(1 - A) \} \theta_n + F(1 - A)(b + k\theta_r) \quad (6.15)$$

Equation 6.15 is a better* approximation than eqn. 6.11. Moreover, equation 6.15 has the important advantage that it coincides with the saturation equations 6.2 and 6.4 at the lower and upper boundaries of region II.

6.2.2 Graphical Solution

As in the case of open loop control, a graphical solution is possible. Equations 6.2, 6.4, and 6.15 are plotted in fig. 6.2, in their respective regions. The curve of fig. 6.2 is drawn for the following parameter values:

$$t_s = 10 \text{ min}, \quad T = 50 \text{ min}, \quad F = 100^\circ\text{C}, \quad \theta_r = 80^\circ\text{C},$$

$$k = 0.01 \text{ } 1/^\circ\text{C}, \quad b = 0.815$$

The straight line with slope 1 (Γ) serves as a link for the increment of n . It is seen from fig. 6.2 that the boundaries of the regions are:

$$\text{Region I (full on)} : \theta_n < V_o = \theta_r - (1 - b)/k = 61.5^\circ\text{C}$$

$$\text{Region II (control)} : 61.5^\circ\text{C} = V_o < \theta_n < U_o = \theta_r + b/k = 161.5^\circ\text{C}$$

$$\text{Region III (full off)} : 161.6^\circ\text{C} = U_o < \theta_n$$

In the above example the straight line approximation in the region II has a maximum absolute error of 0.432°C , which

*See appendix B

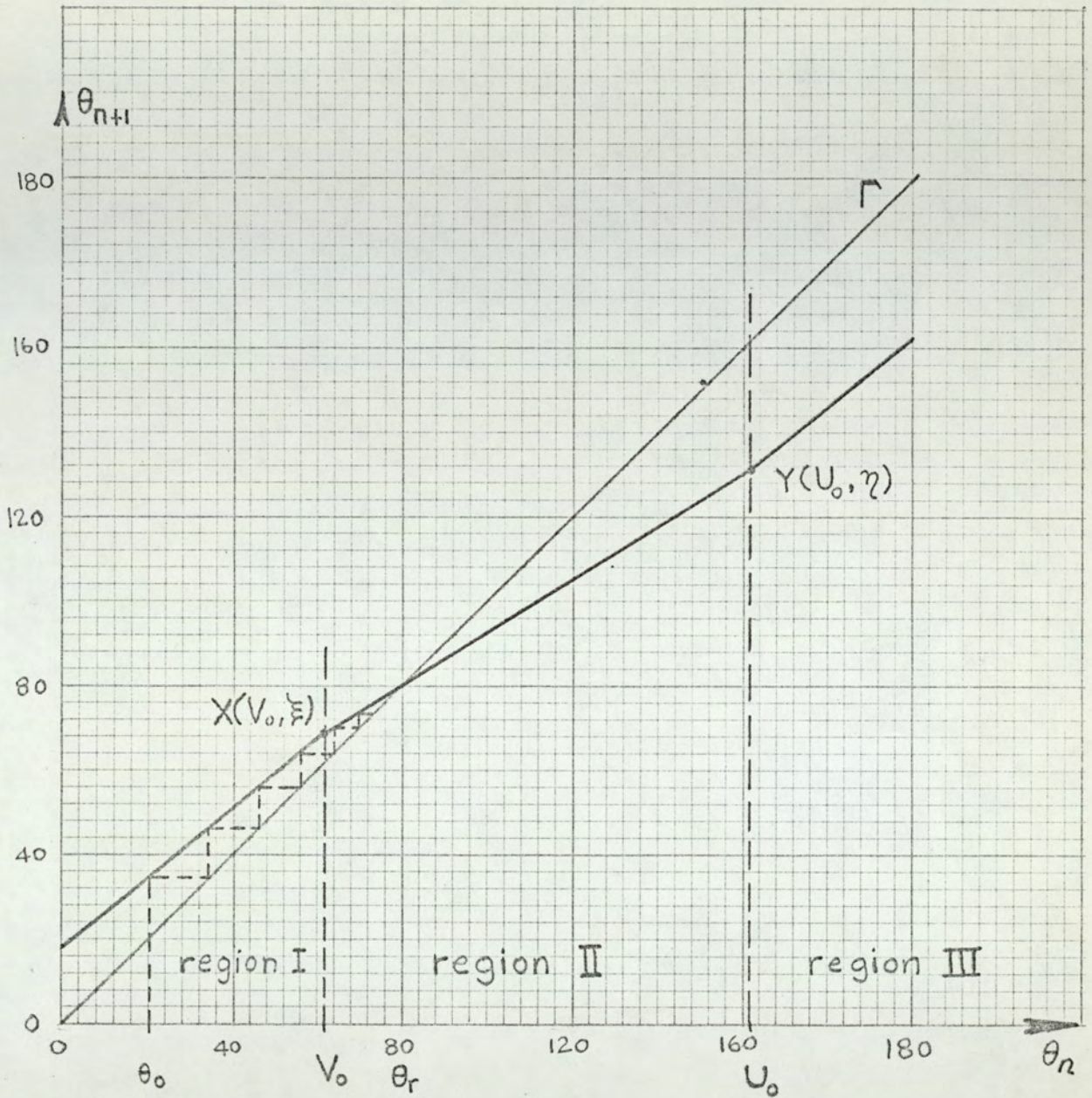


Fig. 6.2

Graphical representation of the system difference equations.
 The parameters of the system are: $t_s=10$ min, $T=50$ min, $F=100^\circ\text{C}$,
 $\theta_r=80^\circ\text{C}$, $k=0.01$ $1/^\circ\text{C}$, $b=0.815$.

A start-up with an initial temperature of 20°C is shown with broken lines; this corresponds to the numerical example of Chapter 5 (fig.5.12)

corresponds to a maximum relative error of 0.467 percent.

Points X and Y which are the boundary points between regions (fig. 6.2) will be encountered frequently in the discussion to follow. The coordinates of X and Y are:

$$\text{Point X: } V_o = \theta_r - (1 - b)/k, \quad \xi = AV_o + F(1 - A) \quad (6.16)$$

$$\text{Point Y: } U_o = \theta_r + b/k, \quad \eta = AU_o \quad (6.17)$$

In the above example, $V_o = 61.5^\circ\text{C}$, $\xi = 68.6^\circ\text{C}$, $U_o = 161.5^\circ\text{C}$ and $\eta = 132^\circ\text{C}$.

In fig. 6.2, a start-up operation from an initial temperature of 20°C is also shown. Since the parameter values are the same as in the example of fig. 5.12, a comparison is possible. It can be seen that the results from state variable analysis of chapter 5 and from the above graphical analysis are in perfect accordance.

6.2.3 Bias considerations

As was mentioned in Chapter 5, the bias is applied to the modulator to obtain a certain output temperature.

When the output temperature θ_n is equal to the command θ_r , the error will be zero. Therefore the bias must be such that:

$$\theta_n = \theta_r \quad \text{when} \quad e_n = 0$$

Moreover, in a stable system, the output will remain constant, for all $t = nt_s$, after it reached the steady state. Therefore

$$\theta_{n+1} = \theta_n$$

The above conditions, applied to eqn. 6.8 yields:

$$\theta_r = A \theta_r + F A (e^{b\phi} - 1) \quad (6.18)$$

which has the solution for b:

$$b = \frac{1}{\phi} \ln [1 + \beta (e^\phi - 1)] \quad (6.19)$$

where $\phi = t_s / T$

$$\beta = \theta_r / F$$

The bias as found according to eqn. 6.19 is used in the programme PWMSYS, (see eqn. 5.39) as well as in the examples of Chapter 5.

One notes that when the sampling period is small compared to the time constant, it is possible to use the approximations*:

$$e^\phi \approx 1 + \phi \quad (6.20)$$

$$\ln(1 + \beta\phi) \approx \beta\phi \quad (6.21)$$

with the above approximations, eqn. 6.19 becomes:

$$b \approx \frac{\theta_r}{F} = \beta \quad (6.22)$$

This approximate value for b was given in eqn. 5.7. This value will be used in the derivation of conditions for limit cycles.

*See Appendix B

Note that the bias value of eqn. 6.19 results an output temperature waveshape with its value at sampling instants being equal to the command value. If we require that the average value of the output temperature equals the command value, a different bias value should be applied.

The bias which is required for $\bar{\theta} = \theta_r$ (rather than $\theta_n = \theta_r$) can be found as follows: Let γ denote the steady state value of pulse width/sampling period ratio. Then, for each sampling period the on time will be γt_s , and the off time will be $(1 - \gamma)t_s$. Then:

$$p = \exp(-\gamma t_s/T) = \exp(-\gamma\phi) \quad (6.23)$$

or

$$\gamma = (1/\phi) \ln(1/p) \quad (6.24)$$

The average temperature at the output is (from eqns. 4.5 and 4.6, with $pq = A$)

$$\bar{\theta} = \frac{(1-p)(1+q)}{2} \frac{F}{1-A} = \frac{F}{2} \left[1 + \frac{A}{p} \frac{1-p}{1-A} \right] \quad (6.25)$$

Eqn. 6.25 is found by replacing q by A/p .

From 6.25, by writing $\bar{\theta} = \theta_r$, and solving for p :

$$p = \frac{-(2\beta - 1)(1-A) + \sqrt{(2\beta - 1)^2(1-A)^2 - 4A}}{2} \quad (6.26)$$

Substitution of the above p into eqn. 6.24 gives γ . Then:

$$\gamma = b + k(\theta_r - \theta_n) \quad (6.27)$$

We note that (since $\theta_{\max} = \theta_{\min}/q$, from eqns. 4.5 and 4.6)

$$\theta_r = \frac{\theta_{\min} + \theta_{\max}}{2} = \frac{\theta_{\min} + \frac{1}{q} \theta_{\min}}{2} = \theta_{\min} \frac{q + 1}{2q}$$

Or since $\theta_{\min} = \theta_n$

$$\theta_n = \theta_r \frac{2q}{q+1}$$

Substituting this value of θ_n into eqn. 6.27 and noting that

$$q = \exp \{ -(1 - \gamma)\phi \} = \exp(-\phi) \exp(\gamma\phi) = A \exp(\gamma\phi)$$

$$\gamma = b + k \theta_r \frac{1 - A \exp(\gamma\phi)}{1 + A \exp(\gamma\phi)} \quad (6.28)$$

Finally, bias can be found from eqn. 6.28:

$$b = \gamma - k \theta_r \frac{1 - A \exp(\gamma\phi)}{1 + A \exp(\gamma\phi)} \quad (6.29)$$

The procedure to find b is as follows:

1. Given t_s , T , θ_r and F find p from eqn. 6.26.
2. With this value of p find γ from eqn. 6.24.
3. With this value of γ , and given k , find the required bias from eqn. 6.29.

One notes the following points:

1. The value of bias becomes dependent on not only t_s , T , θ_r , and F ; but also on k .
2. This derivation of the bias maintaining $\bar{\theta} = \theta_r$ is cumbersome, and mainly of academic interest; since in general practice the difference between $\bar{\theta}$ and θ_n is small.

3. A version of program PWMSYS which calculates the bias according to the eqns. 6.24, 6.26, and 6.29 (instead of eqn. 6.19) is written, and it is verified that the average value of the output temperature (rather than the minimum value) is adjusted by the system to be made equal to command. This version of PWMSYS is not included in this work.

6.3 AN EXACT ANALYSIS OF LIMIT CYCLES IN PWM ELECTROHEAT SYSTEMS

6.3.1 Basic definitions

In this section the plant is assumed mode independent and without lag. The effects of mode dependence and lag will be discussed later. The control law is assumed linear between two saturation regions (fig. 5.6). The effects of saturation is taken into consideration. Two types of limit cycling are distinguished:

1. Saturated-saturated (sat-sat) mode (or "relay mode" as it is referred to by some authors¹⁸). In this mode, the modulator input is either negative or larger than 1, i.e. the modulator is always saturated.
2. Linear-saturated (lin-sat) mode. In this mode the modulator is saturated for some part of the cycling period, and non saturated for the remaining part.

It will be shown that the linear mode, where the modulator remains non-saturated for the whole cycling period is not possible, except for unstable limit cycling.

In the following analysis we shall make use of three operators, H, C, and Q. Their definitions are given below:

H (heat) operator: $\theta_2 = H(\theta_1)$ where θ_1 is the output temperature at $t = nt_s$, and θ_2 is the output temperature at $t = (n + 1)t_s$, when $m = 1$ (power on) for the entire sampling interval.

C (cool) operator: $\theta_2 = C(\theta_1)$ where θ_1 and θ_2 are the output temperatures at $t = nt_s$, and $t = (n + 1)t_s$ respectively, when $m = 0$ (power off) for the entire n th sampling interval.

Q (control region) operator: $\theta_2 = Q(\theta_1)$ where θ_1 and θ_2 are the output temperatures at $t = nt_s$ and $t = (n + 1)t_s$ respectively, when $m = 1$ for $nt_s < t < (n + \gamma_n)t_s$ and $m = 0$ for $(n + \gamma_n)t_s < t < (n + 1)t_s$.

Figure 6.3 shows the interpretation of these operators in time domain and in (θ_n, θ_{n+1}) plane.

These operators and their powers can be represented algebraically as follows:

$$H(\theta) = A\theta + F(1 - A) \quad (6.30a)$$

$$C(\theta) = A\theta \quad (6.30b)$$

$$Q(\theta) = \{A - Fk(1 - A)\}\theta + F(1 - A)(b + k\theta_r) = \\ s\theta + (1 - s)\theta_r \quad (6.30c)$$

$$H^i(\theta) = A^i\theta + F(1 - A^i) \quad (6.30d)$$

$$C^i(\theta) = A^i\theta \quad (6.30e)$$

$$Q^i(\theta) = s^i\theta + (1 - s^i)\theta_r = s^i(\theta - \theta_r) + \theta_r \quad (6.30f)$$

$$H^{-i}(\theta) = \frac{\theta - F(1 - A^i)}{A^i} \quad (6.30g)$$

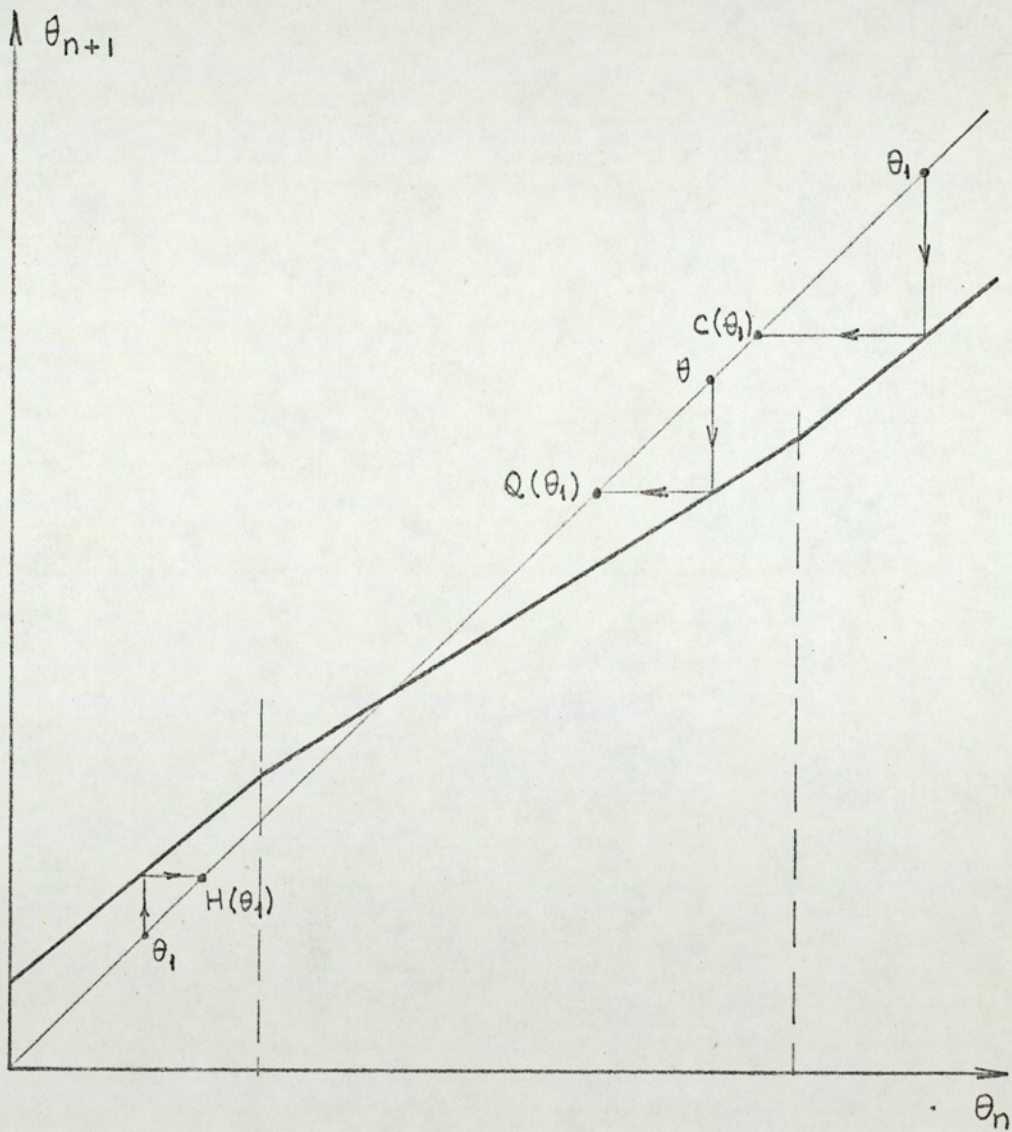
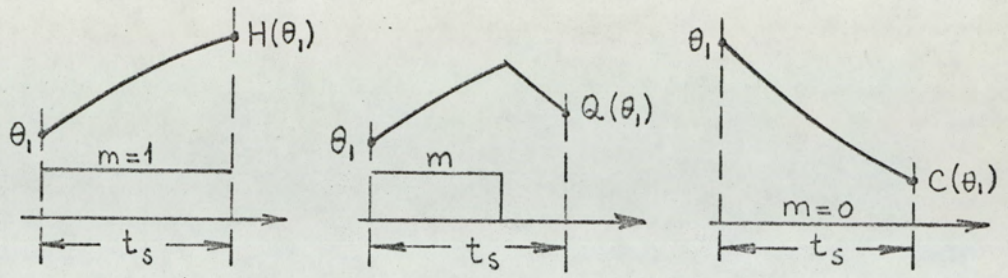


Fig. 6.3

H , C and Q operators.

$$C^{-i}(\theta) = \frac{\theta}{A^i} \quad (6.30h)$$

where $i = 0, 1, 2, 3, \dots$ and S is the slope of the characteristic curve in region II $[S = A - Fk(1 - A)]$.

From the above equations, one notes that

1. Operators H and Q are not linear, while operator C is linear.
2. The operators H, Q, C do not commute with each other, i.e. when two or more operators of different kind operate, their order is important. For example

$$H \{ C(\theta) \} \neq C \{ H(\theta) \}$$

6.3.2 Saturated-saturated oscillations

In sat-sat mode the modulator remains saturated throughout the cycling period. The system should alternate between region I and III, since otherwise the output temperature cannot be periodic. Switching from one saturation region to the other occurs at sampling instants, since the output of the saturated modulator remains constant ($m = 0$ or 1) in a sampling interval. Therefore the system will be in region I for an integral multiple of the sampling period, and in region III for another integral multiple of the sampling period. We shall use the following notation: M will denote the number of heat-up sampling periods (i.e. periods for which $m = 1$) in a cycling period; N will denote the number of cool-down sampling periods ($m = 0$) in a cycling period. It follows that $t_c = (M + N)t_s$ where t_c denotes the period of the limit cycle. Such a sat-sat oscillation mode will be called $M-N$ mode. In fig. 6.4 typical plant and modulator output waveforms are shown for 3-1 mode limit cycling.

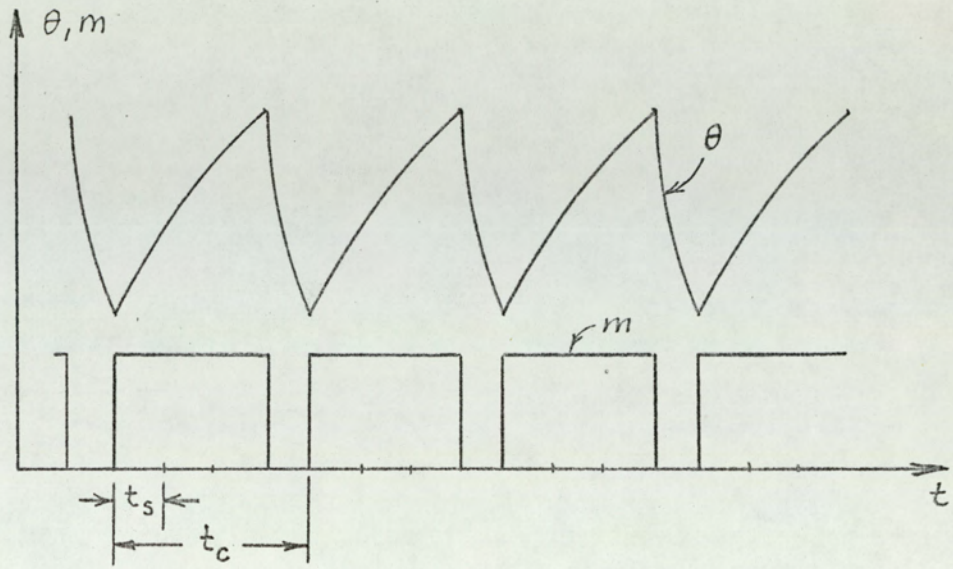


Fig. 6.4

Typical plant output (θ) and modulator output (m) waveforms for 3-1 cycling mode.

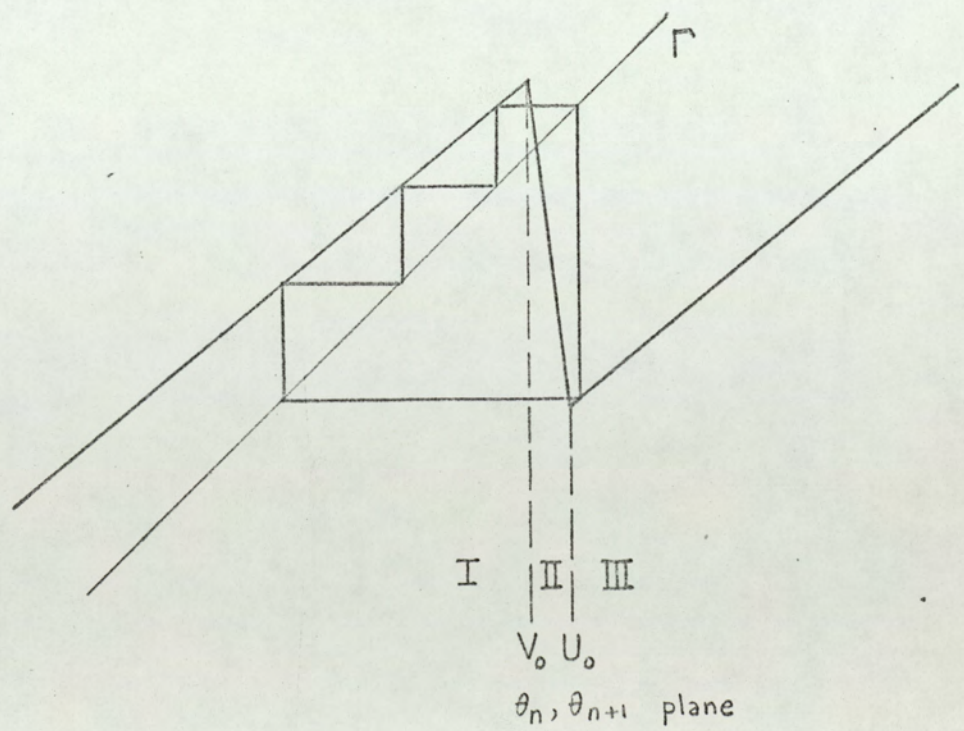


Fig. 6.5

Typical limit cycle trajectory for 3-1 mode

Geometry of the sat-sat trajectory and possible modes
of oscillation

Since the limit cycling is periodic, the trajectory is a closed curve. A typical cycling trajectory is shown in fig. 6.5 For sat-sat oscillations, the cycling trajectory never hits the line Γ between V_0 and U_0 , since this would mean a sampling interval with linear control.

We define temperatures V_i , V^i , U_i , and U^i as follows:

$$\begin{aligned} V_1 &= H^{-1}(V_0) \\ V_2 &= H^{-1}(V_1) = H^{-2}(V_0) \\ &\vdots \\ V_i &= H^{-1}(V_{i-1}) = \dots = H^{-i}(V_0) \end{aligned} \quad (6.31)$$

$$\begin{aligned} V^1 &= H^{-1}(U_0) \\ V^2 &= H^{-1}(V^2) = H^{-2}(U_0) \\ &\vdots \\ V^i &= H^{-1}(V^{i-1}) = \dots = H^{-i}(U_0) \end{aligned} \quad (6.32)$$

$$\begin{aligned} U_1 &= C^{-1}(U_0) \\ U_2 &= C^{-1}(U_1) = C^{-2}(U_0) \\ &\vdots \\ U_i &= C^{-1}(U_{i-1}) = \dots = C^{-i}(U_0) \end{aligned} \quad (6.33)$$

$$U^1 = C^{-1}(V_0)$$

$$U^2 = C^{-1}(U^1) = C^{-2}(V_0)$$

$$\vdots$$

$$U^i = C^{-1}(U^{i-1}) = \dots = C^{-i}(V_0) \quad (6.34)$$

The above quantities correspond to points on the line Γ , shown in fig. 6.6. It is clear from fig. 6.6 that the limit cycle trajectory cannot hit the portions of Γ shown red in fig. 6.6, because this would result in a sampling interval with linear control. Therefore a sat-sat limit cycle trajectory hits Γ only in the intervals shown black in fig. 6.6. These intervals will be called "allowable intervals". Allowable intervals correspond to the portions of Γ for which:

$$V^{i+1} < \theta < V_i \quad i = 0, 1, 2, \dots \quad (6.35)$$

and

$$U_i < \theta < U^{i+1} \quad i = 0, 1, 2, \dots \quad (6.36)$$

From the geometry of the trajectory (figs. 6.5 and 6.6) it can be seen that:

1. The trajectory can hit Γ only once in an allowable interval.
2. The trajectory cannot skip an allowable interval, i.e. the hitting points are in consecutive allowable intervals, starting with the first such interval in region I (interval $V_0 - V^1$) and the first interval in region III (interval $U_0 - U^1$).

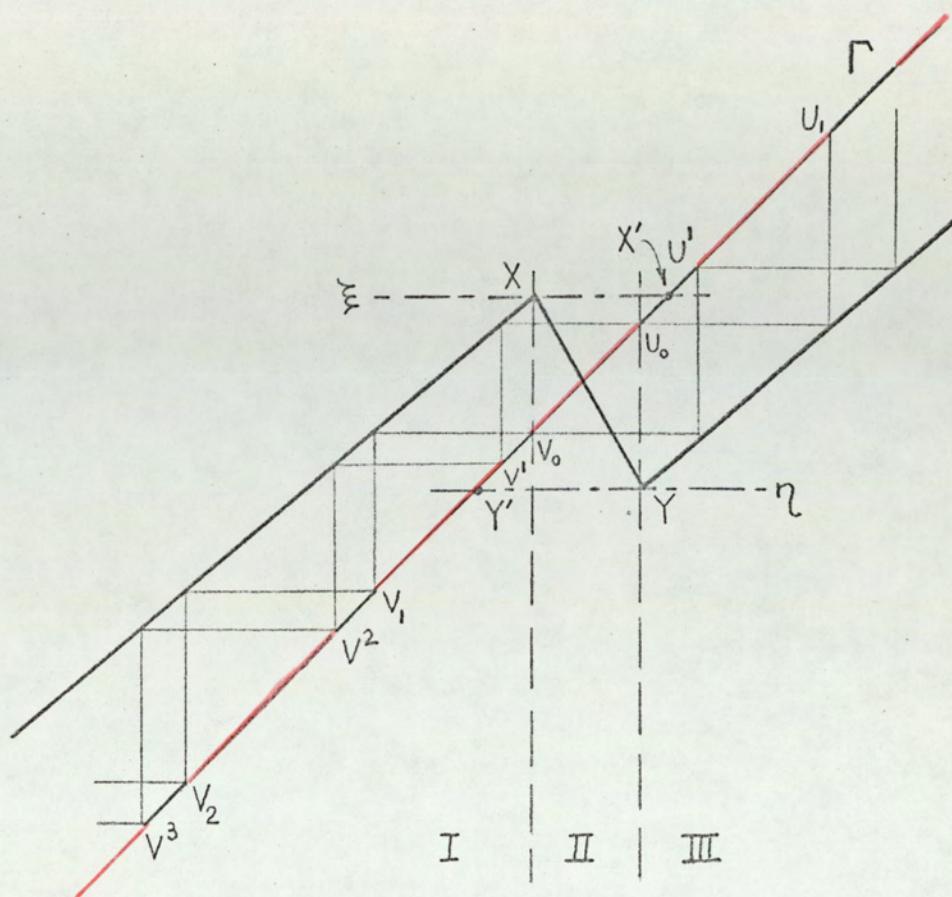


Fig. 6.6

Allowable intervals on Γ (shown black)

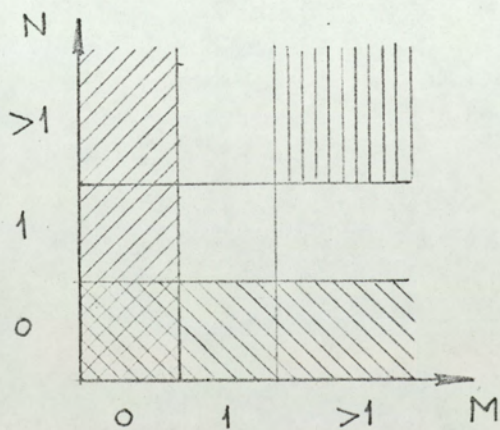
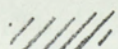
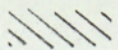


Fig. 6.7

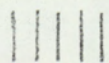
Constraints on M and N



equation 6.39



equation 6-40



assertions 1 and 2 with
eqns. 6.37 and 6.38

3. The trajectory for M-N mode hits Γ M times in region I (below V_0) and N times in region III (above U_0).
4. Since the temperature cannot be larger than ξ and smaller than η , the trajectory is bound to be between two horizontal lines passing through points X and Y.

Let μ denote the number of allowable intervals or interval fractions between points V_0 and Y' , and ν denote the same between U_0 and X' . Then we have:

$$M \leq \mu \quad (6.37)$$

$$N \leq \nu \quad (6.38)$$

Assertion 1: If $\mu > 1$ then $\nu \leq 1$.

Proof: $\mu > 1$ implies Y' is below V_1 i.e. $\eta < V_1$.

$$\therefore C(U_0) < H^{-1}(V_0)$$

Since $U_0 = V_0 + 1/k$

$$C(V_0 + \frac{1}{k}) < H^{-1}(V_0)$$

$$AV_0 + \frac{A}{k} < \frac{V_0 - F(1 - A)}{A}$$

$$A^2V_0 + \frac{A^2}{k} < V_0 - F(1 - A) \quad \text{since } A > 0$$

$$F(1 - A) + \frac{A^2}{k} < V_0 - A^2V_0$$

$$F(1 - A) + \frac{A^2}{k} < V_0(1 - A^2)$$

$$FA(1 - A) + \frac{A^2}{k} < V_0(1 - A^2) \quad \text{since } A < 1,$$

$$F(1 - A) > 0$$

$$FA(1 - A) - \frac{A^2}{k} < V_0(1 - A^2) \quad \text{since } A^2 > 0,$$

$$k > 0$$

$$FA(1 - A) - \frac{1}{k} < V_0(1 - A^2) \quad \text{since } A^2 < 1$$

$$FA(1 - A) < V_0 - V_0A^2 + \frac{1}{k}$$

$$F(1 - A) < \frac{V_0}{A} - V_0A + \frac{1}{Ak} \quad \text{since } A > 0$$

$$F(1 - A) + V_0A < \frac{1}{A} (V_0 + \frac{1}{k}) = \frac{U_0}{A}$$

$$H(V_0) < C^{-1}(U_0)$$

$$\xi < U_1$$

i.e.

$$\nu \leq 1 \quad \text{Q.E.D.}$$

Assertion 2: If $\nu > 1$ then $\mu \leq 1$

Proof: $\nu > 1$ implies $\xi > U_1$, and by similar manipulation, it can be shown that this implies $\eta > V_1$ which means $\mu \leq 1$. Q.E.D.

Since the limit cycle is periodic, we can assert the following:

1. The trajectory is a closed curve.

2. In a cycling period, there is at least one sampling period with $m = 1$, and one with $m = 0$, i.e.:

$$M \geq 1 \quad (6.39)$$

$$N \geq 1 \quad (6.40)$$

Now we have

$$M \geq 1, \quad N \geq 1 \quad \text{from eqns. 6.39 and 6.40}$$

$$M \leq \mu, \quad N \leq \nu \quad \text{from eqns. 6.37 and 6.38}$$

$$\left. \begin{array}{l} \mu > 1, \quad \nu \leq 1 \\ \nu > 1, \quad \mu \leq 1 \end{array} \right\} \text{from the assertions 1 and 2.}$$

The logical result from the above constraints is the following (fig. 6.7):

$$M > 1 \quad N = 1$$

$$N > 1 \quad M = 1$$

Therefore the only possible modes are $M - 1$ and $1 - N$ modes, where $M, N = 1, 2, 3, \dots$

The output waveform

M-1 Mode

A trajectory corresponding to a $M-1$ mode limit cycle is shown in fig. 6.8.a. In fig. 6.8.b. the corresponding

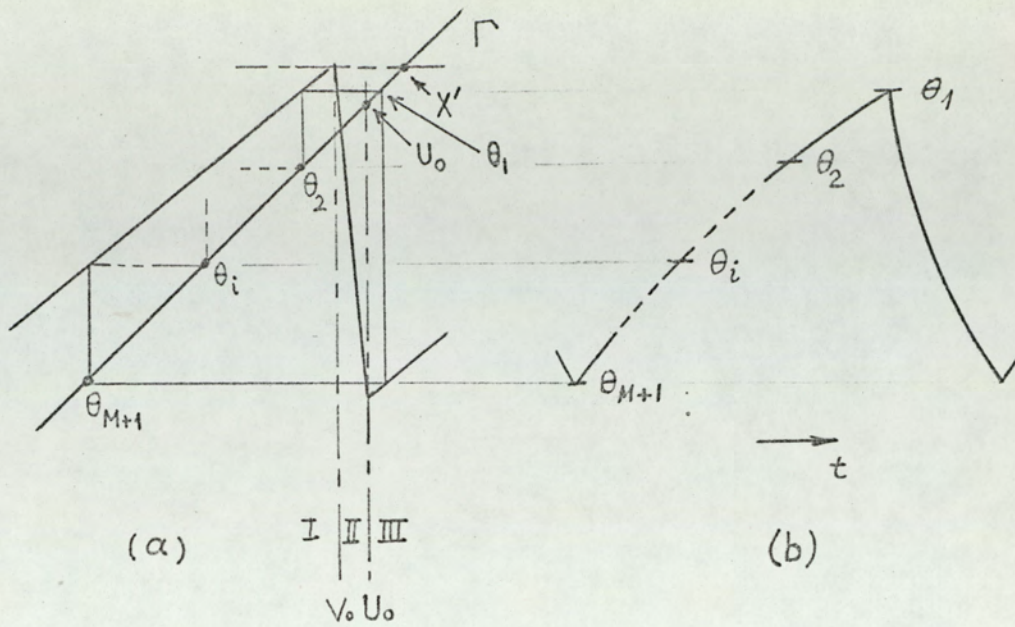


Fig. 6.8

- (a) Trajectory corresponding to M-1 mode limit cycling
- (b) Corresponding output temperature

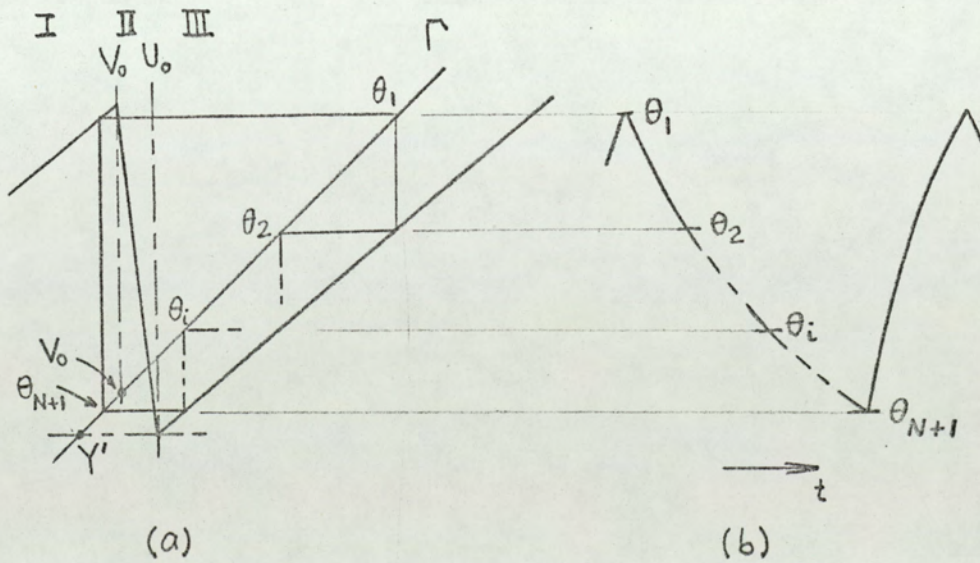


Fig. 6.9

- (a) Trajectory corresponding to 1-N mode limit cycling
- (b) Corresponding output temperature.

output waveshape is shown. From fig. 6.8.a, the maximum output temperature satisfies:

$$H^M \{ C(\theta_1) \} = \theta_1 \quad (6.41)$$

or

$$A^{M+1} \theta_1 + FA(1 - A^M) = \theta_1 \quad (6.42)$$

The solution of eqn. 6.42 for θ_1 gives

$$\theta_1 = F \frac{1 - A^M}{1 - A^{M+1}} \quad (6.43)$$

For θ_i we have

$$\theta_i = H^{-(i-1)} (\theta_1) \quad (6.44)$$

Equation 6.44, with eqn. 6.43 gives

$$\theta_i = F \left[1 - \frac{A^M(1 - A)}{A^{i-1}(1 - A^{M+1})} \right] \quad (6.45)$$

The minimum value of the output temperature, θ_{M+1} , can be found by letting $i = M + 1$ in eqn. 5.45:

$$\theta_{M+1} = F \frac{A(1 - A^M)}{1 - A^{M+1}} \quad (6.46)$$

The cycling amplitude θ_d is given by

$$\theta_d = \theta_1 - \theta_{M+1} = F \frac{(1 - A)(1 - A^M)}{1 - A^{M+1}} \quad (6.47)$$

The average value of the output temperature can be found from:

$$\bar{\theta} = \frac{1}{M+1} \sum_{i=1}^{M+1} \theta_i \quad (6.48)$$

But one notes that the average value \bar{m} over one cycling period is:

$$\bar{m} = \frac{M}{M+1} \quad (6.49)$$

Therefore the average value of the output temperature is:

$$\bar{\theta} = \bar{m}F = F \frac{M}{M+1} \quad (6.50)$$

Substitution of θ_i as given in eqn. 6.45 into eqn. 6.48 yields the same result.

1-N mode

The trajectory and the output waveshape corresponding to 1-N mode limit cycle are shown in fig. 6.9a and b. From fig. 6.9.a:

$$H \{c^N(\theta_1)\} = \theta_1 \quad (6.51)$$

or

$$A^{N+1} \theta_1 + F(1-A) = \theta_1 \quad (6.52)$$

Solution for θ_1 gives:

$$\theta_1 = F \frac{1 - A}{1 - A^{N+1}} \quad (6.53)$$

θ_i is related to the maximum output by

$$\theta_i = C^{i-1} (\theta_1), \quad (6.54)$$

therefore

$$\theta_i = F \frac{A^{i-1} (1 - A)}{1 - A^{N+1}} \quad (6.55)$$

The minimum value of the output, θ_{N+1} , is found by letting $i = N + 1$ in eqn. 6.55:

$$\theta_{N+1} = F \frac{A^N (1 - A)}{1 - A^{N+1}} \quad (6.56)$$

The cycling amplitude, θ_d , is given by:

$$\theta_d = \theta_1 - \theta_{N+1} = \frac{(1 - A)(1 - A^N)}{1 - A^{N+1}} \quad (6.57)$$

The average value of the output temperature is given by:

$$\bar{\theta} = \bar{m}F = F \frac{1}{N + 1} \quad (6.58)$$

Gain and β boundaries for the oscillations

M - 1 mode oscillations

In order that the system sustain an M - 1 mode limit

cycle, the following conditions must be satisfied:

1. $\mu > 0$ (i.e. $\eta < V_0$)
2. $\nu > 0$ (i.e. $\xi > U_0$)
3. A closed trajectory of the form given in fig. 6.8 should be geometrically possible, with θ_1 (max. temperature) satisfying conditions 4 and 5 below.
4. $\theta_1 \leq \xi$
5. $\theta_1 \geq U_0$

Conditions 1 and 2 must be satisfied in order that M and N have values greater than zero (eqns. 6.39 and 6.40). The maximum cycling temperature θ_1 must satisfy condition 4 because the output temperature cannot attain values greater than ξ . Condition 5 must be satisfied, otherwise the limit cycle loses its sat-sat nature, as is evident from fig. 6.8. Conditions 4 and 5 together imply that θ_1 must be between points X' and U_0 (fig. 6.8). Note that conditions 4 and 5 together imply condition 2; therefore we can omit condition 2. Later it will be shown that condition 1 is not independent*. Thus, for the time being, we also leave out condition 1.

A closed M - 1 mode trajectory implies:

$$\theta_1 = F \frac{1 - A^M}{1 - A^{M+1}}$$

as given in eqn. 6.43. Substituting this value of θ_1 and

*See eqn. 6.75.a.

the value of ξ given in eqn. 6.16 into condition 4:

$$F \frac{1 - A^M}{1 - A^{M+1}} \leq AV_0 + F(1 - A) \quad (6.59)$$

Since $V_0 = \theta_r - \frac{1 - b}{k}$ and $b \approx \beta$,

$$F \frac{1 - A^M}{1 - A^{M+1}} \leq A\theta_r - \frac{1}{k} + \frac{\theta_r}{Fk} + F(1 - A) \quad (6.60)$$

by collecting terms, and dividing by F

$$\frac{1 - A^M}{1 - A^{M+1}} \leq A(\beta - 1) + \frac{A}{Fk} (\beta - 1) + 1 \quad (6.61)$$

Since $\beta - 1$ is negative

$$\frac{\frac{1 - A^M}{1 - A^{M+1}} + (1 - \beta)A - 1}{\beta - 1} \geq \frac{A}{Fk} \quad (6.62)$$

and, finally

$$Fk \geq \frac{1 - \beta}{\beta - \left(1 - \frac{A^{M-1}(1 - A)}{1 - A^{M+1}}\right)} \quad (6.63)$$

On the other hand, condition 5 gives:

$$F \frac{1 - A^M}{1 - A^{M+1}} \geq U_0 \quad (6.64)$$

Since $U_0 = \theta_r + b/k$ and $b \approx \beta$,

$$\frac{1 - A^M}{1 - A^{M+1}} \geq \left(1 + \frac{1}{Fk}\right) \beta \quad (6.65)$$

which yields

$$Fk \geq \frac{\beta}{\frac{1 - A^M}{1 - A^{M+1}} - \beta} \quad (6.66)$$

Expressions 6.63 and 6.66 gives the gain and β boundaries for $M - 1$ mode limit cycles.

An examination of the two inequalities 6.63 and 6.64 reveals the following facts:

1. $M-1$ mode limit cycles are possible only for some β values. The ranges of β values for which $M-1$ limit cycling is possible will be called "M-1 zones". The lower and upper boundaries of a $M-1$ zone will be denoted by β_{M-1}^l and β_{M-1}^u . These boundaries can be found by equating the denominators of the right hand sides of eqns. 6.63 and 6.66 to zero:

$$\beta_{M-1}^l = 1 - \frac{A^{M-1} (1 - A)}{1 - A^{M+1}} \quad (6.67)$$

$$\beta_{M-1}^u = \frac{1 - A^M}{1 - A^{M+1}} \quad (6.68)$$

2. In a given $M-1$ zone the minimum required (i.e. critical) gain to sustain the sat-sat oscillations can be found as the minimum Fk value which satisfies both eqn. 6.63 and eqn. 6.66.

3. For β values corresponding to the boundaries of the zones the necessary gain to sustain the oscillations

becomes infinite.

4. In a given zone the critical gain passes through a minimum, this occurs at the β value which makes the right hand sides of eqns. 6.63 and 6.66 equal. If we denote this value of β by β_{M-1}° :

$$\frac{1 - \beta_{M-1}^{\circ}}{\beta_{M-1}^{\circ} - 1 - \frac{A^{M-1}(1-A)}{1-A^{M+1}}} = \frac{\beta_{M-1}^{\circ}}{\frac{1-A^M}{1-A^{M+1}} - \beta_{M-1}^{\circ}} \quad (6.69)$$

which gives:

$$\beta_{M-1}^{\circ} = \frac{1 - A^M}{1 + A^{M-1} - 2A^M} \quad (6.70)$$

The minimum critical gain for the M-1 zone is found by substituting the above value of β_{M-1}° into eqn. 6.69:

$$Fk = \frac{1 - A^{M+1}}{(1 - A)^2 A^{M-1}} \quad (6.71)$$

As an example, let $t_s = 20$ min, and $T = 100$ min, which gives $\phi = 0.2$ and $A = \exp(-0.2) = 0.8187$. We shall investigate the possibility of 2-1 limit cycling. For this case expressions 6.63 and 6.66 become:

$$Fk \geq \frac{1 - \beta}{\beta - 0.6711} \quad (6.72)$$

$$Fk \geq \frac{\beta}{0.7307 - \beta} \quad (6.73)$$

The 2-1 zone is the interval:

162

$$0.6711 = \beta_{2-1}^l < \beta < \beta_{2-1}^u = 0.7307$$

The gain necessary to sustain the 2-1 mode becomes infinite at zone boundaries ($\beta = 0.6711$ and $\beta = 0.7307$), and becomes minimum for:

$$\beta_{2-1}^o = \frac{1 - A^2}{1 + A - 2A^2} = 0.6896 \quad (6.74)$$

The minimum critical gain (for $\beta = 0.6896$) is:

$$F_k = \frac{1 - A^3}{(1 - A)^2 A} = 16.771 \quad (6.75)$$

In fig. 6.10 this zone, and the gain boundary is shown. 2-1 limit cycling is possible only for the F_k and β values corresponding to the shaded area in fig. 6.10.

It can be shown that all M-1 zones lie above $\beta = 0.5$, therefore no M-1 limit cycle is possible for $\beta < 0.5$, with the exception of 1-1 mode, whose zone is centered at $\beta = 0.5$. Using this fact one can prove that condition 1 is always satisfied when conditions 5 and 6 are satisfied. In other words:

$$\left. \begin{array}{l} \text{condition 4} \\ \text{condition 5} \end{array} \right\} \longrightarrow \left. \begin{array}{l} \text{condition 2} \\ \beta \geq 0.5 \end{array} \right\} \longrightarrow \text{condition 1}$$

(6.75a)

This can be proved as follows:

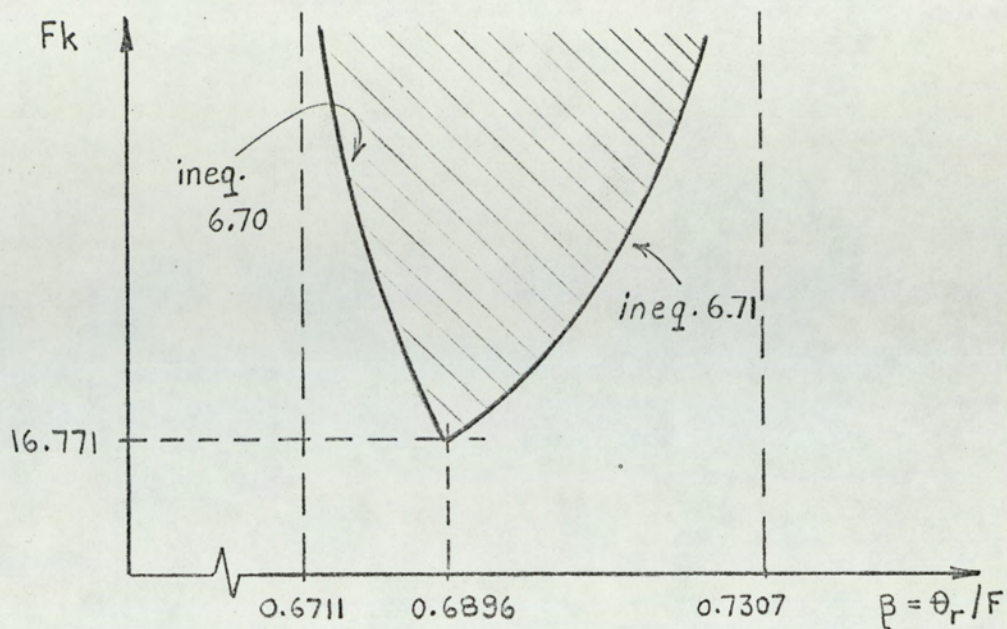


Fig. 6.10

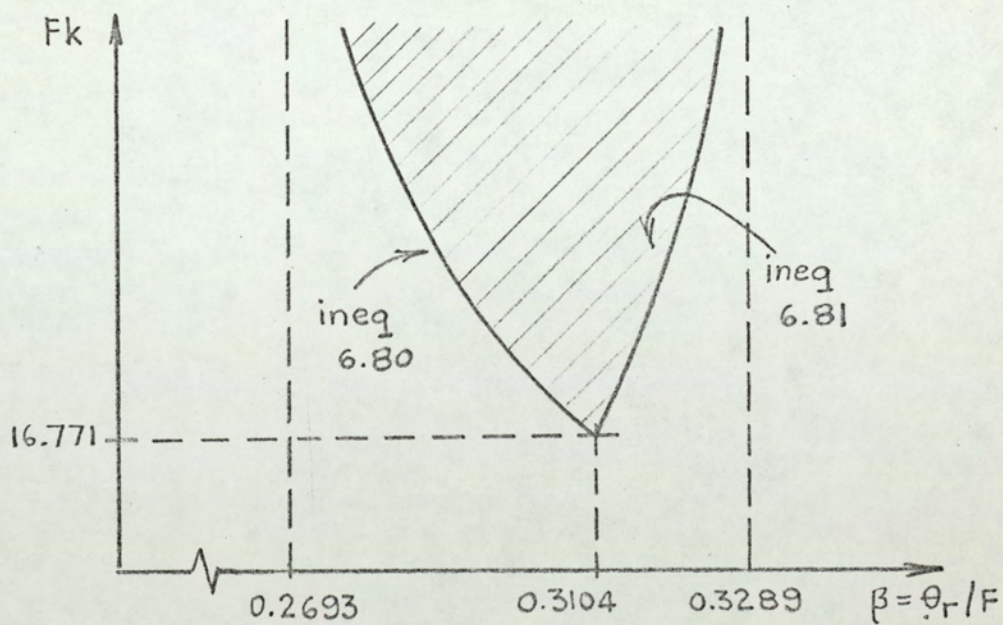
2-1 limit cycling boundaries for $\phi = 0.2$ 

Fig. 6.11

1-2 limit cycling boundaries for $\phi = 0.2$

$$\beta \geq 0.5$$

164

$$2\beta - 1 \geq 0$$

$$F - 2\theta_r \leq 0$$

$$F - \theta_r \leq \theta_r$$

$$F - \theta_r - \frac{b}{k} \leq \theta_r - \frac{(1-b)}{k}$$

since $\beta \approx b > 1 - b \approx 1 - \beta$

$$F - (\theta_r + \frac{b}{k}) \leq \theta_r - \frac{1-b}{k}$$

$$F - U_0 \leq V_0 \tag{6.76}$$

On the other hand, condition 2 gives:

$$\xi > U_0$$

or

$$U_0 - F(1 - A) < AV_0 \tag{6.77}$$

Inequalities 6.76 and 6.77 added side by side gives:

$$FA < V_0 (1 + A)$$

multiplying both sides by $1 - A$, which is positive:

$$FA(1 - A) < V_0(1 - A^2)$$

$$A \{ AV_0 + F(1 - A) \} < V_0$$

$$AU_0 < V_0$$

$$\eta < V_0$$

which is condition 1. Q.E.D.

It is interesting to find the limit values of the zone boundaries for $\phi \rightarrow 0$. When $\phi = t_s/T$ becomes very small, the effects of sampling becomes less significant, therefore we expect that the zones will shrink with decreasing ϕ , and finally disappear when $\phi \rightarrow 0$. From eqns. 6.67 and 6.68:

$$\lim_{\phi \rightarrow 0} \beta_{M-1}^l = \lim_{A \rightarrow 1} 1 - \frac{A^{M-1} (1 - A)}{1 - A^{M+1}} = \frac{M}{M+1} \quad (6.78)$$

$$\lim_{\phi \rightarrow 0} \beta_{M-1}^u = \lim_{A \rightarrow 1} \frac{1 - A^M}{1 - A^{M+1}} = \frac{M}{M+1} \quad (6.79)$$

As expected, lower and upper boundaries of each zone become equal, thus the zones vanish.

1-N mode oscillations*

In order the system sustain a 1-N mode limit cycle, the following conditions must be satisfied:

1. $\mu > 0$
2. $\nu > 0$
3. A closed trajectory of the form given in fig. 6.9

*Since there exists a symmetry between M-1 and 1-N modes, many arguments are somewhat similar, therefore details of some derivations are omitted.

should be geometrically possible, with θ_{N+1} (minimum temperature) satisfying conditions 4 and 5 below,

$$4. \theta_{n+1} \leq V_0$$

$$5. \theta_{n+1} \geq \eta$$

Conditions 4 and 5 imply condition 1 and together with $\beta < 0.5$ they imply condition 2. The fact that $\beta < 0.5$ for 1-N oscillations will be shown later. Conditions 4 and 5 mean that θ_{N+1} must be between points Y' and V_0 (fig. 6.9).

A closed 1-N mode trajectory implies:

$$\theta_{N+1} = F \frac{A^N (1 - A)}{1 - A^{N+1}}$$

as given in eqn. 6.56. Substituting this value of θ_{N+1} and the value of V_0 in condition 4 we obtain:

$$Fk \geq \frac{1 - \beta}{\beta - \frac{A^N (1 - A)}{1 - A^{N+1}}} \quad (6.80)$$

Similarly condition 5 gives:

$$Fk \geq \frac{\beta}{\frac{A^{N-1} (1 - A)}{1 - A^{N+1}} - \beta} \quad (6.81)$$

The following conclusions can be drawn from eqns. 6.80 and 6.81:

1. 1-N mode limit cycles are possible only for some values. The ranges of β values for which 1-N limit cycling is possible will be called 1-N zones. The

boundaries of the 1-N zones will be denoted by β_{1-N}^l and β_{1-N}^u , where:

$$\beta_{1-N}^l = \frac{A^N (1 - A)}{1 - A^{N+1}} \quad (6.82)$$

$$\beta_{1-N}^u = \frac{A^{N-1} (1 - A)}{1 - A^{N+1}} \quad (6.83)$$

2. The boundaries of 1-N and M-1 zones are related to each other by:

$$\beta_{M-1}^l = 1 - \beta_{1-N}^u \quad \Big|_{N=M}$$

$$\beta_{M-1}^u = 1 - \beta_{1-N}^l \quad \Big|_{N=M}$$

This relationship is evident from eqns. 6.67, 6.68, 6.82, and 6.83. From this relationship, it is clear that 1-N and M-1 zones are symmetrical about $\beta = 0.5$.

3. In a given 1-N zone the critical gain is found as the minimum Fk value which satisfies both inequalities 6.80 and 6.81.

4. At zone boundaries the critical gain becomes infinite.

5. In a given 1-N zone the critical gain passes through a minimum, and this minimum occurs at $\beta = \beta_{1-N}^o$, where:

$$\beta_{1-N}^o = \frac{A^{N-1} (1 - A)}{1 + A^{N-1} - 2A^N} \quad (6.84)$$

By comparing eqns. 6.84 and 6.70:

$$\beta_{1-N}^{\circ} = 1 - \beta_{M-1}^{\circ} \quad \Big| \quad M=N \quad (6.85)$$

The value of the minimum critical gain for the 1-N zone is:

$$F_k = \frac{1 - A^{N+1}}{(1 - A)^2 A^{N-1}} \quad (6.86)$$

The above minimum is exactly the same as the minimum critical gain for the symmetrical M-1 zone (eqn. 5.71).

It can be shown that the gain boundaries in the 1-N zone and the M-1 zone are symmetrical with respect to the vertical line passing through $\beta = 0.5$ when $M = N$. The gain boundary of 1-2 mode limit cycling for a system with $\phi = t_s/T = 0.2$ is shown in fig. 6.11. Note that this figure and the one in fig. 6.10 are symmetrical with respect to the line $\beta = 0.5$. 1-2 mode limit cycling is possible only for the F_k and β values corresponding to the shaded area in fig. 6.11.

No 1-N limit cycling is possible for $\beta > 0.5$, with the exception of 1-1 mode. It can be asserted that

$$\left. \begin{array}{l} \text{condition 4} \\ \text{condition 5} \end{array} \right\} \longrightarrow \left. \begin{array}{l} \text{condition 1} \\ \beta < 0.5 \end{array} \right\} \longrightarrow \text{condition 2}$$

The proof follows the same pattern as given for M-1 zones. When $\phi \rightarrow 0$ the zone boundaries approach the limits given below:

$$\lim_{\phi \rightarrow 0} \beta_{1-N}^{\circ} = \lim_{A \rightarrow 1} \frac{A^N (1 - A)}{1 - A^{N+1}} = \frac{1}{N + 1} \quad (6.87)$$

$$\lim_{\phi \rightarrow 0} \beta_{1-N}^u = \lim_{A \rightarrow 1} \frac{A^{N-1}(1-A)}{1-A^{N+1}} = \frac{1}{N+1} \quad (6.88)$$

The zones vanish for $\phi \rightarrow 0$ as it can be seen from the above equations.

The complete gain- β boundaries are given in fig. 6.12 for $\phi = 0.2$ and in fig. 6.13 for $\phi = 0.5$. From these figures it is seen that there are an infinite number of M-1 and 1-N zones. As M and N become larger the zones become narrower, and the critical gains increase.

The zone boundaries are shown in fig. 6.14, for changing ϕ . From this figure it is seen that all zones except the 1-1 zone become narrower as ϕ increases. For large values of ϕ , the 1-1 zone extends over a large range of β values. This shows the increasing tendency of the system towards 1-1 mode as ϕ becomes large.

A three dimensional display of the gain- β boundary for 1-1 mode limit cycling is shown in fig. 6.15.

The 1-1 zone is centered around $\beta = 0.5$. The minimum critical gain for 1-1 zones is given by:

$$Fk = \frac{1+A}{1-A} \quad (6.89)$$

This value is the global minimum of critical gain for sat-sat mode oscillations.

As an example of the digital simulation of a limit cycling system the computer plot in fig. 5.15 is given. The system parameters are: $t_s = 10$ min, $T = 10$ min, $k = 2$ 1/°C, $F = 100$ °C, $\theta_r = 92$ °C, $b = 0.927$, $L = 0$. Therefore $\phi = 0.2$, $A = 0.819$ and $Fk = 200$. It can be seen that the parameter values satisfy the conditions for 6-1 mode cycling. The

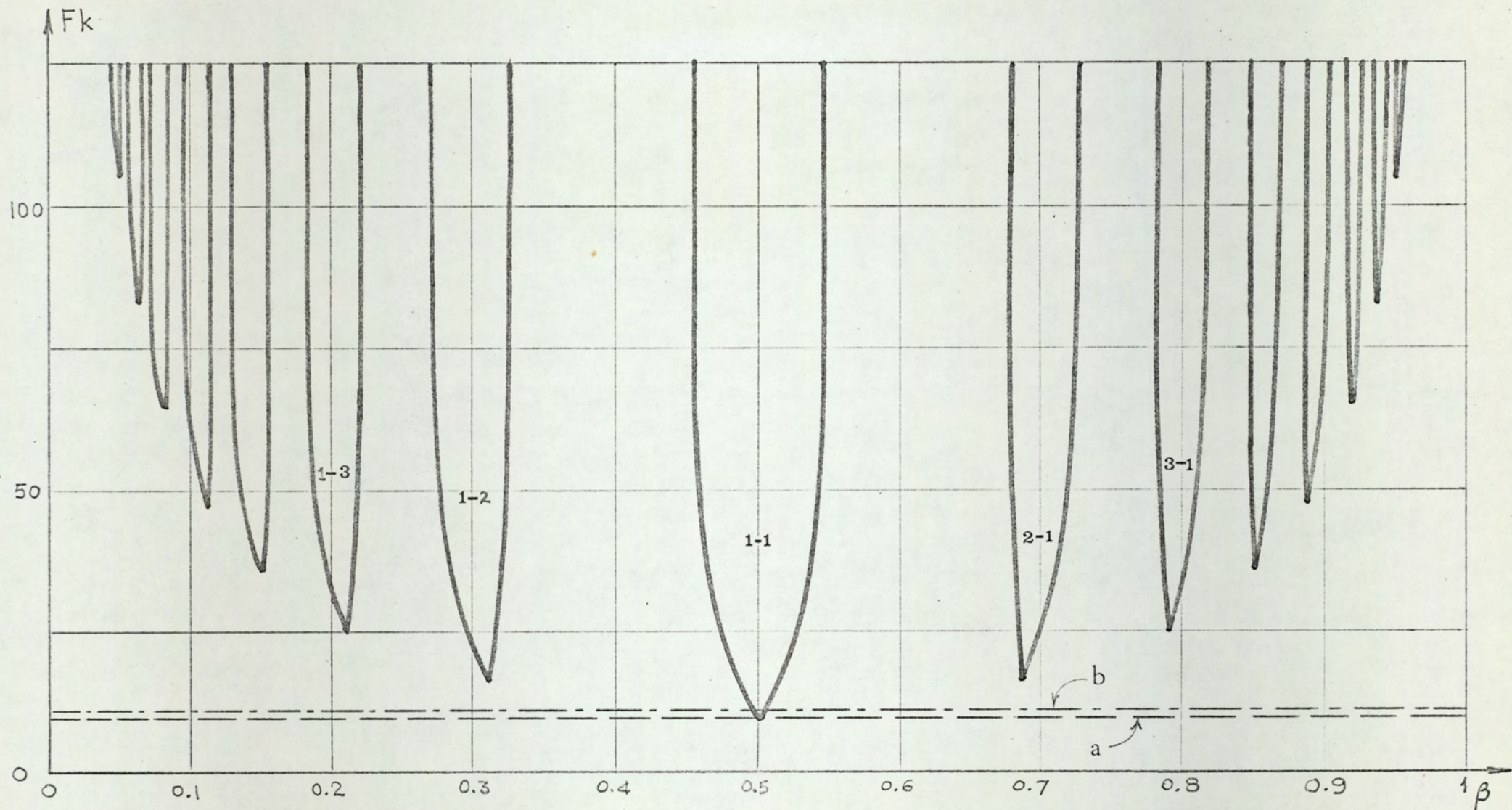


Fig 6.12

Gain- β boundaries for sat-sat limit cycling. $\phi = t_s/T = 0.2$
 a: Stability boundary; b: Upper limit for sat-lin oscillations.

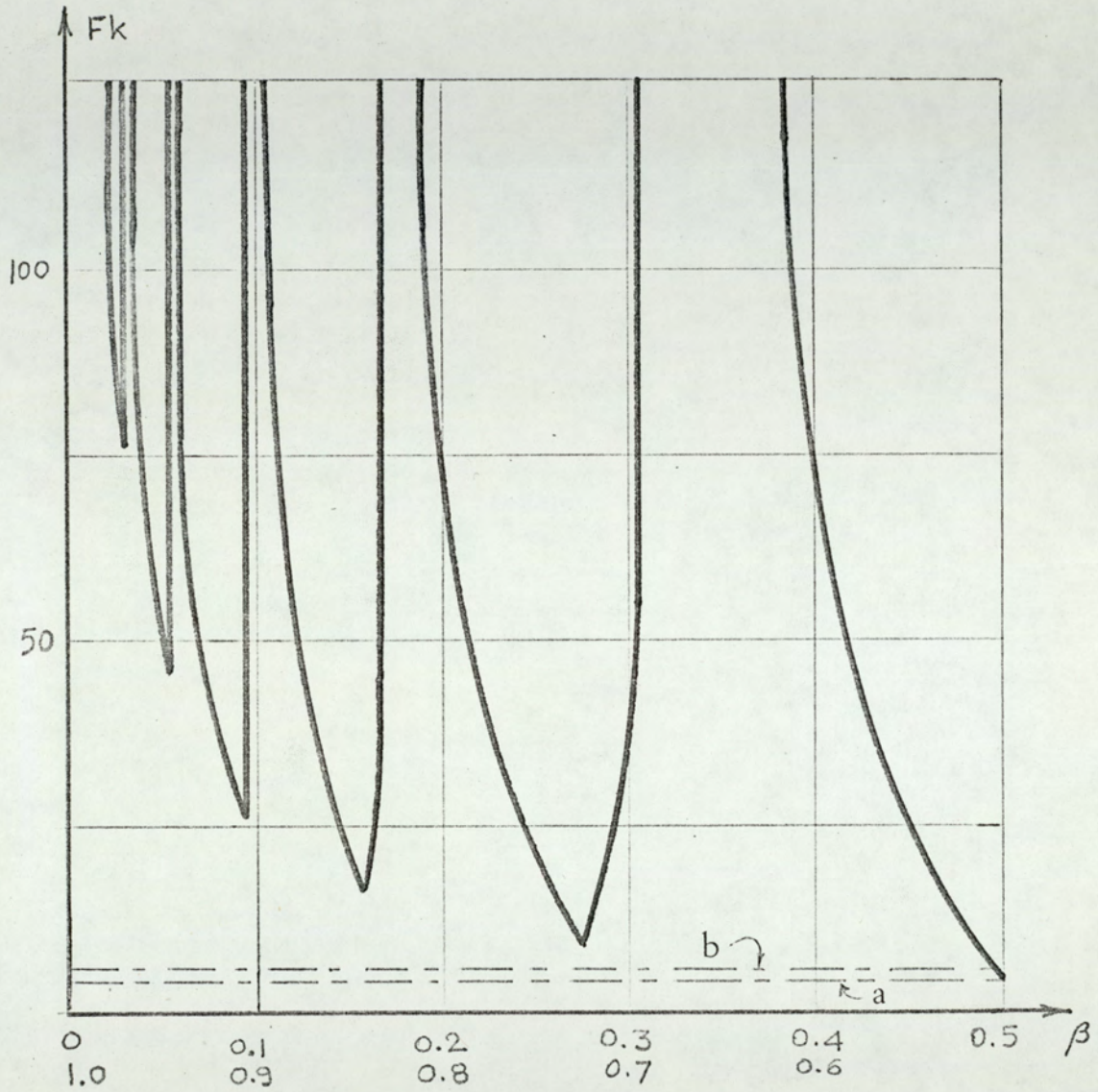


Fig. 6.13

Gain- β boundaries for sat-sat limit cycling.

$$\phi = 0.5$$

a: Stability boundary,
b: Upper limit for sat-lin oscillations.

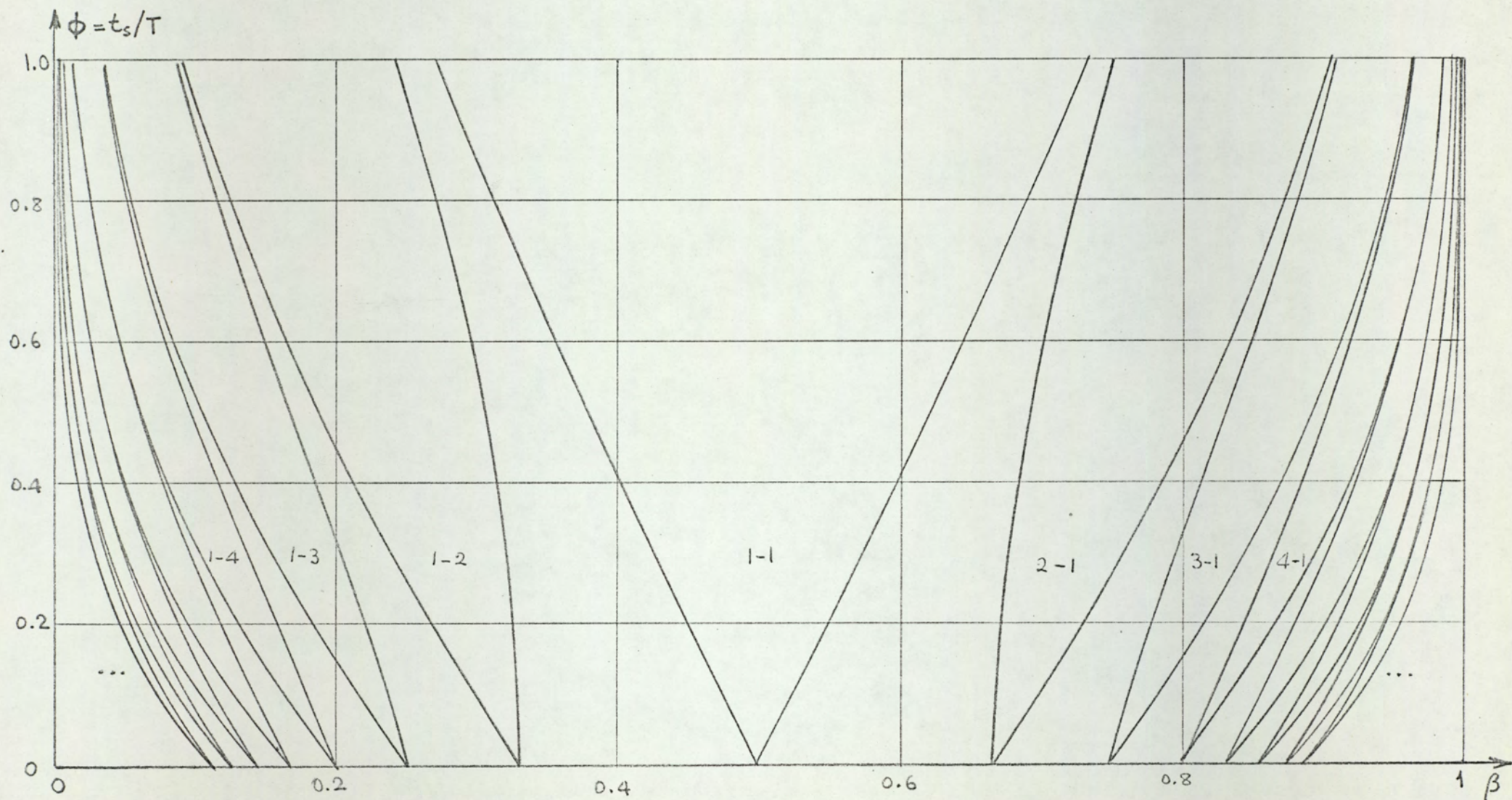


Fig. 6.14
 Zone boundaries for sat-sat limit cycling. Zones for M and N up to 8 are shown.

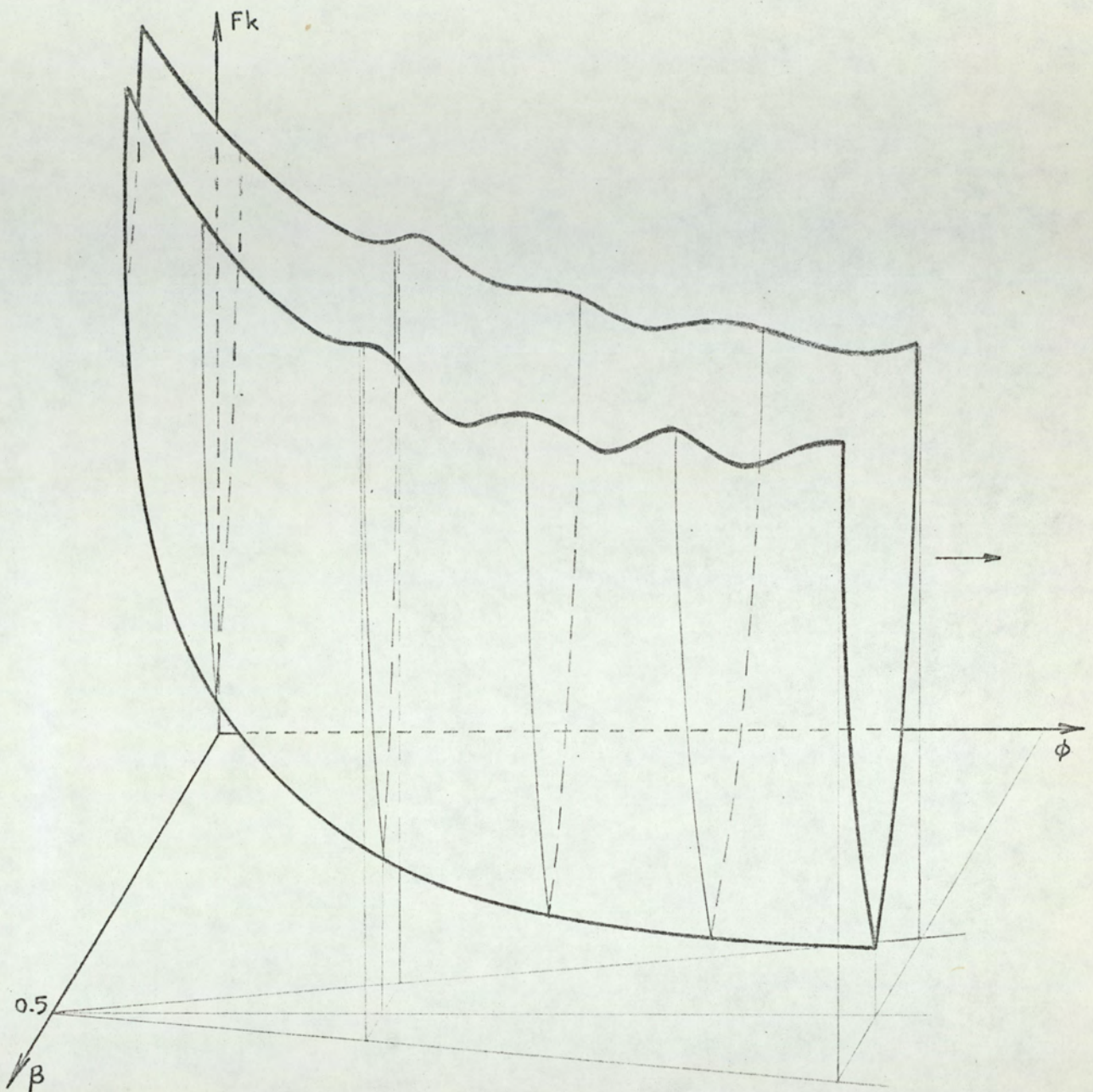


Fig. 6.15

A three dimensional display of 1-1 limit cycling zones.
 A point (a set of values of ϕ , β , and F_k) inside the V-shaped curve corresponds to 1-1 mode limit cycling

system settles into a 6-1 mode limit cycling. The effect of the disturbance will be discussed later.

Stability of sat-sat limit cycles

It is seen from figure 6.16 that for an M-1 limit cycle a perturbation ϵ on the output temperature becomes $A^{M+1} \epsilon$ after one cycling period. The same is true for 1-N limit cycles. Since $A = \exp(-\phi) < 1$ the perturbation will eventually die. It can be shown that even if the perturbation is large enough to drive the system out of the saturation region, the system will eventually return to the original limit cycle. Therefore it can be asserted that all sat-sat limit cycles are stable.

Performance of the system in sat-sat cycling

The average output temperature and offset

The output waveshape for a given M-1 or 1-N mode is independent of the command value, as shown in eqns. 6.50 and 6.58. On the other hand the mode of the oscillations depends on the command. Since the average value of the output is dependent on the mode the command still has an effect on the output temperature. This effect is shown in fig. 6.17. In fig. 6.17 the average output temperature of a sat-sat cycling system is shown as a function of command (both normalized). Line A shows the ideal dependence (i.e. $\theta = \theta_r$), whereas the horizontal line segments show the actual dependence. Figure 6.17 is valid for $\phi = 0.2$, the dependence of θ on θ_r for other values of ϕ can easily be found from fig. 6.14. In fig. 6.17 the boundary for an allowable offset of +7 percent is also shown as an example (line B). It can be seen that for M-1 modes with $M = 4, 5, 6$ and 7 the offset may exceed the allowable limit,

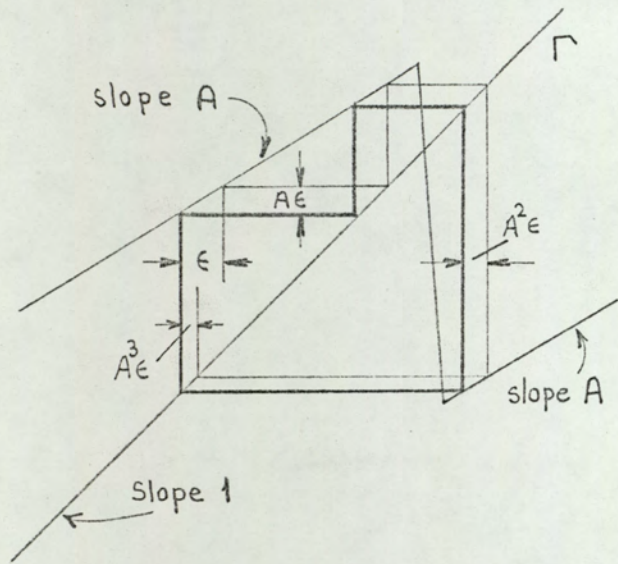


Fig. 6.16

Stability considerations for sat-sat limit cycling. A 2-1 mode cycling is shown. An initial perturbation ϵ becomes $A^3\epsilon$ after one cycling period.

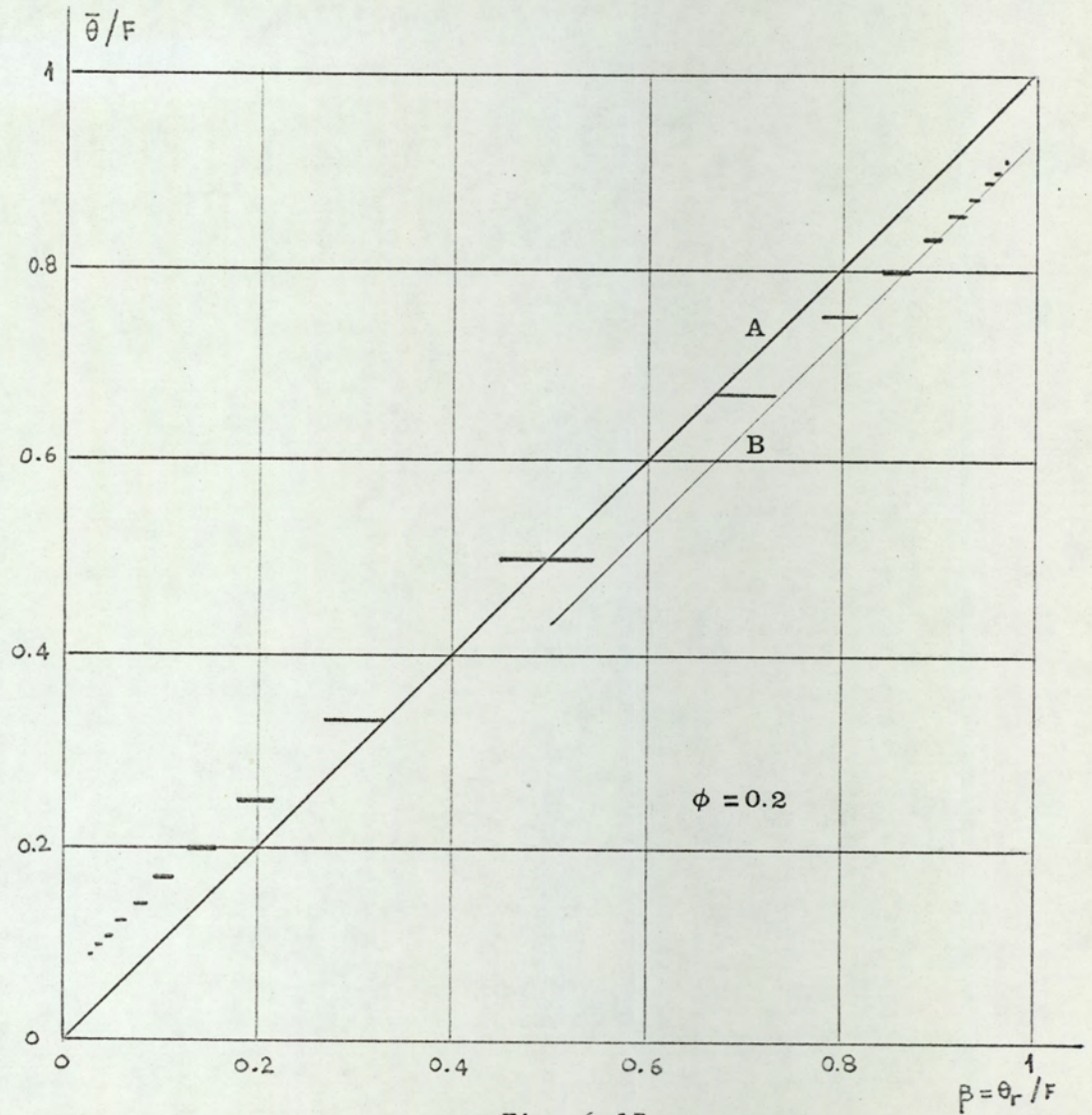


Fig. 6.17

Average output temperature of sat-sat cycling system as a function of command (both normalized). Line A shows the ideal dependence (i.e. $\theta = \theta_r$). Line B is the allowable offset boundary for an offset of 7 percent.

whereas for other values of M the offset is always less than +7 percent. The value of the offset for a given θ_r and M (or N) can precisely be calculated from:

$$\text{relative offset} \left. \vphantom{\frac{\theta_r - \bar{\theta}}{F}} \right\} = \frac{\theta_r - \bar{\theta}}{F} = \begin{cases} \beta - \frac{M}{1+M} & \text{for } \theta_r \geq 0.5 F \\ \beta - \frac{1}{1+N} & \text{for } \theta_r \leq 0.5 F \end{cases}$$

The maximum possible value of the relative offset can be found from:

$$\text{max. possible offset} \left. \vphantom{\frac{\beta^u}{M-1} - \frac{M}{1+M}} \right\} = \begin{cases} \beta^u_{M-1} - \frac{M}{1+M} & \text{for } \theta_r \geq 0.5 F \\ \beta^l_{1-N} - \frac{1}{1+N} & \text{for } \theta_r \leq 0.5 F \end{cases}$$

where upper and lower boundaries of zones are as given in eqns. 6.68 and 6.82. In fig. 6.18 maximum possible offset is shown as a function of ϕ .

Amplitude of oscillations

The amplitude of sat-sat oscillations have been given in eqns. 6.47 and 6.57. These equations are displayed in fig. 6.19. It is clear that as M (or N) increases (i.e. as θ_r/F approaches 0 or 1) the amplitude increases. It can be shown that the maximum possible amplitude is:

$$\lim_{M(N) \rightarrow \infty} \frac{\theta_d}{F} = 1 - A = 1 - \exp(-\phi)$$

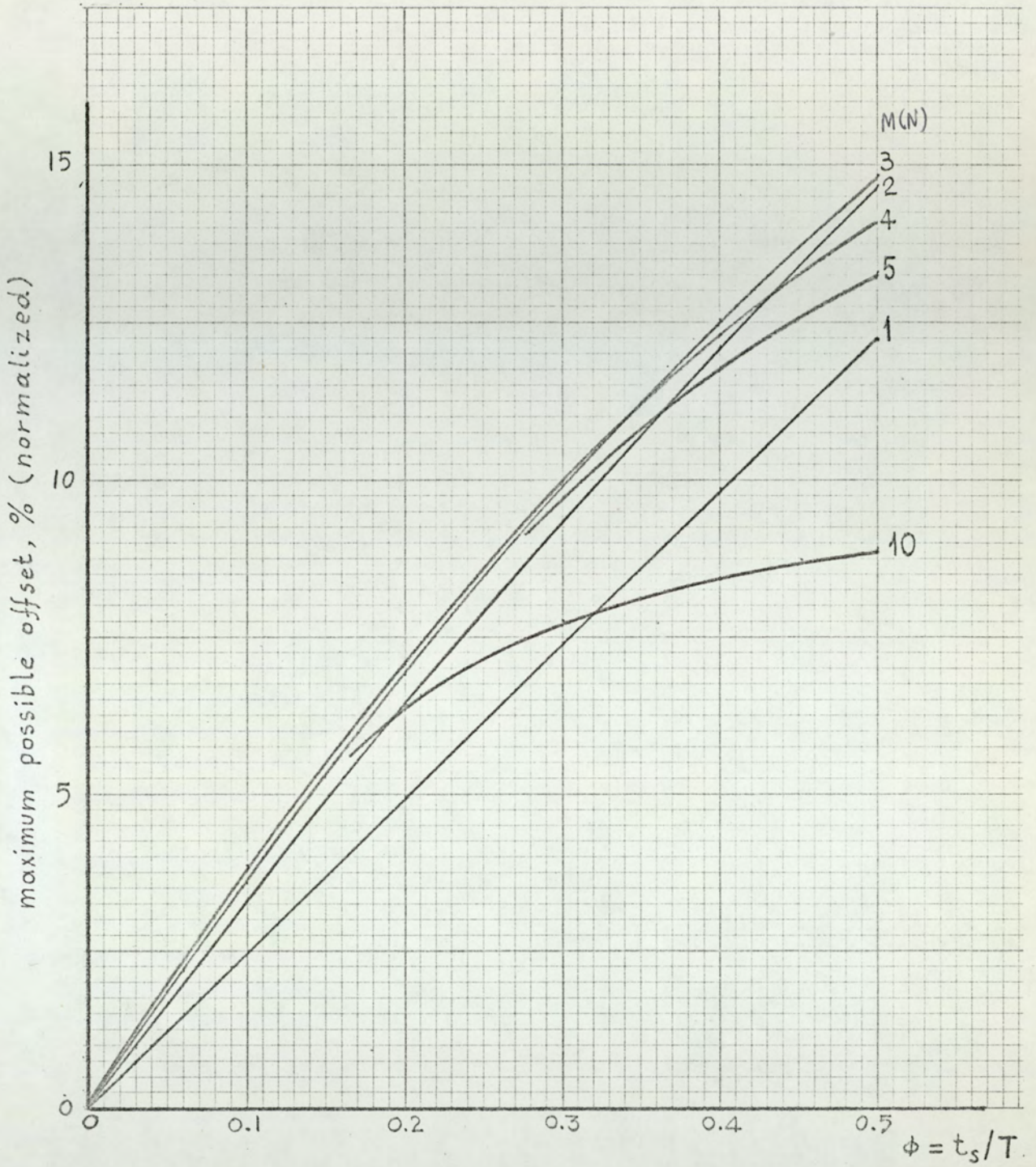


Fig. 6.18

Maximum possible offset as a function of ϕ (sat-sat cycling system).

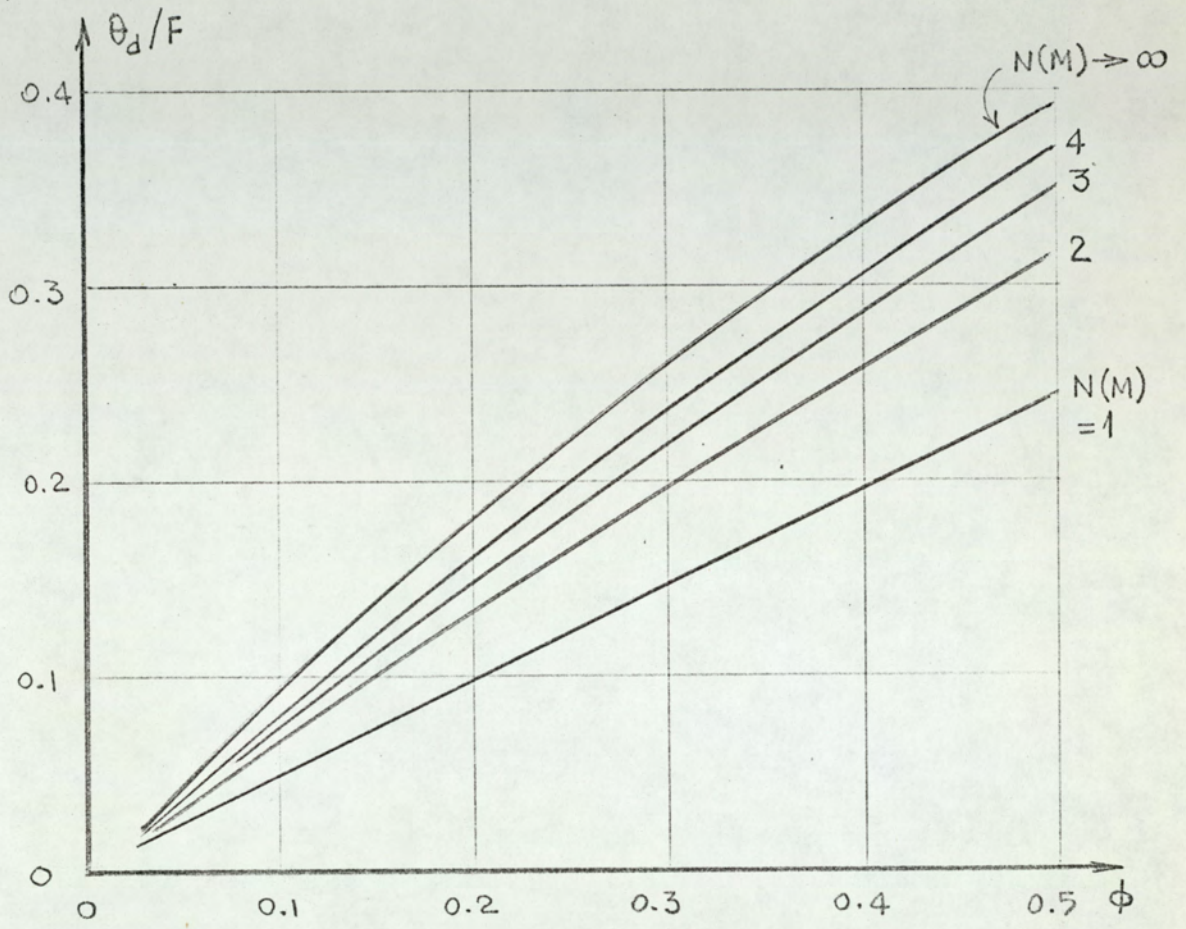


Fig. 6.19

The amplitude of sat-sat oscillations as a function of ϕ .

Figures 6.17, 6.18, and 6.19 provide an easy way for the evaluation of the performance of the system in sat-sat cycling.

6.3.3 Linear and saturated-linear oscillations

As it was mentioned earlier, the term "sat-lin limit cycling" implies the existence of non-saturated as well as saturated sampling intervals in the cycling period. Before examining this type of cycling, we shall investigate the possibility of linear limit cycling, for which the system remains non-saturated for the entire cycling period.

The slope of the system characteristic curve for region II is (eqn. 6.15)

$$S = A - Fk(1 - A) \quad (6.90)$$

No limit cycle of any kind is possible for

$$S > -1 \quad (6.91)$$

This can be shown as follows:

1. From eqn. 6.89 we know that no sat-sat limit cycle is possible for

$$Fk < \frac{1+A}{1-A}$$

This last condition is equivalent to condition 6.91 as it is evident from eqn. 6.90.

2. For any other type of limit cycling the system must pass through region II. Once the system enters into region II the output temperature will have a value θ between U_0

and V_0 (fig. 6.2). The temperature for the next sampling instant will be equal to $Q(\theta)$ and the subsequent temperature values are given by (eqn. 6.30 f) :

$$Q^i(\theta) = S^i (\theta - \theta_r) + \theta_r$$

It is clear that when $|S| < 1$

$$\lim_{i \rightarrow \infty} S^i = 0$$

and

$$\lim_{i \rightarrow \infty} Q^i(\theta) = \theta_r \quad (6.92)$$

Therefore, if $|S| < 1$ the system will remain in region II, and the output temperature approach θ_r .

We note that the maximum value of S is A , which corresponds to $Fk = 0$. If

$$0 < S < A \quad \text{i.e.} \quad 0 < Fk < \frac{A}{1-A}$$

then θ approaches θ_r from either above or below, the system error having the same sign all the time. But if

$$-1 < S < 0 \quad \text{i.e.} \quad \frac{A}{1-A} < Fk < \frac{1+A}{1-A}$$

then θ approaches θ_r by damped oscillations. The damping is dependent on the value of $|S|$. The smaller the value of $|S|$ the faster the transients die out.

The above argument is summarised in fig. 6.20.

For $S = -1$ damping is zero and linear oscillations become possible. This is shown in fig. 6.21. It is also clear that this limit cycling is not stable since, if S is slightly larger than -1 , the oscillations will eventually die out. On the other hand, if S is slightly smaller than -1 the oscillations will increase in amplitude, until the trajectory hits one or both of the saturation characteristics, then the system falls in a sat-sat limit cycle if β and Fk satisfy the conditions for some sat-sat zone. Otherwise sat-lin limit cycling occurs.

Sat-lin limit cycling is basically a two sampling period cycling. One sampling period is saturated ($m = 0$ or 1), the other is non-saturated. The term sat heat-lin will be used if $m = 1$ in the saturated sampling period, whereas a sat-lin limit cycling with $m = 0$ in the saturated period will be called sat cool-lin cycling. Fig. 6.22 shows a typical sat heat-lin cycling. The parameters of the system are:

$$\phi = t_s/T = 0.915, F = 100^\circ\text{C}, \theta_r = 80^\circ\text{C}, b = 0.79 (\approx 0.80), \\ k = 0.04 \text{ l}/^\circ\text{C}.$$

The graphical determination of the limit cycle trajectory is evident from fig. 6.22. Point D is the intersection point of region I characteristic line and Γ . The line DB makes the same angle with Γ as DY. Point B is found as the intersection of lines DB and XY. Point C is found by simply drawing a perpendicular to Γ from point B. Note that the line DB has a slope $1/A$. Any point E on XY corresponds to a pulse duration ratio γ which is given by

$$\gamma = \frac{\overline{YE}}{\overline{XY}}$$

(6.93)

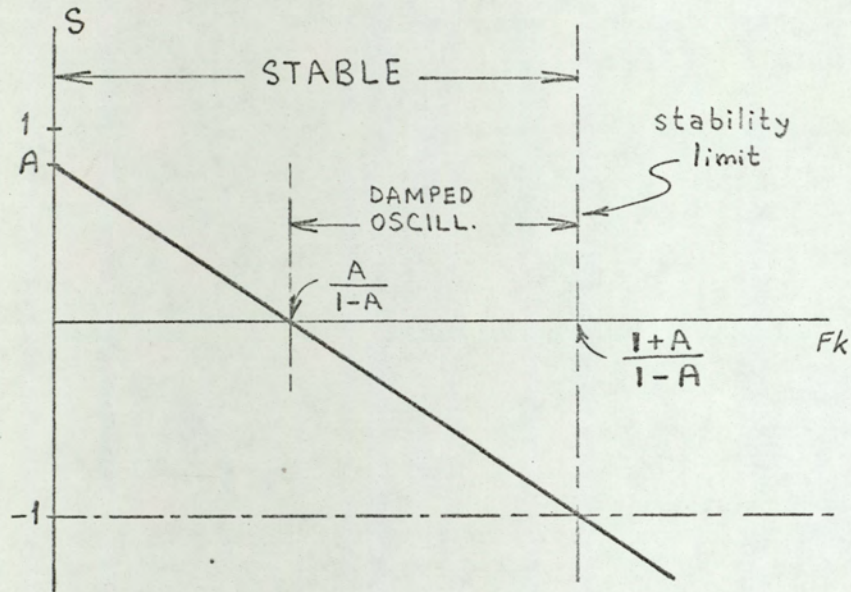


Fig. 6.20

Behaviour of the system in the stable region.

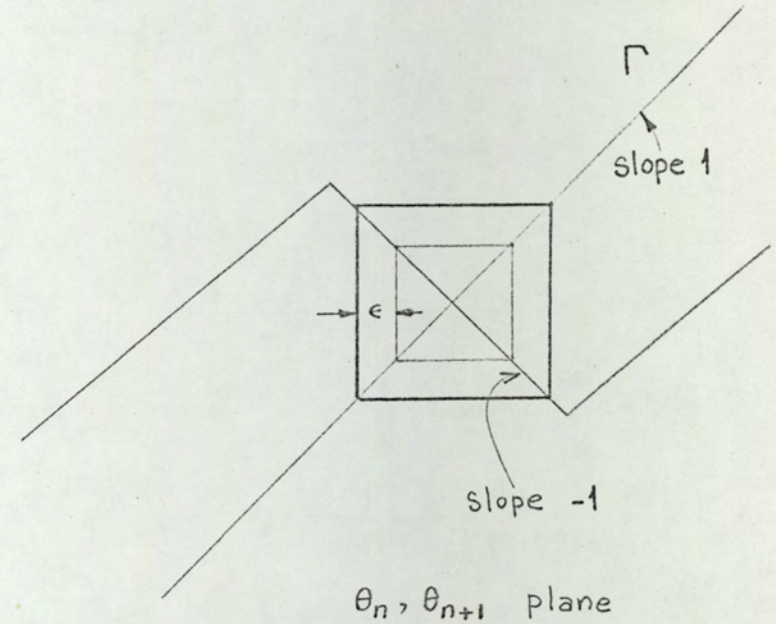


Fig.6.21

Linear cycling. This type of cycling occurs when $Fk = (1 + A)/(1 - A)$. With a small disturbance ϵ the system passes into a new trajectory. This cycling mode is not stable.

For the numerical example, point B corresponds to:

$$\gamma = \frac{\overline{YB}}{\overline{YX}} = 0.53$$

Therefore the limit cycle consists of two sampling periods, one with power continuously on, and another with $\gamma = 0.53$ (fig. 6.22).

The value of the output temperature at sampling instants can be found as follows;

$$\theta_1 = H \{ Q(\theta_1) \} \quad (6.94)$$

$$\theta_1 = H \{ S\theta_1 + (1 - S)\theta_r \} = A \{ S\theta_1 + (1 - S)\theta_r \} + F(1 - A) \quad (6.95)$$

with $S = A - Fk(1 - A)$ the above equation gives

$$\theta_1 = F \frac{1 + \beta A(1 + Fk)}{1 + A(1 + Fk)} \quad (6.96)$$

The minimum temperature is found from

$$\theta_2 = Q(\theta_1) \quad (6.97)$$

which gives

$$\theta_2 = F \frac{A - Fk(1 - A) + (1 + Fk)\beta}{1 + A(1 + Fk)} \quad (6.98)$$

With the parameter values of the above example, eqns.

6.96 and 6.98 yield:

$$\theta_1 = 86.7^\circ\text{C}$$

$$\theta_2 = 66.7^\circ\text{C}$$

which agree with fig. 6.19.

Note that θ_d can no longer be found as $\theta_1 - \theta_2$. This is simply because θ_1 does not represent the maximum output temperature. θ_{\max} occurs in the linear sampling period, as it is seen from fig. 6.22. To find θ_{\max} graphically, one draws line DK which corresponds to

$$\theta' = \theta \exp(-\gamma t_s/T) + F \{1 - \exp(-\gamma t_s/T)\} \quad (6.99)$$

where θ and θ' are abscissa and ordinate values, respectively, and $\gamma = 0.53$.

For sat cool-lin cycling the temperatures at sampling instants are as below:

$$\theta_2 = c [Q(\theta_2)]$$

which gives

$$\theta_2 = F \frac{\beta A(1 + Fk)}{1 + A(1 + Fk)} \quad (6.100)$$

and θ_1 is found from:

$$\theta_1 = c^{-1}(\theta_2)$$

which gives

$$\theta_1 = F \frac{(1 + Fk)\beta}{1 + A(1 + Fk)} \quad (6.101)$$

The graphical construction of the limit cycle trajectory is similar to satheat-lin case.

It can be shown that for $\beta > 0.5$ only satheat-lin oscillations exist whereas only satcool-lin oscillations are possible for $\beta < 0.5$. For $\beta = 0.5$ the system falls into 1-1 mode without passing through sat-lin oscillations, as is evident from eqn. 6.90.

Stability of sat-lin mode oscillations

In fig. 6.23 a small perturbation of magnitude ϵ is assumed. At the end of one cycling period this perturbation becomes $SA\epsilon$ where

$$A = \exp(-\phi) \quad \text{and} \quad S = A - Fk(1 - A)$$

In order that the oscillation be stable we require:

$$|SA| \epsilon < \epsilon \quad (6.102)$$

$$|S| A < 1 \quad (6.103)$$

$$|S| < \frac{1}{A} \quad (6.104)$$

Since oscillations are possible only for $S < -1$, S is negative, therefore $|S| = -S$. Equation 6.104 becomes:

$$-S < \frac{1}{A} \quad (6.105)$$

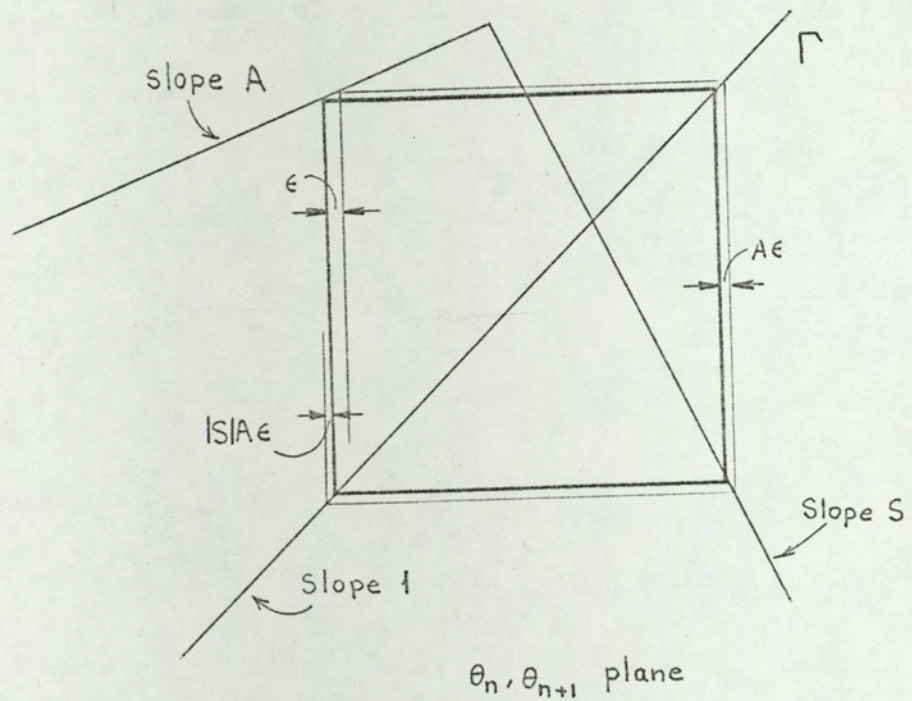


Fig.6.23

Stability considerations for sat-lin oscillations

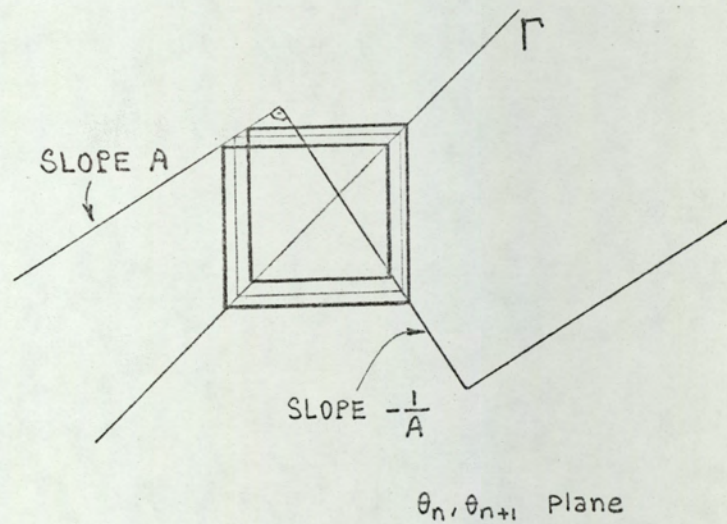


Fig. 6.24

Oscillations when $S = -1/A$
 [i.e. $F_k = (1 + A^2)/A(1 - A)$].

$$S > -\frac{1}{A} \quad (6.106)$$

$$A - Fk(1 - A) > -\frac{1}{A}$$

or

$$Fk < \frac{1 + A^2}{A(1 - A)} \quad (6.107)$$

Therefore, sat-lin oscillations are possible for:

$$\frac{1 + A}{1 - A} < Fk < \frac{1 + A^2}{A(1 - A)} \quad (6.108)$$

Note that for the example of fig. 6.21, $Fk = 4$ whereas $A = 0.4$ and the gain boundaries of sat-lin oscillations are

$$2.34 < Fk < 4.84$$

Therefore, sat-lin oscillations are possible for $Fk = 4$.

Since $\beta = 0.8 > 0.5$ we have sat-lin oscillations.

If $S = -1/A$, i.e. the characteristic lines for saturated and non-saturated regions are perpendicular, the situation shown in fig. 6.24 occurs (sat-lin oscillations of $t_c = 4t_s$). In this type of oscillation the disturbance is carried along indefinitely with alternating signs. This type of oscillation is unstable because, if S is slightly larger than $-1/A$, the oscillations become stable sat-lin, on the other hand, if S is slightly smaller than $-1/A$, then the oscillations become aperiodic, or sat-sat if β and Fk values fit into an oscillation region given in figs. 6.12, 6.13, and 6.14.

Figure 6.25 summarises the conditions given so far.

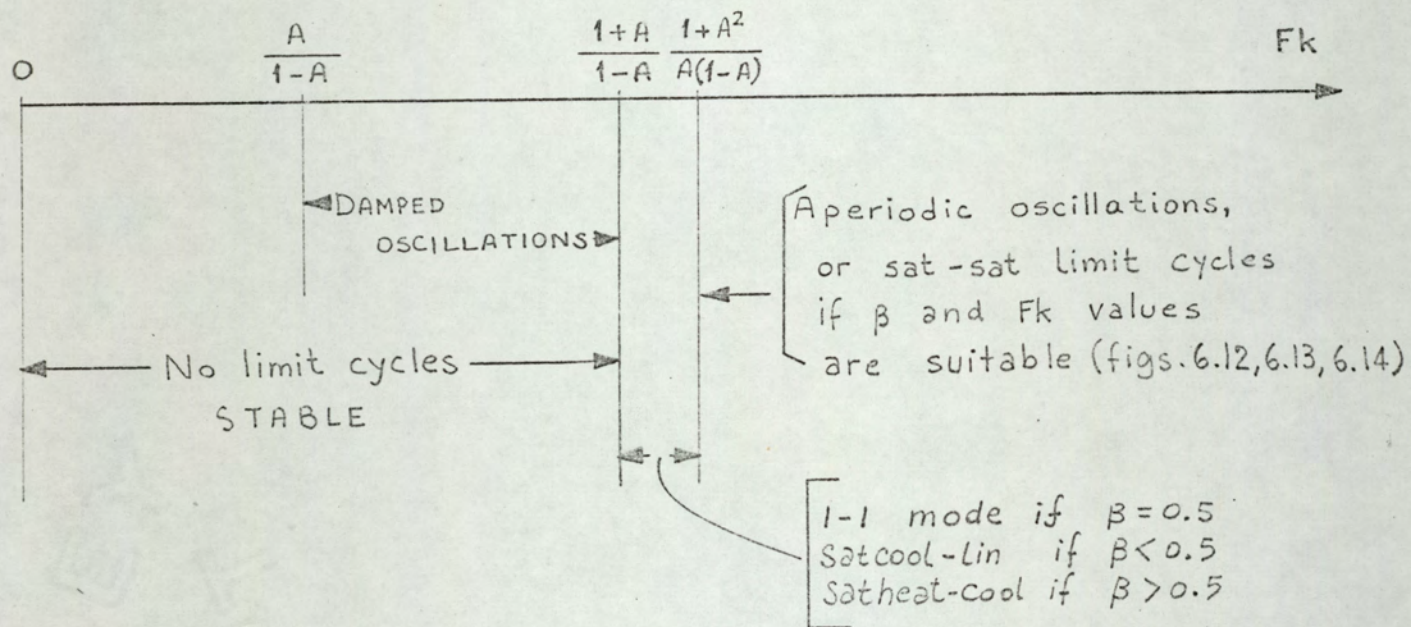


Fig. 6.25

Stability considerations

The functions

$$Fk = \frac{1 + A}{1 - A} \quad (\text{curve 1})$$

$$Fk = \frac{1 + A^2}{A(1 - A)} \quad (\text{curve 2})$$

are displayed in fig. 6.26 as a function of $\phi = t_s/T$. Curve 1 represents the stability of the system. Sat-lin oscillations are possible only for the Fk values between the two curves. It is clear that for the normal range of ϕ sat-lin oscillations are highly improbable.

6.3.4 Plants with transit delay

In this section we consider the plant transfer function

$$F \exp(-sL)/(1 + sT)$$

where $L \neq 0$.

Because of the sampled nature of the system, it is convenient to consider the discrete values of delay which are integer multiples of the sampling period:

$$L = \mu t_s, \quad \mu \text{ integer}$$

The block diagram of the system is shown in fig. 6.27.

From fig. 6.27 and eqn. 6.8:

$$\theta_{n+\mu+1} = A\theta_{n+\mu} + FA \left\{ \exp \left\{ [b+k(\theta_r - \theta_n)] \phi \right\} - 1 \right\} \quad (6.109)$$

With the same approximations used to derive eqn. 6.15, we have:

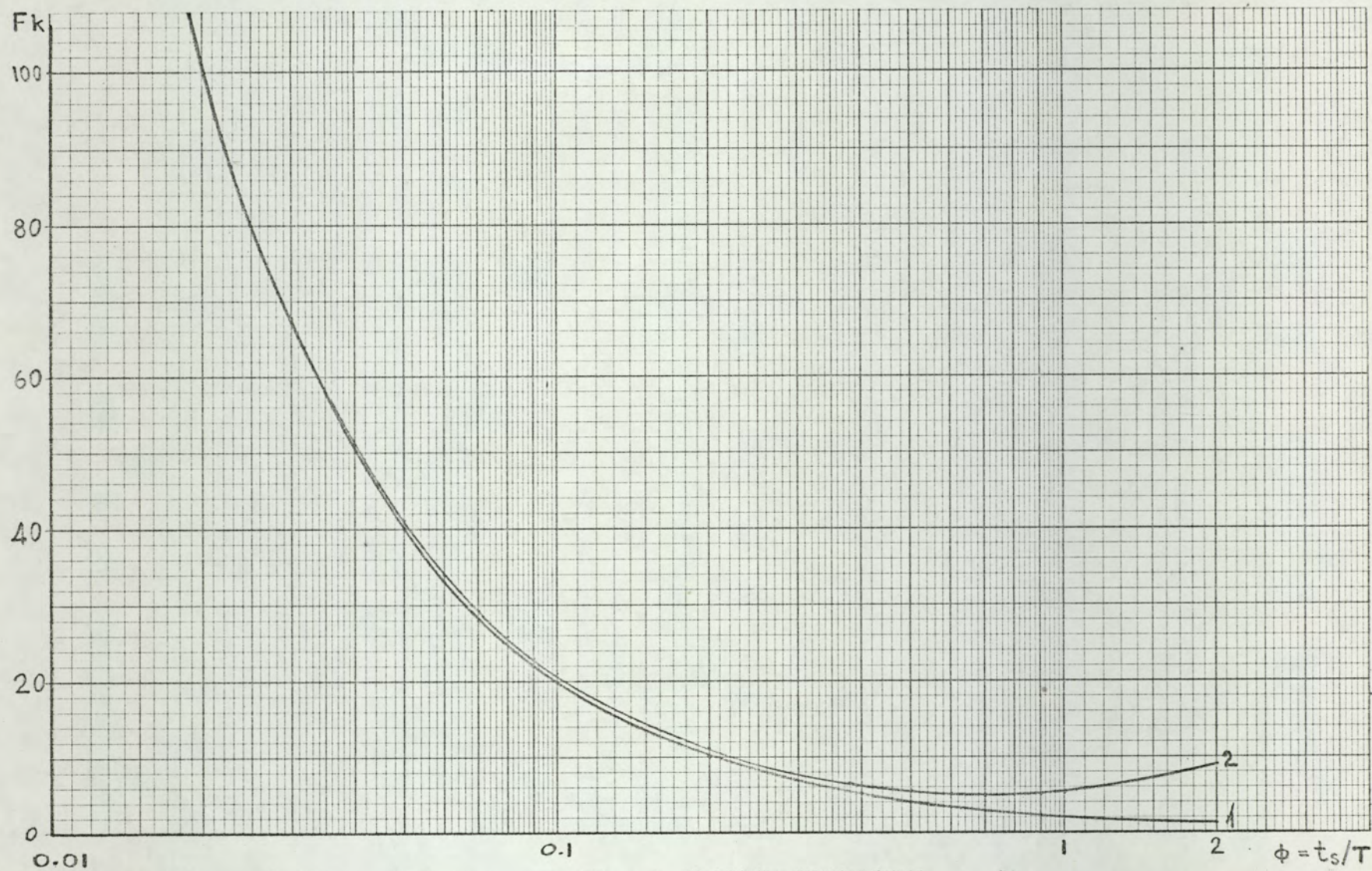


Fig. 6.26

Gain boundaries for $L = 0$.

(1)- Stability boundary

(2)-Upper limit of sat-lin oscillations.

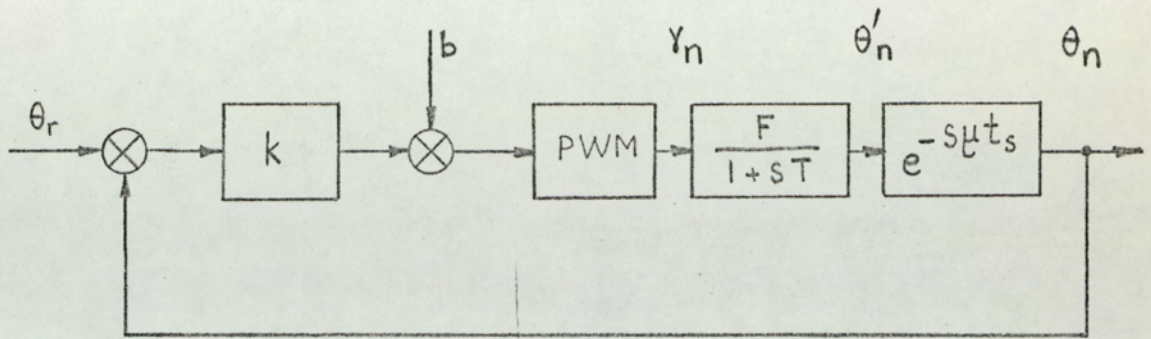


Fig. 6.27

PWM control system with delay in the plant

$$\theta'_n = \theta_{n+\mu}$$

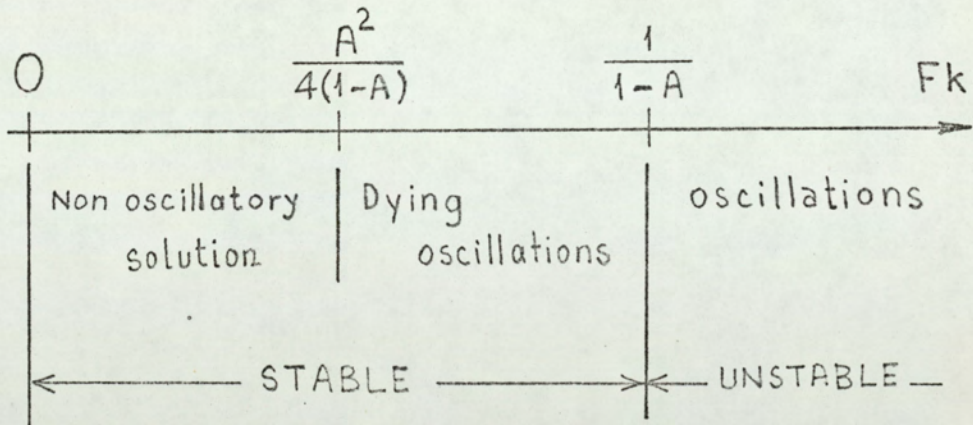


Fig. 6.28

Stability considerations for $L = t_s$

$$\theta_{n+\mu+1} - A\theta_{n+\mu} + Fk(1-A)\theta_n = (1-A)(1+Fk)\theta_r \quad (6.110)$$

Equation 6.110 is a linear ($\mu + 1$) st order difference equation. For $\mu \neq 0$ a graphical solution is very difficult if not impossible. Therefore, we proceed to solve eqn. 6.110 by analytical methods.

Since the range of delays usually encountered in electroheat processes extends from about $T/10$ to at most about $T/5$, and the sampling period is usually of the order of $T/20$ to $T/10$ we consider $L = t_s$ and $L = 2t_s$ (i.e. $\mu = 1$ and $\mu = 2$) in the following analysis.

$$\underline{\mu = 1 \quad (L = t_s)}$$

Solution of system difference equation

For $\mu = 1$ the difference equation 6.110 becomes:

$$\theta_{n+2} - A\theta_{n+1} + Fk(1-A)\theta_n = (1-A)(1+Fk)\theta_r \quad (6.111)$$

The corresponding homogeneous equation is:

$$\theta_{n+2} - A\theta_{n+1} + Fk(1-A)\theta_n = 0 \quad (6.112)$$

The characteristic equation is:

$$m^2 - Am + Fk(1-A) = 0 \quad (6.113)$$

which has the solution

$$m_{1,2} = \frac{A}{2} \pm \frac{\sqrt{A^2 - 4Fk(1-A)}}{2} \quad (6.114)$$

Thus, if

$$\Delta = A^2 - 4Fk(1 - A) \geq 0 \quad (6.115)$$

m_1 and m_2 are real. Inequality 6.115 leads to:

$$Fk \leq A^2/4(1 - A) \quad (6.116)$$

We now distinguish three cases:

$$1. Fk < A^2/4(1 - A)$$

In this case the roots are real and distinct. The solution of eqn. 6.112 is given by:

$$\theta_n = C_1 m_1^n + C_2 m_2^n \quad (6.117)$$

A particular solution of eqn. 6.111 is

$$\theta_n = \theta_r \quad (6.118)$$

Therefore, the general solution of eqn. 6.111 is given by:

$$\theta_n = C_1 m_1^n + C_2 m_2^n + \theta_r \quad (6.119)$$

where C_1 and C_2 are to be determined from the initial conditions.

$$2. Fk = A^2/4(1 - A)$$

In this case, the roots are equal, and the general solution is

$$\theta_n = (C_1 + C_2 n) \frac{A}{2} + \theta_r \quad (6.120)$$

$$3. Fk > A^2/4(1 - A)$$

In this case, the roots of the characteristic equation are given by:

$$m_{1,2} = \frac{A}{2} \pm j \sqrt{4Fk(1-A) - A^2} \quad (6.121)$$

or, in polar form:

$$m_{1,2} = r(\cos \alpha \pm j \sin \alpha) \quad (6.122)$$

where

$$r = \frac{1}{2} \sqrt{A^2 + 4Fk(1-A) - A^2} = \sqrt{Fk(1-A)} \quad (6.123)$$

and

$$\alpha = \tan^{-1} \frac{\sqrt{4Fk(1-A) - A^2}}{A} \quad (6.124)$$

The solution of eqn. 6.111 is given by

$$\theta_n = C_1 r^n \cos(n\alpha + C_2) + \theta_r \quad (6.125)$$

where C_1 and C_2 are to be determined from the initial conditions.

Stability of the system

The condition of stability for a second order difference equation is given by the following theorem¹⁵.

Theorem: Let

$$\Omega = \max(|m_1|, |m_2|) \quad (6.126)$$

where m_1 and m_2 are as given in eqn. 6.114. Then $\Omega < 1$ is a

necessary and sufficient condition for the solution of the homogeneous equation to converge, with limit 0, for all initial conditions.

From eqn. 6.118 it follows that when $\Omega < 1$ the solution of the nonhomogeneous equation will converge to the limit θ_r .

Now we examine the stability for the three cases mentioned above

$$1. Fk < A^2/4(1 - A)$$

In this case we have

$$\Omega = |m_1| = m_1 = \frac{A}{2} + \frac{\sqrt{A^2 - 4Fk(1 - A)}}{2} \quad (6.127)$$

since $A > 0$, $A^2 - 4Fk(1 - A) > 0$.

The condition $\Omega < 1$ gives

$$Fk > -1$$

which is always true, since $Fk > 0$. Therefore, the system is always stable.

$$2. Fk = A^2/4(1 - A)$$

In this case

$$\Omega = m_1 = m_2 = \frac{A}{2} < 1$$

Therefore, the system is always stable.

$$3. Fk > A^2/4(1 - A)$$

In this case

$$\Omega = r = \sqrt{Fk(1 - A)}$$

Therefore, the system is stable when $Fk < 1/(1 - A)$, and unstable when $Fk \geq 1/(1 - A)$.

The period of oscillations, t_{osc} , is found from eqns. 6.122 and 5.124:

$$t_{osc} = \frac{2\pi}{a} t_s \quad (6.128)$$

where a is expressed in radians

The summary of the above discussion is given in fig. 6.28.

In fig. 6.29 the stability boundary (curve a) and the oscillatory solution boundary (curve b) are shown. If the point corresponding to the ϕ and Fk values is in region I the system is stable and non-oscillatory, if it is in region II the system is stable but oscillatory (damped), and if it is in region III the system is unstable. Curve a shows the period of the undamped oscillations (i.e. period of oscillations when $\Omega = 1$) versus ϕ .

Numerical Example

Let the system parameters be $t_s = 10$ min, $T = 50$ min, $L = 10$ min, $F = 100^\circ\text{C}$, $\theta_r = 50^\circ\text{C}$, $b = 0.5$, $A = \exp(-0.2) = 0.819$.

The condition for nonoscillatory solution is:

$$Fk < \frac{A^2}{4(1 - A)} = 0.924 \quad \text{or} \quad k < 0.00924$$

The condition for stability is:

$$Fk < \frac{1}{1 - A} = 5.517 \quad \text{or} \quad k < 0.05517$$

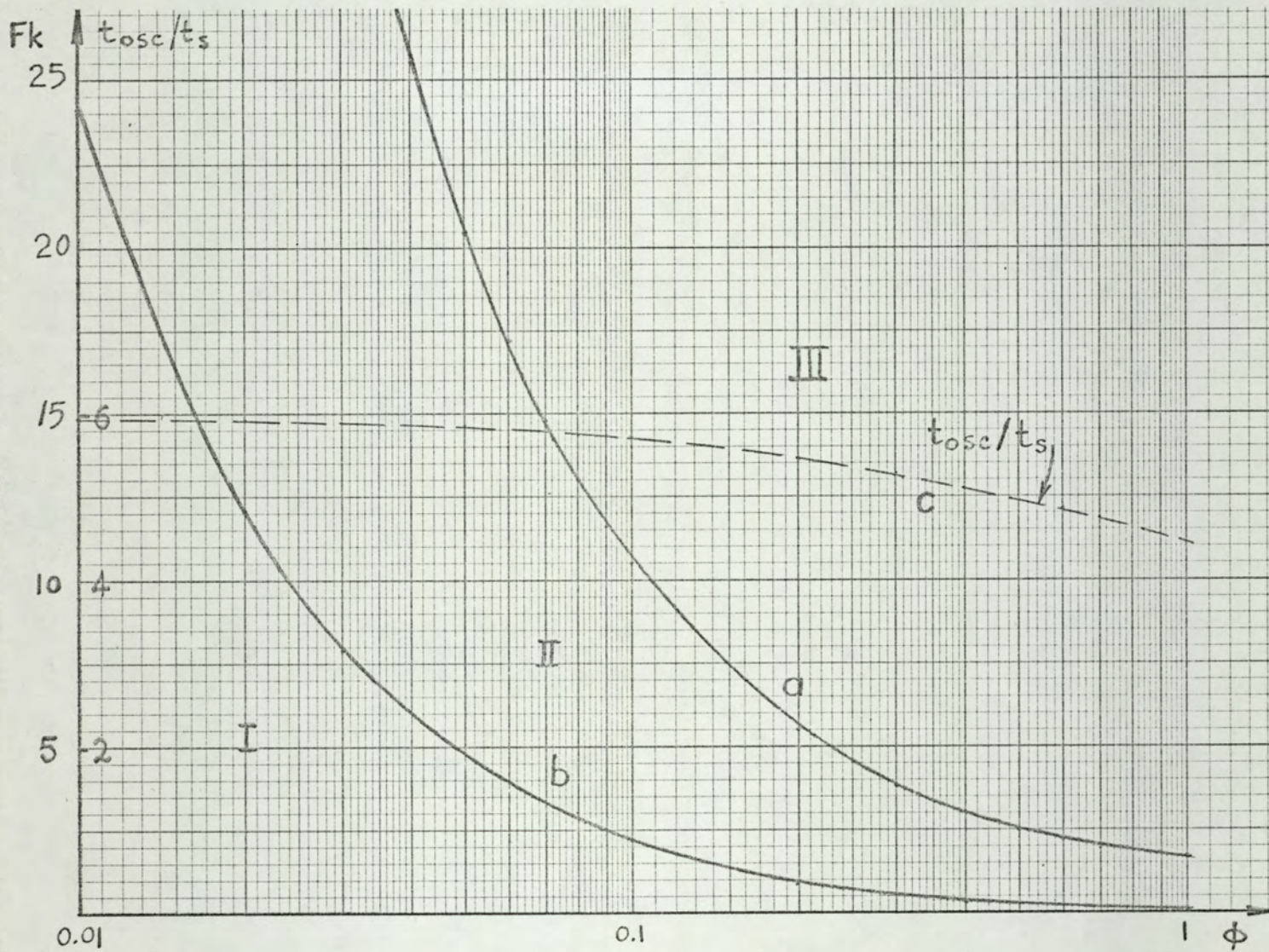


Fig. 6.29

The stability (a), and oscillatory solution (b) boundaries for $L = t_s$. Curve c shows the period of the undamped oscillations (i.e. when $\Omega = 1$).

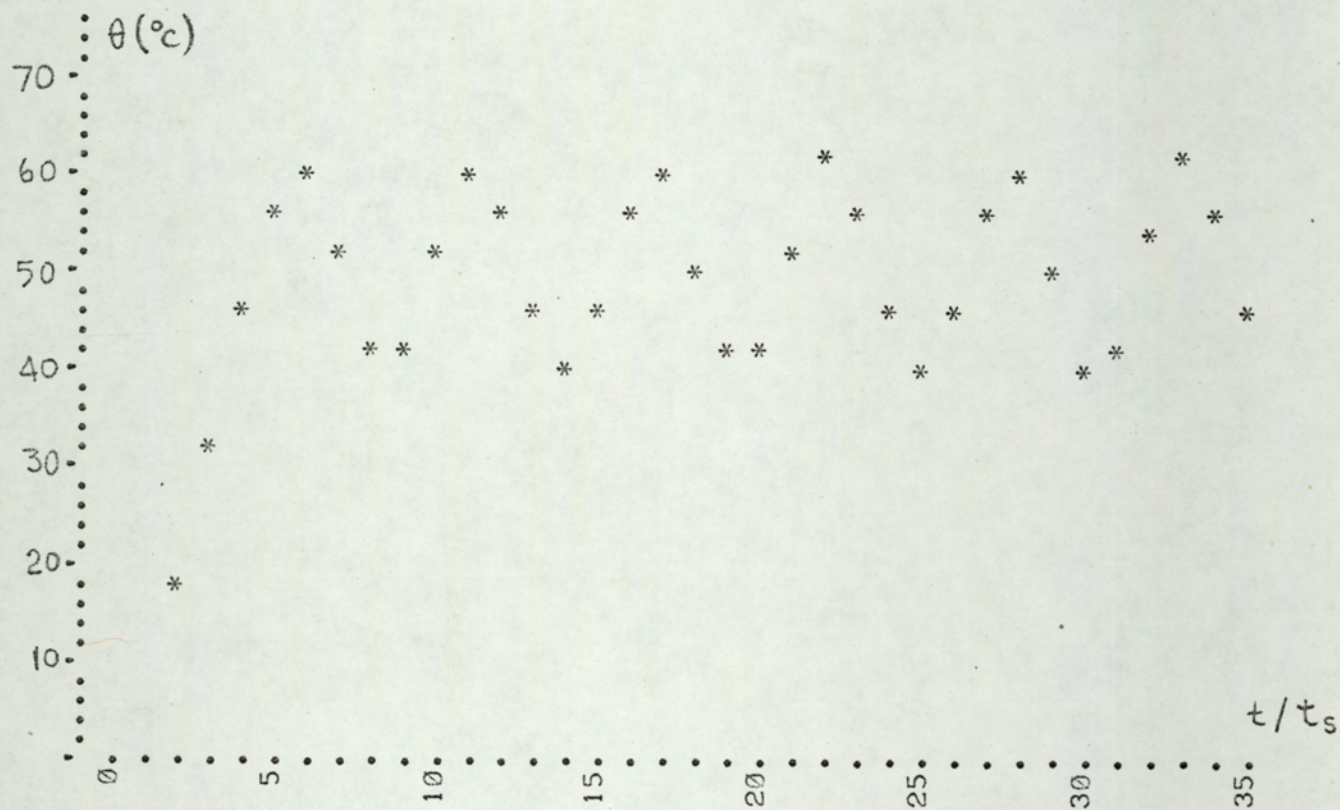


Fig. 6.30
 Digital computer plot of the system output for $t = 10$ min, $T = 50$ min, $F = 100^{\circ}\text{C}$, $\theta_r = 50^{\circ}\text{C}$
 $b = 0.5$ and $k = 0.07$.

If $k = 0.07$ the system will be oscillatory, with oscillations very slowly growing.

r is found from eqn. 6.123

$$r = \sqrt{Fk(1 - A)} = 1.12$$

α is found from eqn. 6.124

$$\alpha = \tan^{-1} 2.56 = 68.7^\circ$$

Therefore, the period of the oscillations is, from eqn. 6.128:

$$t_{osc} = \frac{360}{68.7} t_s = 5.25 t_s = 52.5 \text{ min.}$$

A digital simulation plot corresponding to the above example for $k = 0.07$ is shown in fig. 6.30. There it is seen that the simulation gives an oscillation period of about $5.5 t_s = 55 \text{ min.}$

It must be noted that the difference equation 6.111 is valid only for the linear region. When the gain is large growing oscillations will cause saturation. The saturated oscillations in presence of delay will not be elaborated in this work. Two figures are included to show a typical saturated oscillation (fig. 6.31 and 6.32). Both fig. 6.31 (curve a) and 6.32 are for the same system with $t_s = 10 \text{ min}$, $T = 50 \text{ min}$, $L = 10 \text{ min}$, $F = 100^\circ\text{C}$, $\theta_r = 70^\circ\text{C}$, $k = 0.24 \text{ l/}^\circ\text{C}$, and $b = 0.72$. Figure 6.31 shows the digital simulation result, whereas fig. 6.32 shows the analogue simulation result. From both curves it is clear that the system is in 4-2 mode. We therefore conclude that for systems having delay M-N modes

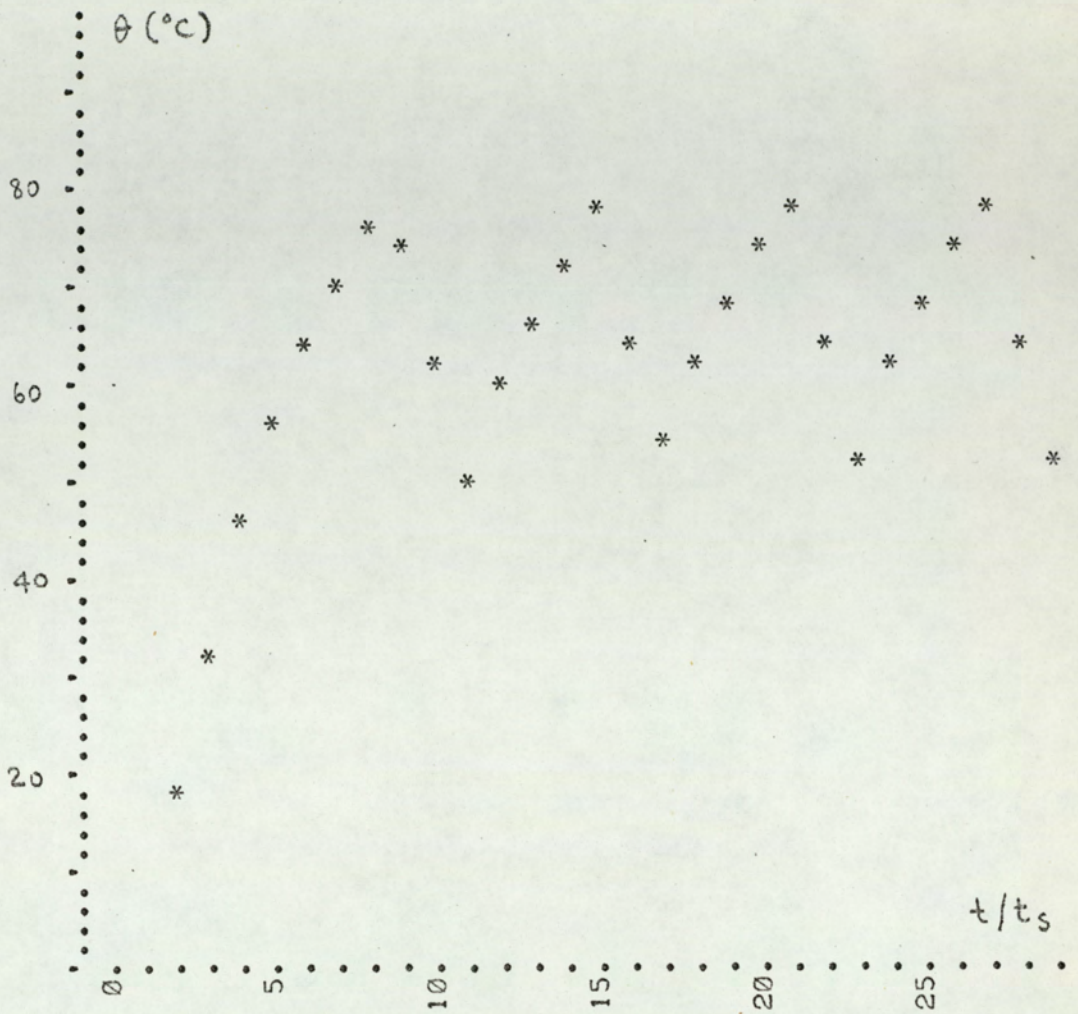


Fig. 6.31

Digital computer plot of the output of a system in saturated limit cycling. System parameters are :

$t_s = 10$ min, $T = 50$ min, $F = 100^\circ\text{C}$, $\theta_r = 70^\circ\text{C}$, $k = 0.24$ $1/^\circ\text{C}$,

$L = 10$ min.

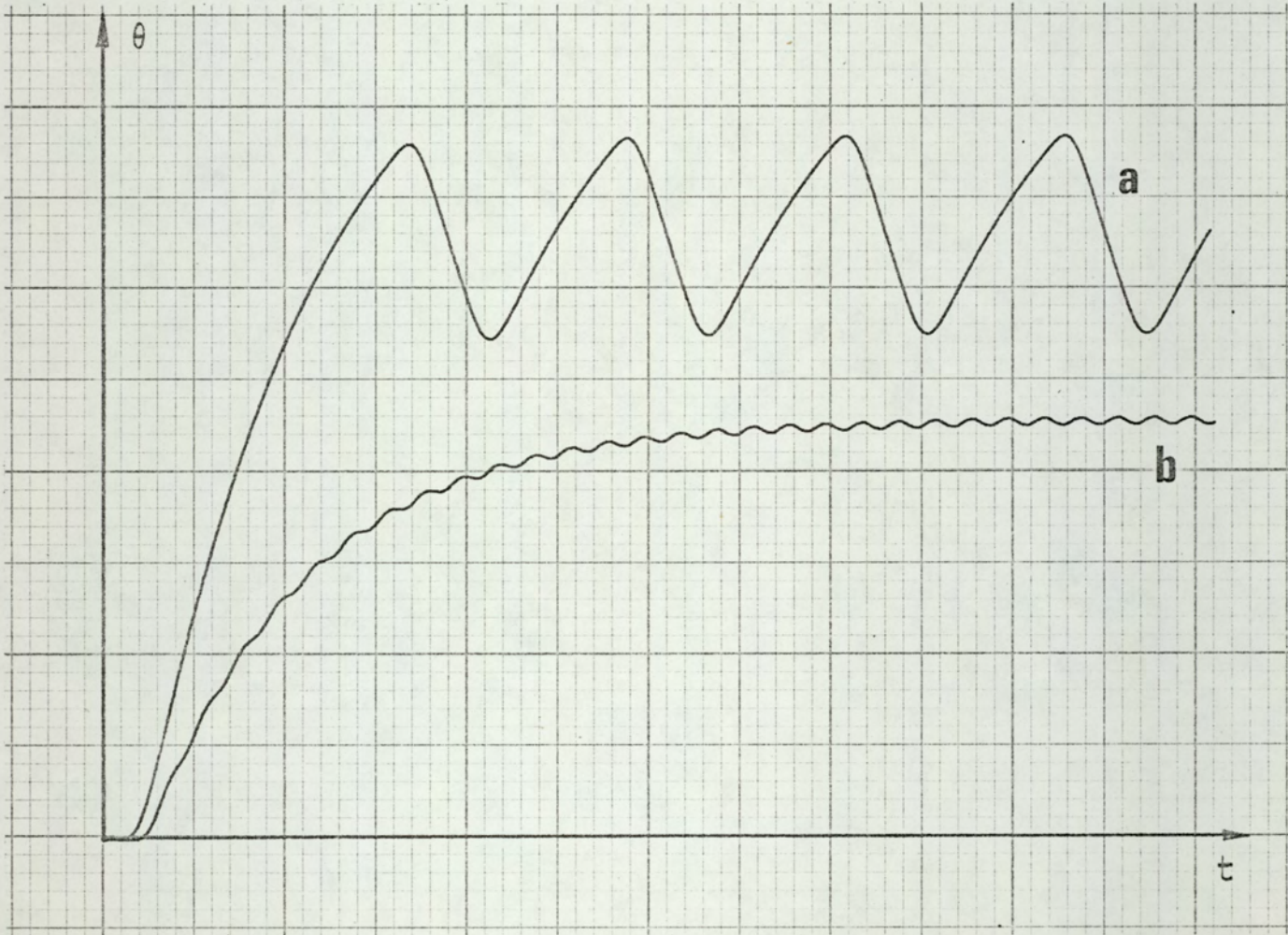


Fig. 6.32

Analogue computer plot of the output of the same system as in fig. 6.31.

a- $k=0.24$, $\theta_r=70$. (sat. limit cycling). b- $k=0.008$, $\theta_r=45$ (stable system).

Time scale: 50 sec/inch; temperature scale: 20°C/inch (2 V/inch).

are possible where both M and N are different from 1. In curve b of fig. 6.32 the response of the same system is shown, but with $k = 0.008$. This value of gain corresponds to non-oscillatory solution, since

$$Fk < A^2 / 4(1 - A) = 0.924$$

$$\underline{\mu = 2 \quad (L = 2t_s)}$$

Solution of system difference equation

For $\mu = 2$, eqn. 6.110 becomes:

$$\theta_{n+3} - A\theta_{n+1} + Fk(1 - A)\theta_n = (1 - A)(1 + Fk)\theta_r \quad (6.129)$$

The characteristic eqn. of the homogeneous difference equation is:

$$m^3 - Am^2 + Fk(1 - A) = 0 \quad (6.130)$$

This cubic equation can be solved analytically by substituting for m the value $x + (A/3)$. The details of the method¹⁷ will not be given.

Let

$$a = -\frac{1}{3} A^2 \quad (6.131)$$

$$b = -\frac{2}{27} A^3 + Fk(1 - A) \quad (6.132)$$

$$\Delta = \frac{b^2}{4} + \frac{a^3}{27} = Fk(1 - A) \left[\frac{1}{4} Fk(1 - A) - \frac{1}{27} A^3 \right] \quad (6.133)$$

$$z_1 = \sqrt[3]{-\frac{b}{2} + \sqrt{\Delta}} \quad (6.134)$$

$$z_2 = \sqrt[3]{-\frac{b}{2} - \sqrt{\Delta}} \quad (6.135)$$

Then the solution of eqn. 6.130 is given by:

$$m_1 = z_1 + z_2 + \frac{A}{3} \quad (6.136)$$

$$m_{2,3} = -\frac{z_1 + z_2}{2} \pm \frac{z_1 - z_2}{2} \sqrt{-3} + \frac{A}{3} \quad (6.137)$$

From eqns. 6.131-6.137 it can be seen that:

If $\Delta > 0$ i.e. $Fk > \frac{4}{27} \frac{A^3}{1-A}$ then there will be one real root and two complex conjugate roots.

If $\Delta \leq 0$ i.e. $Fk \leq \frac{4}{27} \frac{A^3}{1-A}$ then there will be three real roots.

Therefore we conclude that if

$$Fk \leq \frac{4}{27} \frac{A^3}{1-A}$$

the system is non oscillatory, otherwise it is oscillatory.

Note that a particular solution of eqn. 6.129 is θ_r . Therefore, when the homogeneous equation is stable, the output will approach θ_r . The homogeneous equation is stable when $\Omega < 1$, where

$$\Omega = \max (|m_1| , |m_2| , |m_3|) \quad (6.138)$$

In particular, for the oscillatory case, the oscillations will die if $\Omega < 1$.

$|m_1|$, $|m_2|$ and $|m_3|$ are found to be:

$$|m_1| = z_1 + z_2 + \frac{A}{3} \quad (6.139)$$

$$|m_{2,3}| = \sqrt{\left(\frac{z_1 + z_2}{2} - \frac{A}{3}\right)^2 + \frac{(z_1 - z_2)^2}{4}} \cdot 0.3$$

where z_1 and z_2 are as given in eqns. 6.134 and 6.135.

To find the stability condition we have to find the values of ϕ and Fk which make one or more of $|m_1|$, $|m_2|$, and $|m_3|$ larger than 1. Unfortunately, to do this analytically is very difficult. Instead, one can seek the solution of the inequality $\Omega < 1$ by digital computer. This is done and the results are shown in fig. 6.33. In this figure, curve a is the stability boundary and curve b is the oscillatory solution boundary. If the point corresponding to the ϕ and Fk values is in region I the system is stable and non oscillatory, if it is in region II the system is stable but oscillatory (damped), and if it is in region III the system is unstable. Curve c shows the period of the undamped oscillations (i.e. period of oscillations when $\Omega = 1$) versus ϕ .

Numerical example

Let the system parameters be: $t_s = 5$ min, $T = 25$ min, $L = 10$ min, $k = 0.045$ $1/^\circ\text{C}$, $F = 100^\circ\text{C}$, $\theta_r = 50^\circ\text{C}$, $b = 0.52$.

The characteristic equation is:

$$m^3 - 0.819 m^2 + 0.815 = 0$$

The roots of the above equation are:

$$m_1 = -0.725$$

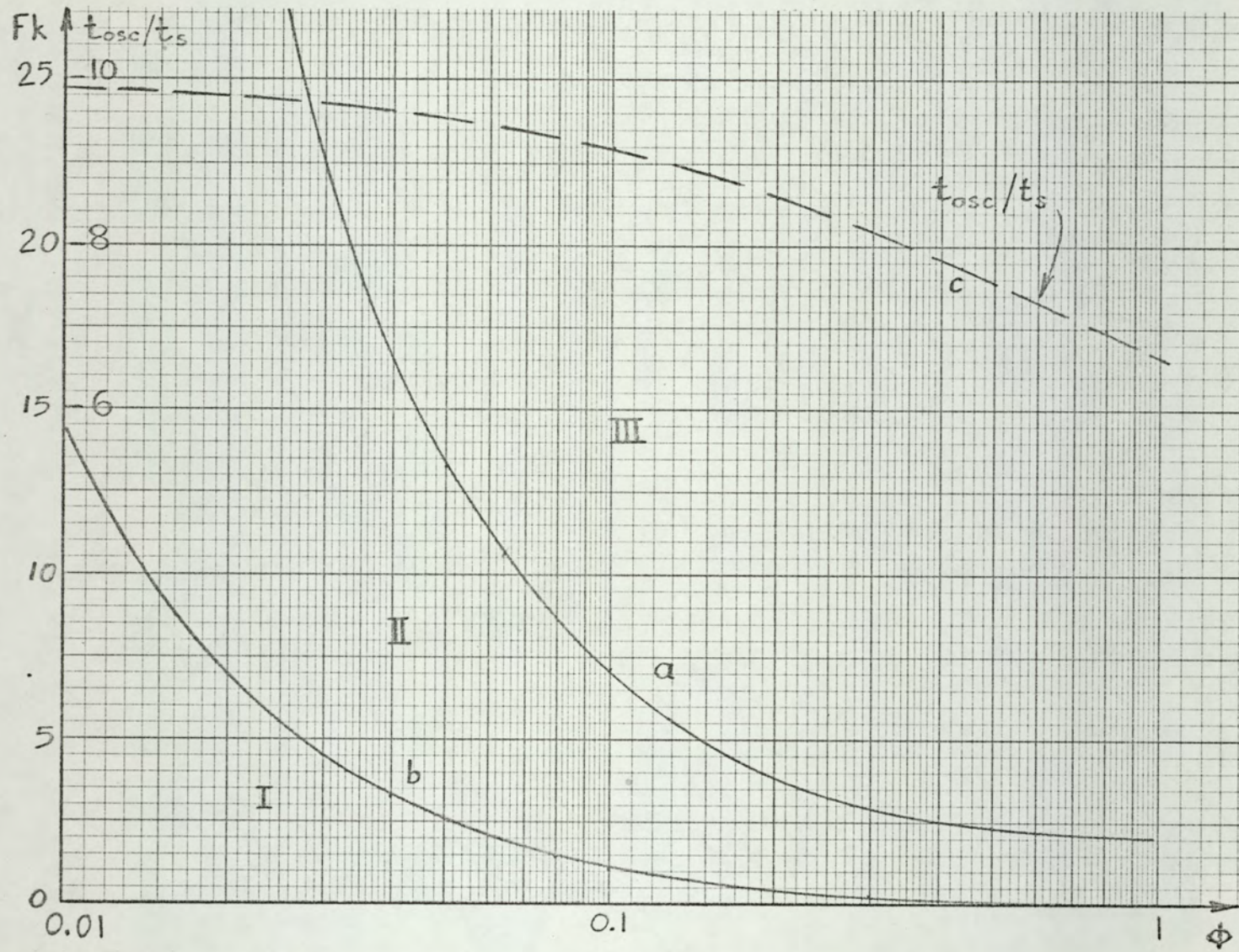


Fig. 6.33

The stability (a), and oscillatory solution (b) boundaries for $L = 2t_s$. Curve c shows the period of undamped oscillations (i.e. when $\Omega = 1$).

$$m_{2,3} = 0.772 \pm j 0.726$$

we see that

$$|m_1| = 0.725$$

$$|m_{2,3}| = 1.06$$

Therefore, the system has slowly growing oscillations.

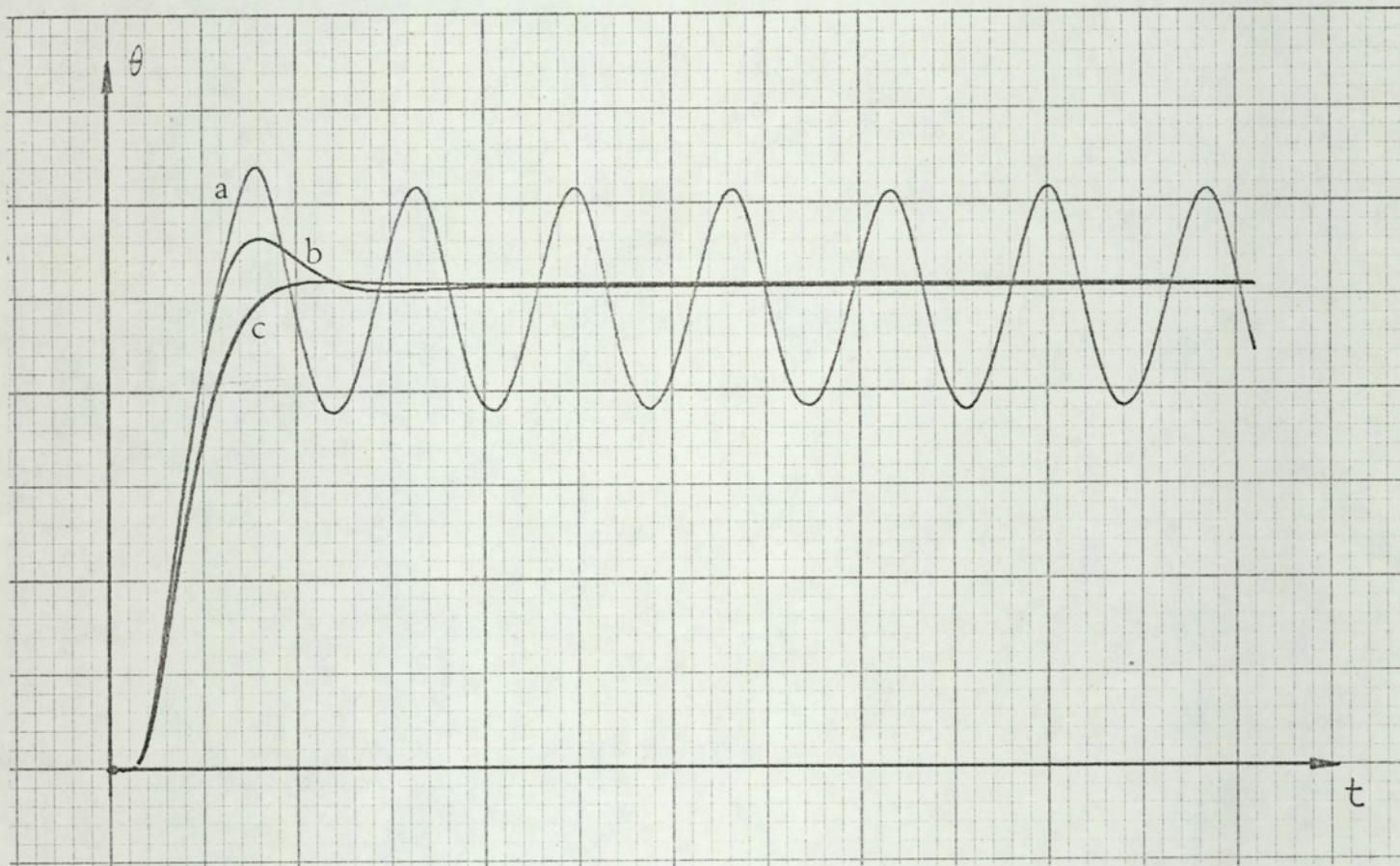
$$\alpha = \tan^{-1} \frac{\text{Im}(m_2)}{\text{Re}(m_2)} = \tan^{-1} \frac{0.726}{0.772} = \tan^{-1} 0.92 = 42.6^\circ$$

Therefore the period of the oscillations are (from eqn. 6.128):

$$t_{\text{osc}} = \frac{360}{42.6} t_s = 8.47 t_s = 42.35 \text{ min}$$

Since $\Omega = |m_2| = 1.06 > 1$, i.e. since the oscillations are nearly undamped, this value of the oscillation period can be found from fig. 6.33.

In fig. 6.34 the output of the system which corresponds to the above example is shown as obtained from analogue simulation. Curve a corresponds to $k = 0.045$ as in the above example. The period of the oscillations is seen to be 42 min. Curve b corresponds to $k = 0.01$. As it can be seen from fig. 6.33 this value of k ($Fk = 1$) corresponds to dying oscillations, and this is evident from fig. 6.34. Curve c corresponds to $k = 0.006$, which is very near to critical damping ($\Delta = 0.000736$). Compare fig. 6.34 with fig. 5.16 (digital plot) and fig. 7.9 (analogue photograph).



a: $k=0.045$
 b: $k=0.01$
 c: $k=0.006$

Fig. 6.34

Analogue computer plot of the output of a system with $L = 2t_s$. The system parameters are:
 $t_s = 5$ min, $T = 25$ min, $L = 10$ min, $F = 100^\circ\text{C}$, $\theta = 50^\circ\text{C}$, $b = 0.52$.
 Time scale: 50 sec/inch, temperature scale: 20°C/inch (2 V/inch)

For large values of gain, analogue simulation has shown 4-4 mode oscillations.

6.4 EFFECTS OF MODE DEPENDENCE

If the plant is mode dependent, the system difference equations can be easily found. Denoting $t_s/T_A = \phi_A$ and $t_s/T_P = \phi_P$, for the on portion of the sampling interval:

$$\theta(\tau) = \theta_n e^{-\tau/T_A} + F(1 - e^{-\tau/T_A}) \quad (6.141)$$

where $\tau = t - nt_s$

Therefore at $\tau = \gamma_n t_s$

$$\theta(\gamma_n t_s) = \theta_n \exp(-\gamma_n \phi_A) + F \{1 - \exp(-\gamma_n \phi_A)\} \quad (6.142)$$

For the remaining portion of the sampling interval:

$$\theta_{n+1} = \theta(\gamma_n t_s) \exp\{-(1 - \gamma_n) \phi_P\} \quad (6.143)$$

From eqns. 6.142 and 6.143:

$$\begin{aligned} \theta_{n+1} = & \theta_n \exp\{\gamma_n(\phi_P - \phi_A) - \phi_P\} + \\ & F \left\{ \exp\{(\gamma_n - 1)\phi_P\} - \exp\{\gamma_n(\phi_P - \phi_A) - \phi_P\} \right\} \end{aligned} \quad (6.144)$$

For region I (fig. 6.2) ($\gamma_n = 1$):

$$\theta_{n+1} = \theta_n \exp(-\phi_A) - F \{1 - \exp(-\phi_A)\} \quad (6.145)$$

For region II $\left[\gamma_n = b + k(\theta_r - \theta_n) \right]$:

Equation 6.144 with $\gamma_n = b + k(\theta_r - \theta_n)$

For region III ($\gamma_n = 0$):

$$\theta_{n+1} = \theta_n \exp(-\phi_p) \quad (6.146)$$

The system difference equation for the control region is, as is seen from eqn 6.144, very complicated. It can be shown that with the approximation $\exp(x) \approx 1 + x$, equation 6.144 can be approximated by a parabola. Therefore, the graphical technique which we used for mode independent systems loses its advantages. Thus we shall not attempt to solve the above difference equations.

The nonlinearity of the characteristic curve in region II does not have any influence on the analysis of sat-sat limit cycling. Therefore, a complete analysis of sat-sat limit cycling is possible using only eqns. 6.145 and 6.146. One notes that these two equations represent two straight lines in the θ_n, θ_{n+1} plane, and the boundaries of regions I and II can easily be found.

6.5 EFFECTS OF DISTURBANCE

6.5.1 Effects of disturbance on regulation characteristic

PWM control is one way of achieving a pseudo-linear control using highly nonlinear elements (relays, thyristors, etc.). Thus, from the point of view of disturbance, a PWM control system is similar to a continuous linear system, if it is stable, and non-saturated.

Two examples are given on the effects of disturbance. In fig. 6.35 the system is subjected to a step disturbance of 10°C at $t = 150$ min. For this system $t_s/T = \phi = 0.2$, $F = 100^\circ\text{C}$, $\theta_r = 50^\circ\text{C}$, and $k = 0.08$. We have

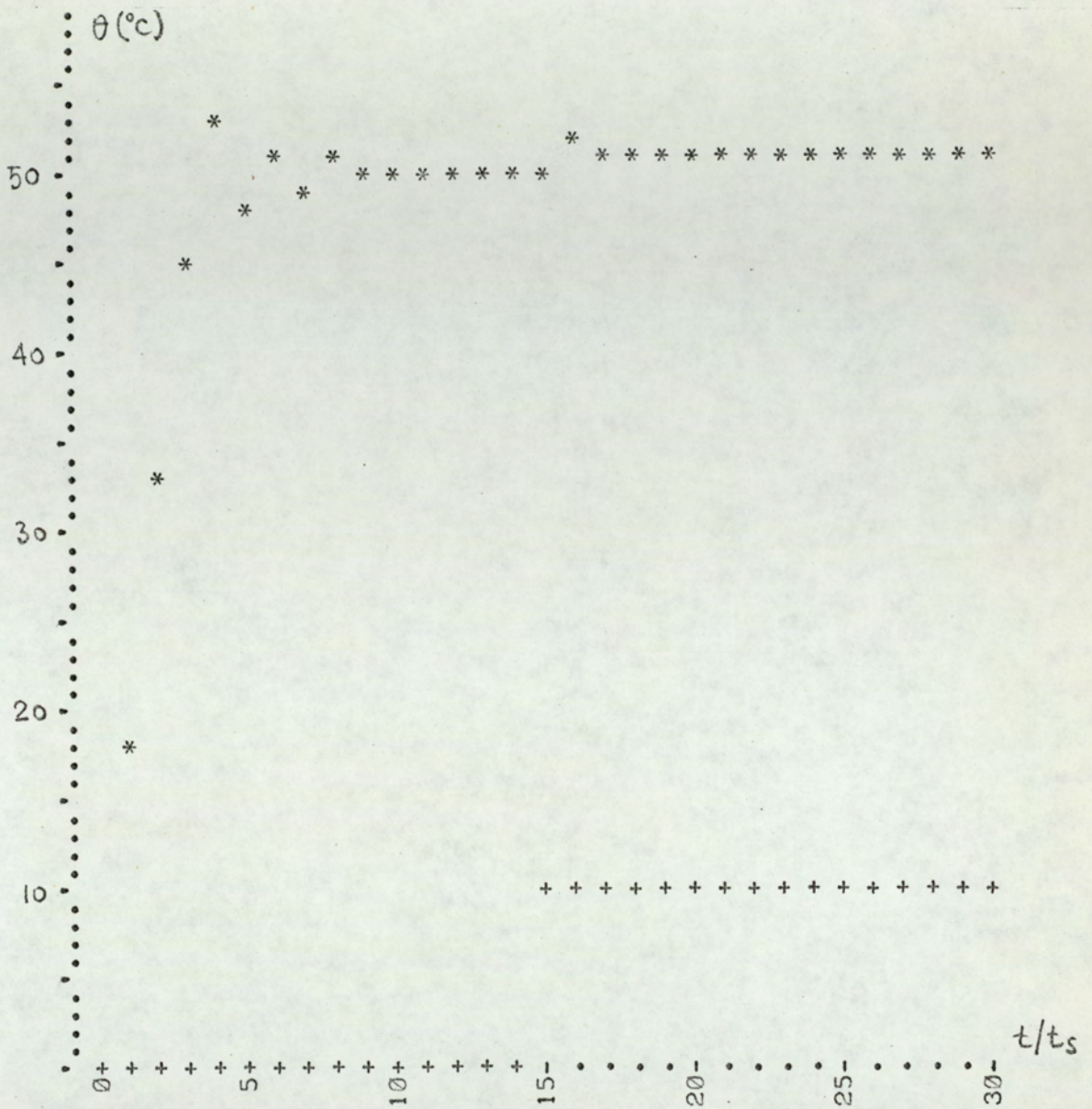


Fig. 6.35

Digital computer plot corresponding to a system subjected to a step disturbance. $t_s = 10$ min, $T = 50$ min, $L = 0$, $F = 100^{\circ}\text{C}$, $\theta_r = 50^{\circ}\text{C}$, $k = 0.08$ $1/^{\circ}\text{C}$.

* output temperature

+ disturbance

$$4.5 = \frac{A}{1 - A} < Fk = 8 < \frac{1 + A}{1 - A} = 10$$

Therefore damped oscillations occur, as is seen from fig. 6.35, but the system is stable. From fig. 6.35 it is seen that a disturbance of 10°C causes a change of 1°C in the output temperature, as the rough calculation below suggests:

$$\frac{\theta_u}{1 + Fk} = \frac{10}{9} \approx 1^{\circ}\text{C}$$

In the second example a sinusoidal disturbance is considered (fig. 6.36). The system parameters are the same as above, except that $k = 0.09$. The system is still stable, but oscillations die slower than they do in the first example. The disturbance is reduced about 10 times.

6.5.2 Effects of disturbance on limit cycles

In terms of the modulator input, and in the steady state, the disturbance can be viewed as opposing the command. Thus, in the presence of disturbance, the zones given for saturation modes will still be valid, provided that β should now be interpreted as $(\theta_r - \theta_u)/F$, instead of θ_r/F .

An example of the effects of disturbance on the limit cycling is given in fig. 5.15. The system parameters are $\phi = t_s/T = 0.2$, $F = 100^{\circ}\text{C}$, $\theta_r = 92^{\circ}\text{C}$ and $k = 2 \text{ l}/^{\circ}\text{C}$. From fig. 6.12 it can be seen that $\beta = 0.92$ and $Fk = 200$ corresponds to 6-1 limit cycling, therefore the system settles in 6-1 limit cycling. When a step disturbance of $\theta_u = 62^{\circ}\text{C}$ is applied the effective β becomes $(96 - 62)/100 = 0.3$ and this

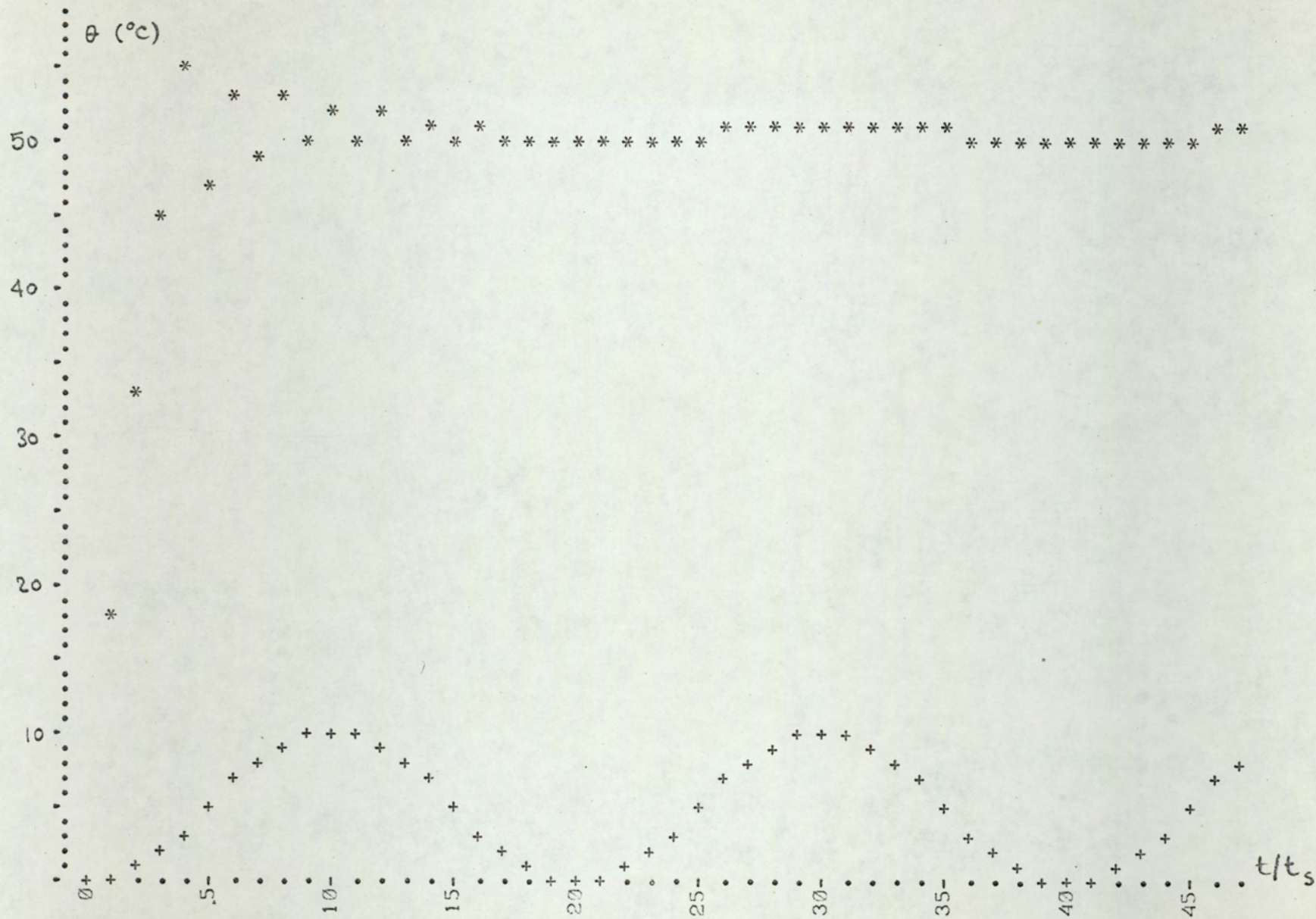


Fig. 6.36

Digital computer plot corresponding to a system subjected to a sinusoidal disturbance. System parameters are same as in fig. 6.35, except that $k=0.09$. * output temperature; + disturbance.

new value of β together with $Fk = 200$ now corresponds to a 1-2 zone. The system changes mode and settles in 1-2 mode oscillations.

Another example is given in fig. 6.37. Here, the system is subjected to a ramp disturbance of

$$\theta_u(t) = 0.05 t \text{ } ^\circ\text{C}$$

where t is in minutes. The system parameters are: $t_s = 10$ min., $T = 50$ min., $F = 100^\circ\text{C}$, $\theta_r = 50^\circ\text{C}$, $L = 0$, $k = 0.1$. Since $Fk = 10$ and $\beta = 0.5$. The system settles in 1-1 mode. When β moves away from 0.5 the required gain for 1-1 mode increases sharply (fig. 6.12). Therefore, when disturbance attains about 5 degrees we expect 1-1 mode cycling to die out and sat-lin oscillations to emerge. Since effective β is now smaller than 0.5 these oscillations are of satcool-lin type. From eqns. 6.100 and 6.101 it is evident that the amplitude of satcool-lin oscillations is proportional to (in contrast with sat-sat oscillations whose amplitude is independent of β). Since the effective β decreases with increasing disturbance, the amplitude also decreases.

6.6 SUMMARY

In this chapter limit cycling in PWM electroheat systems is investigated in detail. An exact analysis, based on the graphical solution of difference equations, is presented.

In section 6.1 basic definitions and a brief survey of the literature on limit cycling in PWM systems are given. In section 6.2 the graphical analysis is presented. This method is used in section 6.3 to analyse limit cycling. Use

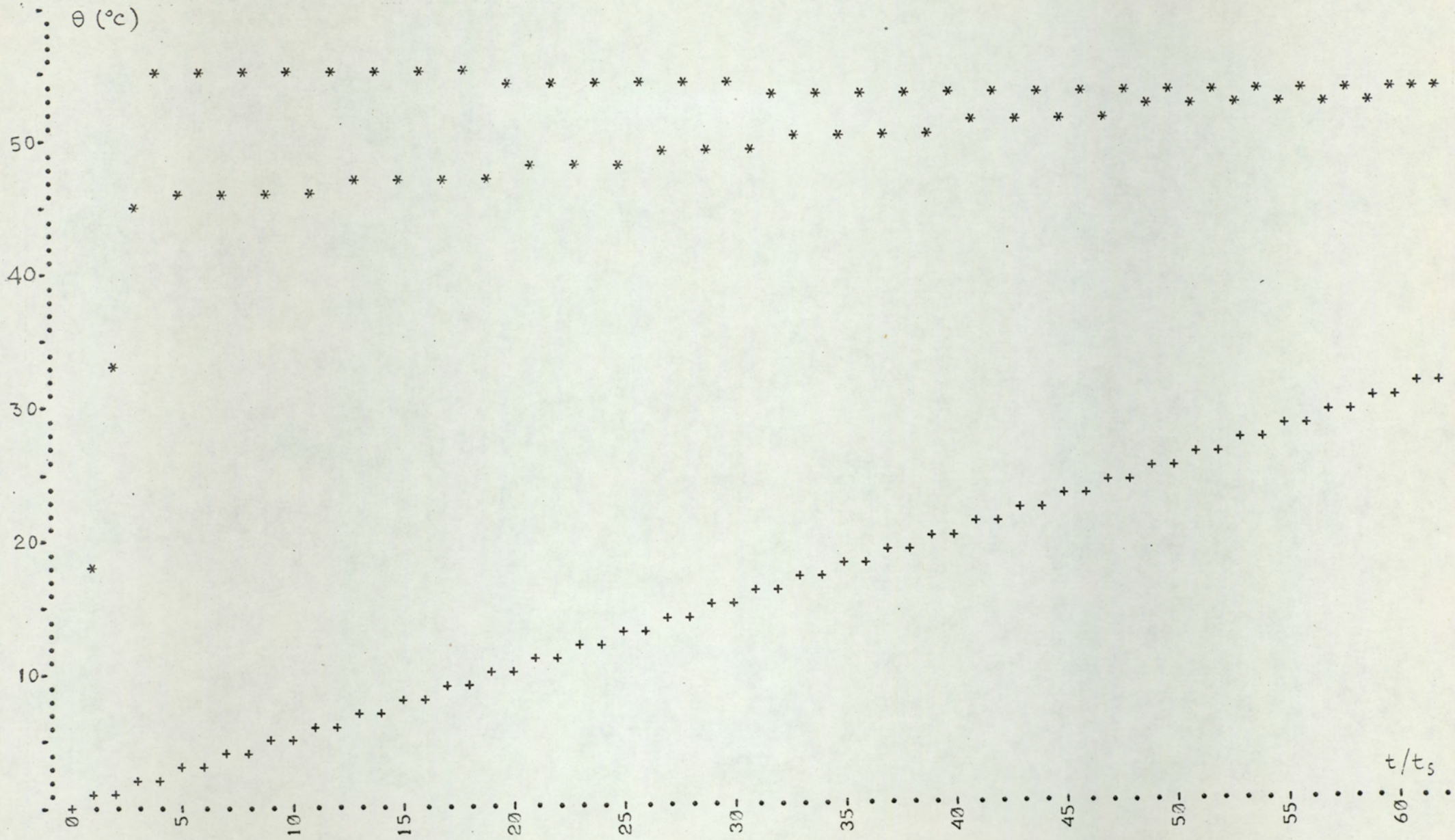


Fig. 6.37

Digital computer plot corresponding to a 1-1 cycling system subjected to a ramp disturbance. System parameters are same as in fig . 6.35 except that $k=0.1$. * output temperature ; + disturbance.

of operator algebra facilitated the analysis. It is proved that for positive pulse PWM, and for the Ziegler-Nichols model without delay, the possible limit cycling modes are those with only one sampling period of heat-up (or cool down) in a cycling period. The waveforms, average value, and oscillation amplitude of the output in presence of limit cycling are found. Stability boundaries for plants with or without delay are given. Stable and unstable modes of limit cycles are considered. All results are verified by digital simulation described in Chapter 5 and by analogue simulation which will be described in Chapter 7. Numerical examples corresponding to typical cases are given, along with the simulation results. In section 6.5 effects of disturbance on regulation performance and on limit cycling are investigated.

7

ANALOGUE SIMULATION OF PWM SYSTEMS

7.1 INTRODUCTION

Digital simulation is a powerful tool for the verification of theoretical results. In fact, all assertions, conditions and critical values found and presented in Chapter 6 are verified by digital simulation. But analogue simulation provides certain interesting possibilities such as the following:

1. Analogue simulation is an efficient method for the investigation of the system behaviour under various conditions. This can be done quickly and in an exhaustive manner by analogue simulation, whereas considerable computer time is necessary to do the same by digital simulation.
2. Analogue simulation gives an overall qualitative picture of the system performance. This enables the experimenter to gain better insight into the system operation. Therefore, analogue simulation provides a useful feedback during the process of theoretical research.
3. Analogue simulation constitutes one of the essential techniques for the verification of results found by theoretical analysis.

Because of these reasons an investigation based on analogue

simulation is necessary for this study to be complete. In this chapter the analogue simulation of the PWM control system is presented. Among the subjects included are the method of simulation, the experimental circuitry, and the qualitative and quantitative results.

7.2 THE PULSE WIDTH MODULATOR

A simple circuit* was used to implement pulse width modulation. This circuit can be realized on the computer patch-board without using additional elements.

The analogue computer diagram of the pulse width modulator is shown in fig. 7.1. In this diagram A23 is a track-store amplifier of unity gain. A track-store amplifier is equivalent to a sampler followed by a zero order hold (fig. 7.2). The track-store operation is achieved by applying a pulse train to the pulse input of the amplifier. The period of this pulse train determines the sampling period. C35 is a comparator which compares the two input voltages (at C_1 and C_2). Since the input C_2 is kept at zero potential the voltage at C_1 is compared with zero level. The output of the comparator is connected to relay R35 in such a way that R35 is operated when the potential of point C_1 is positive, and released otherwise. In other words the output of the modulator (m) is 10V when $w > 0$ and 0V when $w \leq 0$.

Typical waveforms at various points of the modulator circuit are shown in fig. 7.3. In this figure x is the input voltage to the modulator. This voltage becomes the staircase voltage, y , after passing through the two inverters (A16 and A23) and the sampler-hold of the track-store amplifier A23. Note that during the n -th sampled period the value of y is

*A somewhat similar circuit was described by Nelson³².

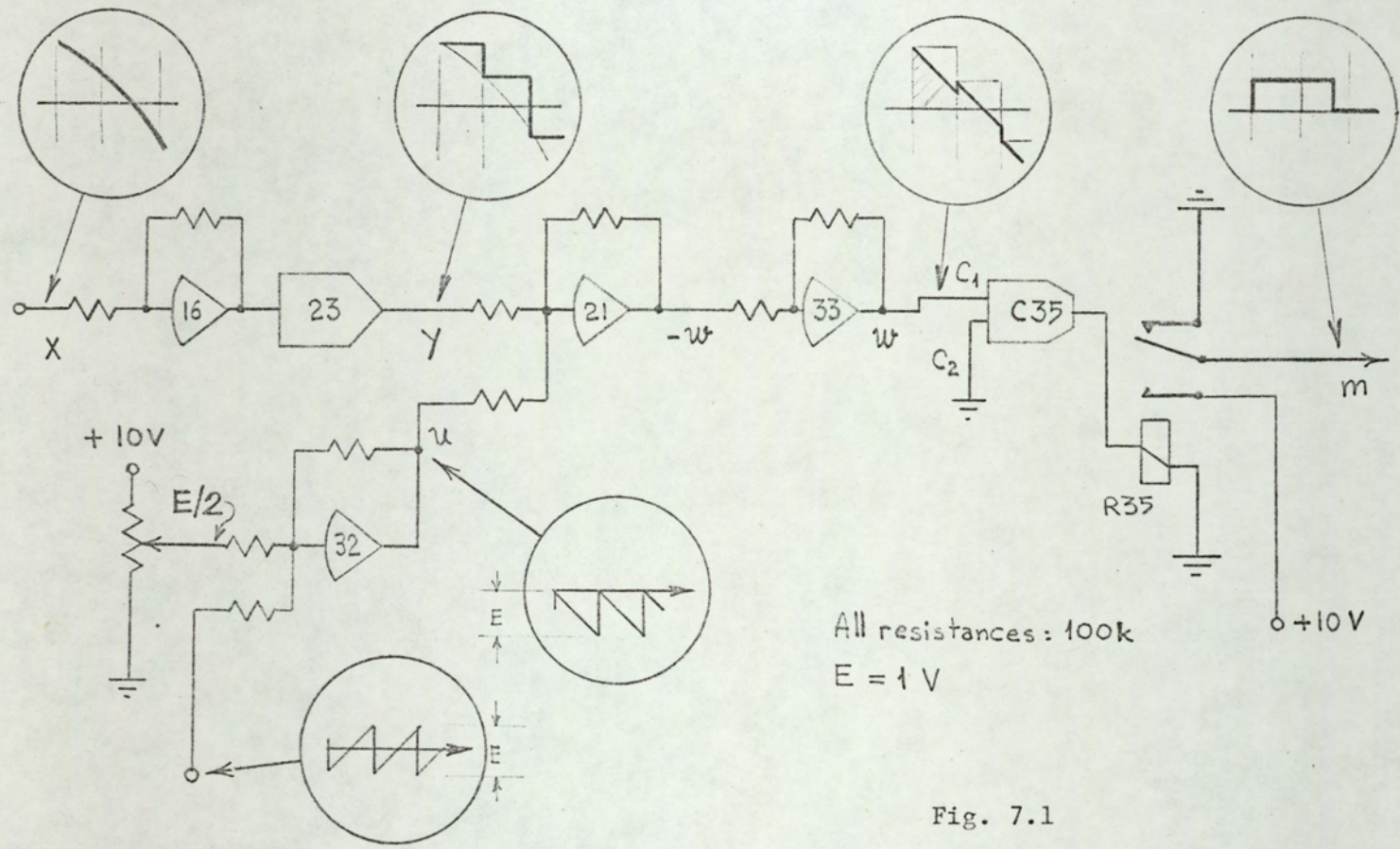


Fig. 7.1
 Analogue computer diagram of the pulse
 width modulator

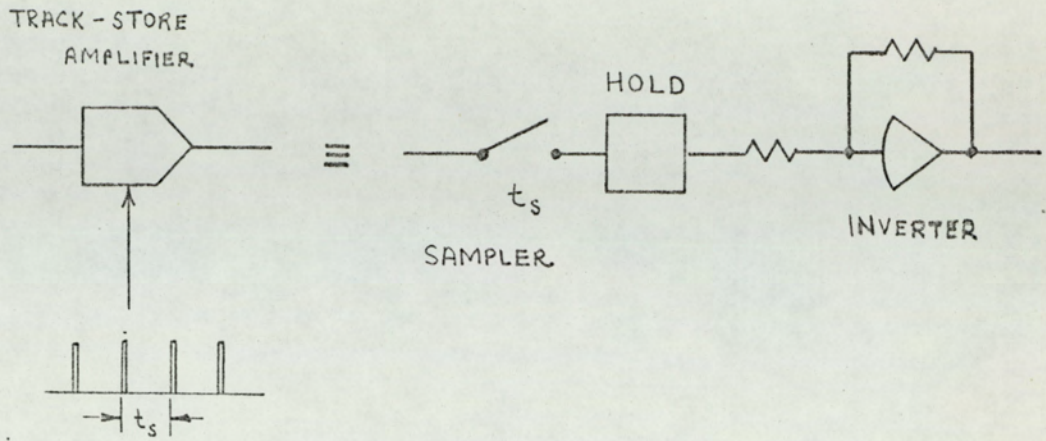


Fig. 7.2

Track-store amplifier
and
sampler-hold circuit

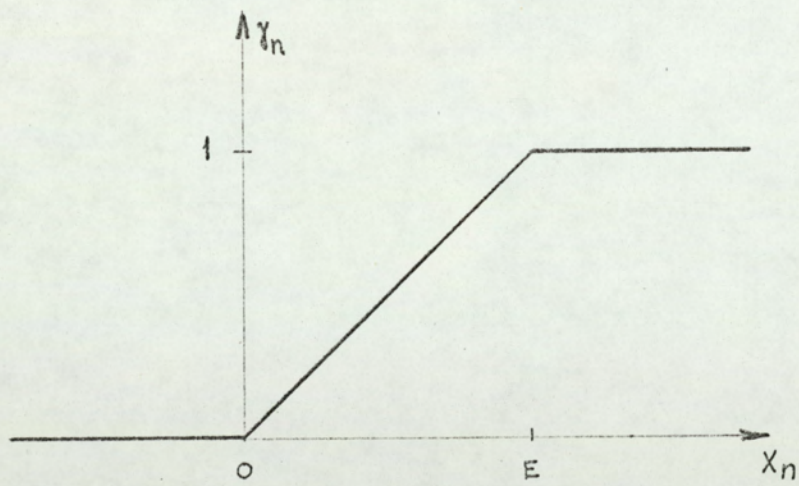


Fig. 7.4

Modulation law,

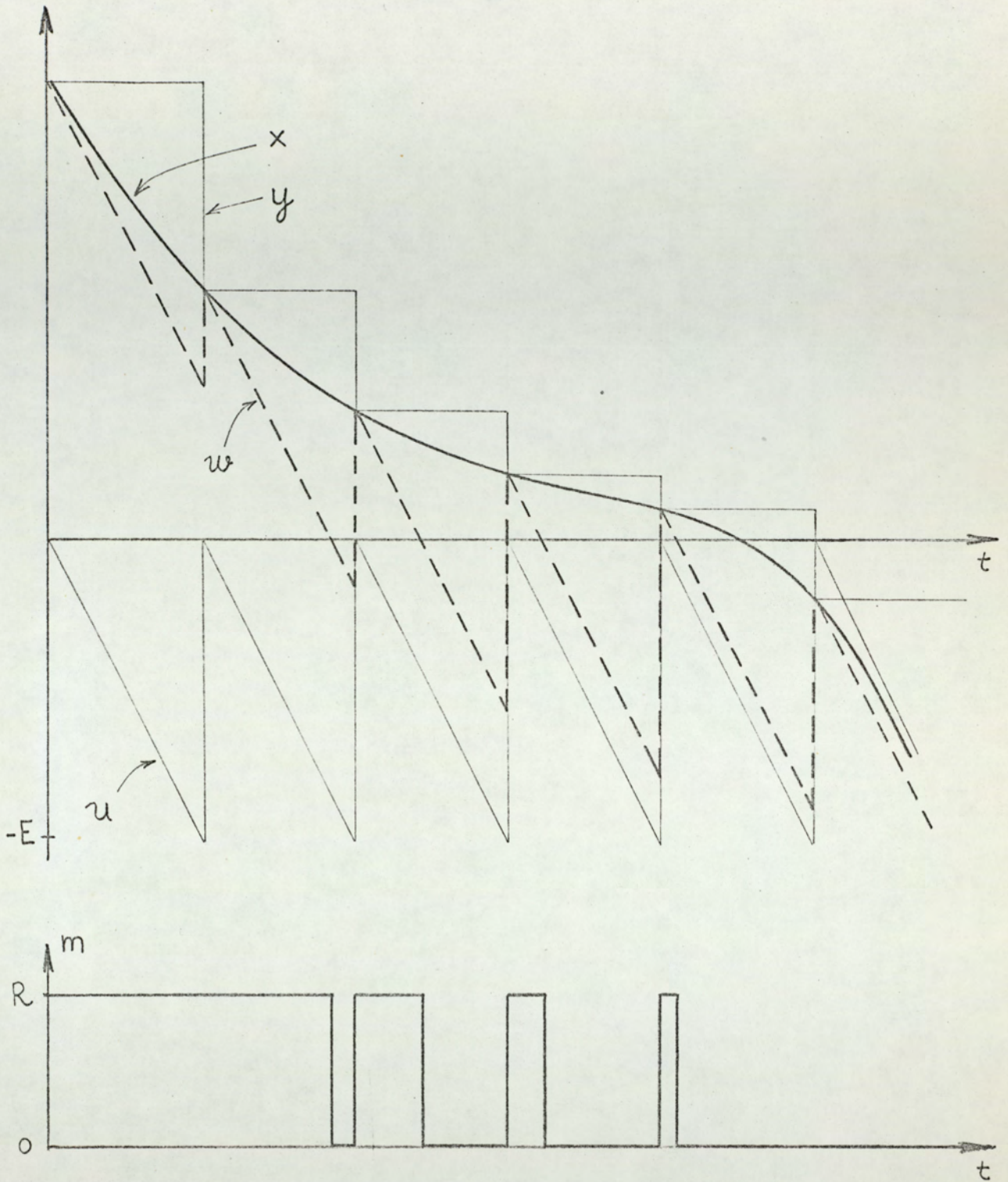


Fig. 7.3

Typical waveforms at various points
of the pulse width modulator.

constant and equal to x_n , where x_n is the value of x at the n -th sampling instant. The voltage, y , is added to the triangular voltage, u , and the sum, $u + y$, is denoted by w . The pulse train is obtained from w in such a way that $m = R$ when $w > 0$ and $m = 0$ when $w \leq 0$. It is clear from fig. 7.3 that the pulse train so obtained is pulse-width modulated according to the modulation law shown in fig. 7.4. It is also evident from figs. 7.1 and 7.3 that the circuit of fig. 7.1 performs the pulse width modulation as shown in figs. 7.3 and 7.4. In the actual experiment R was 10 V and E was 1 V.

7.3 ANALOGUE SIMULATION OF THE PWM CONTROL SYSTEM

7.3.1 Actual process variables and their analogues

In this analogue simulation all process variables are presented by their analogues. The usual dependent analogue variable is voltage. All quantities will be represented by voltages or by voltage ratios (gain or attenuation). Table 7.1 gives the relationship between the actual PWM control system variables and their analogues.

Table 7.1

VARIABLE	UNITS		EQUIVALENCE					
	Actual Process	Analogue	Actual	Analogue				
θ (output temperature) F (runaway temperature) θ_r (command)	°C	V	10°C	1 V				
b (bias) m (pulse height) x (modulator input)					-	V	1	1 V
k (modulator gain)*								

*In the actual process b, m , and x may be represented by voltages, in which case the units of k become $V/^\circ\text{C}$. Units for analogue quantities will remain as given in table 6.1.

7.3.2 Description of the circuit used in simulation

The analogue computer diagram for the simulation of the PWM control system is given in fig. 7.5. This simulation was realized using an EAL 48 Hybrid computer. The simulation circuit utilizes 22 amplifiers, 1 track-store amplifier, 1 comparator, 1 relay and 6 potentiometers. Four additional devices were used: 2 oscilloscopes, 1 x-y recorder and 1 oscillator (servo-mex PF 51). The numbers for amplifiers, comparator, relay and potentiometers in fig. 7.5 correspond to the actual element numbers on the analogue computer.

The value of F was kept constant at 10 V (100°C). The command, θ_r was obtained from P55, and could be adjusted between 0 and 10 V (0 and 100°C). All amplifiers in the circuit had unity gain except A34 (and A31). The gain of A34 was either 1 or 10, depending on the position of switch S1. The modulator gain, k_1 was represented by

$$k \rightarrow G_{34} r_{28}$$

where G_{34} is the absolute value of the gain of A34 (either 1 or 10), and r_{28} is the dividing ratio of P28 (adjustable between 0 and 1). Thus, the quantity $G_{34} r_{28}$ could have values between 0 and 10 which corresponded to actual k values between 0 and $1/^{\circ}\text{C}$.

Bias was obtained from P15 and P16. The voltage at the moving contact of P16 was:

$$b \rightarrow 10 r_{15,16} \text{ volts}$$

where $r_{15,16}$ is the dividing ratio of P15 and P16 in cascade. Note that because of loading $r_{15,16} \neq r_{15} r_{16}$, where r_{15} and

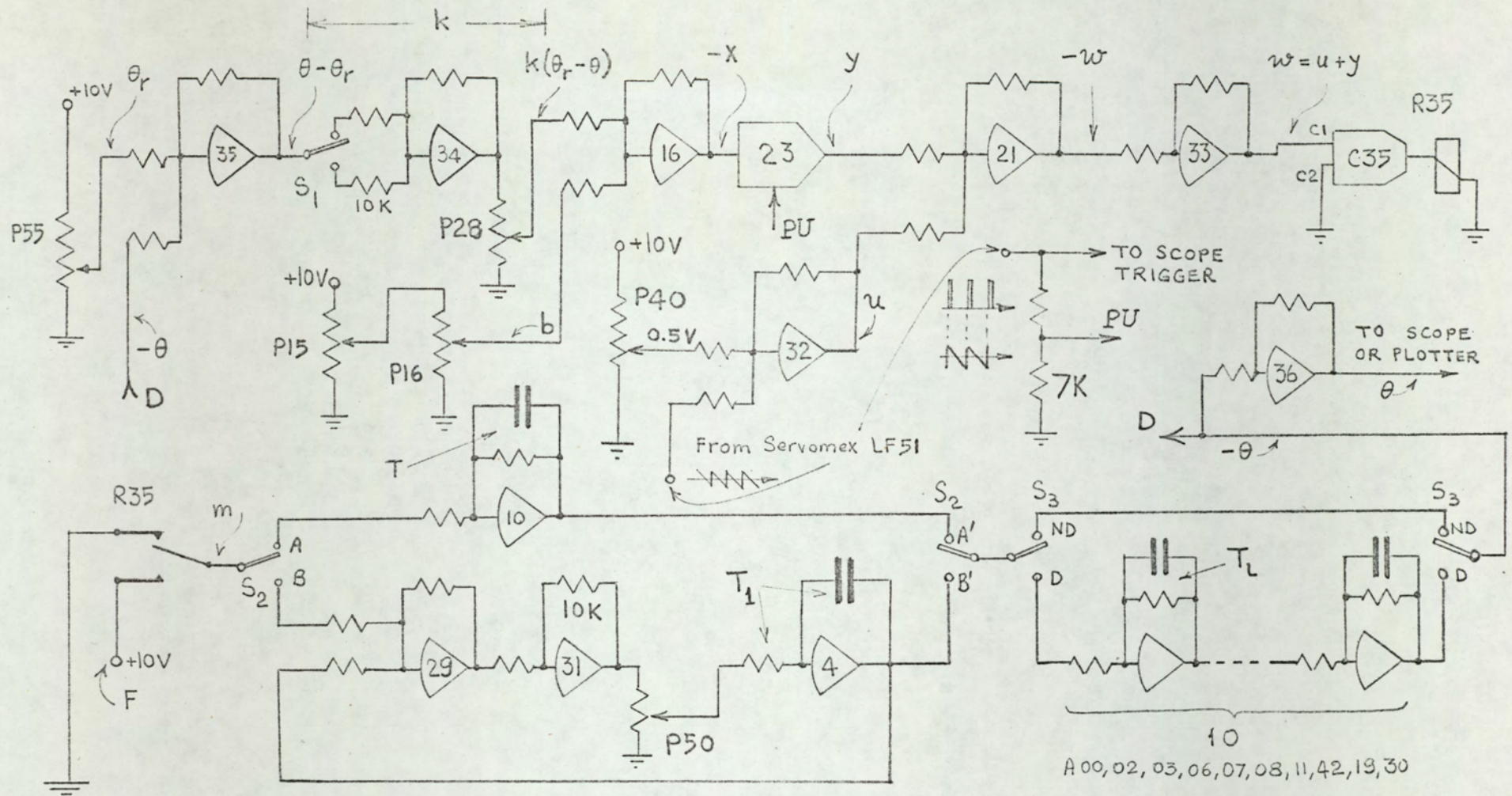


Fig. 7.5

Analogue computer diagram for the simulation of PWM control system.

r_{16} are ratios of P15 and P16 respectively. The ratio $r_{15,16}$ could be adjusted between 0 and 1, therefore the output of the P15-P16 combination was between 0 and 10 volts which corresponds to actual bias values between 0 and 10. Since we did not need actual bias values greater than 1, the P15 setting was kept constant at $r_{15} \approx 0.1$ and the fine adjustment of the bias was achieved by adjusting P16.

Potentiometer P40, together with the triangular voltage source and A32 supplied the sweep voltage u . The amplitude of the triangular voltage (setting on the external generator) and the setting of P40 were adjusted to obtain the waveshape u as shown at the output of A32 in fig. 7.5; and then were kept constant.

It is important to observe that the pulse input to the track-store amplifier (A23) and the triangular input to A32 must be of exactly the same frequency, and they must be in phase as shown in fig. 7.5. This necessitates use of a single generator giving both voltages.

Implementation of time delay

There are various methods to simulate time delay on analogue computers. One method is to use Padé approximants^{43,46}. Another method is to use a tape recorder with spatial separation of record and playback heads. If the signals to be delayed are pulses, monostables can be used to obtain delay. The simplest method to obtain approximate delay is using a network with an n -th order pole, so that in s domain:

$$e^{-sL} \approx \frac{1}{(1 + s \frac{L}{n})^n} \quad (7.1)$$

We know that the above approximation becomes better as n increases. On the analogue computer the right hand side of eqn. 7.1 is equivalent to n cascaded first-order systems with equal time constants ($T_L = L/n$). Since the overall gain of the chain is $(-1)^n$, it is desirable to choose n an even number so as to obtain a gain of $+1$. Among the considerations on the choice of n are the available number of amplifiers and the noise present in the system. For the simulation described in this work a value of $n = 10$ was used. When switch $S3$ is in ND position the amplifier chain is bypassed so that there is no delay in the plant. When $S3$ is in D position, the delay becomes effective.

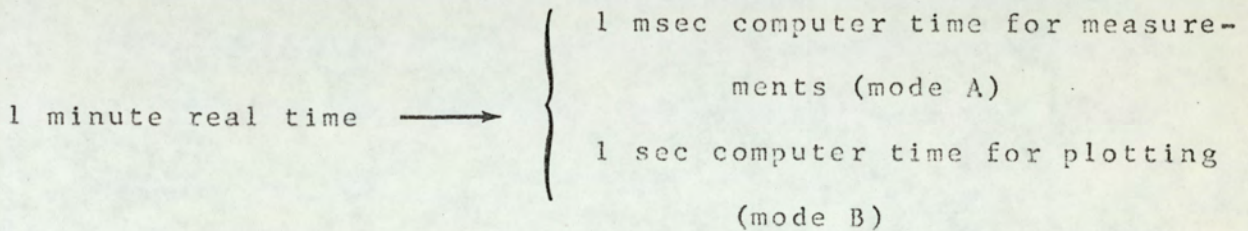
Computer time versus real time

As indicated in fig. 7.5, T denotes the time constant of the plant (A10, when $S2$ is in position A-A'), t_s denotes the sampling period, T_L denotes the time constant of each individual first order network in the delay chain. While doing measurements and taking photographs a fast computer time is preferred, on the other hand while plotting on the x-y plotter slow computer times must be used because of the slow response of the x-y recorders. Therefore two different computer times were used. For measurements and photograph taking 1 minute real time \rightarrow 1 msec computer time equivalence is adopted, whereas a computer time which is 1000 times slower is used for plotting on the x-y recorder. The procedure to set the time constants is described below:

1. $\mu = 0$ (no delay, $S3$ is in position ND)
 - a. Given ϕ ($\phi = t_s/T$)
 - b. $T = 50$ msec. for measurements (mode A)
50 sec. for plotting (mode B)

- c. $t_s = \phi \cdot T$ (set on the generator)
2. $\neq 0$ (delay, S3 is in position D)
- a. Given ϕ and
- b. $L = 10$ msec for measurements (mode A)
10 sec. for plotting (mode B)
- c. Since $n = 10 = \text{constant}$, set $T_L = 1$ msec (for measurements) or $T_L = 1$ sec (for plotting).
- d. Find t_s from $t_s = L/\mu = 10/\mu$ msec (measurements)
sec (plotting)
and set the generator to this t_s .
- e. Find T from $T = t_s/\phi$ and set T to this value.

For both cases 1 (no delay) and 2 (delay):



Some typical examples are given in Table 7.2

Table 7.2

ϕ	μ	Mode A				Mode B			
		t_s	L	T_L	T	t_s	L	T_L	T
		msec				sec			
0.2	0	10	-	-	50	10	-	-	50
0.5	0	25	-	-	50	25	-	-	50
0.2	1	10	10	1	50	10	10	1	50
0.2	2	5	10	1	25	5	10	1	25
0.2	4	2.5	10	1	12.5	2.5	10	1	12.5

It is seen from the procedure above that to simplify the operation some standard values were adopted, e.g. $T = 50$ msec in case 1 and $L = 10$ msec in case 2. Since the performance criteria of the system depends on t_s/T and not on t_s and T

separately, the above procedure does not impose any limitation on the generality of the experiment. Also, as seen in table 7.2, for mode B (plotting) long time constant are required. Since the longest time constant available on the computer was 1 second, the branch which consisted of A29, A31, P50 and A4, was added (fig. 7.5). For this branch:

$$\frac{V_{B'}}{V_B} = - \frac{1}{1 + T's} \quad (7.2)$$

where T' is the equivalent time constant of the branch. It can be shown that

$$T' = \frac{T_1}{G_{31} r_{50}} \quad (7.3)$$

where G_{31} is the absolute value of the gain of A31 and r_{50} is the ratio of P50. In the circuit used $G_{31} = 0.1$ and $T_1 = 1$ sec. Therefore:

$$T' = \frac{10}{r_{50}} \text{ sec} \quad (7.4)$$

when a plant time constant larger than 1 sec was required switch S_2 was put in position B-B' and the required time constant was obtained according to eqn. 7.4 by adjusting P50.

7.4 EXPERIMENTAL RESULTS

7.4.1 Practical considerations

The following practical considerations are worth mentioning:

1. Since a relay was used in the circuit, the computer time was chosen slow enough for the relay to follow the operation of the system.
2. The oscilloscope rise and fall times were very small compared with the time intervals involved, therefore exact waveshapes were displayed.
3. Since the comparators on the analogue computer operate on the sampled-data principle it is important to have a very high sampling rate (at least 50 times larger) for the comparators compared with sampling rate of the system.
4. The time-properties (slow response) of the x-y recorders necessitated the slowing down of the computer time, this resulted in the exact tracing of the waveshapes.
5. For plants with delay the period of oscillations usually is not an integer multiple of the sampling interval. Therefore, since the triggering is obtained from the same generator which supplies the sampling pulses, the oscillation pattern (output waveshape) and the triangular voltage (voltage u in fig. 7.3) move with respect to each other on the oscilloscope screen. Because of this, photographs should be taken by using the single-sweep facility. Figure 7.8 and 7.9 were taken using the single-sweep facility.

7.4.2 Qualitative results

Plants without delay

The existence of lin-sat and sat-sat oscillations are verified. A careful experimental investigation confirmed that:

- a. Lin. oscillations are not possible

- b. Sat-sat oscillations of mode M-N, with both M and N different from 1, are not possible.

Analogue simulation, therefore, provided an experimental verification of the assertions of chapter 6 that lin oscillations and sat-sat oscillations as in b above do not occur. The types and modes of oscillations were monitored from the waveform of m. For example, the 3-1 nature of the oscillations can be clearly seen from the m waveform in fig. 7.7.

The existence of zones and the fact that the critical gain for any particular mode of sat-sat limit cycling passes through a minimum and becomes infinite at zone boundaries (i.e. it is impossible to maintain the oscillations) were verified. Also verified was the fact that the zones, critical gains, etc. are dependent upon $\beta (\theta_r/F)$ and $\phi(t_s/T)$ and not upon $\theta_r, F, t_s,$ and T.

Plants with delay

The experiments on plants with delay also verified the theoretical results given in chapter 6. The n-th order pole approximation to delay (with $n = 10$) proved to be a simple and sufficiently accurate approximation. One of the outcomes of the experiment concerned the saturated limit cycles. It was found that, in contrast to the no delay case, it was possible for the system to have M-N mode limit cycles with both M and N different from 1. It seems that the system goes into an M-N limit cycling where $M+N$ is the nearest integer to t_{osc}/t_s , where t_{osc} is the period of non-saturated oscillations. For example, with $\mu = 1$ ($L = t_s$), t_{osc}/t_s was about 5.5 whereas the period of saturated cycling was found to be 6. The value of the $\beta (\theta_r/F)$ dictates the M/N ratio. For $\beta = 0.5$ ($\theta_r = F/2$) $M = N$, and this explains the tendency of $M+N$ to be an even

number. For $M + N = 6$ there are 5 possible saturated limit cycling modes: 5-1, 4-2, 3-3, 2-4, and 1-5. Therefore, it is logical to divide the range of values of β ($0 < \beta < 1$) into 5 zones, the largest being 3-3 zone, centered around $\beta = 0.5$. Experimental study supported this argument.

7.4.3 Quantitative results

Two sets of experimental data are given in tables 7.3 and 7.4. The corresponding theoretical values, found from the equations of chapter 6 are included for comparison.

Table 7.3

Experimental and theoretical values of critical gains

$L = 0, \phi = 0.2$ ($t_s = 10$ msec, $T = 50$ msec)

θ_r (v)	β	Oscill. start at		Sat-Sat Oscillations		
		(Fk)		Mode	Oscill. start at	
		Exp.	Theor.		(Fk)	
					Exp.	Theor.
5.00	0.500	10.5	10.03	1-1	10.5	10.03
6.90	0.690	10.5	10.03	2-1	18.0	16.77
7.88	0.788	10.1	10.03	3-1	26.0	25.00
8.47	0.847	10.0	10.03	4-1	37.0	35.05
8.86	0.886	10.6	10.03	5-1	49.0	47.33
9.13	0.913	10.5	10.03	6-1	65.0	62.33

$$F = 10 \text{ V } (100^\circ\text{C}), b = \theta_r / F$$

Table 7.4

Experimental and theoretical values of critical gains

$$L = 0, \phi = 0.5 \quad (t_s = 25 \text{ msec}, T = 50 \text{ msec})$$

$\frac{\theta_r}{(V)}$	β	Oscill. start at		sat-sat oscillations		
		(Fk)		mode	oscill.start at (Fk)	
		Exp.	Theor.			exp.
5.00	0.500	4.2	4.08	1-1	4.2	4.08
7.26	0.726	4.1	4.08	2-1	8.6	8.27
8.43	0.843	4.1	4.08	3-1	15.7	15.18
9.08	0.908	4.1	4.08	4-1	27.5	26.57
9.45	0.945	4.1	4.08	5-1	46.0	45.35
9.67	0.967	4.1	4.08	6-1	77.1	76.31

$$F = 10 \text{ V (100}^\circ\text{C)}, b = \theta_r/F$$

It is seen from tables 7.3 and 7.4 that the experimental results for the stability boundary (start of oscillations) correspond closely to the theoretical values. The theoretical values (10.03 for $\phi = 0.2$ and 4.08 for $\phi = 0.5$) are found from eqn. 6.89.

Experimental values for sat-sat oscillation boundaries are slightly higher than expected. The reason for this difference is explained below:

The command values in the first columns of tables 7.3 and 7.4 correspond to β^0 values (the value of β where the sat-sat gain boundary attains its minimum) as given by eqn. 6.70. It is clear from figs. 6.10-6.13 that the gain boundary has a large slope throughout the zone. The significance of this large slope is that a small change in β (i.e. in θ_r) will cause a large change in corresponding critical gain. From eqns. 6.63, 6.66, 6.67, 6.68, 6.70 and 6.71 it can be shown

that the slope of gain boundary at $\beta = \beta_{M-1}^0$ for an M-1 zone is given by:

$$\pm (1 + F k_{M-1}^0)$$

where $F k_{M-1}^0$ denotes the critical gain at $\beta = \beta_{M-1}^0$ in a given M-1 zone. Note that the values listed in the last columns of tables 7.3 and 7.4 correspond to $F k_{M-1}^0$. For example, if $\phi = 0.5$ and $M = 5$, corresponding to the fifth line in table 7.4, the slope of the gain boundary curve at $\beta_{5-1}^0 = 0.945$ is ± 46.35 , which simply means an error in the setting of β (θ_r/F) will be amplified into a gain (Fk) value 46 times larger.

The experimental results related to the system with delay are given in tables 7.5, 7.6, and 7.7.

Table 7.5

Oscillation conditions, $\mu = L/t_s = 1$, $\phi = t_s/T = 0.2$

θ_r (V)	β	Start at Fk=		Period(t_{osc})		Saturated Oscillations Experimental	
		Exp.	The.	Exp ⁽¹⁾	Exp ⁽²⁾	Mode	Starts at Fk =
5	.5	6.0	5.517	$5.5t_s$	$5.25t_s$	3-3	16.3
7	.7	5.9	5.517	$5.5t_s$	$5.25t_s$	4-2	19.0

$$L = t_s = 10 \text{ msec}, \quad T = 50 \text{ msec}, \quad F = 10 \text{ V (100}^\circ\text{C)},$$

$$b = \theta_r/F$$

1 See fig. 7.8

2 From the example in section 6.3.4

Table 7.6

Oscillation conditions, $\mu = L/t_s = 2$, $\phi = t_s/T = 0.2$

θ_r (V)	β	Start at Fk=		Period (t_{osc})		Saturated Oscillations
		Exp	The. (3)	Exp (4)	The.	Experimental
5	.5	3.77	3.80	$8.5t_s$	$8.6t_s$	4-4 mode for large gain
7	.7	3.45	3.80	$8.5t_s$	$8.6t_s$	

$L = 10$ msec, $t_s = 5$ msec, $T = .25$ msec, $F = 10$ V (100°C)

$b = \theta_r/F$

Table 7.7

Oscillation conditions, $\mu = L/t_s = 3, 4, 5$; $\phi = t_s/T = 0.2$

t_s sec	L msec	μ -	T msec	θ_r V	β -	Oscillations Start at Fk= Experimental	Approximate Period (t_{osc}) Experimental
3.33	10	3	16.65	5	0.5	3.75	$11 t_s$
3.33	10	3	16.65	8	0.8	3.10	$11.2t_s$
2.50	10	4	12.5	5	0.5	3.05	$13t_s$
2.50	10	4	12.5	8	0.8	2.60	$13t_s$
2.00	10	5	10	5	0.5	2.70	$15.5t_s$
2.00	10	5	10	8	0.8	1.80	$15.5t_s$

$F = 10$ V (100°C), $b = \theta_r/F$

4 From fig. 6.33

5 See fig. 7.9

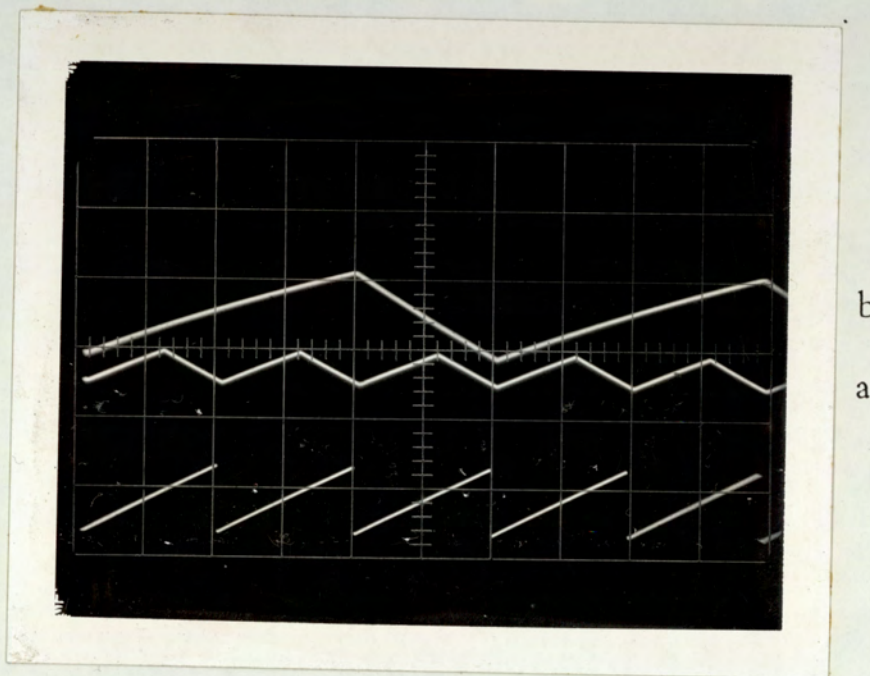


Fig. 7.6

Output temperature of a stable (curve a) and 2-1 cycling (curve b) PWM control system.

$F=10$ V, $t_s=10$ msec, $T=50$ msec, $L=0$.

curve a: $k(\text{actual system})=0.01$, $\theta_r = 6.9$ V.

curve b: $k(\text{actual system})=0.19$, $\theta_r = 6.3$ V.

Horizontal axis: One period of the triangular wave is 10 msec.

Vertical axis:

curve a : max = 7.33 V, min = 6.02 V.

curve b : max = 6.82 V, min = 6.33 V.

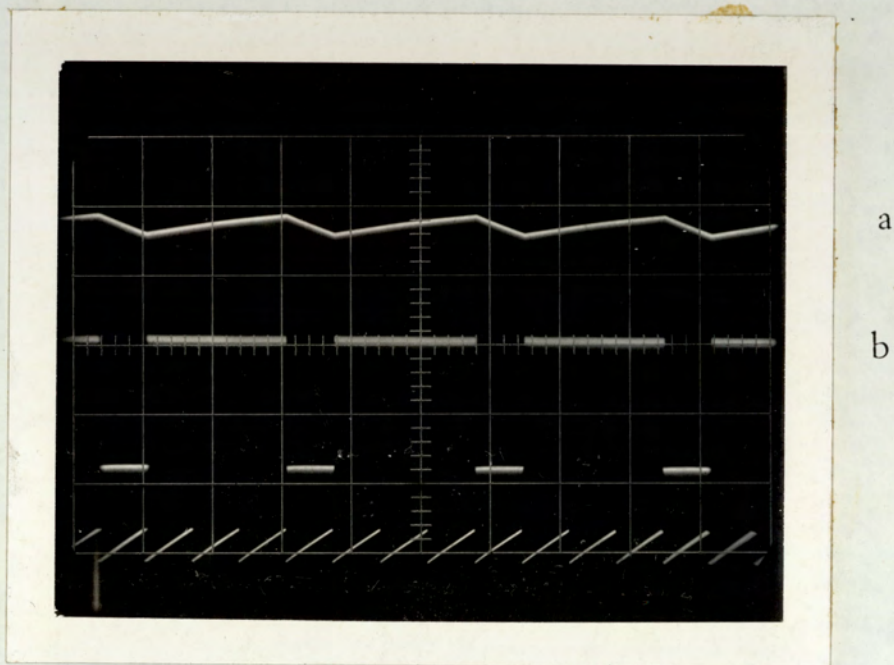


Fig.7.7

Output temperature (curve a) and m (curve b)
for a 3-1 limit cycling system.

$F=10$ V, $t_s=10$ msec, $T=50$ msec, $L=0$, $\theta_r=7.88$ V,
 $k(\text{actual system})=0.3$

Horizontal axis: One period of curve b is 10 msec.

Vertical axis:

curve a : max = 8.32 V, min = 6.68 V.

curve b : max = 10 V, min = 0 V.

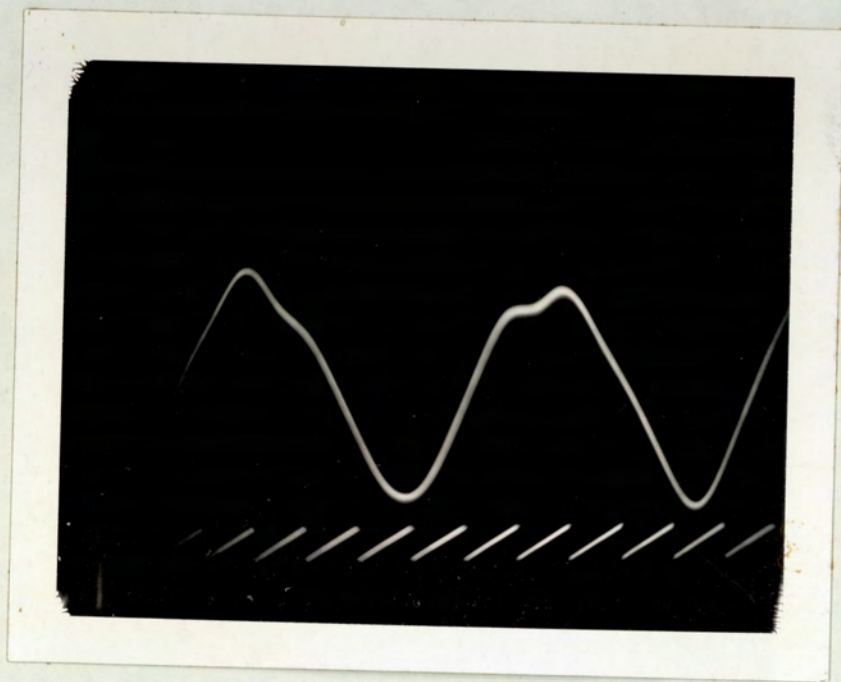


Fig. 7.8

Oscillations in the presence of delay ($L=t_s$)

$F=10$ V, $t_s=10$ msec, $T=50$ msec, $L=10$ msec ,

$T_L=1$ msec, $\theta_r=5$ V, $k(\text{actual system}) = 0.07$.

Horizontal axis: One period of the triangular
wave is 10 msec.

Vertical axis:

Output voltage: max = 5.95 V, min = 4.0 V.

It is seen that $t_{osc} \approx 5.5 t_s$.

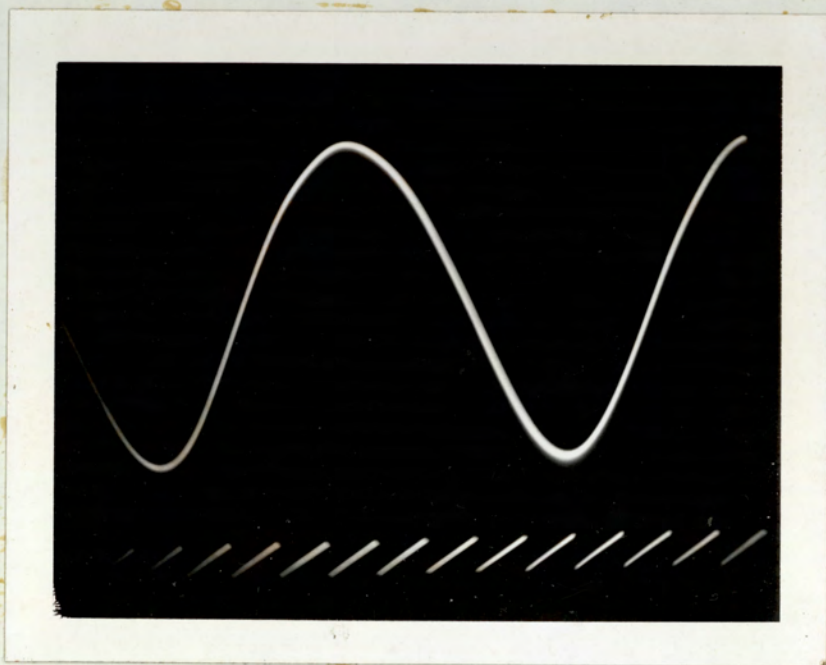


Fig. 7.9

Oscillations in the presence of delay ($L=2t_s$).

$F=10$ V, $t_s=5$ msec, $T=25$ msec, $L=10$ msec,

$L_T=1$ msec, $\theta_r=5$ V, $k(\text{actual system})=0.0455$

Horizontal axis: One period of the triangular wave
is 5 msec.

Vertical axis:

Output voltage: max = 6.2 V, min = 3.71 V.

It is seen that $t_{osc} \approx 8.5 t_s$.

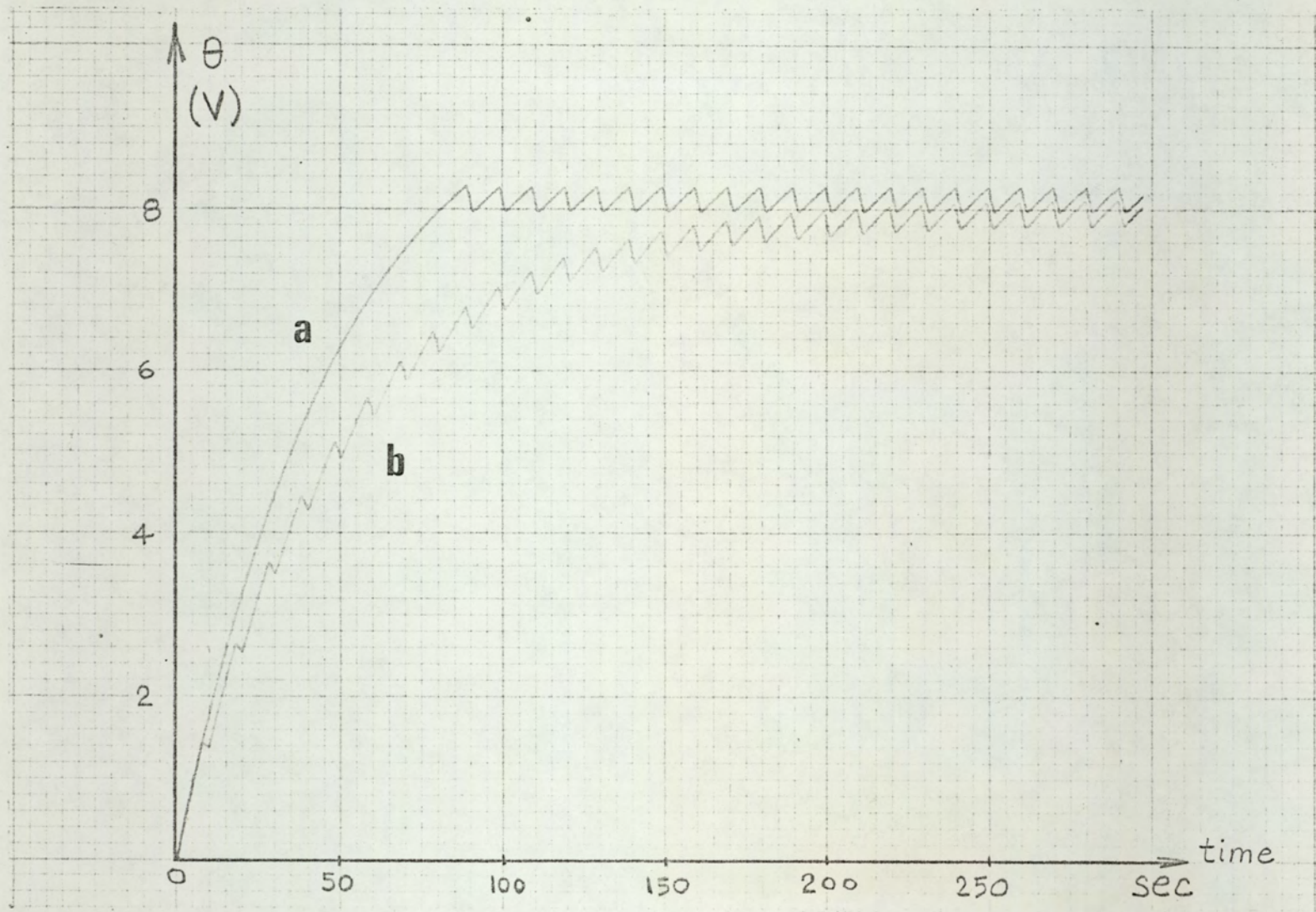


Fig. 7.10

Comparison of PWM control with open loop control. Curve a: PWM system output. $F=10$ V, $T=50$ sec, $L=0$, $\theta_r=8$ V, $t_s=10$ sec, $k(\text{actual system})=0.05$, $b=0.8$. Curve b: Open-loop system output. $F=10$ V, $T=50$ sec, $L=0$, $t_o/t_p=0.8$, $t_q=10$ sec. (corresponds to the above PWM system with $k=0$).

From tables 7.5 and 7.6 it is seen that the experimental data are in close agreement with the theoretical results of chapter 6.

Four photographs are given in figs. 7.6-7.9. The first photograph (fig. 7.6) shows the output temperature for a stable (curve a) and a 2-1 limit cycling system. The triangular wave-shape at the bottom is the sweep voltage u , it is added to the photograph to indicate sampling periods.

In fig. 7.7, system output (curve a) and m (curve b) is shown for a 3-1 limit cycling system.

In fig. 7.8, oscillations in the presence of delay ($L = t_s$) shown. It is seen that the period of oscillations is $5.5 t_s$.

In fig. 7.9 oscillations for larger delay ($L = 2 t_s$) are displayed. The period of oscillations is seen to be $8.5 t_s$, whereas theoretical investigation indicated $8.47 t_s$ (see example in section 6.3.4 and fig. 6.33)

In figs. 6.32 and 6.34 two plots obtained using an x-y plotter are shown. Another plot shown in fig. 7.10 provides a comparison between open-loop and PWM control systems. Curve a in fig. 6.10 corresponds to PWM control. As was stated before, PWM systems operates on on-off basis in the start-up period thereby giving a short (in fact optimal) start-up period. On the other hand, as it is seen from curve b, open-loop control results in considerably longer start-up times.

7.5 SUMMARY

In this chapter methods for the analogue simulation of PWM control systems are described, and the corresponding diagrams are given. Practical considerations concerning the simulation are also discussed.

The results obtained by analogue simulation were found to be in complete agreement with the theoretical results, as well as those obtained by the digital simulation.

8

GENERAL CONCLUSIONS

Individual conclusions have been summarized at the end of each chapter. Here the general conclusions of this study are given.

1. A full analytical investigation of the on-off control systems has been given. This analysis applies to the general case of mode dependent electroheat processes with transit delay which are controlled by hysteretic controllers. It therefore represents a considerable advance on Roots and Woods³⁸ which was restricted to ideal controllers.
2. Open-loop control methods have been examined as a preliminary to indirect and PWM control.
3. Digital simulation programmes for on-off and open-loop control systems have been developed. These programmes are applicable to processes with any transfer function given analytically, with or without transit delay and controlled by hysteretic or ideal controllers.
4. Indirect control has been proposed and examined in depth. It has been shown that with a suitable choice of the model parameters the performance criteria can be substantially improved. Material to facilitate the

design of such control schemes has been included.

5. Pulse width modulation (PWM) control has been thoroughly studied as an electroheat control scheme for the first time. An analysis of PWM control systems has been given. This analysis is based on state space approach and hence can easily be extended to higher order systems.
6. A digital computer programme for the complete simulation of PWM electroheat systems has been developed. This programme serves the double purpose of being a powerful tool in the analysis and design of PWM control systems and as a method of checking the analytical results obtained for such systems. This programme comprises subprogrammes for the simulation of:
 - (a) processes with or without transit delay
 - (b) systems incorporated with various PWM laws
 - (c) systems subjected to various forms of disturbance.

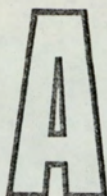
The programme given has been developed in such a way that on-off, open-loop, and multiposition (quasi-continuous) control systems can be simulated by treating them as special cases of PWM control.

7. The most important aspects of control systems, stability criteria and non-oscillatory response criteria have been developed for PWM electroheat control.
8. An exact analysis of limit cycles in PWM electroheat control systems has been presented for the first time. This represents a considerable advance beyond the existing work in this area. The previous results have been restricted to approximate methods or were unsuitable for application to electroheat systems.

The analysis presented in this work provides the necessary means required by the design engineer when considering the use of limit cycling systems for process control and to evaluate the performance characteristics of the system in limit cycling.

9. An analogue simulation method for PWM control systems and the experimental implementation of this method have been described.
10. Stability criteria and non-oscillatory response criteria derived analytically have been verified both by analogue and digital simulations.
11. The existence of limit cycles, their modes and gain- β boundaries (which are predicted, proved and calculated analytically for PWM electroheat control systems) have been verified by analogue and digital simulations.
12. Having thoroughly analysed PWM systems, one is now in a position to compare the use of PWM with derivative and multi-position control schemes from the viewpoint of the accuracy of control thereby obtained. Such an investigation could well be the subject of a future research project.

Pulse frequency modulation control is a possible alternative to PWM control. It has not been hitherto explored in the electroheat field, and so can also form the basis for a separate investigation.



DIGITAL SIMULATION PROGRAMMES

A.1 INTRODUCTION

The programmes developed for the digital simulation of on-off, open-loop, and PWM control systems are given in the following pages. Programmes developed mainly for calculation purposes or alternate forms of the simulation programmes are not included. All programmes are written in FORTRAN language suitable for PDP-9 computer (8k memory), and run through the department computer (PDP-9).

For each programme basic information such as class, purpose, subprogrammes used, basic variables, and data to be supplied are given. Flowcharts are included for two main programmes.

References are given to the relevant sections and figures of the text.

ONOFF

Class: Main programme

Purpose: Simulate the on-off control system shown in fig. 3.1

Subprogrammes used:

1. H(T): A function subprogramme for the step response of the plant. (One of STEP 1, STEP 2, STEP 3).
2. SPLOT4: Subroutine for printing and plotting (see SPOT5)

Flowchart: Figure A-1.

Programme listing: Figure A-2.

Variables in the programme:

<u>Fortran name</u>	<u>Meaning</u>
T	t time
K	i counting index for on-off periods (see fig. 3.11)
J	counting index for time intervals (Δt).
TS(K)	λ_1 switching instant (fig. 3.11)
U	$1 - \text{MOD}(K, 2)$ U = 1 means on, U = 0 means off.
Z	θ output temperature

Data to be supplied:

<u>Fortran name</u>	<u>Meaning</u>
R	θ_r
HYST	h
DELTA	Δt (step length)
START	time value at which plotting starts
SCALE	y-axis scaling for plotting
NN	NN = 0 means print = 1 means plot

JJ skipping ratio (see sect. 3.5.4)

Comments: This programme uses the method described in sect. 3.5. Examples of output of ONOFF are given in figs. 3.10, 3.12, 3.13, 3.14, and 3.15.

OPLOOP

Class: Main programme

Purpose: Simulate open-loop control system

Subprogrammes used:

1. H(T): A function subprogramme for the step response of the plant. (One of STEP 1, STEP 2, STEP 3).
2. SPLOT4: Subroutine for printing and plotting (see SPLOT5)

Programme listing: Figure A-3

Variables in the programme:

<u>Fortran Name</u>	<u>Meaning</u>
TQ	tq period
T	t time
N	n period counting index
M	M = even: off; M = odd: on.
R	θ output temperature

Data to be supplied:

TO	t_o on time
TP	t_p off time
DELT	Δt step length (time increment)
NN	NN = 0: write; NN = 1: plot.
SCALE	y-axis scaling in plotting

Comments: This programme uses the method described in sect. 4.2.3. Examples of output of OPLOOP are given in figs. 4.9,

PWMSYS

Class: Main programme

Purpose: Simulate the PWM control system shown in fig. 5.8.

Subprogrammes used:

1. D(X): A function subprogramme for disturbance. One of FUND, FRAMP2, FSTEP2, FSIN
2. SAT(X): A function subprogramme for control law. One of FUNSAT, SATN2, SATN10.
3. SUBMUL: Subroutine for matrix multiplication.
4. SUBLAG: Subroutine to introduce transit delay.
5. SPLOT5: Subroutine for printing and plotting.

Flowchart: Figure A-4.

Programme listing: Figure A-5.

Variables in the programme:

<u>Fortran name</u>	<u>Meaning</u>
PO	Φ_1
P1	Φ_2
B	B_1
V	$v(nt_s)$
U	$v(n + \gamma_n)t_s$
Z	$v(nt_s^+)$
PSI	ψ
BIAS	b
GAM	γ

Data to be supplied:

<u>Fortran name</u>	<u>Meaning</u>
TQ	t_s
TAU	T
H	k

<u>Fortran name</u>	<u>Meaning</u>
FG	F
R	θ_r
XO	θ_o
MU	ν
SCALE	scaling factor for the y-axis
NV, NU	0,0 means print V and U, 0,-1 means print V only, 1,1 means plot V and U (see comment 5 in sec. 5.4), 1,-1 means plot V only (all plots displayed in this work have been obtained with 1,-1).

Comments: This programme uses the method described in sec.5.3.3. For further explanation see sec. 5.4. Examples of output of PWMSYS are given in figs. 5.15, 5.16, 6.30, 6.31, 6.35, 6.36, and 6.37.

STEP1

Class: Function subprogramme

Purpose: Evaluate the step response of the first order system with transfer function $F \exp(-s DL)/(1+s TC)$

Function reference: H(T)

Programme listing: Figure A-6

Common Statement required: COMMON L, L must be set to 0 before the first encounter of function reference, and it must be set to 1 immediately afterwards.

Data to be supplied: F, DL, TC - system parameters.

STEP2

Class: Function subprogramme

Purpose: Evaluate the step response of the second order system

Function reference: H(T)

Programme listing: Figure A-7.

Common Statement required: Common L (see program STEP1)

Data to be supplied: F, T1, T2 - system parameters.

Comment: T1 and T2 must not be equal.

STEP3

Class: Function Subprogramme

Purpose: Evaluate the step response of a distributed lag system whose transfer function (in s domain) is: $F \exp(-\sqrt{sB})$.

Function reference: H(T)

Subprogrammes used: SUBERF

Programme listing: Figure A-8.

Common statement required: COMMON L (see programme STEP1)

Data to be supplied: F, B: system parameters.

SUBERF

Class: Function subprogramme

Purpose: Evaluate error function of a real argument.

Function reference: ERF(X)

Programme listing: Figure A-9 .

Method of calculation: Error function is calculated according to the polynomial approximation¹:

$$\text{erf}(x) = 1 - \{Ay + By^2 + Cy^3\} \exp(-x^2)$$

where $y = 1/(1 + px)$

$$p = 0.47047$$

$$A = 0.3480242$$

$$B = -0.0958798$$

$$C = 0.7478556$$

The absolute value of the error is less than $2.5 \cdot 10^{-5}$

Class: Subroutine subprogramme

Purpose: Plot or print of up to three dependent functions (B, C, D) of one independent variable (A)

Calling sequence: SUBROUTINE PLOT (N,I,K,A,B,C,D.SCALE)

Description of parameters:

N: determines printing, plotting or skipping modes

0 print values of A,B,C,and D.

1 plot

-1 skip (neither print nor plot)

I: selects the variables to be plotted (immaterial if N≠1).

1 plot only B

2 plot B and C

3 plot B, C, and D

4 plot B and D

K: flag to read data. Set K = 0 in the first call, and

K=1 in all subsequent calls (immaterial if N≠1).

A: independent variable

B,C,D: dependent variables

SCALE: scaling factor for the y-axis. One division on y-axis equals SCALE.

Program listing: Figure A-10.

Data to be supplied:

BLANK - blank (),

DOT - dot (.),

STAR, PLUS, EKS - plotting symbols for B,C, and D, respectively.

PRIME - prime ('),

HYPHEN - hyphen (-),

Comments: In this work, SPL0T5 is used in conjunction with PWMSYS.

A slightly different version of SPL0T5 has been used with

all other main programmes. This programme, SPLOT4, does not indicate time values on x-axis. To obtain SPLOT4 from SPLOT5 the following changes should be done:

1. Delete 7 lines between statements 350 and 950 (inclusive).

2. Insert, instead of deleted lines:

```
350 WRITE (2,203) LINE
203 FORMAT (1X,70A1)
      LCOUNT = LCOUNT + 1
```

SUBMUL

Class: Subroutine subprogramme.

Purpose: Multiply two matrices A and B (each up to the order 10×10)

Calling sequence: SUBROUTINE MLTPLY (A,B,C,M,N,L)

Description of parameters:

A: matrix of order $M \times N$

B: matrix of order $N \times L$

C: result of the multiplication AB

Programme listing: Figure A-11.

Comment: M, N, and L must be equal or less than 10.

SUBLAG

Class: Subroutine subprogramme.

Purpose: Shift a sequence of numbers stored in a one dimensional array.

Calling sequence: SUBROUTINE DELAY (A,MU)

A: the number to be shifted

MU: amount of shift (0,1,2,...)

Programme listing: Figure A-12.

Common statement required: COMMON ICOUNT

ICOUNT must be set to 0 before the first call, and it

must be set to 1 immediately afterwards.

Comment: This subroutine has been used to introduce transit delay into the PWMSYS program, by shifting values of $GAM(\gamma_n)$. MU , then, equals μ . $SUBLAG$ must be used with $FUND$.

FUNSAT

Class: Function subprogramme

Purpose: Evaluate saturation function (fig. 5.6)

Function reference: $SAT(X)$

Programme listing: Figure A-13

Comment: FUNSAT is used with PWMSYS as the modulation law.

SATN2

Class: Function subprogramme

Purpose: Evaluate the function displayed in fig. A-15a.

Function reference: $SAT(X)$

Programme listing: Figure A-14

Comments: SATN2 is used with PWMSYS as a modulation law. It is evident from fig. A-15a that this function is a rough approximation to the three level control law of fig. 5.7b. A better approximation has been obtained by using SATN10 subprogramme which evaluates the function displayed in fig. A-15b. To obtain SATN10 from SATN2 the following change should be done: Replace statement $N = 2$ by $N = 10$. In fact any even value can be assigned to N .

FUND

Class: Function subprogramme

Purpose: Assign $D(X) = 0$

Function reference: $D(X)$.

Programme listing: Figure A-16.

Comment: FUND supplies zero disturbance to the programme PWMSYS. A subprogramme is used (which may seem unnecessary) to achieve flexibility in obtaining various types of disturbances (see FRAMP2, FSTEP2, FSIN). Examples of PWMSYS using FUND are given in figs. 5.16, 6.30 and 6.31.

FRAMP2

Class: Function subprogramme

Purpose: Evaluate the function $D(X) = 0.05X$

Function reference: $D(X)$

Programme listing: Figure A-17

Comment: FRAMP2 supplies a ramp disturbance to the programme PWMSYS. See figure 6.37 for a display. The slope of the ramp can easily be changed by changing the statement $D = X * 0.05$ accordingly.

FSTEP2

Class: Function subprogramme

Purpose: Evaluate the function $D(X) = A u(X - TW)$, where

$u(t)$ is unit step function

Function reference: $D(X)$

Programme listing: Figure A-18

Common statement required: COMMON T

T must be set to 0 before the first reference to $D(X)$, and it must be set to a value other than 0 immediately afterwards.

Data to be supplied:

A: magnitude of the step function

TW: time instant when the step function is applied.

Comment: Two examples are given in figs. 5.15 and 6.35.

FSIN

Class: Function subprogramme

Purpose: Evaluate the function $D(X) = A - B \cos(\pi CX)$

Function reference: D(X)

Programme listing: Figure A-19

Common statement required: COMMON T (see FSTEP2)

Data to be supplied:

A, B, C: parameter values for the D(X) function.

Comment: An example is given in fig. 6.36.

A.3 FLOWCHARTS AND PROGRAMMES

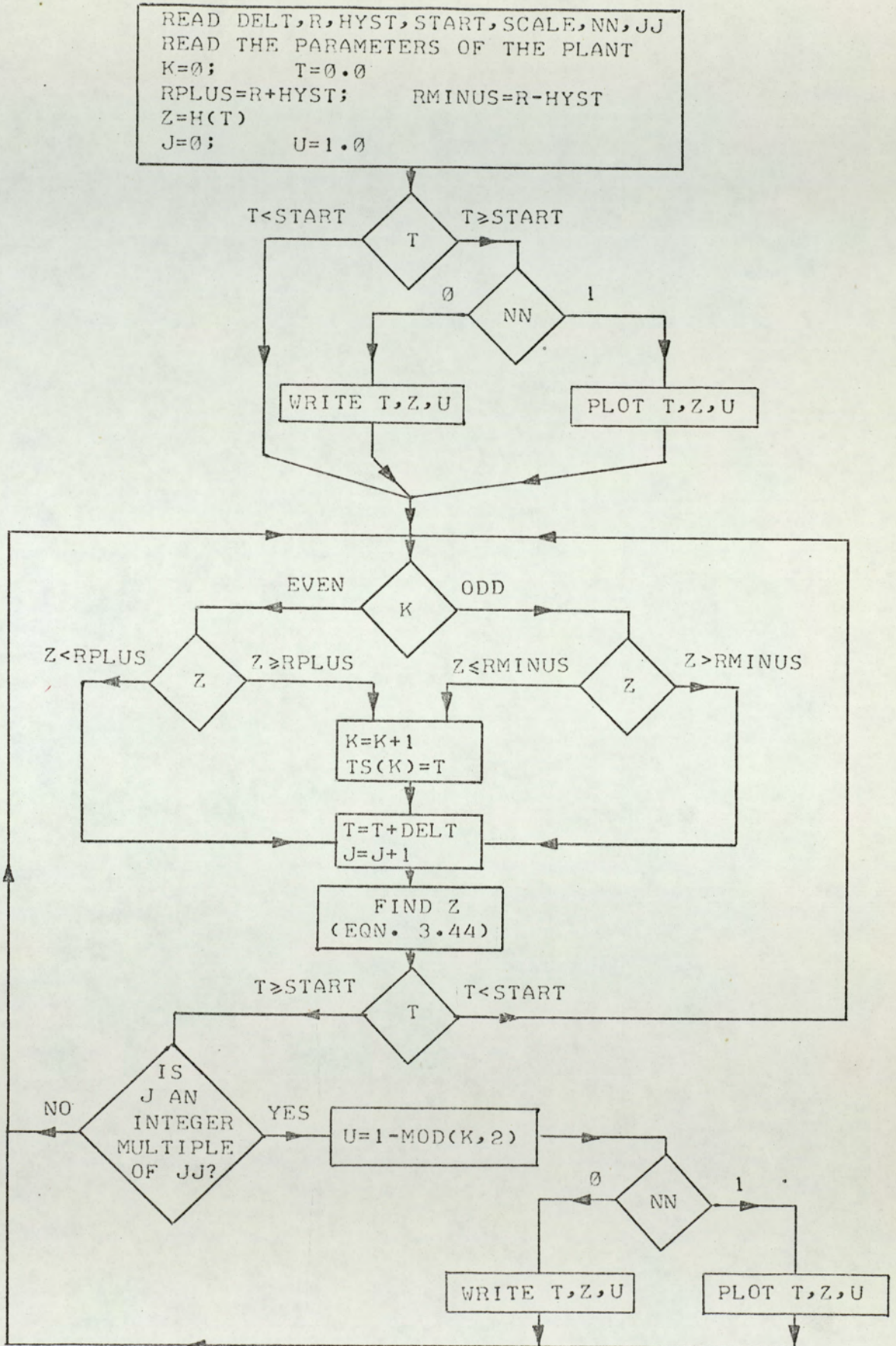


Fig. A-1 Flowchart-Programme ONOFF

```

DIMENSION TS(50)
COMMON L
READ (1,115) DELT,R,HYST,START,SCALE,NN, JJ
115 FORMAT (5(F7.3,2X),I1,2X,I3)
T=0.0
L=0
Z=H(T)
L=1
K=0
U=1.0
I=0
RPLUS=R+HYST
RMINUS=R-HYST
KK=0
IF (T.LT.START) GO TO 90
N=NN
95 CALL PLOT (N,2,KK,T,Z,U,Z,SCALE)
KK=1
11 IF (MOD(K,2).EQ.1) GO TO 30
IF (Z.GE.RPLUS) GO TO 40
15 T=T+DELT
I=I+1
Z=H(T)
IF (K.EQ.0) GO TO 20
DO 70 M=1,K
Q=(-1.0)**M
70 Z=Z+Q*H(T-TS(M))
20 IF (T.LT.START) GO TO 50
N=NN
30 MOD J=MOD(J, JJ)
IF (MOD J.NE.0) N=-1
U=1-MOD(K,2)
CALL PLOT (N,2,KK,T,Z,U,Z,SCALE)
GO TO 11
30 IF (Z.GT.RMINUS) GO TO 15
40 K=K+1
TS(K)=T
GO TO 15
50 N=-1
GO TO 30
90 N=-1
GO TO 95
END

```

Fig. A-2 Programme Listing - ONOFF

```

COMMON L
READ (1,81) TO,TP,DELT,NN,SCALE
81 FORMAT (3(F5.1,2X),I1,2X,F5.3)
T=0.0
M=1
TQ=TO+TP
K=0
L=0
20 R=H(T)
L=1
CALL PLOT (NN,1,K,T,R,R,R,SCALE)
K=1
T=T+DELT
IF (T.GE.TO) GO TO 30
GO TO 20
30 M=M+1
IF (M.GE.250) STOP
N=(M-1)/2
AN=N
B=(AN+1.0)*TQ
35 R=0.0
I=N+1
DO 40 J=1,I
AK =J-1
40 R=R+H(T-AK*TQ)-H(T-TO-AK*TQ)
CALL PLOT (NN,1,K,T,R,R,R,SCALE)
T=T+DELT
IF (T.GE.B) GO TO 50
GO TO 35
50 M=M+1
N=(M-1)/2
AN=N
C=AN*TQ+TO
55 R1=0.0
I=N+1
DO 60 J=1,I
AK= J-1
60 R1=R1+H(T-AK*TQ)
R2=0.0
DO 70 J=1,N
AK =J-1
70 R2=R2+H(T-TO-AK*TQ)
R=R1-R2
CALL PLOT (NN,1,K,T,R,R,R,SCALE)
T=T+DELT
IF (T.GE.C) GO TO 30
GO TO 55
END

```

Fig. A-3 Programme Listing - OPLOOP

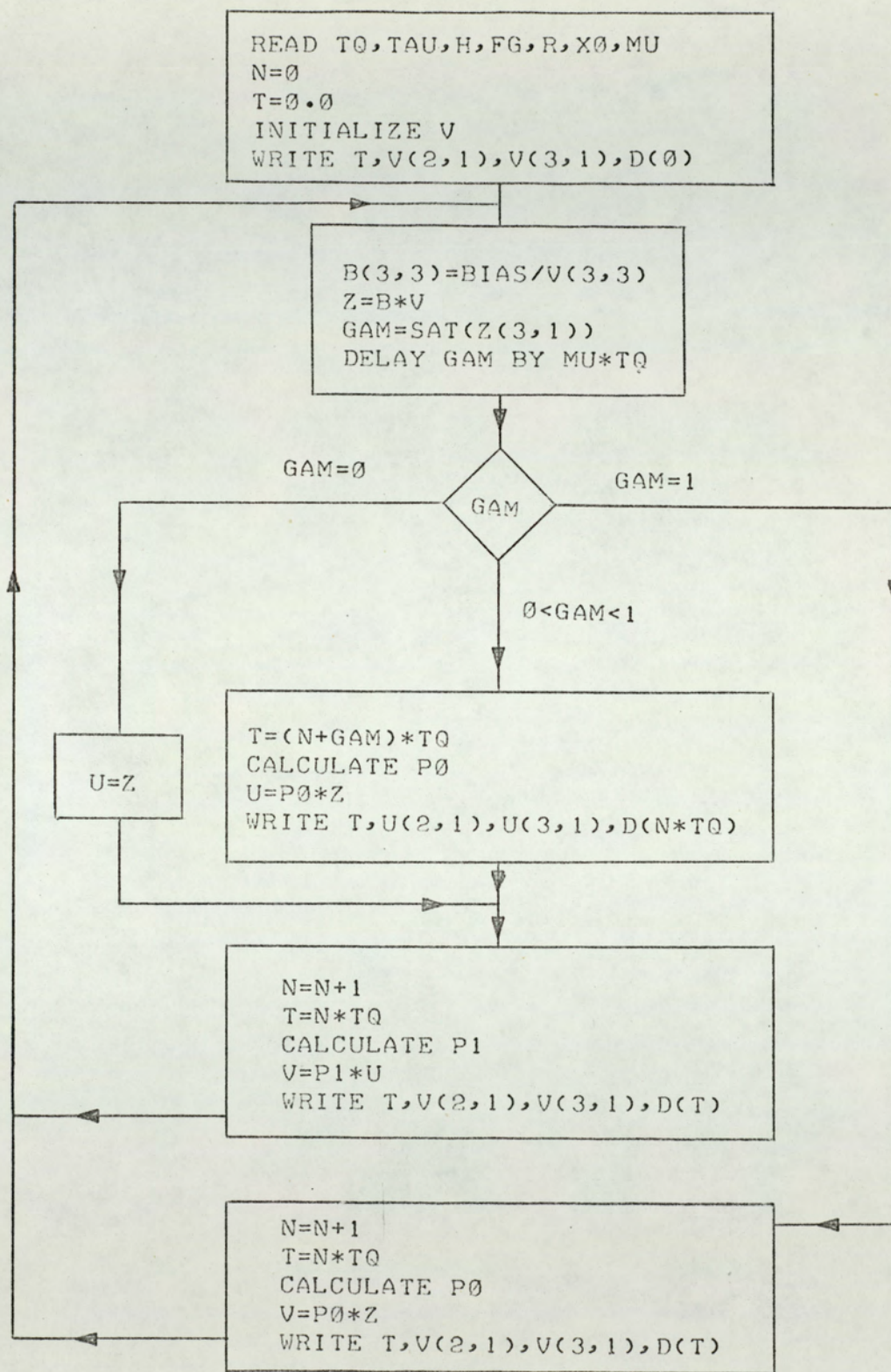


Fig. A-4 Flowchart - Programme PWMSYS

```

DIMENSION P0(3,3),P1(3,3),B(3,3),V(3,1),U(3,1),Z(3,1)
COMMON ICOUNT
COMMON T
READ (1,62) T0,TAU,H,FG,R,X0
WRITE (2,63) T0,TAU,H,FG,R,X0
63 FORMAT(10X,2(F5.1,2X),F6.3,3(2X,F5.1))
62 FORMAT (2(F5.1,2X),F6.3,3(2X,F5.1))
READ (1,64) NV,NU,SCALE
64 FORMAT (2(I2,2X),F5.2)
READ (1,67) MU
67 FORMAT (I2)
ICOUNT = 0
DO 12 I=1,3
DO 12 J=1,3
P0(I,J)=0.0
P1(I,J)=0.0
12 B(I,J)=0.0
P0(1,1)=1.0
P0(3,3)=1.0
P1(1,1)=1.0
P1(3,3)=1.0
B(1,1)=1.0
B(2,2)=1.0
B(3,1)=H
B(3,2)=-H
PSI=T0/TAU
BIAS=(1./PSI)*ALOG(1.+(R/FG)*(EXP(PSI)-1.))
WRITE (2,65) BIAS
65 FORMAT (/10X,5HBIAS=,F8.5)
V(1,1)=R
V(2,1)=X0
V(3,1)=BIAS
N=0
T=0.0
D0=D(T)
CALL PLOT (NV,4,0,T,V(2,1),V(3,1),D0,SCALE)
14 B(3,3)=BIAS/V(3,1)

```

Fig. A-5 Programme Listing-PWMSYS

```

CALL MLTPLY (B,V,Z,3,3,1)
GAM=SAT (Z(3,1))
CALL DELAY (GAM,MU)
ICOUNT=1
IF (GAM.EQ.0.0) GO TO 15
IF (GAM.EQ.1.0) GO TO 17
RN=N
T=(RN+GAM)*TQ
P0(2,2)=EXP(-(GAM*TQ/TAU))
P0(2,3)=((FG+D(RN*TQ))/Z(3,1))*(1.0-P0(2,2))
CALL MLTPLY (P0,Z,U,3,3,1)
C=D(RN*TQ)
CALL PLOT (NU,4,1,T,U(2,1),U(3,1),C,SCALE)
IF (N.GE.100) STOP
GO TO 21
15 U(1,1)=Z(1,1)
   U(2,1)=Z(2,1)
   U(3,1)=Z(3,1)
21 N=N+1
   RN=N
   T=RN*TQ
   P1(2,2)=EXP(-(1.0-GAM)*TQ/TAU)
   P1(2,3)=(D((RN-1.0)*TQ)/Z(3,1))*(1.0-P1(2,2))
   CALL MLTPLY (P1,U,V,3,3,1)
   E=D(T)
   CALL PLOT (NV,4,1,T,V(2,1),V(3,1),E,SCALE)
   GO TO 14
17 N=N+1
   IF (N.GE.100) STOP
   RN=N
   T=RN*TQ
   P0(2,2)=EXP(-(TQ/TAU))
   P0(2,3)=((FG+D((RN-1.0)*TQ))/Z(3,1))*(1.0-P0(2,2))
   CALL MLTPLY (P0,Z,V,3,3,1)
   Q=D(T)
   CALL PLOT (NV,4,1,T,V(2,1),V(3,1),Q,SCALE)
   GO TO 14
END

```

Fig. A-5 ctd.

```

FUNCTION H(T)
COMMON L
IF (L.NE.0) GO TO 115
READ (1,635) F,DL,TC
635  FORMAT (3(F5.1,2X))
115  IF (T.LE.DL) GO TO 125
     H=AMAX1(0.0,(F*(1.0-EXP(-(T-DL)/TC))))
     RETURN
125  H=0.0
     RETURN
END

```

Fig. A.6 Programme Listing-STEP1

```

FUNCTION H(T)
COMMON L
IF (L.NE.0) GO TO 115
READ (2,635) F,T1,T2
635  FORMAT (3(F5.1,2X))
115  IF (T.EQ.0.0) GO TO 125
     H=AMAX1(0.0,(F*(1.0+(T2*EXP(-T/T2)-T1*EXP(-T/T1))/(T1-T2))))
     RETURN
125  H=0.0
     RETURN
END

```

Fig. A-7 Programme Listing-STEP2

```

FUNCTION H(T)
COMMON L
IF (L.NE.0) GO TO 115
READ (1,625) F,B
625  FORMAT (2(F5.1,2X))
115  IF (T.EQ.0.0) GO TO 125
     H=AMAX1(0.0,(F*(1.0-ERF(0.5*SQRT(B/T))))
     RETURN
125  H=0.0
     RETURN
END

```

Fig A-8 Programme Listing-STEP3

```

FUNCTION ERF(X)
IF (X.EQ.0.0) GO TO 100
P=0.47047
A=0.3480242
B=-0.0953798
C=0.7478556
Y=1./(1.+P*X)
ERF=1.-(A*Y+B*Y*Y+C*Y*Y*Y)*EXP(-(X*X))
RETURN
100 ERF=0.0
RETURN
END

```

Fig A-9 Programme Listing-SUBERF

```

SUBROUTINE PLOT (N,I,K,A,B,C,D,SCALE)
REAL LINE (70)
IR(X) = INT(2.0*X-AINT(X))
IF (N) 300,305,310
305 WRITE (2,610) A,B,C,D
610 FORMAT (10X,4(F8.3,4X))
RETURN
300 RETURN
310 IF (K) 100,100,104
100 READ (1,201) BLANK,DOT,STAR,PLUS,EKS,PRIME,HYPHEN
201 FORMAT (7A1)
DO 101 J=1,70
101 LINE (J)=DOT
DO 102 J=1,70,5
102 LINE (J)=PRIME
LCOUNT=0
WRITE (2,202) LINE
202 FORMAT (3X,70A1)
104 DO 103 J=1,70
103 LINE (J) = BLANK
IF(MOD(LCOUNT,5)) 810,820,810
810 LINE (1) =DOT
GO TO 830
820 LINE (1) =HYPHEN
830 GO TO (320,330,340,320),I
340 L=IR(D/SCALE)+1
IF (L.GT.70) GO TO 710
LINE (L) =EKS
710 IF (I.EQ.4) GO TO 350
330 M=IR(C/SCALE)+1
IF (M.GT.70) GO TO 320
LINE (M) = PLUS
320 J=IR(B/SCALE) +1
IF (J.GT.70) GO TO 720
LINE(J) = STAR
720 IF (I.EQ.4) GO TO 340
350 IF (MOD(LCOUNT,5)) 910,910,920
910 WRITE (2,930) LCOUNT,LINE
930 FORMAT (1X,I2,70A1)
GO TO 950
920 WRITE (2,940) LINE
940 FORMAT (3X,70A1)
950 LCOUNT=LCOUNT+1
RETURN
END

```

Fig. A-10 Programme Listing-SPL0T5

```

SUBROUTINE MLTPLY (A,B,C,M,N,L)
REAL A(10,10), B(10,10), C(10,10)
DO 1 I=1,M
DO 1 J=1,L
C(I,J)=0.0
DO 1 K=1,N
1 C(I,J)=C(I,J)+A(I,K)*B(K,J)
RETURN
END

```

Fig. A-11 Programme Listing-SUBMUL


```

SUBROUTINE DELAY (A,MU)
DIMENSION S(100)
COMMON ICOUNT
IF (ICOUNT.NE.0) GO TO 30
DO 20 I=1, 100
20 S(I)=0.0
30 DO 10 K=1,99
   N = 101-K
10 S(N)=S(N-1)
   S(1)=A
   A=S(MU+1)
   RETURN
END

```

Fig. A-12 Programme Listing-SUBLAG

```

FUNCTION SAT (X)
IF (X.LT.0.0) GO TO 1
IF (X.LT.1.0) GO TO 2
SAT = 1.0
RETURN
1 SAT =0.0
  RETURN
2 SAT = X
  RETURN
END

```

Fig. A-13 Programme Listing-FUNSAT

```

FUNCTION SAT(X)
N=2
IF (X.LE.0.0) GO TO 1
IF (X.LE.0.49) GO TO 2
IF (X.LE.0.51) GO TO 3
IF (X.LT.1.0) GO TO 4
SAT=1.0
RETURN
1 SAT=0.0
  RETURN
2 SAT=0.5-(2.**N-1)**(X-0.5)**N
  RETURN
3 SAT=0.5
  RETURN
4 SAT=(2.**N-1)**(X-0.5)**N+0.5
  RETURN
END

```

Fig. A-14 Programme Listing-SATN2

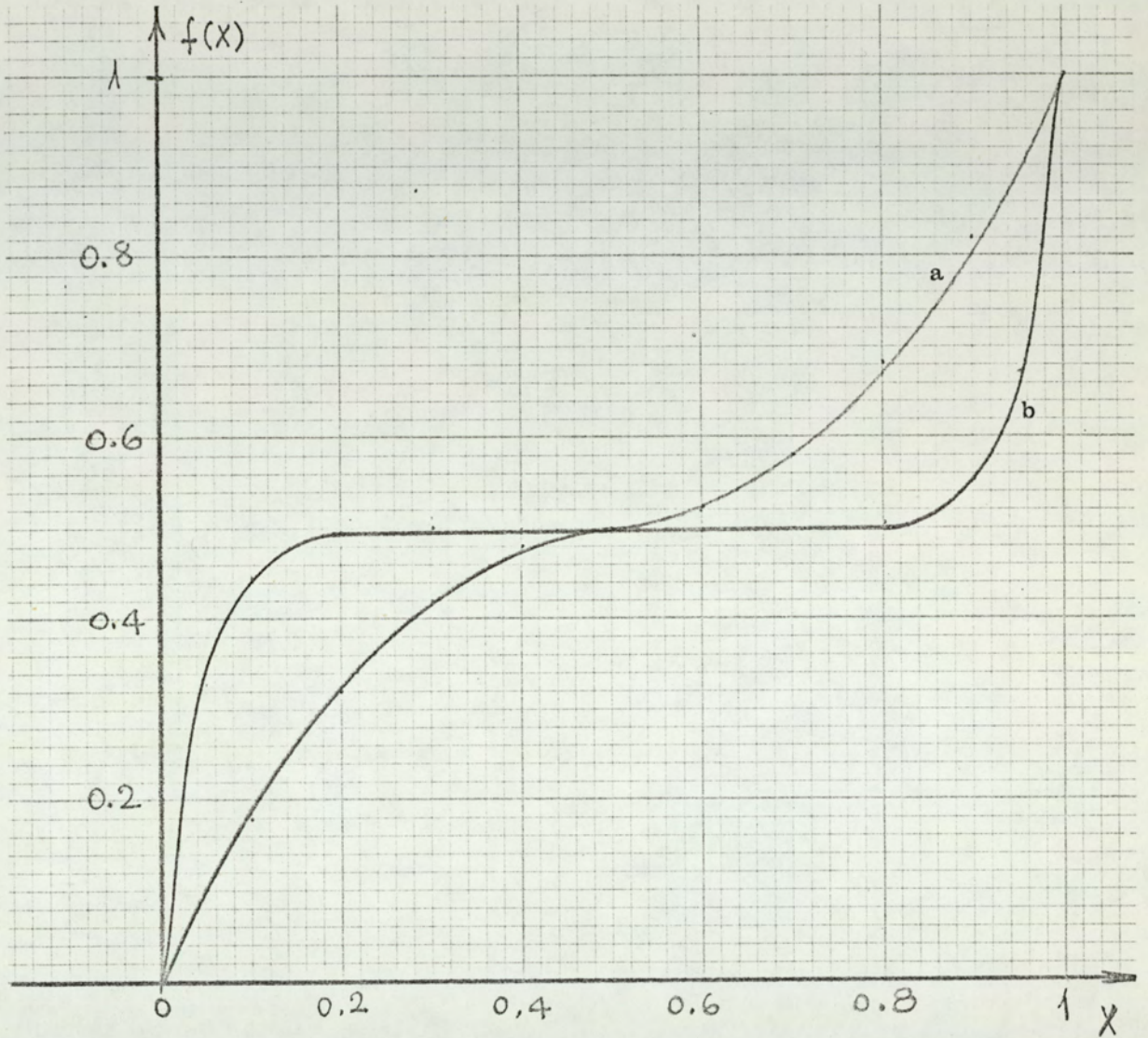


Fig. A-15

Modulation laws realized by the programmes SATN2 and SATN10

a- SATN2

b- SATN10

```

FUNCTION D(X)
D = X*0.0
RETURN
END

```

Fig. A-16 Programme Listing-FUND

```

FUNCTION D(X)
D = X*0.05
RETURN
END

```

Fig. A-17 Programme Listing-FRAMP2

```

FUNCTION D(X)
COMMON T
IF (T) 11,10,11
10 WRITE (2,71)
71 FORMAT (10X,40HVALUE OF STEP,TIME APPLIED ----)
READ (1,72) A,TW
72 FORMAT (F5.2,2X,F6.2)
11 IF (X-TW) 20,21,21
20 D=X*0.0
RETURN
21 D=X*0.0+A
RETURN
END

```

Fig. A-18 Programme Listing-FSTEP2

```

FUNCTION D(X)
COMMON T
IF (T) 11,10,11
10 WRITE (2,71)
71 FORMAT(10X,37HA-BCOS(C 3.14 X),A B C-- --)
READ (1,72) A,B,C
72 FORMAT (F3.1,2X,F3.1,2X,F5.3)
11 D=A-B*COS(C*3.14159*X)
RETURN
END

```

Fig. A-19 Programme Listing-FSIN

B

APPROXIMATIONS USED IN THE TEXT

B.1 APPROXIMATIONS TO $\exp(x)$

Two approximations to $\exp(x)$ are used in the text:

$$\exp(x) \approx 1 + x \quad (\text{B.1})$$

$$\exp(x) \approx 1 / (1 - x) \quad (\text{B.2})$$

Approximation B.1 is used in eqns. 3.33 and 6.20, and B.2 is used in eqn. 3.12. Errors of the above approximations relative to $\exp(x)$ are shown below:

<u>x</u>	<u>relative error, per cent</u>	
	<u>(B.1)</u>	<u>(B.2)</u>
0.0	0.00	0.00
0.1	-0.47	0.54
0.2	-1.75	2.34
0.3	-3.69	5.83
0.4	-6.16	11.72
0.5	-9.02	21.31

The ranges of these approximations, for errors less than 10 per cent, are given below:

$$\exp(x) \approx 1 + x \quad 0 < x < 0.53$$

$$\exp(x) \approx 1/(1 - x) \quad 0 < x < 0.38$$

B.2 APPROXIMATIONS TO $\exp(-x)$

Two approximations to $\exp(-x)$ are used in the text:

$$\exp(-x) \approx 1 - x \quad (\text{B.3})$$

$$\exp(-x) \approx 1/(1 + x) \quad (\text{B.4})$$

Approximation B.3 is used in eqn. 4.8 and B.4 is used in eqn. 6.12. Errors of the above approximations relative to $\exp(-x)$ are shown below:

<u>x</u>	<u>relative error, per cent</u>	
	<u>(B.3)</u>	<u>(B.4)</u>
0.0	0.00	0.00
0.1	- 0.53	0.47
0.2	- 2.29	1.78
0.3	- 5.51	3.84
0.4	-10.49	6.56
0.5	-17.56	9.91

The ranges of these approximations, for relative errors less than 10 per cent, are given below:

$$\exp(-x) \approx 1 - x \quad 0 < x < 0.39$$

$$\exp(-x) \approx 1/(1 + x) \quad 0 < x < 0.50$$

Another approximation to $\exp(-x)$ is found as:

$$\exp(-x) \approx (2.35 - x)/(2.35 + 1.35x) \quad (\text{B.5})$$

The relative error of this approximation is given below:

<u>x</u>	<u>relative error of B.5</u>
	<u>per cent</u>
0.0	0.00
0.5	0.83
1.0	- 0.82
1.1	- 2.08
1.2	- 3.83
1.3	- 6.14
1.4	- 9.14
1.5	-12.93

From the above table it is seen that the approximation of B.5 is better than B.3 and B.4. In fact this approximation is better than

the Taylor approximations $[1 - x + x^2/2]$ and $[1 - x + x^2/2 - x^3/6]$, and the Pade approximations of relatively higher orders. Since the exponents encountered in the text (L/T and ϕ) were generally in the range of $0 < x < 0.4$ we used the approximations B.3 and B.4. If better approximations or larger ranges are required, the approximation of eqn. B.5 can be used.

B.3 APPROXIMATIONS TO $\ln x$

Two approximations to $\ln x$ are used in the text:

$$\ln x \approx x - 1 \quad (\text{B.6})$$

$$\ln x \approx 2(x - 1)/(x + 1) \quad (\text{B.7})$$

Approximation B.6 is used in eqns. 3.32 and 6.21, and B.7 is used in eqn. 4.47. The ranges of these approximations, for relative errors less than 10 per cent, are given below:

$$\ln x \approx x - 1 \quad 0.8 < x < 1.25$$

$$\ln x \approx 2(x - 1)/(x + 1) \quad 0.33 < x < 3.3$$

B.4 APPROXIMATION USED FOR THE DIFFERENCE EQUATION 6.8

A detailed investigation using digital computer showed that for V_0 values larger than $0.2F$ the error associated with the eqn. 6.15 is less than 10 per cent. $V_0 > 0.2F$ is the usual case in practice which means that the linear control region does not extend to very low temperatures. The range of parameter values in the error investigation was:

$$0.1 < Fk < 1000 \quad (\text{B.8})$$

$$0.1 < \beta < 0.9 \quad (\text{B.9})$$

$$0.1 < \phi < 0.9 \quad (\text{B.10})$$

Values of Fk given in B.8 cover the practical range of gain values. Values of β given in B.9 cover approximately the whole range (0-1). The range of ϕ given in B.10 also covers all the practical values.

LIST OF SYMBOLS

A	$\exp(-t_s/T)$; coefficient matrix
B	state transition matrix
C	cool operator
F	runaway temperature of the plant
G	gain of the plant ; gain of the amplifier
H	normalized hysteresis width (h/F); heat operator
I	unit matrix
L	transit delay
L_e	equivalent transit delay (Ziegler-Nichols)
L_s	equivalent transit delay (Strejc)
M	number of heat-up periods in the limit cycling period
N	number of cool-down periods in the limit cycling period
P	plant
Q	linear region operator
S	slope
T	time constant
T_c	equivalent time constant (Chaussard)
T_e	equivalent time constant (Ziegler-Nichols)
T_s	equivalent time constant (Strejc)
T_A, T_P	active and passive mode time constants
V	State vector, s domain
W	power into plant
a(t)	step response
b	bias
e	error signal
f	modulation law
h	half hysteresis width

$h(t)$	impulse response
k	gain of the modulator
m	controller output (0 or 1)
p	$\exp (-t_o/T_A)$
q	$\exp (-t_p/T_P)$
r	command; voltage dividing ratio of potentiometer
s	Laplace variable
t	time
t_c	limit cycling period
t_o	on time
t_{osc}	period of oscillations ($L \neq 0$)
t_p	off time
t_q	$t_o + t_q$
t_s	sampling period
t_w	start-up time
u	disturbance
$u(t)$	unit step function
v	state vector
x	modulator input
Δ	discriminant; increment
Θ	temperature, s domain
Φ	overall transition matrix; controller
α	$\exp (L/T), \exp (L/T_P)$
β	θ_r/F
γ	$\exp (L/T_A)$; pulse width/ t_s
δ	T_A/T_P
ε	disturbance
θ	temperature
θ_r	command
θ_d	amplitude of oscillations
θ_u	disturbance
$\bar{\theta}$	average output temperature
λ	t_q/T_1 ; switching instant
μ	number of possible heat-up periods; L/t_s
ν	number of possible cool-down periods

ρ	T/T_1
σ	T_1/T_2
τ	$t-nt_s$
ϕ	t_s/T
ψ	t_o/t_p

dec dynamic equilibrium cycling

lpi location of prime importance

REFERENCES

1. Abramovitz, M. and Stegun, I. A., Handbook of Mathematical Functions, Dover, New York, 1965.
2. Andeen, R. E., "Analysis of pulse duration sampled-data systems with linear elements", IRE Trans. Aut. Cont., v. AC-5, 1960, pp 306-313.
3. Ball, B. J., "Analysis of two branches of the root locus which originate from a simple pole in system containing distributed lag." Proc. 6th Annual Allerton Conf. on Circuit and System Theory, Oct. 1968, Allerton, Illinois, pp. 880-888.
4. Benyon, P. R., "Review of numerical methods for digital simulation", Simulation, Nov. 1968, pp. 219-238.
5. Brych, A., "Optimalization de la régulation d'un four par tout ou rien", Automatisme, vol. 10, no. 6, 1965, pp. 245-249.
6. Carslaw, H. S., and Jaeger, J. C., Conduction of Heat in Solids. Oxford University Press, London, 1959.
7. Chaussard, R. et al., "Rational adjustment of the controls of a thermal power station". 3rd Congress of the International Federation of Automatic Control, London, June, 1966, paper 21A.
8. Cheng, D. K., Analysis of Linear Systems. Addison Wesley, Reading, Mass., 1959.
9. Chu, Y., "Feedback Control Systems with dead time lag or distributed lag by root-locus method". Trans. AIEE, pt II, Vol. 71, No. 11, 1952, pp 291-296.
10. Cypkin, Ja. Z., Théorie des Asservissements par plus-ou-moins. Dunod, Paris, 1962.
11. Da-Chuan, S., "On the possibility of certain types of oscillations in sampled-data control systems," Automation and Remote Control, vol.10, January 1959, pp. 77-82.

12. Delfeld, F. R. and Murphy, G. J., "Analysis of pulse-width modulated control systems", IRE Trans. Aut. Cont. v. AC-6, no. 3, 1961, pp. 283-292.
13. Erdélyi, A. et al., Tables of Integral Transforms. McGraw-Hill, New York, 1954.
14. Gelb, A. and Vander Velde, W. E., Multiple-input Describing Functions and Nonlinear System Design, McGraw-Hill, New York, 1968.
15. Goldberg, S., Introduction to Difference Equations, John Wiley, New York, 1958.
16. Gouy, M., "On a constant temperature oven", J. Physique, v. 6., ser. 3., 1897, pp. 479-483 (quoted in Lindorff²⁴ and Andeen²).
17. Hodgman, C. D., ed, Mathematical Tables From Handbook of Chemistry and Physics, Chemical Rubber Publishing Co., Cleveland, Ohio, 1963.
18. Jury, E.I. and Nishimura, T., "On the periodic modes of oscillation in pulse-width-modulated feedback systems", Trans. ASME. Jl. Basic Engineering, v. 84, 1962. pp. 71-84.
19. Jury, E. I., and Nishimura, T., "Stability Study of PWM feedback Systems," Trans. ASME, V. 86, March 1964, pp. 80 - 86.
20. Kadota, T. T. and Bourne, H. C., "Stability conditions of PWM systems through the second method of Lyapunov" IRE Trans. Aut. Cont., v. AC-6, 1961, pp. 266-276.
21. Kilomeitseva, M. B. and Netushil, A. V., "Transients in automatic control systems with irrational transfer functions", Aut. Rem. Control, v. 26, no. 2, 1965, pp. 353-358.
22. Kuntsevich, V. M. and Chekhovoi, Yu. N., "Stability of control systems with double (pulse-frequency and pulse-width) modulation". Automatic and Remote Control, 1967, no. 7, pp. 1044-1052.
23. Kutz, M., Temperature Control, John Wiley, New York, 1968.
24. Lindorf, D. P., Theory of Sampled-Data Control Systems, John Wiley, New York, 1965.
25. Michalski, L., "Ein elektrischer Widerstandofen als Regelstrecke", in Proc. 6th International Congress on Electro-heat, Brighton, England, paper 621, published by UIE, Paris, 1968.
26. Michalski, L., "Unstetige und stetigähnliche Regelung der Temperatur in Elektrowarme-anlagen", Electrotechnik, vol. 42, 1964, pp. 1-15.
27. Monroe, A. J., Digital Processes for Sampled Data Systems, John Wiley, New York, 1962.
28. Nease, R. F., "Analysis and design of nonlinear sampled-data control systems", Mass. Inst. Tech., Cambridge, Mass., Tech.

29. Nelson, W. L., "Pulse -width relay control in sampling systems", Trans. ASME, II. Basic Eng., D, v. 83, 1961, 65-76.
30. Polak, E., "Stability and Graphical Analysis of first-order pulse-width-modulated sampled-data regulator systems", IRE Trans. Aut. Cont., v.AC-6, no. 3, 1961, pp. 266-276.
31. Pyshkin, I. V., "Self oscillation in pulse width modulated systems," in "Theory and Application of Discrete Automatic Systems" (book in Russian), Academy of Science, USSR, Moscow, 1960, pp. 134-150. (Quoted in Jury and Nishimura¹⁸)
32. Roots, W. K., Fundamentals of Temperature Control, Academic Press, New York, 1969.
33. Roots, W. K. et al, "Mode depeident time constants in electric heating processes", IEEE Trans. Industry and General Applications, vol. IGA-3, no. 4, 1967, pp. 315-322.
34. Roots, W. K., and Gönenc, G., "Electroheat control, comparison and extension of three recent contributions". Trans. Inst. Meas. Cont., v.2, no. 2, 1969, pp. T18-T28.
35. Roots, W. K., and Gönenc, G., "Indirect electroheat regulation". Proc. IEE., vol. 116, no. 8, 1969, pp. 1471-1474.
36. Roots, W. K., and Tulunay, E., "Electroheated Fluidised beds", Proc. IEE, vol.116, no. 5, 1969, pp. 827-833.
37. Roots, W. K., and Walker, F., "Secondary feedback in on-off electric heating processes". IEEE Trans. on Industry and General App., vol. IGA-3, no. 5, 1967, pp. 401-420.
38. Roots, W. K., and Woods, J. T., "Design parameters for thermal processes with on-off controllers". J. Inst. Fuel, vol. 41, no. 324, 1968, pp 5-15.
39. Shapiro, S., "On-off temperature control", in Polytechnic Institute of Brooklyn, New York, Report to the Joint Services Technical Advisory Committee, no. R-452.31-67, 1967, pp. 183-184.
40. Shnaidman, M. A., "Pulse width modulation element is used to investigate control systems" (in Russian), Avtomatika i Telemekhanika, v.17, 1956, pp. 910-920 (quoted in Nelson²⁹).
41. Strejc, V., "Determination approchee des caracteristiques de regulation d'un processus aperiodique". Automatisme, v.5, no. 3., 1960, pp. 109-111.
42. Svenchanski, A., Polischuk, Ya. and Edemski, V., "Automatic temperature control of resistance furnaces for precision heating", in Proc. 6th International Congress on Electro-heat, Brighton, England, paper 315, published by UIE, Paris, 1968.
43. Thaler, G. J. and Pastel, M. P., Analysis and Design of Nonlinear Feedback Control Systems, McGraw-Hill, New York, 1962.

44. Tou, J. J., Modern Control Theory, McGraw-Hill, New York 1964.
45. Treizon, Z. and Polischuk, Ya., "Dynamic characteristics of electric resistance furnaces and a method for selecting an automatic temperature controller". l'Union Internationale d'Electrothermie, Paris, Automatic Control Working Group paper no. 69-4, 1969.
46. Truxal, J. G., Automatic Feedback Control System Synthesis, McGraw-Hill, New York, 1955.
47. Tüdös, T., "On the temperature control of electric resistance furnaces by means of discontinuous controllers", in Proc. 6th International Congress on Electroheat, Brighton, England paper 602, published by UIE, Paris, 1968.
48. Ziegler, J. G., and Nichols, N. B. "Process Lags in Automatic-Control Circuits", Trans. ASME, v.65, 1943, pp. 433-444.

PRESENT PUBLICATIONS RESULTED FROM THIS WORK

"Analysis of Recent Contributions to Discontinuous Electroheat Control". Automatic Control Working Group Report No. ACWG68-1, International Union for Electroheat, Paris, France, dec. 1968.

"Electroheat Control, A Comparison and Extension of Three Recent Contributions" Transactions of the Institute of Measurement and Control (London), vol.2, no.2, feb. 1969, pp. 18-28.

"Indirect Electroheat Regulation" Proceedings of the IEE (London), vol 116, no.8, aug. 1969, pp. 1471-1474.

"Temperature Control in Industrial Processes" IEEE Trans. Ind. Electronics and Control Instrumentation (New York), vol. IECI-16, no.2, sep 1969, pp. 147-156.

"Use of Models to Control Electroheat Processes" Accepted by IEEE Transactions on Industry and General Applications (New York).